



Passive antenna systems printable on conformable supports

Hong Duc Nguyen

► To cite this version:

Hong Duc Nguyen. Passive antenna systems printable on conformable supports. Electronics. Ecole nationale supérieure Mines-Télécom Atlantique, 2018. English. NNT : 2018IMTA0075 . tel-02051066

HAL Id: tel-02051066

<https://theses.hal.science/tel-02051066>

Submitted on 27 Feb 2019

HAL is a multi-disciplinary open access archive for the deposit and dissemination of scientific research documents, whether they are published or not. The documents may come from teaching and research institutions in France or abroad, or from public or private research centers.

L'archive ouverte pluridisciplinaire **HAL**, est destinée au dépôt et à la diffusion de documents scientifiques de niveau recherche, publiés ou non, émanant des établissements d'enseignement et de recherche français ou étrangers, des laboratoires publics ou privés.

THESE DE DOCTORAT DE

L'ÉCOLE NATIONALE SUPERIEURE MINES-TELECOM ATLANTIQUE
BRETAGNE PAYS DE LA LOIRE - IMT ATLANTIQUE
COMUE UNIVERSITE BRETAGNE LOIRE

ECOLE DOCTORALE N° 601
*Mathématiques et Sciences et Technologies
de l'Information et de la Communication*
Spécialité : *Electronique*

Par

Hong Duc NGUYEN

Passive Antenna Systems Printable on Conformable Supports

Thèse présentée et soutenue à Brest, le 23 mai 2018
Unité de recherche : Labsticc (UMR 6285)
Thèse N° : 2018IMTA0075

Composition du Jury :

Président :	Than-Phu Vuong	Professeur des universités, laboratoire IMPE/LAHC – INP – Grenoble
Rapporteurs :	Valérie Vigneras Cyril Decroze	Professeur des universités, Laboratoire IMS – ENSCBP - Pessac Maître de conférences (HDR), Université de Limoges
Examineurs :	Dominique Lo Hine Tong Anwar Shoaib Jean-Philippe Coupez	Ingénieur R&D, Technicolor Connected Home – Cesson Sévigné Ingénieur R&D, MGV Industries Directeur d'études, IMT Atlantique
Dir. de thèse :	Christian Person	Professeur, IMT Atlantique

----- To my father and grandfather

"Everything is theoretically impossible, until it is done"
_____ *Robert A. Heinlein*

"The science of today is the technology of tomorrow."
_____ *Edward Teller*

"The important thing is not to stop questioning.
Curiosity has its own reason for existing."
_____ *Albert Einstein*

Acknowledgements

This dissertation is the outcome of my PhD thesis which was realized in the Microwaves department at IMT Atlantique, a leading french engineering school in Brest, France from October 2014 to March 2018.

Firstly, I would like to express my sincere thanks and gratitude to Prof. Christian Person, my thesis director, for giving me the wonderful opportunity to work under his patronage on an extremely rich and enchanting research area. His superlative research spirit and aptitude really inspired my intuitive and critical approach towards science. Aside from his valuable guidance and support, he is exceptionally kind, welcoming and friendly to me as a sincere friend. It was also my magnificent experience to work in Lab-STICC laboratory surrounded by gifted minds and smart scientists.

I would also like to express my sincere thanks to Prof. Jean-Philippe Coupez, the supervisor of my research work for his valuable guidance and directions throughout the course of my thesis. He is the most important person to help me complete this dissertation over 3 years. I have learned a lot from his endless knowledge as well as his wonderful experimental skills.

I would also like to express my special thanks to ANR (Agence Nationale de la Recherche) to financially sponsor the STICK'IT project under grant ANR-IG-CE26-0033-01 and hence, this thesis. I additionally thank the excellent partners in the ANR STICK'IT project for helping me to accomplish successfully this research work.

I would like to acknowledge Pascal Coant, Jean-Marc Autret, Jérémie Hemery, Vincent Castel, Maïna Sinou, and Raymond Jezequel from the Microwaves department for their technical support during various measurements realized in this thesis and Yannick Marinette for his administrative support.

I am also very grateful to Prof. Emmanuel Daniel from Optics department for his insightful suggestions about interconnection solution and valuable guidelines.

A special mention goes to all my great vietnamese friends (Vinh Loc, Thanh Huy, Trung Kien, Tran Vu, Quang Thang, ...) in the Maisel student residence and my brilliant colleagues in the Microwaves department especially Ankit Jain, Rizwan Masood, Jialai Weng, Emna Bel Kamel, Malika Tlili, Lyes Rahmouni to name only a few for the wonderful time and cherishing moments that we spent together.

Above all, I would like to express my profound thanks and gratefulness to my father, younger sister and all other family members for their special love, affection and cares for me regardless of the geographical distances.

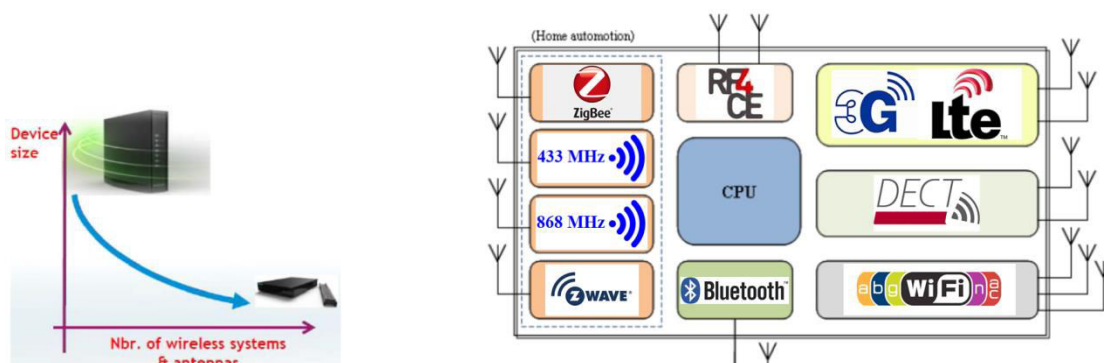
Résumé en français

Au cours des dernières années, en raison de la demande croissante de produits de plus en plus légers, plus petits et moins chers à l'intérieur des appareils portables, l'électronique flexible émerge sur le marché commercial comme une nouvelle génération d'électroniques. Les substrats rigides conventionnels sont remplacés par des matériaux plus minces, flexibles et à faible coût tels que papier, polymère, plastique pour la fabrication des composants et circuits. En même temps, les futurs boîtiers électroniques demandent de plus en plus de nombreux systèmes sans fil afin d'offrir de multiples services et applications (ZigBee/Z-Wave, WLAN, DECT, Bluetooth, RF4CE, 3G/4G, etc.). À cause de l'intégration d'un très grand nombre d'antennes pour satisfaire l'opération de toutes ces applications, les connectivités deviennent donc un grand défi pour les exigences de coût. C'est pourquoi on voudrait remplacer l'ensemble du système d'alimentation/d'interconnexion à la carte mère PCB par une technologie homogène, collective.

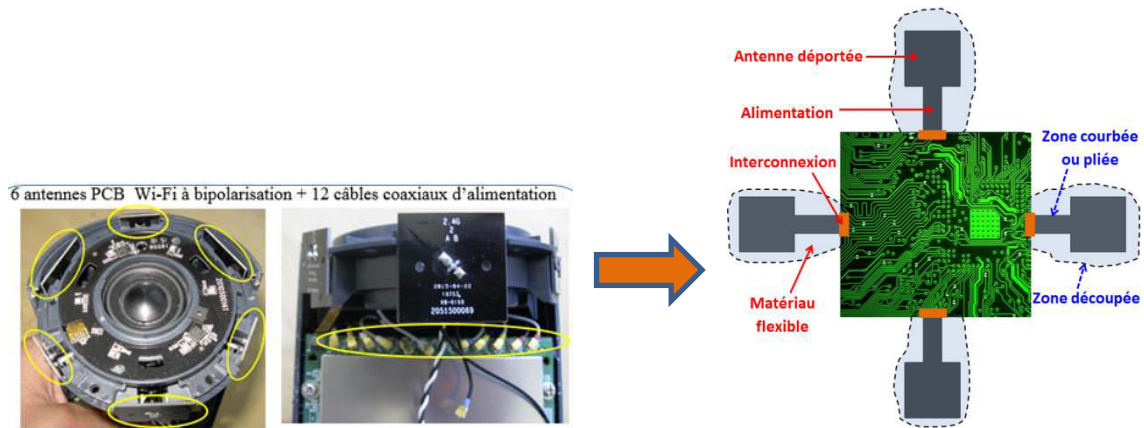
Ce travail de thèse vise à développer une nouvelle technologie "verte" et faible coût dédiée à la conception et réalisation de systèmes antennaires et d'interconnexions sur les matériaux flexibles (tels que papier) à base d'encre conductrice et de procédés de fabrication additifs comme impression. Le défi scientifique est de concevoir des systèmes antennaires répartis spatialement sur les faces internes en plastique du boîtier électronique sous forme des stickers RF 3D et connectés directement à la carte PCB par une solution innovante, à faible coût pour des applications multimédia sans fil dans la gamme de fréquences de 1.8-6 GHz.

Contexte et Objectifs

Ce sujet de recherche est dérivé de la tendance du développement des boîtiers électroniques. Plus spécifiquement ici, on a vraiment un besoin d'intégrer un grand nombre d'antennes et systèmes sans fil à l'intérieur du set-top-box pour satisfaire tous les communications multistandards, multi-bandes demandées (comme ZigBee/Z-Wave, Bluetooth, RF4CE, DECT, GPS, réseau cellulaire 3G/4G, Wi-Fi). Cependant, la taille du boîtier électronique est de plus en plus diminuée en raison de l'esthétique. Donc, il n'y a pas suffi de place pour mettre tous les antennes sur la carte mère. Et cela introduit une solution d'intégration d'antennes déportées dans tout le volume du boîtier.



La solution out-of-board actuelle utilise un système des câbles d'alimentation très encombrant. Cela coûte très cher le coût et le temps pour la soudure de toutes les parties connectiques. C'est pourquoi, on voudrait remplacer l'ensemble de tout le système: antennes + alimentation/interconnexion par une autre technologie plus homogène et collective.



Deuxièmement, des divers facteurs de forme des futurs boîtiers électroniques demandent des matériaux flexibles (tels que polymère ou papier) pour les substrats des antennes pour que ces antennes puissent être collées sur les faces internes du boîtier.

Troisièmement, pour économiser le coût avec le développement durable, les antennes sont proposées à développer sur des substrats flexibles, biodégradables, à faible coût comme papier.

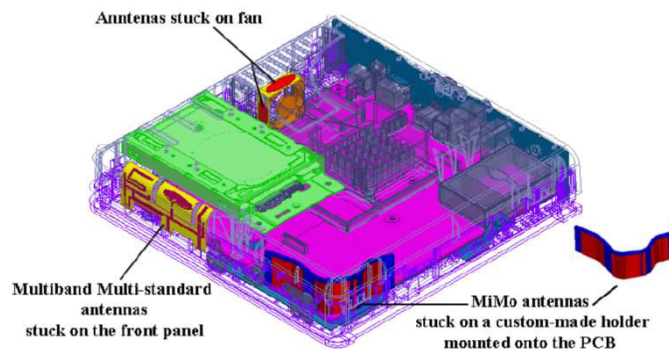
Dans la littérature, des antennes RFID sur papier sont déjà validées largement sur plusieurs tags pour des applications dans la détection ou identification ... Alors, on se pose une question toujours ouverte: est-il possible de transposer cette technologie pour des applications de type communication (à fort niveau de performances) ? Et c'est aussi l'enjeu du projet ANR STICK'IT dans lequel IMT Atlantique a travaillé en collaboration avec 3 autres partenaires: un laboratoire à INP Grenoble, un centre technique du papier à Grenoble et une entreprise Technicolor Connected Home à Rennes.



4 partenaires	Type
IMT Atlantique (IMT-TB) - Brest	LABO
Institut Polytechnique (INPG) - Grenoble	LABO
Centre Technique du Papier (CTP) - Grenoble	CTI
Technicolor (TCHN) - Rennes	Entreprise



À partir de ce contexte, le principal objectif posé est la réalisation d'un système antenne déporté vis-à-vis de la carte mère PCB, pour des applications multimédia sans fil dans lequel les éléments rayonnants sont collés sur les faces internes du boîtier électronique ou sur des supports mécaniques spécifiques (sous forme des stickers 3D) pour satisfaire des communications multistandards, multibandes dans la bande de fréquence 1.8-6 GHz (solutions multi-bandes ou très large bande).



Ces antennes conformables possèdent des interconnexions directes, flexibles, à faible coût avec la carte PCB.

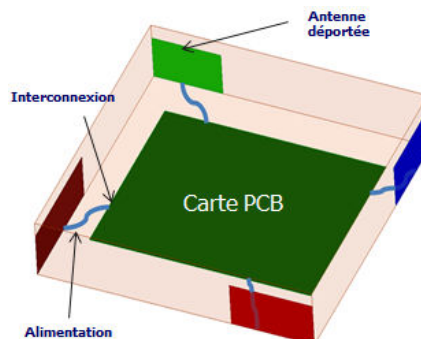
Vers une éco-conception, nous avons utilisé des matériaux recyclables, bio-sourcés, comme le papier pour les substrats des antennes.

Et on promeut aussi les technologies d'impression qui sont compatibles avec le matériau papier pour la métallisation.

Positionnement du sujet

À partir de l'état de l'art et vu dû l'objectif posé du sujet, j'ai déterminé le positionnement du travail de thèse:

- a) Des antennes sont montées dans un environnement complexe, très perturbateur avec la présence du boîtier, de plastique et des éléments métalliques à proximité qui font nuire à la performance des antennes. Et on a besoin des couplages inter-antennes pour les isoler.
- b) Il faut choisir une solution appropriée pour la structure des antennes comme: taille compacte pour intégrer facilement à l'intérieur du boîtier, réalisation sur les substrats papiers (faible coût, flexible, respectueux de l'environnement), fabrication par une technologie d'impression utilisant l'encre métallique, et à base des éléments rayonnants multi-bandes, de configuration plus simple que possible pour fabriquer facilement avec la technologie actuelle.
- c) C'est l'interconnexion entre la carte mère PCB, les antennes déportées et les lignes d'alimentation. On utilise des lignes d'alimentation sur substrat papier flexible, à faible coût et développe aussi une solution d'interconnexion directe avec la carte PCB sans utiliser de câble coaxial.



L'ensemble de tous ces points là ne sont pas encore existés dans la littérature et ne sont jamais développés. Alors, c'est l'originalité du travail de thèse que j'ai poursuivi. Donc, les points clés de ma thèse sont: développement d'une technologie

papier métallisé, validation/utilisation de cette technologie sur des éléments rayonnants basiques et extension à l'intégration de systèmes antennaires complets.

Caractérisation du substrat papier

Le matériau papier est constitué de fibres cellulosiques et d'additifs, donc c'est un matériau non homogène, non isotropique. Ce matériau est aussi original, non habituel pour la fabrication de composants RF.

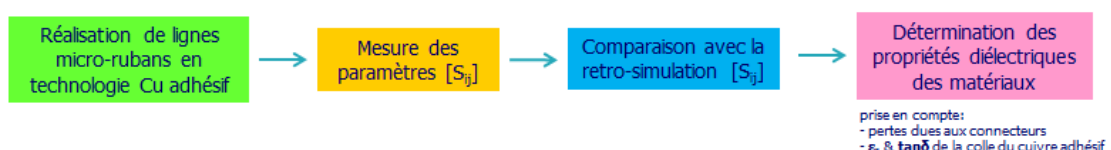
Il possède des avantages comme: très faible coût (0.1 cents/dm²), très léger et flexible et respectueux de l'environnement. Pourtant, il montre aussi des inconvénients si l'on veut l'utiliser pour fabriquer des composants RF. La surface est très rugueuse et la porosité est importante, donc besoin de traitement de surface préconisé. La tolérance en température très faible (< 200°C) ne permet pas la soudure. Et plus important, les pertes diélectriques sont relativement élevées ($\tan\delta > 0.04$) qui limite son utilisation à haute fréquence.

Pour réaliser des circuits et systèmes complexes sur ce matériau papier, il faut connaître les plus précises que possibles ses propriétés diélectriques, telles que permittivité relative ou tangente de pertes. Donc, tout d'abord, la procédure de caractérisation électromagnétique est très importante.

Nous avons utilisé une méthode de caractérisation à base de résonateur de type ligne de transmission micro-ruban pour exploiter les phénomènes stationnaires sur une très large bande de fréquence par exemple de 0-20 GHz. C'est une ligne micro-ruban d'impédance caractéristique différente de 50 ohms, résonante à différentes fréquences selon sa longueur physique. Sa structure est aussi très simple et facile à réaliser. Cependant, elle montre des inconvénients comme pas de distinction simultanée des pertes diélectriques avec des pertes métalliques et "imprécision" due aux pertes des connecteurs, pour une calibration de type OSLT.



Tout d'abord, j'ai commencé par la métallisation cuivre adhésif (40 μm Cu + 25 μm adhésif), une méthode de prototypage très simple et rapide au stade laboratoire avec une bonne valeur de conductivité. En fait, j'ai réalisé plusieurs lignes micro-rubans avec techno cuivre adhésif sur différents substrats papiers (carton, papier Image Laser, papiers photo, papier synthétique Teslin, différents papiers fournis par CTP, ...). Puis, j'ai mesuré des paramètres $[S_{ij}]$ et comparé avec les rétro-simulations. Enfin, j'ai déterminé les propriétés diélectriques du substrat flexible sur la base du principe suivant: En prenant en compte les pertes en transmission liées aux connecteurs (par calibrage de type OSLT), nous choisissons des valeurs de permittivité relative ϵ_r et de tangente de pertes $\tan\delta$, telles que la rétro-simulation, à l'aide de Momentum, colle au mieux que possible avec la mesure réalisée sur toute la bande choisie. Cette détermination a déjà pris en compte les pertes dues aux connecteurs et les propriétés diélectriques estimées de la gomme du cuivre adhésif.



Les résultats des propriétés diélectriques de plusieurs substrats papiers différents à la première fréquence de résonance (autour de 2 GHz) sont présentés dans le tableau suivant:

Paper substrates	Thickness (μm)	ϵ_r	$\tan\delta$
Teslin	250	2.26	0.051
Kodak Polycontrast	245	2.95	0.056
Kodak Polymax	245	2.95	0.062
Couverture magazine	245	3.67	0.065
Ilford	250	3.05	0.067
Silver Image Laser	250	3	0.085
Carton blanc	265	2.85	0.093
PWC	230	2.82	0.069
PRP60	75	3.7	0.093
PRJ	60	4.4	0.098
BL200	245	3.25	0.108
PRC	60	5.3	0.111
SP3	330	2.55	0.065
E4D_75	330	2.68	0.066
FS2	170	3.2	0.081

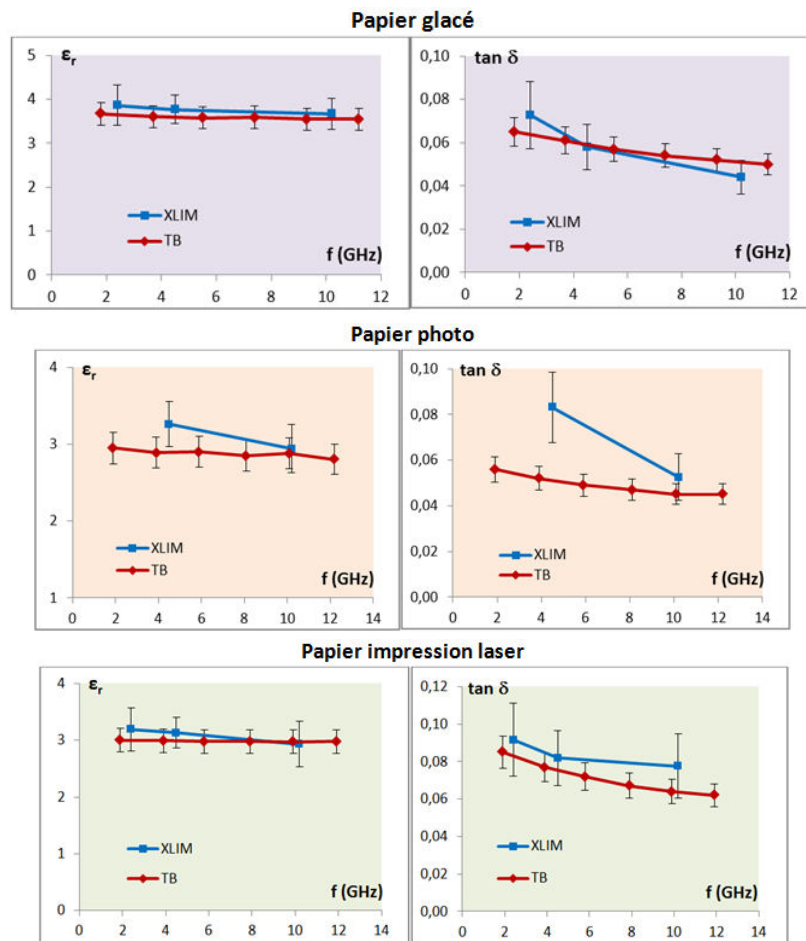
La difficulté dans cette détermination est clairement l'incertitude des propriétés de la colle adhésive. C'est pourquoi, pour la suite, j'ai étudié des lignes de transmission réalisées avec les métallisations directes: impression par sérigraphie Ag sur papier ou gravure d'aluminium sur PET. J'ai calculé aussi les propriétés diélectriques à chaque fréquence de résonance comme montré dans les tableaux ci-dessous:

E4D_240 μm paper									
Resonance mode	1	2	3	4	5	6	7	8	9
f (GHz)	1.95	4	6.02	8.08	10.17	12.22	14.37	16.39	18.44
ϵ_r	2.68	2.53	2.51	2.47	2.43	2.43	2.39	2.4	2.4
$\tan\delta$	0.056	0.05	0.049	0.048	0.046	0.046	0.043	0.045	0.043

PET film_130 μm											
Resonance mode	1	2	3	4	5	6	7	8	9	10	11
f (GHz)	1.77	3.56	5.36	7.14	8.94	10.74	12.53	14.34	16.11	17.9	19.69
ϵ_r	2.91	2.89	2.86	2.86	2.85	2.85	2.85	2.84	2.85	2.85	2.85
$\tan\delta$	0.013	0.01	0.009	0.01	0.009	0.009	0.01	0.008	0.01	0.009	0.01

On constate que les propriétés diélectriques sont particulièrement stables en hautes fréquences. Toutefois, le matériau papier montre une caractéristique légèrement plus dispersive que PET, notamment en $\tan\delta$.

Nous avons comparé nos résultats de mesures avec ceux de XLIM. XLIM a utilisé 3 cavités résonantes à 2.45 GHz, 4.3 GHz et 10 GHz. Ces résultats de mesures prouvent une bonne convergence entre deux méthodes différentes réalisées par chaque laboratoire.



Choix du substrat papier et du procédé d'impression

Après avoir testé une douzaine de substrats papier différents, nous avons choisi le papier E4D grâce aux caractéristiques: imprimable sur les deux faces et tangente de pertes plus petite parmi tous les papiers testés permettant une impression recto-verso.

Nous avons étudié les deux technologies d'impression sur papier qui sont disponibles chez notre partenaire CTP: flexographie et sérigraphie.

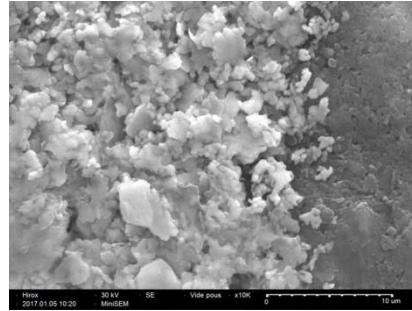
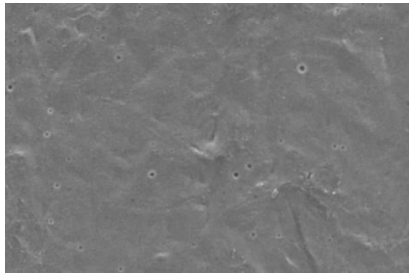
Avec flexographie, on trouve des problèmes comme la manque d'encre argent au bord du motif, l'épaisseur du dépôt très faible (en moyenne $2.25 \mu\text{m}$) avec une conductivité aussi très faible ($\sigma = 7.7 \times 10^5 \text{ S/m}$). Donc, les pertes d'insertion dans une ligne 50Ω sont très élevées (1.2 dB/cm à 5 GHz).

Tandis que avec sérigraphie, nous recevons une meilleure qualité de dépôt avec une épaisseur du dépôt beaucoup plus élevée (en moyenne $7.6 \mu\text{m}$) et une conductivité aussi améliorée ($\sigma = 1.5 \times 10^6 \text{ S/m}$). C'est pourquoi, il y a moins de pertes d'insertion dans une ligne 50Ω (0.8 dB/cm à 5 GHz).

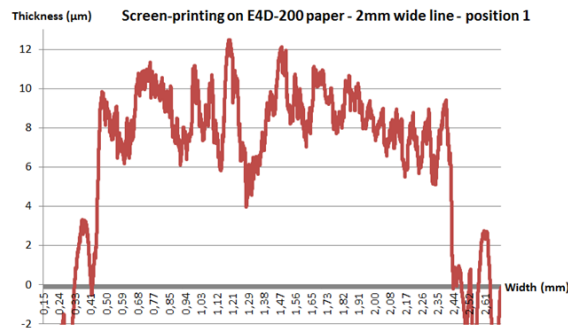
Alors, notre choix définitif pour la métallisation sur papier est: impression Ag par sérigraphie.

L'image microscopie a montré que la qualité de surface du substrat papier est très rugueuse avec la présence des piqûres et des fibres celluliques. La métallisation

par impression sérigraphie associée est un dépôt aléatoire de particules d'encre argent avec beaucoup de gaps d'air à l'intérieur.



Nous avons utilisé un profilomètre mécanique pour mesurer l'épaisseur du dépôt avec rugosité. La rugosité moyenne estimée est $\Delta = 2.8 \mu\text{m}$ et l'épaisseur moyenne estimée du dépôt est $t = 7.6 \mu\text{m}$.



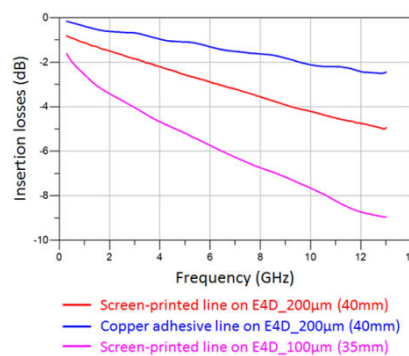
Parmi les différents types de papier E4D, nous avons testé E4D-100 et E4D-200.

Le papier E4D-100 est très fin (épaisseur $106\mu\text{m}$) permettant de plier ou de courber facilement. Mais sa tangente de pertes est trop élevée. C'est pourquoi, les pertes d'insertion dans une ligne 50Ω sont très élevées (1.1 dB/cm à 2.4 GHz et 1.6 dB/cm à 5.5 GHz).

Le papier E4D-200 a une tangente de pertes relativement similaire. Pourtant, la ligne 50Ω plus large permet de diminuer considérablement les pertes métalliques. C'est la raison pour laquelle les pertes d'insertion sont significativement réduites (0.49 dB/cm à 2.4 GHz et 0.76 dB/cm à 5.5 GHz).

À 5GHz:

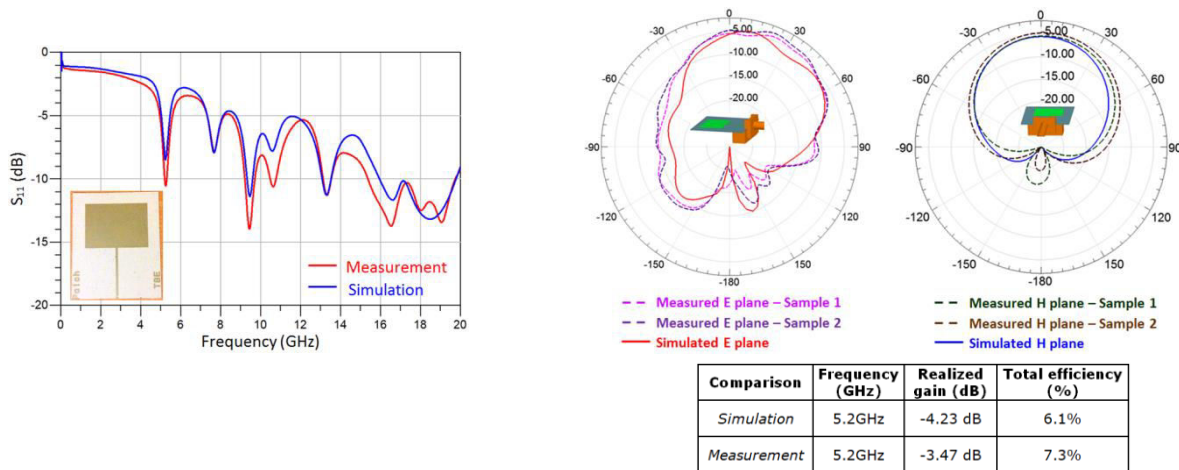
Paper substrate	Thickness (μm)	ϵ_r	$\tan\delta$
E4D-100	106	2.85	0.06
E4D-200	204	2.57	0.05



Donc, notre choix définitif est le papier E4D-200.

Étude et conception d'antennes imprimées élémentaires sur substrats papier flexibles

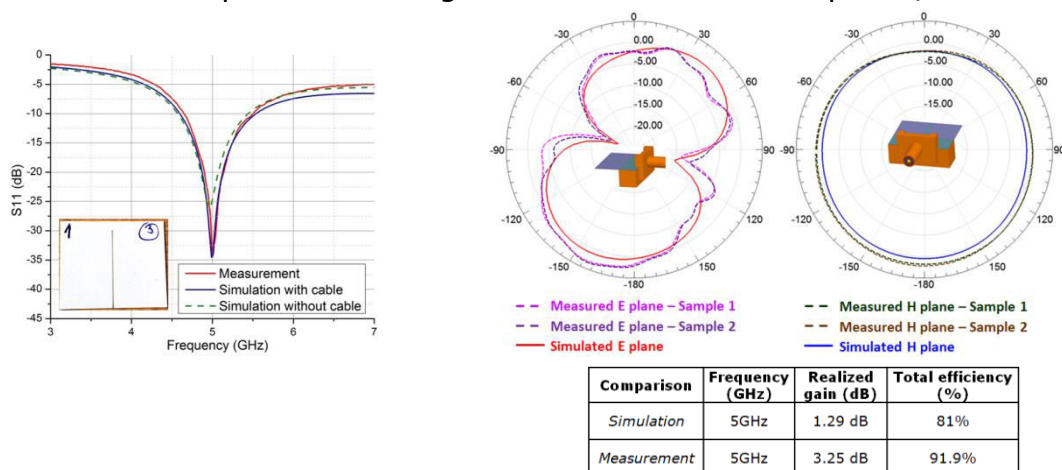
Tout d'abord, pour valider des performances électriques de la technologie "papier imprimé", nous avons utilisé des antennes patch.



On voit bien une excellente adéquation entre les résultats de mesures et les simulations sur une très large bande de fréquence (par exemple, jusqu'à 20 GHz). Cela permet de valider les résultats de caractérisation des propriétés diélectriques du substrat papier utilisé ainsi que la métallisation sérigraphie Ag associée.

Le gain et l'efficacité de rayonnement sont très faibles à cause de l'influence très importante des pertes diélectriques du substrat papier.

C'est pourquoi, nous avons ensuite expérimenté un autre type d'antenne visant à augmenter la bande passante et augmenter l'efficacité: monopôle $\lambda/4$.

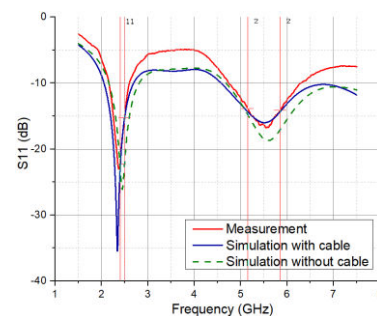
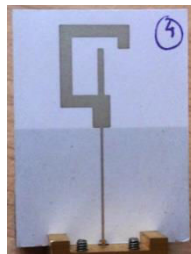
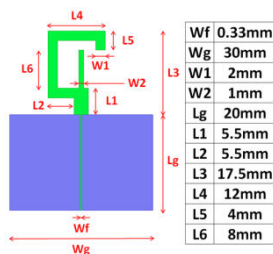


De nouveau, on reçoit une excellente adéquation entre les mesures et les simulations. Le diagramme de rayonnement est dépointé dû au connecteur et au support métallique attaché.

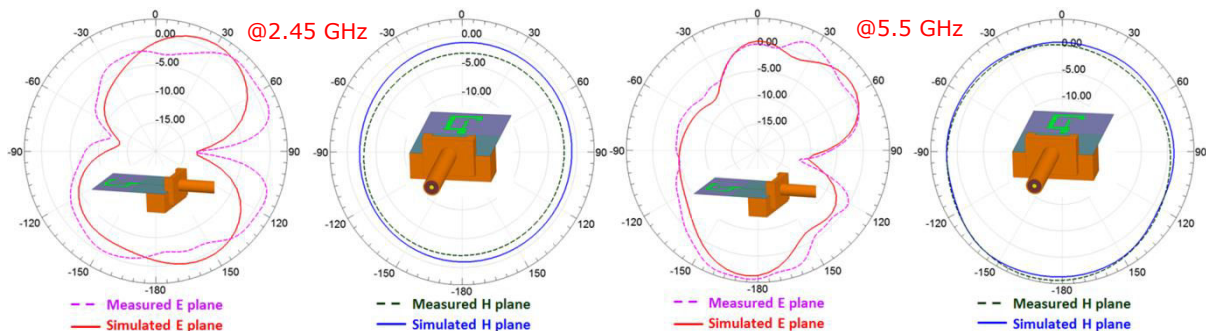
L'efficacité de rayonnement de l'antenne est augmentée considérablement grâce à la plus grande transparence du substrat papier vis-à-vis du champ EM rayonné. Donc, ce type d'antenne (monopôle ou dipôle) est totalement approprié en termes de large bande passante, de diagramme de rayonnement quasi-omnidirectionnel et d'efficacité améliorée (efficacité > 60%) pour construire le système antenne final.

Des principales contraintes posées pour l'antenne sont: configuration simple pour une réalisation facile et robuste; taille compacte pour une intégration aisée dans le set-top-box (avec la hauteur maximum de 3 cm); comportement bi-bandes: 2.4 - 2.5 GHz et 5.15 - 5.85 GHz; rayonnement de type omnidirectionnel; et l'efficacité de rayonnement > 60%.

Nous avons conçu une antenne Wi-Fi bi-bande de type combinaison de monopôles pour une application de type WLAN afin de répondre aux exigences données au début de cette thèse. L'antenne est imprimée par sérigraphie Ag sur le papier E4D-100 μ m. Ce monopôle, de taille compacte 17.5 x 12 mm², a deux fréquences et deux bandes passantes associées qui peuvent être contrôlées indépendamment en jouant sur la longueur et la largeur de chaque branche. Sa structure est aussi simple et appropriée avec le procédé d'impression double face et il n'y a pas d'élément critique au niveau réalisation.



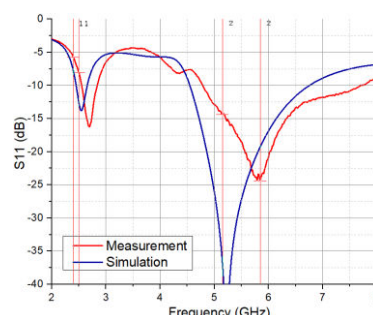
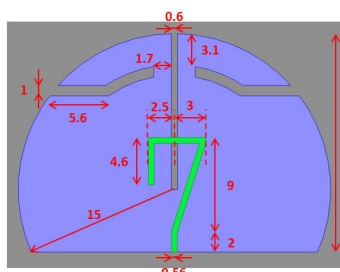
On constate une bonne concordance entre la mesure et la simulation HFSS du coefficient de réflexion S_{11} . Les deux bandes passantes mesurées à -10 dB sont comprises entre 2.16 – 2.6 GHz (0.44 GHz, 18%) et 4.74 – 6.29 GHz (1.55 GHz, 28.2%). Elles couvrent totalement les deux bandes des standards WLAN IEEE.802.11a/b/g/n/ac.



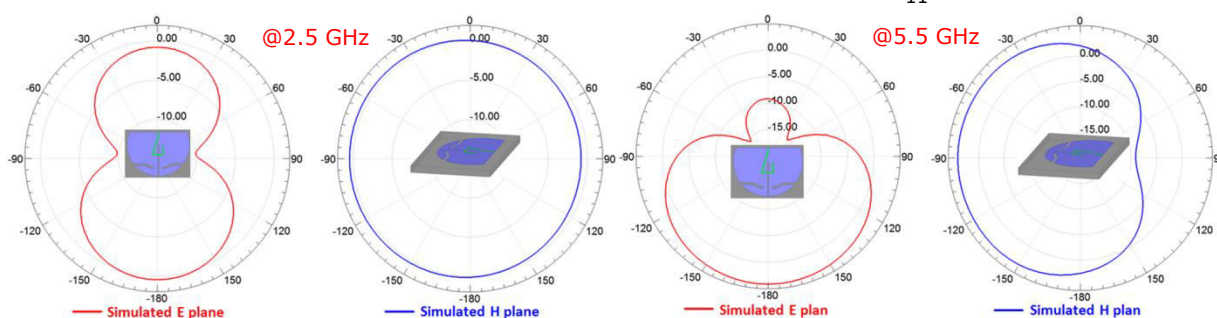
Comparison	Frequency (GHz)	Realized gain (dB)	Total efficiency (%)
Simulation	2.45 GHz	1.3 dB	80.4% (-2.6 dB)
	5.5GHz	3.21 dB	92.6% (-3.4 dB)
Measurement	2.45 GHz	1.87 dB	64.5% (-4 dB)
	5.5GHz	4.1 dB	93.4% (-2.5 dB)

Les diagrammes de rayonnement mesurés à 2.4 GHz et à 5.5 GHz sont en bonne concordance avec les simulations sous HFSS. On constate également que les diagrammes de rayonnement sont quasiment omnidirectionnels en plan H aux deux fréquences de résonance 2.4 et 5.5 GHz. Le diagramme de rayonnement en plan E à 5.5 GHz est déformé à cause de l'influence du monopôle en "C". L'efficacité de rayonnement à 2.45 GHz est plus petite que celle à 5.5 GHz à cause de l'épaisseur du dépôt Ag insuffisante à cette fréquence.

Nous avons continué à concevoir une antenne originale de type dipôle "double ailette" pour un autre type de diagramme de rayonnement omnidirectionnel et une bande passante plus large que le monopôle. Ce dipôle avec balun intégré directement dans l'élément rayonnant est inspiré d'un brevet inventé à IMT Atlantique de M. Coupez.



Ce dipôle bi-bande, collé sur plastique ABS, possède deux bandes passantes simulées de 2.4 – 2.63 GHz (0.23 GHz ou 9.2%) et 4.59 – 6.43 (1.84 GHz ou 36.1%) GHz, correspondant à deux bandes de fréquences de WLAN. Un assez bon accord est obtenu entre la mesure et la simulation HFSS de S_{11} .



Comparison	Frequency (GHz)	Realized gain (dB)	Total efficiency (%)
Simulation	2.5GHz	-0.23 dB	54.8%
	5.5GHz	3.3 dB	92.2%

Le diagramme de rayonnement à 5.5 GHz est beaucoup plus directionnel parce que la grande surface de dipôle à l'arrière des fentes joue le rôle d'un réflecteur. L'efficacité de rayonnement à 2.45 GHz est plus petite que celle à 5.5 GHz en raison de la transition ligne micro-ruban/fente non optimisée à cette fréquence.

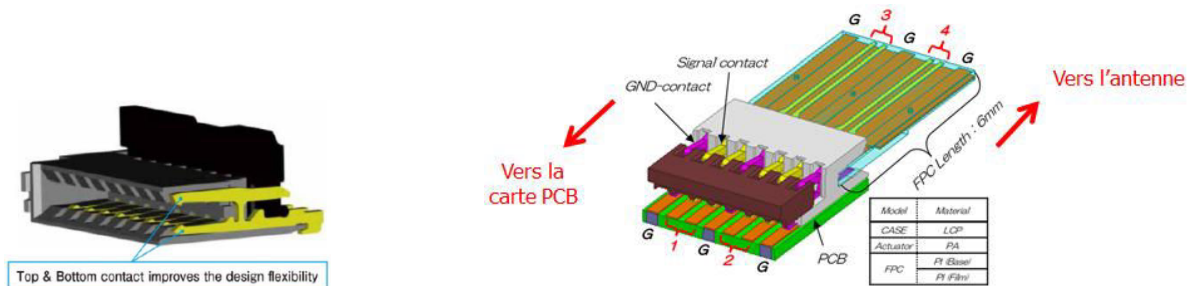
En général, les études sur ces antennes de base ne permettent pas seulement de valider des propriétés diélectriques du substrat papier, caractérisées initialement mais aussi de vérifier la bonne reproductibilité technologique de cette filière papier imprimé. En fait, la technologie est stable, satisfaisante pour la fabrication de circuits RF (ne nécessitant pas cependant d'étapes technologiques critiques: besoin de largeurs de fente ou de ruban très faibles, réalisation de vias métallisés, ...). Toutes les performances sont correctes pour les solutions d'antennes monopôle/dipôle étudiées: efficacité supérieure à 50%, en excluant les pertes d'insertion propres aux lignes d'alimentation. Nous avons constaté un point critique: les pertes d'insertion dans les lignes d'alimentation micro-ruban sont très élevées (1dB/cm à 5 GHz, à comparer au micro câble coaxial: 0.1 dB/cm à 5GHz). Donc, il faut raccourcir au maximum les lignes d'interconnexion/alimentation.

Interconnexion RF à la carte PCB

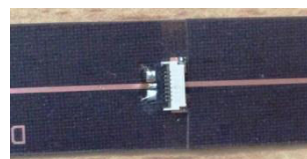
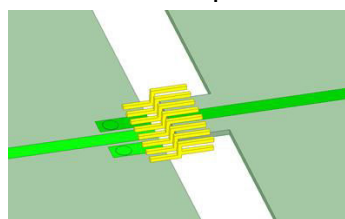
Il faut chercher une solution d'interconnexion flexible entre les antennes et la carte mère PCB avec des caractéristiques: faible coût pour favoriser une production de masse, compatibilité technologique avec les antennes élémentaires, simplicité et rapidité de mise en œuvre.

Nous avons choisi le connecteur ZIF en nappe pour cette interconnexion RF à la carte PCB:

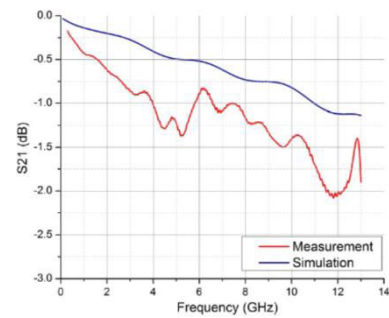
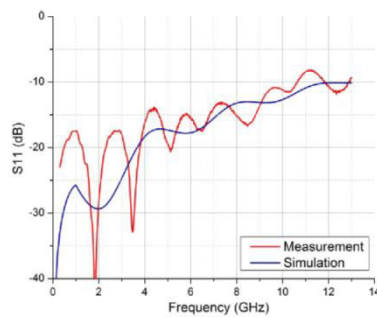
- Ce composant CMS de petite taille permet d'économiser l'espace sur la carte électronique
- Il procure une connexion électrique et mécanique fiable avec une insertion facile des lignes "flex"
- Compatibilité avec des circuits imprimés souples standard d'épaisseur de 200 - 300 μm
- Solution de connexion avec contacts mono ou double faces
- Utilisation actuelle standard: transmission de signaux numériques en mode différentiel jusqu'à des débits de 10 Gb/s.



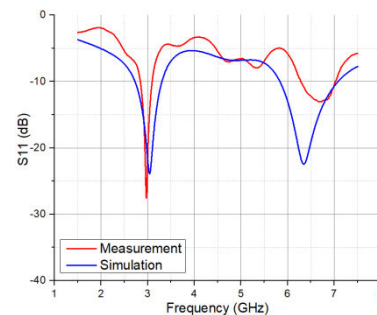
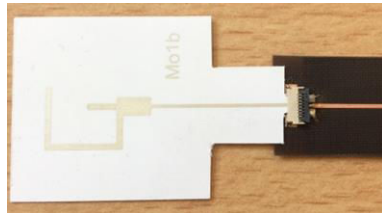
Afin de vérifier la compatibilité de ces connecteurs pour les opérations à radiofréquence, l'interconnexion entre deux lignes de transmission microruban de 50 Ω a été testé via un connecteur ZIF. Un test préliminaire a été réalisé sur le substrat Teflon™ (épaisseur 250 μm , $\epsilon_r = 2.2$, $\tan\delta = 0.0003$). Le connecteur ZIF est soudé sur la surface d'une ligne; la ligne restante peut être insérée dans l'ouverture de ce connecteur pour former une interconnexion.



On voit bien une excellente adaptation pour des fréquences < 3 GHz, puis dégradation progressive avec la fréquence (-10 dB en bande X). Les pertes d'insertion estimées sont relativement petites et acceptables, au moins jusqu'à 6 GHz: 0.43 dB/connecteur à 2.4 GHz et 0.73 dB/connecteur à 5.5 GHz. Il permet d'éliminer aussi des opérations de soudure sur le côté de ligne "flex" en comparaison avec une solution micro câble coaxial.



Pour préparer le démonstrateur final, nous avons testé la transition d'une antenne imprimée sur un substrat papier à une ligne d'alimentation sur la carte PCB. L'antenne, sérigraphiée sur le papier E4D-200, est insérée dans un connecteur ZIF, soudé préalablement sur le substrat TeflonTM pour connecter avec la ligne de transmission micro-ruban 50Ω.



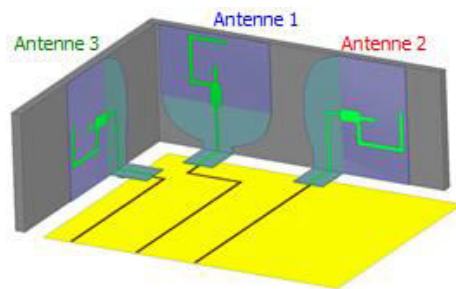
Une bonne concordance est obtenue entre la mesure et la simulation de pertes en réflexion S_{11} .

Intégration de systèmes antennaires au sein de boîtiers électroniques

Pour répondre aux multiples attentes en terme de capacités de communication des boîtiers électroniques (multistandards, contraintes de couvertures), on a besoin de développer des systèmes antennaires:

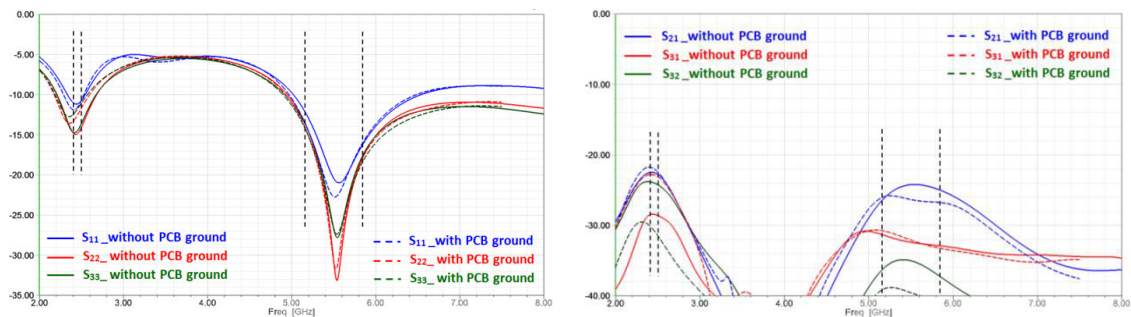
- comportant un grand nombre d'éléments rayonnants, distribués au sein du boîtier (choix des antennes avec positions, orientations)
- réalisés dans une technologie permettant:
 - la mise en forme des éléments rayonnants
 - leur report/montage aisé au sein de la structure globale
 - leur alimentation et leur interconnexion RF avec la carte mère PCB
- prenant en compte de l'effet perturbateur de l'environnement (boîtier diélectrique, carte mère PCB, batterie, ...)

Nous avons construit une première configuration de système combinant 3 monopôles bi-bandes:



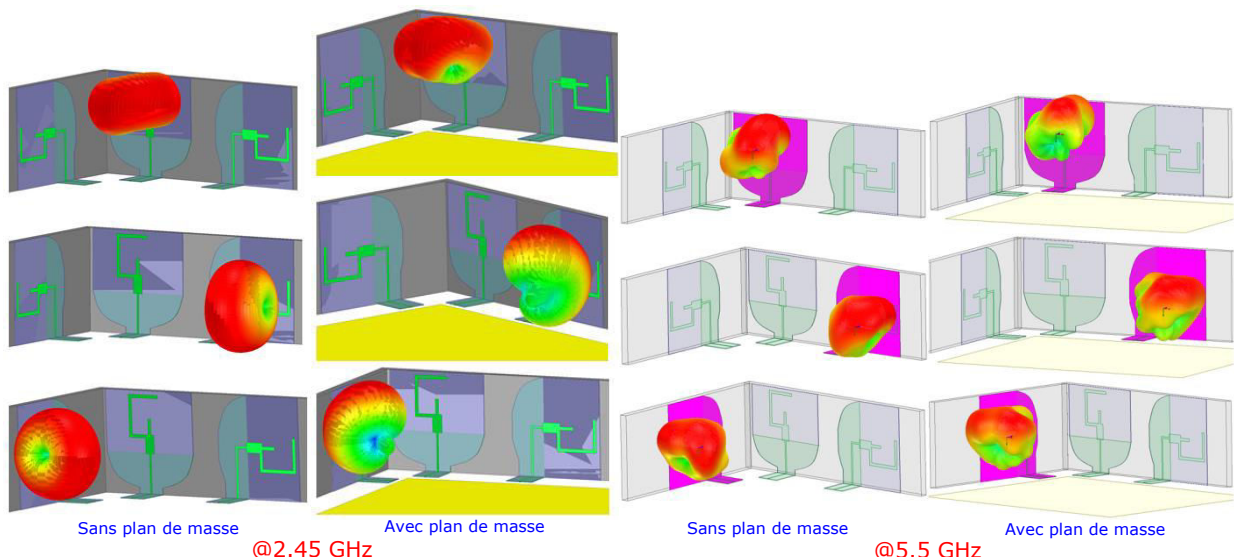
Pour une diversité de polarisation, des antennes sont orientées de sorte que les 3 plans H (ou 3 plans E) soient orthogonaux les uns aux autres. Ces antennes sont positionnées au plus proche tout en satisfaisant le critère d'isolation (> 20 dB). Et, les lignes d'alimentation sont réduites au maximum.

Résultats de simulation (adaptation et isolation) sont présentés dans les figures ci-dessous:



Les bandes passantes sont vérifiées en prenant en compte la présence du boîtier plastique. On voit bien une bonne isolation entre des antennes (couplages < -20 dB). Les pertes en réflexion S_{ii} et couplages S_{ij} sont quasi inchangés en présence du plan de masse (PCB).

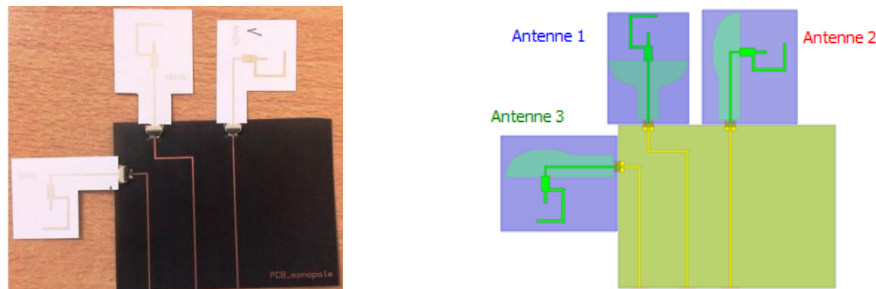
Avec la présence du plan de masse, les diagrammes de rayonnement des antennes en direction du PCB sont déformés (surtout pour les antennes latérales).



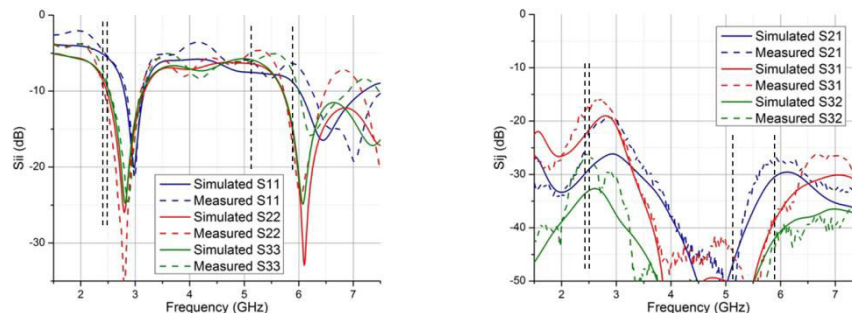
Dans le cas avec plan de masse PCB, les efficacités de rayonnement des antennes sont supérieures à 55% à 2.45 GHz et supérieures à 75% à 5.5 GHz.

Comparison	Frequency (GHz)	Realized gain (dB)	Total efficiency (%)
Antenna 1	2.45 GHz	2.11 dB	55.2%
	5.5GHz	4.89 dB	77.7%
Antenna 2	2.45 GHz	2.87 dB	60.8%
	5.5GHz	5.6 dB	81.5%
Antenna 3	2.45 GHz	2.24 dB	57.1%
	5.5GHz	5.32 dB	79.8%

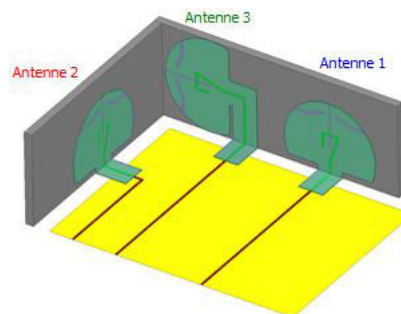
Puisque le contact entre la partie interconnexion sur papier E4D-200 et le connecteur ZIF n'est pas serré (principalement en raison de la compatibilité d'épaisseur) et le problème lié au risque de microfissure du dépôt d'encre d'argent n'est pas encore traité, nous ne pouvons pas encore plier la ligne d'interconnexion sur papier pour créer la configuration 3D finale. Par conséquent, nous devons investiguer temporairement le système d'antenne dans un état planaire, comme illustré dans la figure ci-dessous.



On trouve une bonne adéquation entre les mesures et les simulations pour toutes les antennes du système et une bonne isolation entre les antennes.

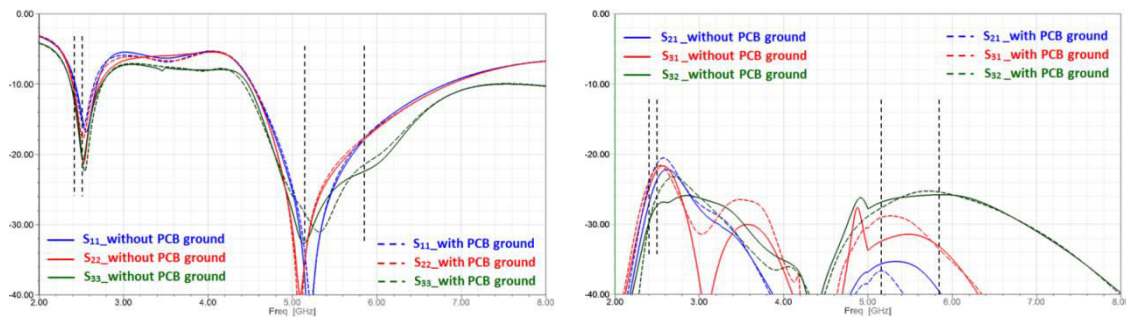


Nous avons développé aussi un système combinant 3 dipôles bi-bandes pour créer une autre configuration de diagramme de rayonnement et élargir la bande passante, notamment sur la 2nde fréquence:

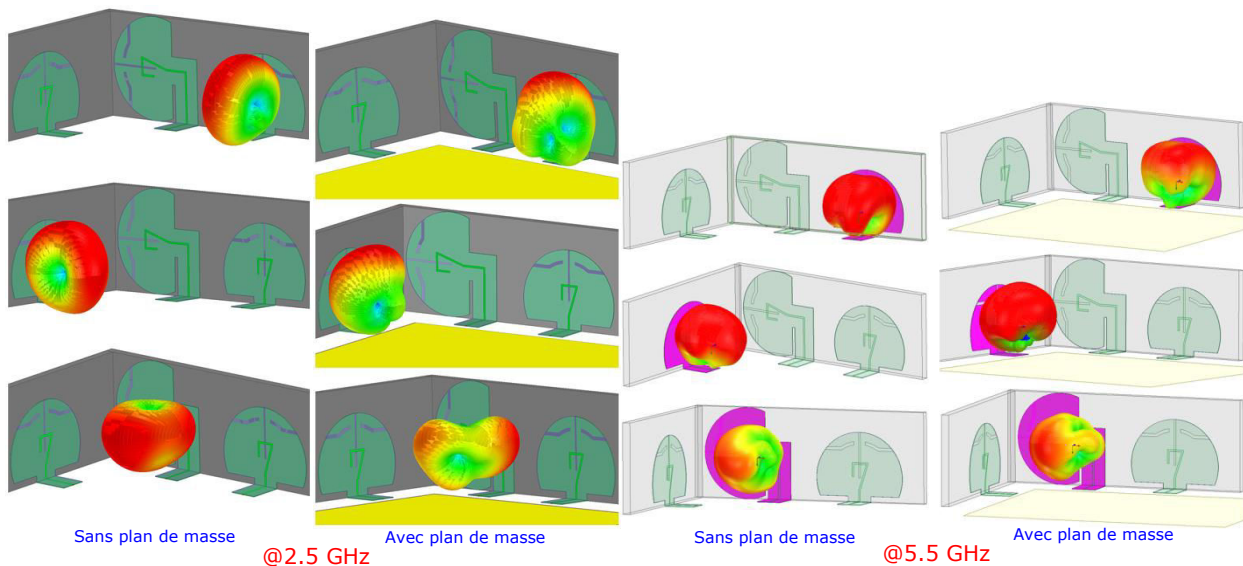


Les antennes sont toujours orientées de sorte que les 3 plans H (ou 3 plans E) soient orthogonaux les uns aux autres. Et elles sont positionnées au plus proche tout en satisfaisant le critère d'isolation (> 20 dB).

Comme dans la configuration précédente avec 3 antennes monopôles, les pertes en réflexion S_{ii} et les couplages S_{ij} sont pratiquement inchangés.



En présence du plan de masse, à 2.5 GHz, les diagrammes de rayonnement de toutes les antennes en direction du PCB sont fortement déformés ; tandis que à 5.5 GHz, les diagrammes de rayonnement des antennes sont peu modifiés car ils sont déjà directifs vers l'extérieur du boîtier.



Dans le cas avec plan de masse PCB, les efficacités de rayonnement des antennes sont supérieures à 50% à 2.45 GHz et supérieures à 90% à 5.5 GHz.

Comparison	Frequency (GHz)	Realized gain (dB)	Total efficiency (%)
Antenna 1	2.45 GHz	2.52 dB	48.2%
	5.5GHz	5.58 dB	92.4%
Antenna 2	2.45 GHz	1.11 dB	55.7%
	5.5GHz	5.28 dB	92.2%
Antenna 3	2.45 GHz	1.68 dB	65.1%
	5.5GHz	5.01 dB	97.5%

Conclusions et Perspectives

En résumé, nous avons utilisé le matériau papier comme un substrat d'antennes RF imprimées, répondant à des critères faible coût et respect de l'environnement. Nous avons caractérisé précisément des propriétés diélectriques du substrat papier flexible sur une large bande de fréquences, ainsi que de la métallisation sérigraphie associée. Puis, nous avons validé la technologie "papier sérigraphié" par la réalisation de prototypes d'antennes élémentaires. Ensuite, nous avons développé une solution d'interconnexion directe, faible coût, avec la carte PCB sans utiliser de câble coaxial. Enfin, nous avons conçu des systèmes antennaires déportés sur les faces internes en plastique du set-top-box et connectés avec la carte PCB comme une première illustration du démonstrateur final.

En conclusion, la technologie papier sérigraphié argent est opérationnelle en RF, avec toutefois quelques limitations (notamment pertes matériau élevées). C'est pourquoi, aujourd'hui, cette solution est juste pertinente pour des applications à niveau de performance non critiques comme capteur sans fil ou tags RFID ...

Pour compléter le démonstrateur final souhaité, il reste encore beaucoup de problèmes à étudier ultérieurement.

Au niveau technologie papier imprimé:

- Optimiser le montage/collage sur supports diélectriques (transparence du film adhésif, fiabilité, reproductibilité, ...).
- Optimiser le pliage/courbure de motifs conducteurs (sans dégradation de la qualité des motifs (absence de microfissures), ...).
- Étendre les possibilités de cette technologie papier imprimé (vias métallisés, substrats multicouches (scellement papier/papier), ...).
- Compléter l'évaluation entre les technologies: papier imprimé (Ag) – polymère flexible gravé.

Au niveau dispositifs RF imprimés sur papier:

- Diminuer des pertes en ligne, notamment dans les éléments d'alimentation (privilégier les solutions où le papier est "transparent" (ligne coplanaire, rubans coplanaires)).
- Optimiser l'interconnexion papier imprimé/connecteur ZIF CMS (sur les plans technologique et électrique).

Au niveau systèmes antennaires:

- Finaliser la conception du démonstrateur multi-antennes (constitution et configuration du système) et la caractérisation des performances associées.
- Simplifier l'interconnexion système antenne/carte mère PCB: connecteur multi-ports unique (simplification de montage, réduction de coût, ...).

Table of Contents

Introduction	1
Chapter 1: Context and state of the art	4
1.1 Introduction.....	5
1.2 Context and Objective	5
1.2.1 Context	5
1.2.2 Objective	9
1.3 State of the art of flexible electronics	10
1.3.1 Technology	10
1.3.1.1 <i>Flexible substrate</i>	11
1.3.1.2 <i>Metallization process on flexible substrate</i>	15
1.3.1.3 <i>Treatment process on paper</i>	23
1.3.2 Applications	26
1.3.2.1 <i>RFID tag</i>	26
1.3.2.2 <i>Wireless Local Area Network (WLAN)</i>	31
1.3.2.3 <i>Ultra-wide-band or multi-frequency antenna</i>	34
1.3.2.4 <i>3D antenna</i>	39
1.3.2.5 <i>Wireless sensor nodes</i>	42
1.3.2.6 <i>Radar system</i>	47
1.4 Conclusion about the state of the art and positioning of this thesis	49
Chapter 2: Characterization of flexible substrate and conductive layer	51
2.1 Introduction.....	52
2.2 Dielectric characterization of flexible substrate	52
2.2.1 State of the art.....	52
2.2.1.1 <i>Two planar transmission lines</i>	52
2.2.1.2 <i>Microstrip ring resonator</i>	54
2.2.1.3 <i>T-resonator</i>	57
2.2.1.4 <i>Cavity resonator</i>	60
2.2.2 Realized method	65
2.2.2.1 <i>First tests</i>	65
2.2.2.2 <i>Dielectric characterization</i>	69
2.2.3 Discussion	73
2.2.4 E4D paper.....	75
2.3 Characterization of conductive layer.....	76
2.3.1 SEM image of ink deposit surface.....	77
2.3.2 Printing process on paper	79
2.3.2.1 <i>Flexography printing</i>	80
2.3.2.2 <i>Screen-printing</i>	83
2.3.3 Measurement of thickness and conductivity of ink deposit	86
2.4 Conclusion of chapter 2	88
Chapter 3: Antenna realization on flexible substrate	90

3.1	Introduction.....	91
3.2	Patch antenna.....	91
3.3	Planar monopole antenna	94
3.4	Dual-band Wi-Fi monopole antenna (2.4 GHz/5.5 GHz)	97
3.5	Planar dual-band dipole antenna (2.4 GHz/5.5 GHz)	104
3.6	Conclusion of chapter 3	112
Chapter 4: Antenna system integrated within the set-top-box environment.....		114
4.1	Introduction.....	115
4.2	RF interconnection to PCB mainboard.....	115
4.2.1	Miniature coaxial cables – Available solutions and limitations.....	115
4.2.2	Identification of interconnection solutions compatible with paper & flex technologies - State of the art	117
4.2.2.1	<i>Classical interconnection using conductive glue and assembling techniques</i>	118
4.2.2.2	<i>Interconnect through direct or pseudo-direct compression techniques</i>	119
4.2.2.3	<i>ZIF (zero insertion force) connector for RF applications</i>	123
4.2.3	Investigations: characterization of flexible interconnections using advanced ZIF connectors	126
4.2.3.1	<i>Interconnection between 2 transmission lines</i>	127
4.2.3.2	<i>Interconnection from antenna to PCB mainboard</i>	133
4.2.4	Conclusion	136
4.3	Antenna system on flexible substrate	137
4.3.1	Three dual-band Wi-Fi monopole antenna	138
4.3.2	Three dual-band Wi-Fi dipole antenna	143
4.4	Conclusion of chapter 4	147
General conclusions and perspectives		149
ANNEX A: Measurement of conductivity of ink deposit.....		152
ANNEX B: Dielectric properties of ABS plastic.....		155
REFERENCES		157
PUBLICATIONS		163

List of tables

Table 1-1: Summary of the basic characteristics of some flexible substrates	14
Table 1-2: Electrical characterization of Cu (electroless deposition) and Ag (inkjet printing followed by sintering at 120°C) test strips	19
Table 1-3: Summary of the metallization processes on flexible substrates	23
Table 1-4: Summary for the via-hole realization on paper substrate	26
Table 1-5: Bandwidth of flat and curved antenna for $S_{11} < -10$ dB	37
Table 2-1: Sample dimensions and unloaded resonance frequency of each cavity at XLIM Limoges	62
Table 2-2: Summary of some basic dielectric characterization methods for paper substrates	65
Table 2-3: Estimation of the connector losses through two different transmission lines.....	66
Table 2-4: Dielectric properties results of characterized paper substrates at 2 GHz	69
Table 2-5: Dielectric properties results of E4D_240 μ m paper substrate in function of frequency	72
Table 2-6: Dielectric properties results of PET substrate in function of frequency	72
Table 2-7: Dielectric property results of some paper substrates realized by XLIM Limoges using cavity resonator method	73
Table 2-8: Dielectric property results of some paper substrates realized by INP Grenoble using cavity resonator method	75
Table 2-9: Dielectric properties of E4D type papers at 5 GHz	76
Table 3-1: Performance comparison of this patch antenna in various test cases	94
Table 3-2: State of the art of the planar dual-band monopole for Wi-Fi application	99
Table 3-3: Simulation and measurement results of the proposed monopole	103
Table 3-4: Performance comparison with the other planar multi-band monopole	104
Table 4-1: Comparison of some ZIF connectors available in the commercial market.....	127
Table 4-2: Simulation results of the 3 monopole antennas stuck on the plastic sidewall of set-top-box in the case with PCB ground plane.....	142
Table 4-3: Simulation results of the 3 dipole antennas stuck on the plastic sidewall of set-top-box in the case with PCB ground plane	146

List of figures

Figure 1-1: Wireless systems potentially embedded in home-networking device	5
Figure 1-2: Illustration of Set-Top Box architecture with myriad of RF antennas	6
Figure 1-3: Future trend of home-networking device.....	6
Figure 1-4: Current out-of-board solutions for the antenna integration.....	6
Figure 1-5: Out-of-board antenna system integrated into an electronic device using the bulky feeding coaxial cables.....	7
Figure 1-6: Illustration of an innovative solution for direct interconnection between out-of-board antenna systems and PCB mainboard without using coaxial cables	8
Figure 1-7: Form factor in near future of home-networking devices	8
Figure 1-8: View of a Set-Top-Box with stuck peripheral antennas.....	9

Figure 1-9: Structure of paper material with a description of cellulose fibers	12
Figure 1-10: Side view of the metallized paper substrate, consisting of a stack of paper layer and aluminum foils, attached by epoxy glue	15
Figure 1-11: Process steps for the circuit fabrication using Cu tape: (a) the photo-resist is deposited on the conductive tape and patterned using UV; (b) the conductive layer is wet-etched; (c)–(e) the etched conductor is transferred on the paper substrate by means of a sacrificial layer. M: metal, A: adhesive, P: protection, R: photo-resist, S: sacrificial layer, SUB: hosting substrate	16
Figure 1-12: Cross-section of an elementary microstrip line exploiting the Cu tape. The thin adhesive layers remain interposed between metal and substrate	16
Figure 1-13: Schematic of film metallizing system (metaliser)	17
Figure 1-14: Aluminum dry process on paper substrate based on laser patterning	18
Figure 1-15: Dimatix Materials Inkjet Printer DMP-2800 Series [L] and Roll-to-roll inkjet printing process used in an industrial environment [R]	19
Figure 1-16: SEM images of a layer of inkjet-printed nanoparticle silver ink, before and after sintering at 180°C for 10 minutes [Konstas 2009]	20
Figure 1-17: Flexographic process description	21
Figure 1-18: "Halo" phenomenon on the edges	21
Figure 1-19: Surface pretreatment process with the corresponding substrate surface views	24
Figure 1-20: Different steps of the fabrication process of SIW components on paper substrate: (a) Inkjet print the pattern; (b) Stack the multi-layer substrate after sintering; (c) Drill via holes; (d) Insert copper rivets; (e) Encapsulate	25
Figure 1-21: Metallized via holes process on paper	26
Figure 1-22: T-match folded bow-tie RFID tag module configuration [L] and its return loss, which covers the universal UHF RFID band [R]	27
Figure 1-23: Bow-tie dipole antenna magnetically coupled to RFID chip	28
Figure 1-24: Layout [L] and paper-based prototype [R] of the frequency doubling tag	28
Figure 1-25: Dual-radiating-body RFID antenna inkjet-printed on paper	28
Figure 1-26: Screen-printed prototype of RFID bow-tie antennas on paper substrate	29
Figure 1-27: Prototypes of RFID tag bowtie antennas on different flexible substrates using different printing processes	29
Figure 1-28: Inkjet-printed RFID quadrate bowtie antenna on HP and Kodak photopaper .	30
Figure 1-29: (a) Chipless RFID tag based on multiple 3-gap loop resonators; (b) Tag prototype printed on glossy paper by flexography	30
Figure 1-30: HF RFID antenna roll produced industrially with a metallizer [L]; HF tag prototype fabricated on paper substrate (85.6×53.98 mm ² with 1µm aluminum thickness) [R]	31
Figure 1-31: Prototype of the Z-shaped CPW-fed inkjet-printed monopole antenna on paper substrate with attached SMA connector [L]. The simulated and measured return loss of the inkjet-printed and copper-tape fabricated monopole [R]	32
Figure 1-32: Fabricated PIFA antenna prototype on organic paper-based substrate [L]; Simulated total efficiency comparison of the antenna on paper (82%) and the antenna on a high-frequency laminate (95%) [R]	32
Figure 1-33: Inkjet-printed antenna on paper bent around cylindrical structures with different radii. It showed no sign of permanent deformation, conductivity deterioration (i.e. cracks) or ink detachment after extensive and repeated bending	33

Figure 1-34: 2.4 GHz meander monopole on Teslin® paper fabricated by Ag inkjet printing [L] and electroless Cu deposition [R]	33
Figure 1-35: Simulated and measured insertion losses (S_{11} , dB) of the meander monopoles	33
Figure 1-36: H-plane and E-plane radiation pattern obtained from simulation and measurement of the Cu and Ag monopole antennas.....	34
Figure 1-37: Model of the UWB monopole [L] and Simulated and measured S_{11} performance of the inkjet-printed antenna prototype [R]	34
Figure 1-38: Antipodal Vivaldi design [L] and prototype fabrication on paper [R]	35
Figure 1-39: Measurement of the antipodal Vivaldi antenna with: (a) S_{11} ; (b) gain versus frequency	35
Figure 1-40: Layout [L] and inkjet-printed prototype [R] of U-slot tri-band monopole antenna	36
Figure 1-41: Simulated and measured S_{11} and realized gain of the proposed antenna	36
Figure 1-42: Layout of proposed wide frequency independently controlled monopole	37
Figure 1-43: Fabrication process for the curved prototype: flat monopole was mounted on a cylindrical surface and was sintered	37
Figure 1-44: Simulated and measured co-polarization in X-Z and X-Y directions at (a) 1.9 GHz, (b) 2.4 GHz and (c) 5 GHz for flat and curved antenna	38
Figure 1-45: Measured S_{11} [L] and peak gain [R] for flat and curved monopole	38
Figure 1-46: Model [L] and realized prototype [R] of cubic RFID antenna	39
Figure 1-47: 3D RFID antenna using meander line configuration	40
Figure 1-48: S_{11} vs. frequency for this 3D RFID antenna	40
Figure 1-49: Simulated model [L] and manufactured prototype [R] of the 18-steps origami helical antenna.....	40
Figure 1-50: Simulated S_{11} [L] and realized gain at the axial direction [R] of folded and unfolded states	41
Figure 1-51: Designed origami accordion antenna [L] and its simulation model [R].....	41
Figure 1-52: Simulated return loss [L] and realized gain [R] for different heights of accordion	41
Figure 1-53: Origami spring antenna	41
Figure 1-54: Simulated return loss [L] and realized gain [R] for unfolded and folded states	42
Figure 1-55: (a) System level diagram of the wireless sensor module; (b) RFID-enabled dipole-based wireless sensor transmitter using inkjet-printing on paper	43
Figure 1-56: Monopole-based wireless sensor module (two layers)	44
Figure 1-57: Assembled prototype showing the key components of the RFID tag packaged on a flexible paper substrate	45
Figure 1-58: Self-powered RFID shoe with mounted electronics	45
Figure 1-59: 3D RFID tag cube for wireless sensing [L] and fully fabricated prototype [R]	45
Figure 1-60: Proposed 3D sensor model inkjet-printed on paper.....	46
Figure 1-61: Inkjet-printed sensor platform for SenSprout agriculture application: (a) block diagram, (b) proposed design	47
Figure 1-62: Block diagram [L] and prototype fabricated by copper adhesive on paper [R] of the 24GHz CW radar front-end	48
Figure 1-63: Return loss [L] and simulated radiation pattern [R] of the fabricated patch array antenna	48

Figure 1-64: Concept of printed rollable GPR radar system	49
Figure 1-65: Illustration of antenna systems having direct interconnections with the PCB mainboard	50
Figure 2-1: Implemented copper-tape microstrip lines on cardboard	54
Figure 2-2: Measured properties of cardboard: (a) Relative permittivity, (b) Loss tangent	54
Figure 2-3: Microstrip ring resonator configuration diagram [Yang 2007-1].....	56
Figure 2-4: Measured and simulated S_{21} of the ring resonator configuration A. Peak positions and -3dB bandwidth at the three resonant frequencies were used to extract the relative permittivity and the loss tangent of the paper substrate	56
Figure 2-5: (a) Extracted relative permittivity of paper at the resonant frequencies; (b) Paper loss tangent versus frequency measured with the microstrip ring resonator method and TL method.....	57
Figure 2-6: Fabricated T-Resonators and TRL calibration lines [Cook 2012-1]	59
Figure 2-7: Measured S_{21} of the 1 GHz T-Resonator.....	59
Figure 2-8: (a) Extracted permittivity using 1–12.5 GHz T-Resonators and (b) extracted loss tangent data from the fabricated T-Resonator	60
Figure 2-9: (a) Split-cylinder cavity in unloaded and loaded status; (b) Simulated field distributions at TE_{011} mode	60
Figure 2-10: Measured modes shifting of the unloaded/loaded split-cylinder cavity	61
Figure 2-11: Loaded and empty cavities used by XLIM for characterization	61
Figure 2-12: Required points for thickness measurements in order to obtain an average thickness of the sample.....	62
Figure 2-13: Open cavity.....	63
Figure 2-14: Measurement bench with the insertion of a test sample into the cavity	63
Figure 2-15: (a) Prototypes and (b) measured S_{21} parameter of the two transmission lines (20 mm and 50 mm of length) fabricated using copper etched on Teflon substrate.	66
Figure 2-16: Model of transmission line fabricated by using an adhesive copper tape	67
Figure 2-17: Measured and simulated S_{ij} -parameters of a 2 mm width transmission line fabricated on Teflon glass by using an adhesive copper tape.	67
Figure 2-18: Measured and simulated S_{ij} -parameters of a 2 mm width transmission line fabricated on Teslin paper by using an adhesive copper tape	68
Figure 2-19: Measured S_{11} of a microstrip transmission line (2 mm width, 50 mm length, and 7.6 μ m ink thickness) screen-printed using silver ink on E4D-240 μ m paper.....	70
Figure 2-20: Measured and simulated S_{ij} -parameters of a 2 mm width transmission line screen-printed on E4D paper by using silver ink: $\epsilon_r = 2.54$ & $\tan\delta = 0.05$	72
Figure 2-21: Measured and simulated S_{ij} -parameters of a 2 mm width transmission line fabricated on PET film by using aluminum etched: $\epsilon_r = 2.85$ & $\tan\delta = 0.009$	72
Figure 2-22: Comparison between the characterized dielectric properties of some paper substrates realized by XLIM and IMT: (a) Magazine cover, (b) Silver Image Laser paper, (c) Kodak photo paper	74
Figure 2-23: Comparison of the insertion losses between different 50 Ω lines on E4D paper substrates	76
Figure 2-24: Perspective view of a screen-printed pattern on paper substrate using silver ink	77
Figure 2-25: SEM image of the silver ink deposit surface at 500 μ m scale.....	78
Figure 2-26: SEM image of the silver ink deposit surface at 20 μ m [L] and 10 μ m [R] scale	78
Figure 2-27: SEM image of the aluminum etched deposit surface at 500 μ m [L] and 50 μ m [R] scale	79

Figure 2-28: SEM image of the aluminum etched deposit surface at 20 μ m [L] and 10 μ m [R] scale	79
Figure 2-29: Schematic of: (a) Flexography printing and (b) Screen-printing	80
Figure 2-30: Microscope image of a flexography printed pattern on E4D paper	80
Figure 2-31: Thickness measurement of the flexography printed deposit on E4D paper	81
Figure 2-32: Measured S_{ij} -parameters of two samples of 2 mm width transmission line flexography-printed on E4D paper	81
Figure 2-33: Measured S_{11} of two samples of patch antenna flexography-printed on E4D paper	82
Figure 2-34: Determination of dielectric properties of E4D-290 μ m paper through a 2 mm width transmission line flexography printed: $\epsilon_r = 2.75$ & $\tan\delta = 0.05$ at 5 GHz	82
Figure 2-35: Measured and simulated S_{11} of a patch antenna flexography-printed on E4D paper	83
Figure 2-36: Microscope image of a screen-printed pattern on E4D paper	83
Figure 2-37: Thickness measurement of the screen-printed deposit on E4D paper	84
Figure 2-38: Performance comparison of three identical 2mmx5cm transmission lines fabricated using various metallization technologies like adhesive copper tape, screen printing and flexography printing on the same E4D paper substrate	84
Figure 2-39: Measured S_{ij} -parameters of two samples of 2 mm width transmission line screen-printed on E4D paper	85
Figure 2-40: Measured S_{11} of three samples of patch antenna screen-printed on E4D paper	85
Figure 2-41: Determination of dielectric properties of E4D-240 μ m paper through a 2 mm width transmission line screen-printed: $\epsilon_r = 2.54$ & $\tan\delta = 0.05$ at 5GHz	85
Figure 2-42: Measured and simulated S_{11} of a patch antenna screen-printed on E4D paper	85
Figure 2-43: Measurement of the deposit thickness with a Veeco mechanical profilometer at UBO	86
Figure 2-44: Measurement of the paper roughness at two different positions on E4D paper	86
Figure 2-45: Measurement of the ink deposit roughness at two different positions on screen-printed line	87
Figure 2-46: Measurement of the ink deposit thickness at two different cross-sections on the 2mmx4cm screen-printed line	87
Figure 2-47: Thickness measurement of the aluminum etched deposit on PET	88
Figure 3-1: Design and prototype of the patch antenna, screen-printed on E4D-240 μ m paper	91
Figure 3-2: Measured and simulated return loss of a patch antenna screen-printed using silver ink on E4D paper	91
Figure 3-3: Return loss S_{11} of this patch antenna	92
Figure 3-4: Setup of the antenna measurement in the MVG Stargate [®] system (SG-24)	92
Figure 3-5: Radiation pattern in E-plane and H-plane at 5.2 GHz of the patch antenna screen-printed on E4D-240 μ m paper	93
Figure 3-6: Return loss S_{11} of this patch antenna in various test cases	93
Figure 3-7: Layout and prototype of the 5GHz monopole antenna, screen-printed on E4D-100 μ m paper	95
Figure 3-8: Return loss S_{11} of the classic monopole antenna screen-printed on E4D-100 μ m paper	95

Figure 3-9: Radiation pattern in E-plane and H-plane at 5 GHz of this classic monopole antenna	96
Figure 3-10: Layout and prototype of the dual-band Wi-Fi monopole antenna, screen-printed on E4D-100 μ m paper	99
Figure 3-11: Simulated current distribution at: (a) 2.4 GHz and (b) 5.5 GHz.....	100
Figure 3-12: Effects of changing L1, length of the hook-shaped branch #1, on the 2.4 GHz frequency band	100
Figure 3-13: Effects of changing L2, length of the straight branch #2, on the 5.5 GHz frequency band	101
Figure 3-14: Return loss S_{11} of this dual-band Wi-Fi monopole antenna.....	101
Figure 3-15: E-Plane and H-Plane radiation patterns obtained from simulation and from measurement of dual-band Wi-Fi monopole antenna at: (a) 2.4 GHz and (b) 5.5 GHz	102
Figure 3-16: Simulated and measured realized gain of the antenna versus frequency	103
Figure 3-17: Geometry of printed dipole antennas with integrated microstrip balun: (a) open-stub structure, (b) via-hole structure.	105
Figure 3-18: Dual fin antenna (patent at IMT Atlantique).....	105
Figure 3-19: Layout and prototype of the ultra-wideband dipole antenna, fabricated with adhesive copper tape on Teslin-250 μ m paper	106
Figure 3-20: Return loss S_{11} of this ultra-wideband dipole antenna	106
Figure 3-21: Radiation pattern in E-plane and H-plane at 5 GHz of this ultra-wideband dipole antenna	107
Figure 3-22: Layout and prototype of the modified ultra-wideband dipole antenna, screen-printed on E4D-200 μ m paper	107
Figure 3-23: Return loss S_{11} of this modified ultra-wideband dipole antenna	108
Figure 3-24: Radiation pattern in E-plane and H-plane at 5.7 GHz of this modified ultra-wideband dipole antenna	108
Figure 3-25: Design process of the dual-band dipole antenna	109
Figure 3-26: Layout and prototype of the proposed dual-band Wi-Fi dipole antenna, screen-printed on E4D-200 μ m paper	110
Figure 3-27: Return loss S_{11} of the proposed dual-band Wi-Fi dipole antenna.....	110
Figure 3-28: Simulated current distribution at: (a) 2.5 GHz and (b) 5.5 GHz.....	111
Figure 3-29: Radiation pattern of this dual-band Wi-Fi dipole antenna: (a) at 2.5 GHz; (b) at 5.5 GHz.....	112
Figure 4-1: Micro-coaxial cables and interconnection – Solutions from industrial markets: (a) Miniature Surface Mounted Connector for Mobile RF devices interconnect; (b) Coaxial connector for wireless laptop connectivity; (c) PCB connector for automotive applications	116
Figure 4-2: RF micro connectors from Hirose: Ultra miniature Surface mounted Connectors (50 ohms, high electrical performance up to 6GHz).....	116
Figure 4-3: Different solutions of plug-in coaxial connectors (Rosenberger™): (a) Miniature Plug in connectors; (b) Elastic board to board connectors	117
Figure 4-4: View of a coaxial interconnection directly soldered to the PCB (courtesy of Technicolor Connected Home Company)	117
Figure 4-5: Interconnects for commercial electronic devices: a myriad of technical solutions (https://www.hirose.com/product/en/products/industry/mobile/smartphones/)	118
Figure 4-6: Isometric view of a microstrip flexible interconnect circuit.....	119
Figure 4-7: Illustration of the interconnection technique between the flexible microstrip line and the strip transmission line on the circuit board.	119

Figure 4-8: Exploded view of a portion of an interconnection system comprising an RF flex circuit, an elastomeric interconnect and a printed circuit board.....	120
Figure 4-9: Side view of this interconnection system.....	121
Figure 4-10: SuperButton® industrial solution for elastomeric compression interconnect..	122
Figure 4-11: Application of SuperButton® in interconnection for Flexible Circuit Board (FPC)	122
Figure 4-12: TI DLP® Technology Interposer Family from Neocomix™ (www.neoconix.com)	123
Figure 4-13: Different solutions for Flexible Circuit Board (FPC) to Board interconnections	123
Figure 4-14: SlimStack™ Board-to-Board Connectors.....	124
Figure 4-15: FFC/FPC connections with clipping - illustration	124
Figure 4-16: Perspective view of a SMC type ZIF connector	125
Figure 4-17: Modeling of the interconnection between FPC and PCB card through the ZIF connector [FH34-SRJ]	125
Figure 4-18: Simulation results of FH34SRJ connector for eDP 1.3 standard.....	126
Figure 4-19: Illustrated model of FH34 family's connector	128
Figure 4-20: Connector dimensions of FH34 family (FH34SJ: contacts only on the top of the flex line. FH34SRJ: contacts on the both sides of the flex line)	129
Figure 4-21: Design for the interconnection in the case of using connector with contacts on top side of the flex line.....	129
Figure 4-22: Simulation model (a) and prototype (b) of the interconnection using connector with contacts on top side of the flex line	130
Figure 4-23: S_{ij} parameters of the transmission line through ZIF connector having contacts on top side of the flex line	131
Figure 4-24: Description of the top-bottom contacts	131
Figure 4-25: Design for the interconnection in the case of using connector with contacts on both sides of the flex line	131
Figure 4-26: Simulation model (a) and prototype (b) of the interconnection using connector with contacts on both sides (top and bottom) of the flex line	132
Figure 4-27: S_{ij} parameters of the transmission line through ZIF connector having contacts on both sides (top and bottom) of the flex line	133
Figure 4-28: Prototype (without ABS (a) and with ABS (b)) and HFSS simulation model (c) of the interconnection from feed line on PCB to monopole antenna screen-printed on paper	134
Figure 4-29: Return loss of the monopole antenna screen-printed on paper with taking into account the interconnection with the feed line on PCB.....	135
Figure 4-30: Prototype (without ABS (a) and with ABS (b)) and HFSS simulation model (c) of the interconnection from feed line on PCB to dipole antenna screen-printed on paper..	136
Figure 4-31: Return loss of the dipole antenna screen-printed on paper taking into account the interconnection with the feed line on PCB.....	136
Figure 4-32: Transition from microstrip line to CPW line in the interconnection.....	137
Figure 4-33: Model of the antenna system stuck on the plastic sidewall of set-top-box: (a) 3 monopole antennas and (b) 3 dipole antennas	138
Figure 4-34: Simulation model of the 3 monopole antennas stuck on the plastic sidewall of set-top-box in the case without PCB ground plane	139
Figure 4-35: Coupling between the two dual-band Wi-Fi monopole antennas in function of angle α	139

Figure 4-36: Coupling between the two dual-band Wi-Fi monopole antennas Ant 1 and Ant 2 in function of the distance d_{12} between them	140
Figure 4-37: Simulated return loss and S_{ij} coupling coefficients of each antenna in the system in both cases: with and without PCB ground plane	140
Figure 4-38: Simulated 3D Radiation pattern of each monopole at 2.45 GHz in the case: (a) without PCB ground plane and (b) with PCB ground plane	141
Figure 4-39: Simulated 3D Radiation pattern of each monopole at 5.5 GHz in the case: (a) without PCB ground plane and (b) with PCB ground plane	141
Figure 4-40: Prototype [L] and simulation model [R] of the system with 3 monopole antennas in the planar state	142
Figure 4-41: Return loss and S_{ij} coupling coefficients of each antenna in the system in the planar state	143
Figure 4-42: Simulation model of the 3 dipole antennas stuck on the plastic sidewall of set-top-box in the case without PCB ground plane.....	144
Figure 4-43: Simulated return loss and S_{ij} coupling coefficients of each antenna in the system in both cases: with and without PCB ground plane	144
Figure 4-44: Simulated 3D Radiation pattern of each dipole at 2.5 GHz in the case: (a) without PCB ground plane and (b) with PCB ground plane	145
Figure 4-45: Simulated 3D Radiation pattern of each dipole at 5.5 GHz in the case: (a) without PCB ground plane and (b) with PCB ground plane	145
Figure 4-46: Prototype [L] and simulation model [R] of the system with 3 dipole antennas in the planar state.....	146
Figure 4-47: Return loss and S_{ij} coupling coefficients of each antenna in the system in the planar state	147

Introduction

Over the past few decades, communication systems have become an important part of society. The transmission of information is, therefore, a crucial issue, particularly through the electromagnetic waves. This is the reason why most current devices incorporate an antennary function to transfer data from the device to the outside and vice versa. From there, in order to meet the growing demand, people continue to improve and develop electronic devices such as reducing the cost, miniaturizing the size, increasing the flexibility, minimizing the energy consumption ...

In just a few years, flexible electronics are increasingly invading the commercial market and creating a new generation of electronics. Flexible electronics show many advantages over classical rigid electronics such as low cost, flexibility, and lightweight. Apart from the ultra-low cost of paper or polymer such as PET, the real cost saving of flexible electronics comes from the ability to operate in a roll-to-roll scheme. This allows for a continuous stream of devices to be produced without interruption, resulting in also the saving of production time. In addition, the flexibility and light weight allow it for portable and wearable applications such as flexible displays, portable devices, clothing-embedded electronics and packaging materials. The most fundamental difficulty is probably the electromagnetic compatibility of the substrate because polymer or paper is not produced for this purpose. In fact, OLEDs, organic transistors, polymer memories are already manufactured at lab and pilot stages and some of them at the industrial level. These low-cost components are produced to replace conventional ones and they are the basis of new products and markets. Flexible antennas, RF electronics and sensors fabricated on paper and polymer substrates (e.g. Liquid Crystal Polymer (LCP), Kapton®) are introduced as a system-level solution for ultra-low-cost mass production of communication, Radio Frequency Identification (RFID) Tags and Wireless Sensor Nodes (WSN) in an approach that could be easily extended to other microwave and wireless applications.

Concurrently with the powerful development of flexible electronics, the eco-system of set-top-boxes (STB) and gateways (GW) has drastically evolved with the pushing demand of new services and new connectivity, becoming the Smart-Home devices for wireless home automation service. Most of them require the integration of many wireless systems including, for instance, ZigBee/Zwave wireless home automation service, high-speed Wireless LAN (WLAN) connectivity, DECT cordless phone system, Bluetooth low-rate and short-range connectivity, radio-based RF4CE remote control, and in the near future, WWAN (Wireless Wide Area Network) connectivity using the high data rate service offered by 3G and 4G (LTE) networks. Therefore, the multi-connectivity becomes a key issue for consumer device manufacturers. Interconnections between the numerous access ports of different radio chipsets mounted on the main PCB (Printed Circuit Board) and multiple antennas spatially distributed on the plastic casing become consequently a great challenge for cost and performances motivations.

The research work about the integration of flexible electronics into wireless systems embedded in GW & STB done in this thesis will undoubtedly contribute to pave the road towards future emerging and highly competitive markets of the Smart-Home devices and wireless home automation industry. Miniaturization with increased functionality at a reduced cost will be the key driver for the evolution of electronics products.

This thesis has been realized in the framework of the ANR project entitled STICK'IT with the collaboration between four partners: two laboratories IMT Atlantique Brest (ex. Telecom Bretagne) and Grenoble Institute of Technology (INPG), Paper Technical Center (CTP) in Grenoble and the Technicolor Connected Home enterprise (TCH) in Rennes. So, STICK'IT is conducted comprising of a versatile consortium working on various sub-projects towards the common goal of the final demonstrator. In which, IMT Atlantique focuses mainly on the designs, developments and innovations concerning the antenna system on flexible materials as well as the intelligent flexible interconnections dedicated to wireless communication systems integrated into STICK'IT demonstrator. The major scientific contributions of this thesis are focused on two main topics for set-top-box application: (i) realization of a flexible, ultra-low-cost antenna system that could be stuck on the sidewalls of the set-top-box and (ii) direct, flexible and inexpensive interconnection solution to PCB mainboard. However, the ideas proposed in the dissertation could also be developed and extended to other electronics boxes for wireless communication. The thesis has been carried out in the microwave department of IMT Atlantique Brest, under the direction of Mr. Christian Person and Mr. Jean-Philippe Coupez. The use of paper as a flexible, low-cost substrate in antenna structures has been also studied for the first time in this research laboratory.

The thesis work is organized as follows with four main chapters:

First of all, chapter 1 aims to present the context and objective of the study. Then, the state of the art of flexible electronics is introduced, which allows us to have an overview of the current development level of RF components and circuits on flexible substrates, especially paper. From there, we can precisely define its positioning in the current international research by comparison with those already realized in the same theme.

Secondly, chapter 2 is devoted to the characterization process of the flexible substrate like paper along with the associated conductive layer. This step is very important to obtain the most accurate parameters of the material such as the relative permittivity, loss tangent of the substrate and the thickness, conductivity of the metallization layer before proceeding to design antenna or other RF components.

Then, chapter 3 is dedicated to the realization of elementary antennas on the flexible substrate, namely paper. They give us the first assessments on paper antennas. Then, the planar dual-band antennas have been also designed and fabricated to meet the initial objectives of this thesis work. They are the fundamental elements for building the antenna system in the following chapter.

In chapter 4, the remaining issues will be resolved in order to integrate the whole antenna system into the set-top-box environment. The direct interconnection solution from the antennas to the PCB mainboard, one of the most difficult

problems, is addressed first. Then, the antenna systems, which are printed on the flexible substrate (e.g. paper) and which can be stuck on the plastic sidewall of the set-top-box, are also modelled. They include three antennas arranged on two sidewalls of the set-top-box for a diversity of polarization as well as their direct interconnection to the PCB mainboard.

Finally, the thesis conclusions along with future perspectives will be highlighted.

Chapter 1: Context and state of the art

Principal content

1.1	Introduction.....	5
1.2	Context and Objective.....	5
1.2.1	Context	5
1.2.2	Objective	9
1.3	State of the art of flexible electronics	10
1.3.1	Technology	10
1.3.2	Applications	26
1.4	Conclusion about the state of the art and positioning of this thesis	49

1.1 Introduction

This first chapter aims to define the subject of this thesis and position it in the international context. Firstly, the context which engenders the ideas for the thesis work, as well as the main objectives, is addressed. Then, the state of the art in detail of the antennas printed on the flexible substrate is targeted. Not only the electromagnetic characteristics of the flexible substrates like paper but also the metallization processes on them are also discussed. And the actual applications of paper substrate in antennas, as well as RF modules and circuits, through the research work around the world are also presented so that we can visualize their current level of development.

1.2 Context and Objective

1.2.1 Context

According to the development of the technology, the future home networking devices, such as Set-Top Boxes (STB) and GateWays (GW), will need a plethora of antennas, whose quantity, if compared to Smartphone eco-system (an extensive network of interconnected devices, services and applications, spanning from hardware to software), can easily be twice or even three times more. In addition to this, most of the wireless systems embedded in these devices require more than one antenna to accommodate the demand for high performance and robust connectivity. The significant example regards MIMO (Multiple Input Multiple Output) systems which use two or more transmitting and receiving antennas in order to enhance the channel capacity. This is usually the case for WLAN and LTE networks. Another illustrative example concerns systems which need antenna diversity in order to ensure a high quality of service. This doubles the number of antennas to integrate into the device. Systems requiring this diversity include, for instance, RF4CE, DECT and 3G systems.

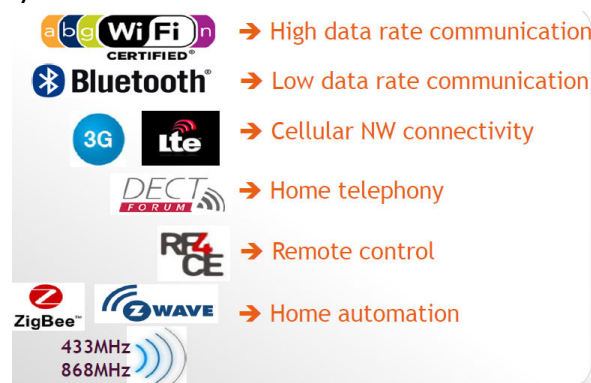


Figure 1-1: Wireless systems potentially embedded in home-networking device

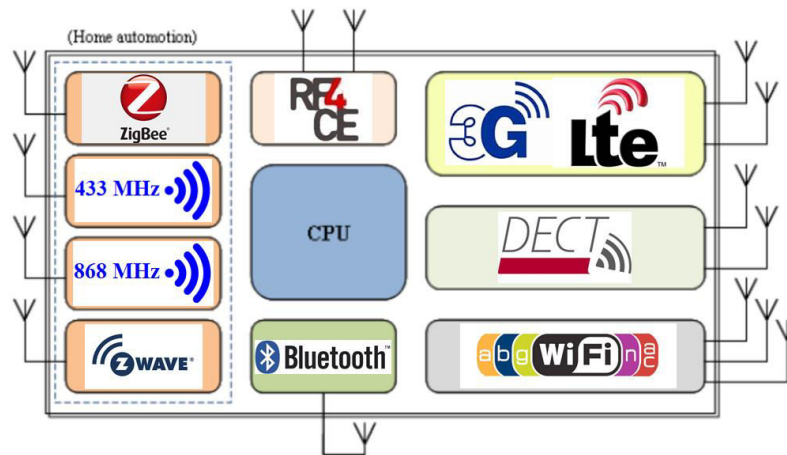


Figure 1-2: Illustration of Set-Top Box architecture with myriad of RF antennas

Furthermore, concurrently with this high-density integration trend, size of STB is decreasing continuously for cost and aesthetic purposes along with consumer demand.



Figure 1-3: Future trend of home-networking device

Therefore, the requested high number of antennas is a real problem in terms of cost and integration. Traditionally, antennas are printed directly on the main board and interconnected with the RF transceiver circuit using printed transmission lines. The high number of antennas makes this no longer possible because there are not enough places to put all the antennas on the PCB mainboard. Finally, on-board integration of the antennas is extremely constraining because of all the parasitic metal parts (e.g. hard disk drive, shielding covers, heat-sinks, Ethernet/USB/HDMI/SATA connectors, cables etc.) that can impair their performance (antenna efficiency, radiation pattern, isolation ...). All these constraints come to figure out out-of-board solutions for the antenna integration. The current out-of-board solutions usually employed are stamped metal, FR4 based PCB, flexible PC (FPC) and MID, as illustrated below.

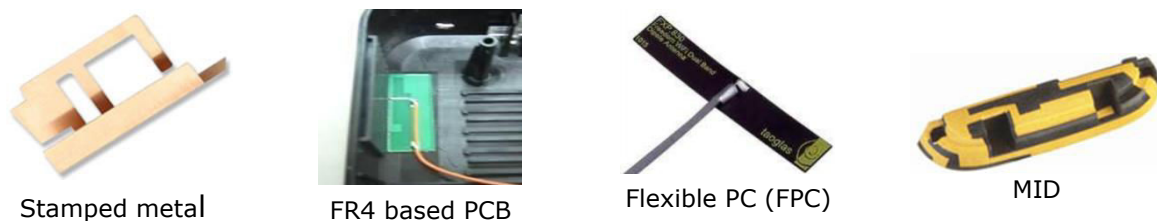


Figure 1-4: Current out-of-board solutions for the antenna integration

The less costly one is stamped metal antenna; however, this technology does not allow integrating several antennas in a single piece. Instead, traditional FR4-based PCB technology features this advantage and offers design flexibility thanks to the multilayer structure; its main drawback is the higher cost (more than 15 times higher if compared to stamped metal technology), with performance degradation due to dielectric losses. Regarding now flexible antennas (on FPC), the technology is originally widely used for the manufacturing of flexible cables, mostly realized on a very thin polyimide substrate. Using a double-sided adhesive, the antennas can be easily affixed to the side walls of the device housing. This technology, however, is ranked by STB manufacturers as very expensive, with a ratio of the price higher than 5 if compared to FR4-based antennas. The second drawback is its single-layer structure which makes it not appropriate for the design of sophisticated multiband multimode antennas. The last technology (MID) allows metalizing selectively plastic parts; it is the most costly one, therefore is only employed when the three others are not mechanically usable.

The current commonly out-of-board solution uses a bulky feeding coaxial cable system, for example, in *Figure 1-5*. It takes too much cost and time for the soldering of all connectivity parts. Therefore, we would like to replace all of the system: antennas + feeding/interconnection by another more homogeneous and collective technology, as illustrated in *Figure 1-6*.

6 antennes PCB Wi-Fi à bipolarisation + 12 câbles coaxiaux d'alimentation

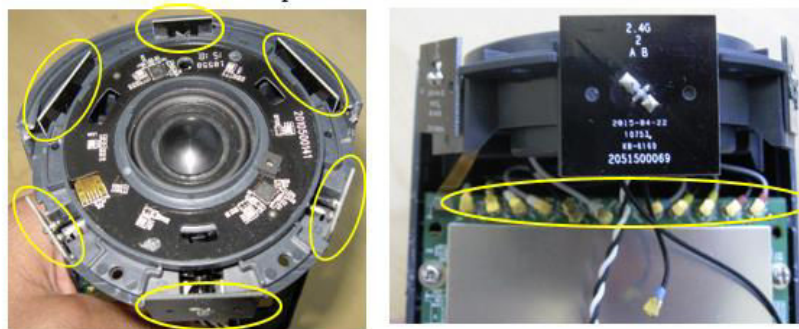


Figure 1-5: Out-of-board antenna system integrated into an electronic device using the bulky feeding coaxial cables

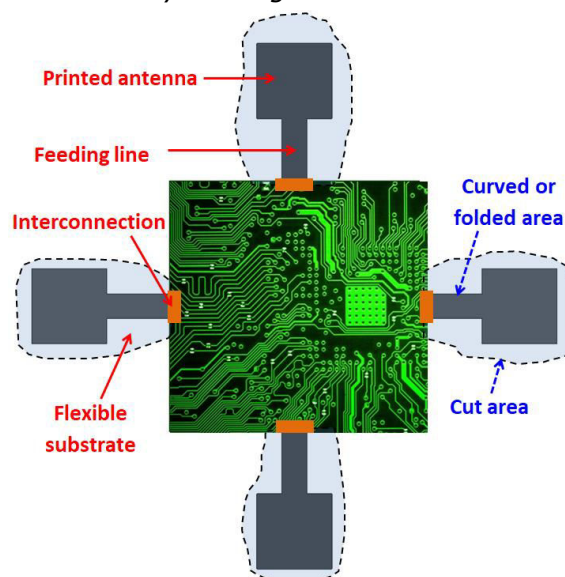


Figure 1-6: Illustration of an innovative solution for direct interconnection between out-of-board antenna systems and PCB mainboard without using coaxial cables

As can be seen, the current common technologies do not respond to the demand of an extremely low-cost solution for the integration of a high number of antennas. Furthermore, concurrently to cost, they can not meet the multilayer process for technical requirements of these antennas, such as multiband, multi-standard. This calls for figuring out another outstanding and innovative technology that we propose to investigate in this thesis. The antennas, fabricated on a low-cost substrate by printing technology, are glued on the inner sidewalls of the electronic box and connected to the PCB main-board such as the RF Stickers. In addition, the form factor of the future box is also changing (ovoid, cylindrical, 3D). So, the flexible substrate i.e. plastic, polymer, paper must be chosen to be able to glue on such non-planar surfaces. In consequence, to save cost with sustainable development, the antennas are proposed to develop on flexible, biodegradable, and low-cost substrates like paper.



Figure 1-7: Form factor in near future of home-networking devices

In the literature, RFID antennas on paper are already validated through multiple tags for applications in the detection or identification. So, we wonder whether it is possible to transpose this technology for applications in communication (with high performance)? And this is also the challenge of the ANR STICK'IT project, in which IMT Atlantique has worked in collaboration with 3 other partners: Grenoble Institute of Technology (INPG), Paper Technical Center (CTP) in Grenoble and the Technicolor Connected Home enterprise (TCH) in Rennes.

Thus, our research work has concentrated in low-cost RF printed electronics on flexible substrates by realizing RF components and systems based on conductive inks and low-cost printing processes. The scientific challenge lies on the design for the first time of RF sub-function stickers integrated into future electronic devices, affixed for instance on any sidewall of their housing. The targeted wireless multimedia applications are primary the home-networking devices such as set-top boxes. The outstanding results can be exploited for other applications for which RF components integration and cost are key parameters. Our ambition takes benefit from the compelling growth and evolution of printed and flexible electronics technologies which mostly address applications such as sensors, displays, and RFIDs. Thence, printing and associated techniques are promoted to develop new ultra-low-cost RF front-end passive components mainly including antenna, filter,

and interconnections, with specific research activities on new material engineering, RF design and characterization.

1.2.2 Objective

This thesis aims at developing "green", low-cost and innovative technology devoted to the design of 2D, 2.5D or 3D antenna and interconnection systems, printed on flexible materials (e.g. paper, polymer) and integrated into home-networking devices, in which the following main objectives are introduced.

The most important goal is realizing of an "out of PCB" conformable antenna system on a low-cost flexible substrate for wireless multimedia applications. This antenna system has the radiating elements stuck on the inner plastic sidewalls or on specific mechanical supports of the Set-top-box like an original "stickers 3D" solution and especially is then connected directly to the PCB mainboard by innovative, low-cost and flexible interconnections without using coaxial cables.

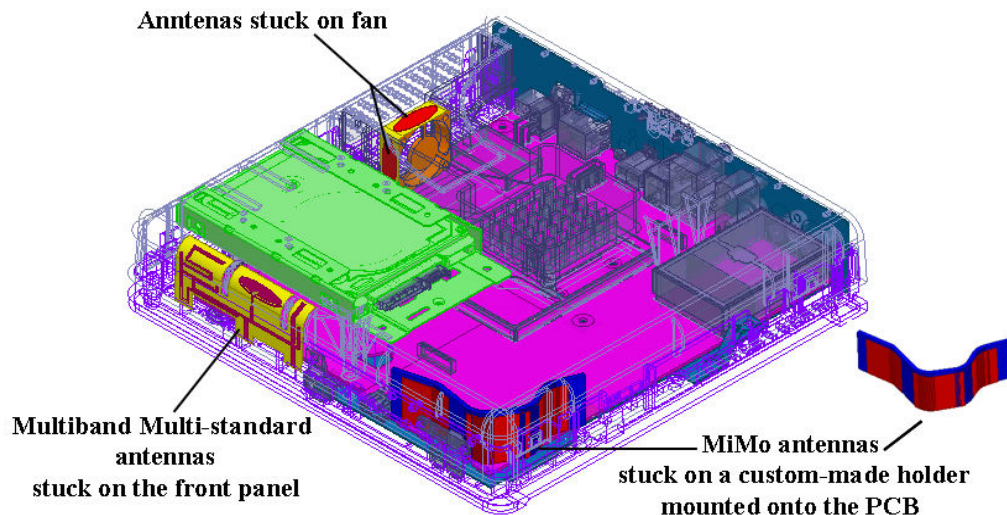


Figure 1-8: View of a Set-Top-Box with stuck peripheral antennas

So, the conventional approaches (like MID, flexible polymer, folded metal etc.) for antenna system design are replaced by a new conformable technology based on flexible paper or polymer film and printing process. This will also promote and reinforce the national printing industry.

The proposed antenna system in 3D configuration exhibits multi-standard, multiband communications enough for the normal operation of all required applications for home-networking and smart-home devices in the frequency range of 1.8 – 6 GHz, for example ZigBee/Z-Wave, Bluetooth, RF4CE (2.4 – 2.5 GHz), DECT (1880 – 1930 MHz), GPS (1565 – 1606 MHz), mobile cellular network (1800 – 2600 MHz) and WLAN (low-band: 2400 – 2483.5 MHz, high band: 5150 – 5850 MHz), etc. There are two possible solutions: multi-band or ultra-wideband. The multi-band solution is preferred because the risks of electromagnetic pollution are much higher when using the ultra-wideband antennas. Specifically, in the

framework of this thesis, we have proposed and developed the dual-band antennas: 2.4 – 2.5 GHz and 5.15 – 5.85 GHz.

And, towards an eco-design, the use of natural, renewable, recyclable, low-cost and environmentally friendly materials, such as paper or other lignocellulosic substrates, will decrease the fabrication cost and the environmental impact. And we also promote printing technologies, that are compatible with the paper material, for metallization. Obviously, this research proposes an alternative solution to mainstream semiconductor technologies: the environmentally friendly "green" and low-cost materials and manufacturing.

Therefore, the most significant objective of this dissertation is paving the way for the realization of RF components along with their interconnection systems under the form of the out-of-board 3D stickers conveniently integrated into future electronic devices. In which, the key parameters are the direct integration of RF components into the electronic devices and the ultra-low cost by taking benefit the emerging of the printed flexible electronics technologies.

1.3 State of the art of flexible electronics

As the growing demand for lighter, smaller and cheaper electronic products inside portable devices, clothing and packaging materials, flexible electronics is emerging as an efficient manufacturing technology which allows printing conductive traces and implanting electronic devices on conformable substrates. Organic and polymer substrates offer the unique advantages of low-cost, lightweight and flexibility than classical rigid substrates such as silicon and FR-4. Therefore, these flexible substrates (paper, polymer, plastic) married with printing technologies like inkjet printing, screen printing or flexography are increasingly investigated for the mass production of a new generation of electronic devices.

In addition, along with an ultra-low-cost target, the environmentally friendly aspect is also the key element toward sustainable development. This is the reason why paper electronics have stimulated the interest of researchers and engineers.

The scope of activities carried out by the various research groups all over the world ranges from purely technological concerns to the integration of complete systems. It includes technological studies on flexible materials (such as paper) and associated treatments, their metallization (implemented processes, chosen inks, etc.), mounting and assembly problems on these materials and the construction of single-layer or multi-layer structures, in 2D or 3D configurations. These activities also cover the realization of basic antennas and develop to the integration of complete modules and systems on paper, for example RFID tags, sensors, microfluidic modules, energy harvesting devices, up to entirely integrated radar systems on paper. All these studies provide particularly original solutions in multiple applications such as detection, control, tracking, monitoring, protection, security, identification ... and in many domains i.e. logistics, transportation, security, medical, pharmacy ...

1.3.1 Technology

1.3.1.1 Flexible substrate

1.3.1.1.1 *Polymer and plastic*

Polymer and plastic have been used extensively in flexible electronics thanks to their ease of bending, their lightness, their hydrophobicity, and particularly their very low dielectric losses (such as polyimide, LCP) for ultra-wide band applications up to beyond 100 GHz, for example ultra-wide band SIW applications on flexible polyimide substrate in the frequency range of 110 to 170 GHz [Göttel 2013].

- **Polyimide (PI):**

Polyimide has been a part of the electronics industry for decades and well-known as the basic substrate for flexible-based technologies. It is available commercially from DuPont as a product called Kapton®. Its advantages include a very high glass transition temperature allowing for processing around 350°C, chemical resistance and a permeability competitive with many other untreated polymers [Nothorn 2007]. But it is prone to swelling in high humidity environments due to high moisture absorption [Göttel 2013]. Polyimide is not optically transparent, that limits its uses in display applications. However, for products such as RFIDs, it could prove to be a very competitive option. It has the dielectric constant of about 3.5 and the loss tangent of about 0.003 up to 5 GHz. [Hsuan-Yu 2012]

- **Polyethylene (PET & PEN):**

Two polymers in the polyethylene family showing significant promise are polyethylene terephthalate (PET) and polyethylene naphthalate (PEN). PET is probably best known for being the plastic that most soda bottles are made from. PET and PEN films are commercially available from DuPont under the names Melinex® and Teonex® respectively. As compared to polyimide films, they offer transparency, but at the expense of lower glass transition temperature (only in the range of 100-200°C). [Nothorn 2007]

PEN has the dielectric constant of about 2.9 and the loss tangent of about 0.025 up to 40 GHz. [Bisognin 2013]

PET has good surface state, lowest cost among the plastic films, and good mechanical and thermal properties. It has the dielectric constant of about 2.8 and the loss tangent of about 0.008 at 1 GHz.

(<http://members.tm.net/lapointe/Plastics.htm>)

- **Polyester Sulfone (PES):**

Polyester has a good heat-resisting property, a high transparency and a good flexibility. The glass transition temperature of PES is 230°C and it shows stable electrical and mechanical properties at high temperature, which enables the fabrication of electronic devices at a relatively high temperature. Unlike other flexible substrates such as polycarbonate (PC) and polyethylene terephthalate (PET), the soldering and bonding processes on PES can be easily performed, which facilitates the packaging process. In addition, a very thin thickness is effective for the miniaturization of RF components. Besides the mentioned properties, the PES shows good water resistance. PES showed dielectric

constant of about 3.3 and dielectric loss tangent of about 0.007 at 2.45 GHz [Kharrat 2014]. PES is suitable for applications such as a transparent flexible display for mobile communications.

- **Liquid Crystal Polymer (LCP):**

LCP is a good material with an impressive loss tangent for high-frequency applications: constant relative permittivity of about 3.2 and loss tangent below 0.005 up to 110 GHz. This material is also suitable for reel-to-reel (or roll-to-roll) processing, in which electronic devices are created on a roll of flexible substrate while having good flexibility [Hsuan-ling 2011]. LCPs are recyclable, impervious to most chemicals, has low water absorption coefficient and can withstand relatively high temperatures (up to 350°C). Thus, this polymer is attractive for high-performance microwave applications and potentially useful in the conformal packaging of many antenna systems and circuits, particularly in the mm-Wave indoor communication, sensing, and imaging applications up to 94 GHz. [Shaker 2010]

Polymer and plastic have proved their potential in the commercial market of printed flexible electronics. However, to find out a more environmentally friendly alternative, in the recent years, a high number of researches have been concentrated in the development of another flexible substrate type that paves a road towards paper electronics.

1.3.1.1.2 Cellulosic substrate

The paper material consists of cellulosic fibers and additives, so it is a non-homogeneous and non-isotropic material. The cellulose fibers in the paper material are wood cells (or parts of wood cells), which can be up to 2-5 mm long and 20-40 μm wide depending on their origin. The cellulose-based cell wall consists of smaller fibrils, which in turn are made of microfibrils that have a diameter of around 3–20 nm. While the amorphous parts between the fibrils mainly consist of hemicellulose and lignin, the microfibrils consist of cellulose chains that partly form crystalline regions of cellulose and are held together by hydrogen bonding. Cellulose is a polysaccharide consisting of thousands of β -linked glucose units, corresponding to a 5 μm long linear chain. [Tobjörk 2011]

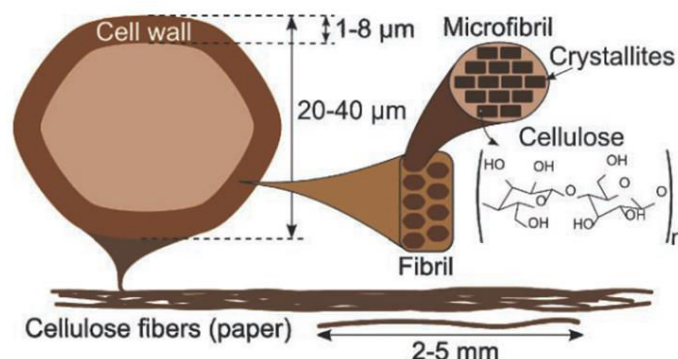


Figure 1-9: Structure of paper material with a description of cellulose fibers

There are many aspects of paper that make it an interesting substrate for RF components and applications.

Firstly, paper is ubiquitous in everyday life and a truly low-cost organic-based substrate. The mass production and the high demand make it the lowest cost material made by human. The price of paper, approximately 0.1 cent/dm², is substantially lower than that of polymer substrates such as polyethylene terephthalate (PET price \approx 2 cents/dm²) and polyimide (PI price \approx 30 cents/dm²) [Tobjörk 2011]. Therefore, electronics on paper have the potential to be extraordinarily cheap.

Secondly, it is lightweight and flexible. From a manufacturing point of view, paper is well suited for reel-to-reel or roll-to-roll processing. The speed of the roll-to-roll (R2R) manufacturing process of paper sometimes exceeds 100 km/h.

Thirdly, paper also has a low surface profile and can be made hydrophobic and fire-retardant by adding certain textiles to it. So, with an appropriate coating, it can host conductive paste on top of its surface which enables modules such as antennas, IC, memory, batteries, and sensors to be easily mounted on or embedded in. This is very crucial since printing processes (such as screen printing, flexography printing, inkjet printing) can be used efficiently to print these modules on a paper substrate.

In addition to this, the paper substrate is also less dilative than low-cost polymer and plastic substrates upon heating, which extends the annealing and sintering (thermal treatment) possibilities of the metallic ink solvent for metallization process. It is also more flexible than polymer because polymer can not be folded easily.

Finally, paper is also environmentally friendly in order to allow for the easy disposal of a massive number of components, since it is biodegradable, recyclable and made from renewable raw materials. Its high biodegradability, with respect to other conventional substrates such as FR4[®], Taconic[®], and Rogers[®], allows it to turn into organic matter in landfills in only a few months and renders it one of the most environmentally friendly materials. [Tentzeris 2012-1]

In summary, paper material is considered one of the new candidates that could potentially open a breakthrough in the flexible electronic world thanks to its ultra-low-cost and environmentally friendly characteristics. Therefore, in the scope of this thesis work, we have concentrated on the realization of antennas and circuits on the paper substrate.

However, applying electronics on paper is challenging because the paper surface is not only very rough compared to plastics, but is also porous and contain chemical compounds that often are considered to be impurities. Plus, its dielectric properties depend on the relative humidity (RH) and temperature. And the low-temperature tolerance ($< 200^{\circ}\text{C}$) of paper prevents the applicability of soldering process. Most importantly, its relatively high dielectric losses ($\tan\delta > 0.04$) limit also its use at very high-frequency applications.

Some cellulosic substrates have been used for RF components:

- Photo paper (Kodak, HP, Mitsubishi ...): This kind of paper is very common and used by most of the research groups. Its thickness is about 250 μm . It has the dielectric constant of about 3.3 and the loss tangent of about 0.08 (in the range of 0.5–2.5 GHz) [Amin 2012-1] [Mariotti 2013]. In particular, the photo paper

has a hydrophobic polymer coating which prevents the conductive ink to get absorbed in the porous paper substrate.

- Teslin paper: Teslin substrate is a durable synthetic paper that offers easy, high-quality printability and strong adhesion. As a single-layer, polyolefin-based material, it is engineered with a micro-porous matrix that allows it to absorb and create strong interlocking bonds with inks, adhesives, coatings and laminating films. This type of paper has the lowest loss tangent value in comparison with the state-of-art [Cook 2013-1]. The 250 μm thickness paper sheet has the dielectric constant of about 2.1 and the loss tangent of about 0.03 at 1.6 GHz.
- Cardboard: This kind of cellulosic substrate has a loss tangent value lower than classical paper thanks to air layer inside, but it is very thick. Saghlatoon et al. from Tampere University have used a highly fibrous cardboard, which has thickness 560 μm , a dielectric constant of about 1.78 and a loss tangent of about 0.025 at 2.45 GHz [Saghlatoon 2014]. Kharrat et al. from INP Grenoble have also used corrugated cardboard to fabricate many antenna prototypes. Cardboard C4, with thickness 3 mm, has a dielectric constant of about 1.41 and a loss tangent of about 0.042 at 2.45 GHz. [Kharrat 2015]

Flexible substrate	Thickness (μm)	ϵ_r	$\tan\delta$	Flexibility	Cost	Bio-degradable
<i>Polyimide</i>	106	3.5	0.003	medium		
<i>PET</i>		3.3	0.008	medium	cheap	
<i>PEN</i>		2.9	0.015	medium		
<i>PES</i>		3.3	0.007	medium		
<i>LCP</i>		3.2	0.005	medium	cheap	
<i>Photo paper</i>	250	3.3	0.08	high	ultra-cheap	X
<i>Teslin paper</i>	250	2.1	0.03	high		uncertain
<i>Cardboard</i>	560	1.78	0.025	low	ultra-cheap	X

Table 1-1: Summary of the basic characteristics of some flexible substrates

Looking at the comparison table above, we can easily see that photo paper is a suitable substrate for purposes of ultra-low cost, high flexibility and environmentally friendly design, despite its very high dielectric losses. Therefore, in simple applications, like RFID or domestic/domotic monitoring, that do not require a very high performance and in which the ultra-low cost is the most important factor, the flexible substrates such as paper become a very potential and interesting candidate.

1.3.1.2 Metallization process on flexible substrate

This section describes the most used manufacturing techniques for fabricating the RF components on a flexible substrate such as paper. For each method, the process, advantages and disadvantages are briefly presented.

1.3.1.2.1 Metal laminating followed by etching

This is currently the oldest and most popular technique for the production of printed electronic components and circuits. This subtractive process is carried out in several steps from a substrate on which is rolled or electrodeposited uniformly a conductor layer, usually copper or aluminum from 10 μ m to 20 μ m thick. Then a mask is made on this layer to protect the areas that will be kept. The mask is made by photolithography using a photosensitive resin. Finally, the unprotected conductive parts are removed in a chemical solution bath. There are two variants of the etching process: the dry and the wet, which have been described in more details by Elsherbeni et al. in [Elsherbeni 2010]. The wet process permits to attain good resolution and antenna performance, but it needs a lot of steps and is incompatible with the paper substrate, so we are obliged to use more expensive polymer substrates like PET, PVC or PC.

The copper laminating process followed by dry etching on the paper substrate was described by Bhattacharya in [Bhattacharya 2007]. 18 μ m copper was laminated and followed by etching to form 50 and 100 μ m lines and spaces. It is also used as reference techno to compare with the antenna performance realized by silver ink inkjet-printing.

Virili et al. from Perugia University have presented a standard aluminum laminating followed by physical dry etching. This technique avoids chemical solutions and the metallization is realized with aluminum (a high conductivity and fully recyclable material). Two aluminum foils of 20 μ m thickness were pressed on the paper substrate by adopting a thin film of epoxy glue and heated for four hours at low temperature (60°C) in order to solidify the glue. Then, a computer-controlled milling machine was adopted for the metal etching. This process also allowed the fabrication of metallized via holes because milling machines are typically equipped with spiral drills tools that enable this feature (cf. *section 1.3.1.3*). [Virili 2015]

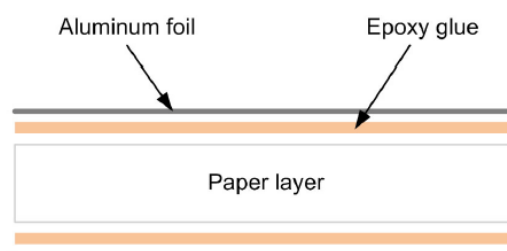


Figure 1-10: Side view of the metallized paper substrate, consisting of a stack of paper layer and aluminum foils, attached by epoxy glue

1.3.1.2.2 Adhesive copper tape

Alimenti et al. from Perugia University have relied on the copper adhesive tape, shaped by a photo-lithographic process and then transferred to the hosting substrate by means of a sacrificial layer. The main advantages of the Cu tape are a superior conductivity with respect to cured Ag ink and the possibility to solder instead of using epoxy to mount lumped components. However, the thin adhesive layers, interposed between each metal and the substrate, have a significant thickness ($30\mu\text{m}$) in comparison with Cu ($35\mu\text{m}$) and influences in the effective permittivity. So, the effect of the adhesive layers must be taken into account in the simulation tool. In addition, this technique is usually just adopted in laboratory scale to create the test prototypes. [Alimenti 2012]

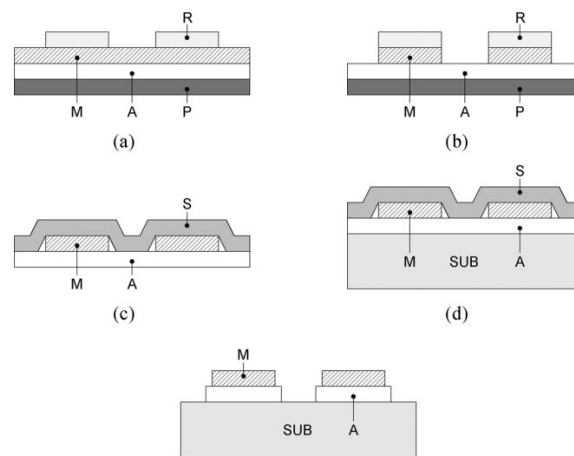


Figure 1-11: Process steps for the circuit fabrication using Cu tape: (a) the photo-resist is deposited on the conductive tape and patterned using UV; (b) the conductive layer is wet-etched; (c)–(e) the etched conductor is transferred on the paper substrate by means of a sacrificial layer. M: metal, A: adhesive, P: protection, R: photo-resist, S: sacrificial layer, SUB: hosting substrate

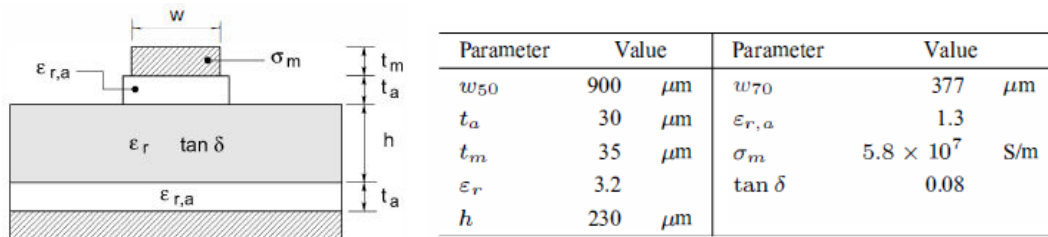


Figure 1-12: Cross-section of an elementary microstrip line exploiting the Cu tape. The thin adhesive layers remain interposed between metal and substrate

Some other researchers, e.g. Gonçalves at Aveiro University and Kharrat at INP Grenoble, have also used copper adhesive to create the antenna prototypes but in a much simpler way. They have just cut a copper strip and pasted directly into the paper substrate. [Gonçalves 2014-1], [Gonçalves 2014-1], [Kharrat 2015]

1.3.1.2.3 Aluminum thermal evaporation

Ramade et al. from Montpellier University have described a depositing technique using thermal evaporation for growing metallic film directly on PET or paper substrates [Ramade 2012]. This technique is well-known in microelectronics and is already used industrially for packaging metallization and for roll-to-roll coating. This coating was carried out with industrial machines that run with a high-speed roll-to-roll process under vacuum. It allowed obtaining thin and homogeneous metal layers with a high electrical conductivity (e.g. $\sigma_{\text{Alu}} = 2.8 \times 10^7 \text{ S/m}$). Thermal evaporation offers numerous advantages: firstly this is a "dry" and fast technique, without baths or drying stages. This is possible thanks to a quick and reusable masking system. Secondly, the use of aluminum material is economical compared to copper or silver inks which are both very expensive. Finally, it allows working with a paper substrate that is ecological, economical, printable and easily convertible into labels without any additional process stages. The evaporation permits to produce the antenna directly onto a printable paper substrate without any additional step. The resolution of the antennas is sufficient depending on the masking system used. It is also environmentally friendly because it does not use harmful chemicals products such as solvents or acids during the production process. The main disadvantage of this method is the small thickness of metal deposited (just about few micrometers) which subsequently complicates the matching between the antenna and the chip and most importantly increases the metallic losses.

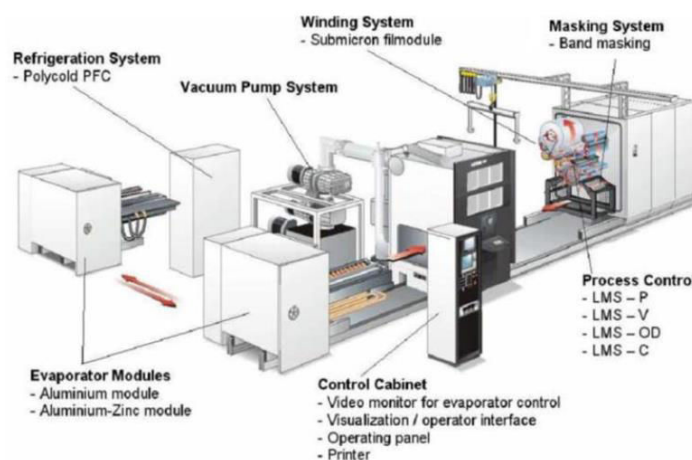


Figure 1-13: Schematic of film metallizing system (metaliser)

For large-scale manufacturing of RFID tags, the metallization method by thermal evaporation can be easily transferable to industrial machines called "metalisers", as shown in Figure 1-13 above, which run with a high-speed roll-to-roll process under vacuum (10 m/min) and enable production of several thousand of antenna in few hours with good reproducibility.

1.3.1.2.4 Aluminum dry process based on laser patterning

Walki® Pantenna has proposed an aluminum laminating followed by dry process based on laser patterning in order to produce flexible circuit boards for a number of different applications, ranging from RFID antennas to flexible displays. The

precision of the laser cutting allows for greater repeatability in the production process and higher accuracy in the antenna. This technique gives us also a flexible choice of substrate (paper or different plastic films). No chemicals are needed in the manufacturing process, resulting in environmentally friendly benefit. Furthermore, the process residue is fully recyclable as metallic aluminum and the absence of chemicals also makes it easier to recycle the final product. Especially, the laser technology in this dry process provides a production speed up to ten times faster than that of wet etching. [Walki 2012]

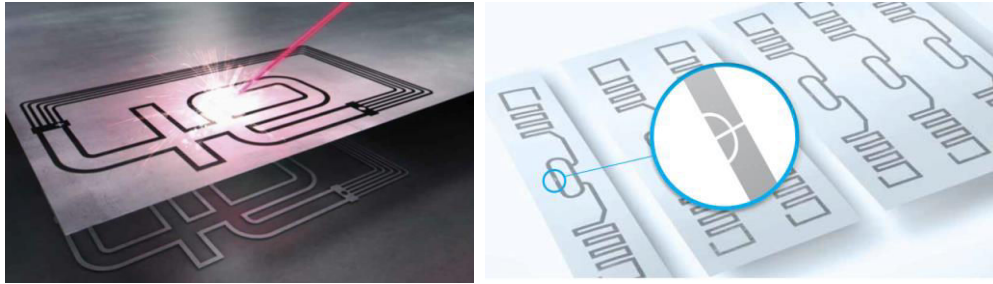


Figure 1-14: Aluminum dry process on paper substrate based on laser patterning

1.3.1.2.5 Inkjet catalyst printing and electroless copper deposition

Cook et al. from Georgia Tech have demonstrated in [Cook 2013-1] a scalable, low-cost process for fabricating copper-based microwave components on flexible, paper-based substrates. First, a Palladium Chloride catalyst-bearing solution was inkjet-printed at a desired pattern on the paper substrate. This catalyst-bearing paper was then immersed in an aqueous copper-bearing solution to allow for electroless deposition of a conformal layer of copper in the inkjet-derived pattern. With increasing electroless deposition time, the conformal Cu films increased in thickness and the sheet resistance values decreased. After 50 minutes (shorter time than multilayer ink inkjet-printing and thermal sintering), the thickness of Cu deposition was attained $4\text{ }\mu\text{m}$ with DC conductivity of $3.4 \times 10^6\text{ S/m}$. This method avoids nozzle-clogging problems and high costs associated with noble metal particle-based inks in comparison with inkjet-printing of silver nanoparticle ink. And it is readily scalable on virtually any substrate and may be used to generate a variety of copper-based microwave devices on flexible substrates.

Specimen Type*	Average Thickness (μm)	Sheet Resistance (Ω/\square)	Electrical Conductivity (S/m)
Cu/10 min	0.61 ± 0.13	7.6	2.2×10^5
Cu/50 min	3.87 ± 0.90	0.099	3.4×10^6
Ag/1 layer/1 h	0.49 ± 0.08	4.6	4.4×10^5
Ag/3 layers/1 h	1.35 ± 0.16	0.63	1.2×10^6
Ag/5 layers/1 h	2.39 ± 0.10	0.20	2.1×10^6
Ag/5 layers/2 h	2.39 ± 0.10	0.15	2.8×10^6

Table 1-2: Electrical characterization of Cu (electroless deposition) and Ag (inkjet printing followed by sintering at 120°C) test strips

1.3.1.2.6 Inkjet printing

Tentzeris et al. have used frequently inkjet-printing technology in their researches. This printing method is a direct-write technology by which the design pattern is transferred directly to the substrate. Unlike traditional metal etching techniques which is a subtractive method by removing unwanted metal from the substrate surface, it sprays the single ink droplet from the printer's nozzle to the desired position. Therefore, no waste is created, resulting in an economical fabrication solution. The conventional masks for fabrication are not necessary for inkjet printing, which means that designed circuit pattern is transferred to the substrate without any byproducts. Therefore, dangerous chemicals, such as etchants are eliminated.

In addition, this new technology may rapidly fabricate prototype circuits without iterations in photolithographic mask design or traditional etching techniques that have been widely used in industry. Printing is a simple, fast and safe process that is completely controlled from the designer's computer and does not require a clean room environment.

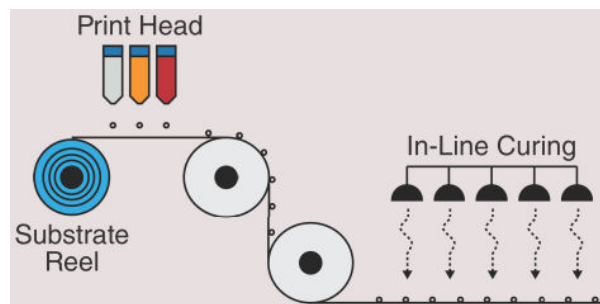


Figure 1-15: Dimatix Materials Inkjet Printer DMP-2800 Series [L] and Roll-to-roll inkjet printing process used in an industrial environment [R]

This fast printing approach on paper is very repeatable, allows for features down to 20µm and enables components such as antennas, filters, baluns, IC, and sensors to be easily embedded in organic modules and in single or multilayer (multi-sheet) configurations. [Tentzeris 2010]

After printing, it is essential to follow the sintering process in order to remove the excess solvent in metallic ink and to remove material impurities from the depositions. A second benefit provided by the sintering process is increasing the bond of the deposition with the flexible substrate and enhancing the conductivity of the conductive ink. Thermal sintering in industrial oven is used most often. The conductivity of the silver ink varies from $0.4 \sim 2.5 \times 10^7$ S/m depending on the curing temperature and duration time. *Figure 1-16* shows a Scanning Electron Microscope (SEM) image of nano-silver ink before and after sintering at 180°C for 10 minutes,

however, no scale information was provided by the authors. Before the cure, large gaps exist between the particles, resulting in a poor connection. After the cure, the high temperature has caused the particles to expand and the gaps between them to diminish [Konstas 2009]. The roughness of the inkjet-printed deposit is very small (root mean squared value $R_q \sim 14.4$ nm) so that the inkjet printing technique can be applied to radiofrequency applications [Tentzeris 2012-2]. Alternatively, other sintering methods such as UV or photonic curing, which takes up only a few seconds, can achieve similar results. [Traillie 2009]

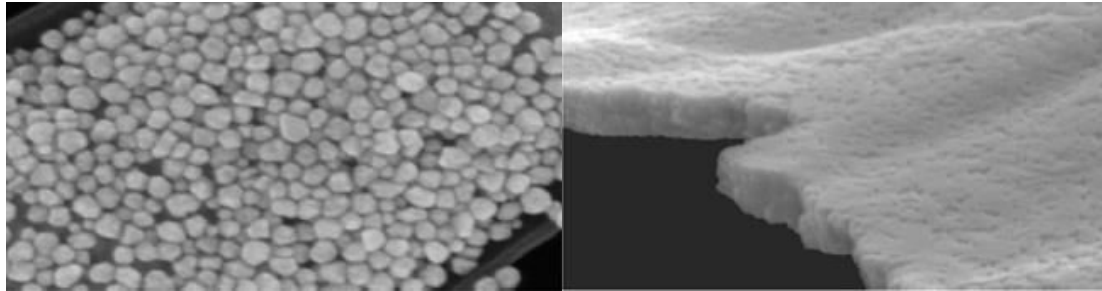


Figure 1-16: SEM images of a layer of inkjet-printed nanoparticle silver ink, before and after sintering at 180°C for 10 minutes [Konstas 2009]

In general, inkjet printing can be used efficiently to print electronics on flexible organic substrates, leading to an increased deployment in printed electronics, such as flexible displays, RFIDs, sensors, solar panels, fuel cells, batteries, and most recently in antennas.

Its primary disadvantages may have noticed as a requirement of a slow step of ink drying, an expensive price of the ink charged with silver particles and a low value of conductivity which affects the antenna performance if the thickness of conductive ink is not sufficient. In particular, it is evaluated by Amin et al. from Royal Institute of Technology (KTH) as the most expensive method to fabricate the RFID tag antennas among printing technology. [Amin 2012-1]

1.3.1.2.7 Flexography printing

Flexography (or flexo) is a form of the printing process which utilizes a flexible relief plate. It is essentially a modern version of letterpress which can be used for printing on almost any type of substrate, including plastic, metallic films, cellophane, and paper. It is widely used for printing on the non-porous substrates required for various types of food packaging.

Kharrat et al. from INP Grenoble have described this additive manufacture process in [Kharrat 2013]. The design is drawn on a photopolymer mask called a printing plate. The ink supply to the mask is taken from a fountain roller through another roller called "anilox". This roll, wherein etched micro pores, allows ink to be transported. The plate cylinder holds the printing plate, which is soft flexible rubber. The impression cylinder applies pressure to the plate cylinder, where the image is transferred to the substrate. But, the flexography method has the

disadvantage of having an extra thickness on the edges, called "Halo" phenomenon. It concentrates the printed ink on the contour printing. Therefore, the pattern dimensions (line width, antenna size ...) are enlarged and the fabrication techno causes a small shift in the resonance frequency of antenna towards lower frequencies.

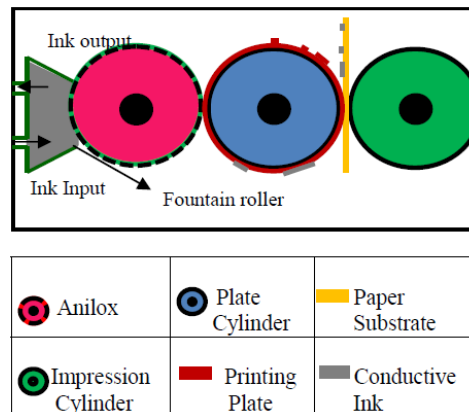


Figure 1-17: Flexographic process description



Figure 1-18: "Halo" phenomenon on the edges

Amin et al. have evaluated that flexography printing is the cheapest solution in the fabrication of RFID antennas among printing technology. The line thickness is typically 10-15 μm and the sheet resistance is 30m Ω /square by additional oven drying. The best print quality is obtained using a printing speed of 2 m/min. [Amin 2012-1]

1.3.1.2.8 Screen-printing

Screen printing is a printing technique whereby a mesh is used to transfer ink onto a substrate, except in areas made impermeable to the ink by a blocking stencil. A blade or squeegee is moved across the screen to fill the open mesh apertures with ink, and a reverse stroke then causes the screen to touch the substrate momentarily along a line of contact. This causes the ink to wet the substrate and be pulled out of the mesh apertures as the screen springs back after the blade has passed.

Amin et al. have used the semi-automatic screen printer to fabricate some antenna prototypes on Kapton HN and Korsnas paper. The 25 μm thick layer is achieved with stable ink distribution all over the printed patterns. The samples are post-annealed for 2 hours at 140°C to achieve improved conductivity. [Amin 2012-1]

The commonly used metallization processes for fabricating the circuit patterns on flexible substrates like paper are summarized in *Table 1-3* below. Each method shows its own advantages and disadvantages. However, as mentioned in the objective, a technological process inspired from smart paper printing techniques, is promoted in this thesis work, aiming at establishing a new paradigm in the implementation of low-cost passive antennas and interconnection systems at radio frequencies. In the conditions of facilities and equipment available, we have tested two printing methods: flexography printing and screen-printing, that will be presented in detail in *section 2.2.2*.

Method	Advantage	Disadvantage
<i>Metal laminating followed by etching</i>	Mature technology. Thick metallic layer (10 μ m to 20 μ m). Very good conductivity.	Requirement of a long etching process.
<i>Adhesive copper tape</i>	Very good conductivity. Possibility of solder.	Influence of the adhesive layers, interposed between each metal and the substrate. Just adopted in laboratory scale to create the test prototypes.
<i>Aluminum thermal evaporation</i>	Fast technique, without baths or drying stages, so do not use harmful chemicals products or acids.	Very thin deposited metal (about few micrometers)
<i>Aluminum dry process based on laser patterning</i>	Great repeatability and very high resolution thanks to the precision of the laser cutting. No chemicals are needed.	Expensive cost
<i>Inkjet catalyst printing and electroless copper deposition</i>	Low cost.	Requirement of a long electroless deposition time. Thin deposited copper layer (about 4 μ m). Fairly low conductivity.
<i>Inkjet printing</i>	Direct-write printing technology. No need of mask and etchant byproduct.	Nozzle-clogging problems and high cost of noble metal particle-based inks. Requirement of a long sintering process.
<i>Flexography printing</i>	Low cost. Higher throughput than screen printing	Requirement of a long sintering process. Very low conductivity. Extra thickness on the edges.
<i>Screen-</i>	Low cost. Thicker conductive	Requirement of a long sintering

<i>printing</i>	layer than flexography printing.	process. Fairly low conductivity
-----------------	----------------------------------	----------------------------------

Table 1-3: Summary of the metallization processes on flexible substrates

1.3.1.3 Treatment process on paper

In addition to the metallization process, the treatment on paper substrate is also extremely important especially with the metallization methods by a printing process. For example, the pre-treatment of the paper surface before printing allows the best quality of the printed pattern as well as the best performance of the RF components. The via-hole realization determines the feasibility of the 2.5 D circuit designs on the paper substrate.

a/ Multilayer paper-glue compound realization

In many designs, the thickness of one paper layer is not enough for a good performance, so some researchers have attempted to paste several sheets of paper together to create a thicker layer.

Moro et al. from University of Pavia have utilized a PolyVinylPyrrolidone (PVP)-based glue to bond the paper substrates because of ease of fabrication and its electrical permeability is very close to that of the paper. [Moro 2013]

Lolli et al. from Perugia University have then investigated for the first time the dielectric properties (permittivity and loss tangent) of a compound material made of sheets of paper stacked using commercial low-cost PVP-based glue. This characterization is the first fundamental step for the future development of a new class of systems in package circuits based on paper-glue compound materials. [Lolli 2012]

b/ Surface pretreatment by using multilayer primer

Since 2011, Denneulin et al. from INP Grenoble have developed a UV-curing inkjet-printable primer layer to avoid the deterioration of the ink functionality due to different paper surface properties. This pre-treatment enabled homogeneous surface properties such as smoothness, absorption capacity and surface energy to be obtained, for almost all the tested substrates. Significant improvement of conductivity was measured for all paper materials and similar conductivity (close to reference PET film) was obtained whatever the substrate involved. This innovative solution was expected to pave a road toward the production of low-cost and flexible paper-based electronics. [Denneulin 2011]

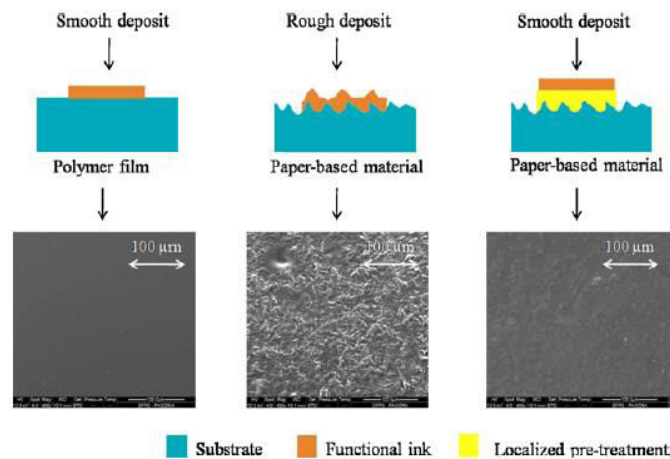


Figure 1-19: Surface pretreatment process with the corresponding substrate surface views

Saghlatoon et al. have also recognized that the ink penetrates into the cardboard (about 55 μm) due to its highly fibrous nature [Saghlatoon 2014]. By penetration of the ink into the fibrous substrate, the printed silver ink is not cured properly in the sintering process. Hence, the conductivity diminishes because the printed silver nanoparticles cannot make a uniform conductor. Therefore, he also used a conventional primer to make the surface smooth and ink proof. For this purpose, four layers of primer were printed separately on the rough surface of cardboard. After the printed deposition of each layer, it was cured using ultraviolet light (UV) for 15 min, and then 1 h at 150°C in an oven. Afterwards, the silver ink was inkjet-printed on the treated surface utilizing the conventional sintering approach. The mean roughness and the root mean squared surface roughness are improved from 1.68 μm and 2.13 μm before treatment to 1.3 μm and 1.62 μm after treatment, respectively. And the value of DC conductivity was found to be almost double. However, the cost of this pre-treatment has not been mentioned.

c/ Via-holes realization

The drilling and laser processing are suitable processing for the paper substrate because those are complete dry processing and no surface treatment is required. In addition, those processes have very good aspect ratios (ratio between the thickness substrate and the via hole size) and feature sizes. The aspect ratios of drilling and laser processing are larger than 10 and 20, respectively. The general achievable feature size of drilling is 300 μm and of laser processing is 5 μm . [Polyakov 2004]

Vyas et al. from Georgia Tech have described, in 2007, a via realization method in [Vyas 2007]. Via-holes were drilled through the laminated structure using a 400 μm micro-drill. Fiducial marks (small crosses or others type of marks located precisely on each of the four corners of the design layout for the circuit fabrication) printed along the borders were used to ensure that the top and bottom layers were aligned properly. The drilled via-holes were then filled using silver epoxy. A small area of the adhesive was left to spill over from the via-holes across the top and bottom

silver traces to ensure connection. The structure was then cured at 120°C for 20 min.

In 2013, Moro et al. from University of Pavia have also utilized drilling to make via holes because it does not damage the substrate and the rim of via holes. But for the via hole metallization, cylindrical copper rivets with an outer diameter of 0.8 mm were inserted into the via hole. He has commented that the epoxy filled via hole, in previous works of Vyas, cannot guarantee a tight contact to the side wall of the via hole and the ink-filling technique cannot be applied to thick paper substrates. [Moro 2013]

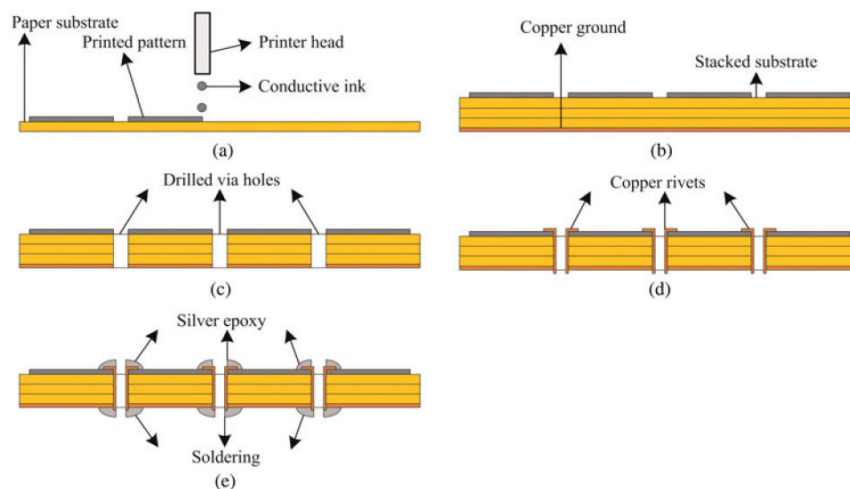


Figure 1-20: Different steps of the fabrication process of SIW components on paper substrate: (a) Inkjet print the pattern; (b) Stack the multi-layer substrate after sintering; (c) Drill via holes; (d) Insert copper rivets; (e) Encapsulate

Virili et al. from University of Perugia have presented, in 2015, the fabrication of via holes on paper based-substrate metallized by aluminum laminating and etching. The via holes were first drilled by milling machine. Then, a preliminary coating thin film of epoxy glue was distributed on the inner wall of via holes to avoid the diffusion of conductive paste into porous paper. A fast heating process was required to cure the coating. Finally, the conductive paste was adopted to fill the holes and guarantee ohmic contact between top and bottom conductive layer, following by a final heating process in order to increase the conductivity of the conductive paste. [Virili 2015]

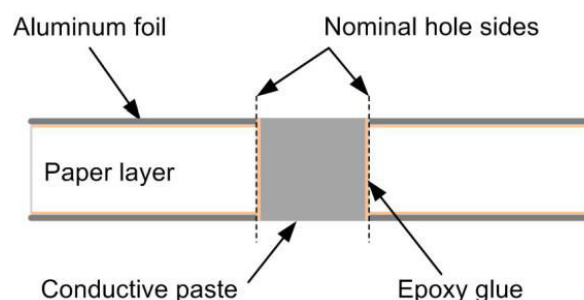


Figure 1-21: Metallized via holes process on paper

Process	Option	Feature size	Cost
Perforation	Drilling	300 μ m	Cheap
	Laser processing	5 μ m	Expensive
Process	Option	Advantage	Disadvantage
Via-hole metallization	Copper rivet	Very good conductivity and fast process	Requirement of the large perforated hole size, so cannot be applied to the narrow pattern
	Silver epoxy or Conductive paste	Applicable for all size of perforated hole	Low conductivity and requirement of the two-step process: metallization followed by the sintering process

Table 1-4: Summary for the via-hole realization on paper substrate

The through holes realization is one of the manufacturing challenges for creating multi-layers structures and 2.5 D configuration on the flexible paper substrate. However, the research works all over the world show that this is entirely feasible. Seen the summarized *Table 1-4* above, a low-cost process could be fully realized by the combination of drilling perforation and via-hole metallization using conductive silver paste.

1.3.2 Applications

As mentioned above, in the framework of this thesis, we have focused on researching the implementation of circuits and systems on paper substrates. So only the applications relating to paper substrate presented and analyzed herein. The most primary applications on low-cost paper substrates are the multi-functionality inexpensive Radio Frequency Identification (RFID) tags and Wireless Sensor Nodes (WSN) that could be easily extended to other microwave and wireless applications. The applications are arranged in order from simple to complex gradually to show what the researchers around the world have attained on paper substrates and how complicated the circuits could be: RFID tag, Wireless Local Area Network (WLAN), Ultra-wide-band or multi-frequency antenna, 3D antenna, radar system.

1.3.2.1 RFID tag

RFID is a wireless technology for the identification of objects. In recent years, the demand for flexible RFID tags has increased dramatically due to the requirements of automatic identification, tracking, monitoring in the various areas such as logistics, Aero-ID, anti-counterfeiting, supply chain, space, healthcare, pharmaceutical tracking, access control, automatic payment, real-time location ... However, the major challenge that hinders its widespread deployment for the realization of a completely ubiquitous network is the inexpensive cost to be realized in mass production amounts. And then, an environmentally-friendly material is also important for making "green" electronics in order to allow the easy disposal of a

massive number (in the billions) of RFID's [Traille 2009]. Therefore, paper becomes one of the interesting organic substrate candidates and embedded paper electronics is a promising solution for realization of complex circuitry on the cheapest synthetic material made by humankind with the consideration of environmental impact.

Georgia Tech has appeared as the reference laboratory for RF electronics on paper, especially Athena group of Professor M. M. Tentzeris, who is undisputed leader and has considerable influence in this field at international level. Since the middle of the last decade, many researchers, in direct collaboration with professor M. M. Tentzeris, have carried out a great number of research activities about the first "green" RFID tags and antennas on an ultra-low-cost organic substrate like paper.

a/ Inkjet-printed RFID tag

Since 2006, Yang has developed for the first time many UHF RFID tag modules on an ultra-low-cost paper substrate with the inkjet-printing technology, proving this approach could function as a fabrication method of low-cost and flexible electronics. A compact RFID tag module with a T-match folded bow-tie structure to match the antenna to the IC was inkjet printed on a paper substrate. It had a designed bandwidth of 190 MHz, corresponding to 22% around the center frequency of 854 MHz, which covers the universal UHF RFID bands. In order to verify the performance of the inkjet-printed RFID antenna, a copper-metallized antenna prototype with the same dimensions was fabricated on the same paper substrate, using the slow-etching technique. Overall, good agreement in term of return loss between the copper-etched and the inkjet-printed antennas was observed, despite the higher metal loss of the silver-based conductive ink. The radiation pattern of this inkjet-printed antenna was almost uniform (omnidirectional) at 915 MHz, with directivity around 2.1 dBi. [Yang 2007-1]

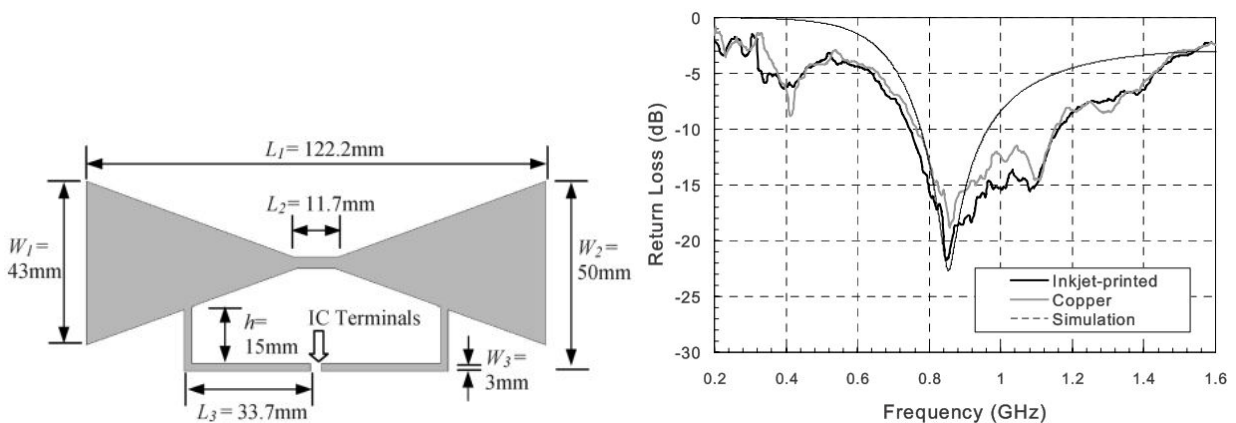


Figure 1-22: T-match folded bow-tie RFID tag module configuration [L] and its return loss, which covers the universal UHF RFID band [R]

Then, the researchers at the University of Perugia, who have a close relationship with Tentzeris, have also continued the development of UHF RFID tags on paper substrates with more functionality.

Alimenti et al. have designed a bow-tie dipole antenna with magnetic coupling to a UHF RFID chip at the operating frequency of 868 MHz. The dipole was fabricated using inkjet printing technology ($\sigma = 2.5 \times 10^7 \text{ S/m}$, $2\mu\text{m}$ ink thickness). Its size was reduced by exploiting a meander line configuration. The magnetic coupling was realized by means of a heterogeneous transformer, in which the primary winding

was implemented on the same paper-substrate of the antenna and the secondary winding was directly fabricated on the RFID chip. [Alimenti 2011-2]

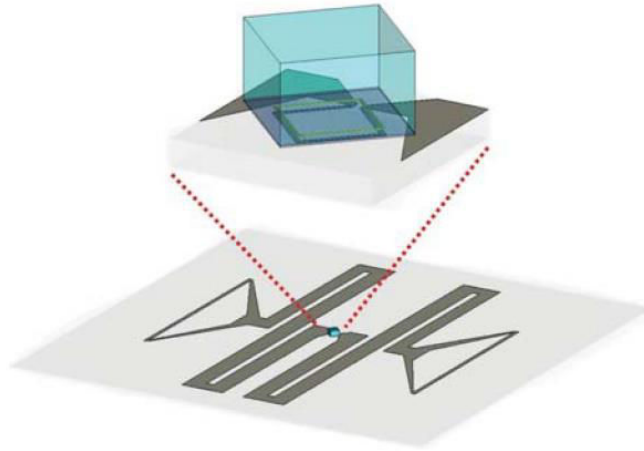


Figure 1-23: Bow-tie dipole antenna magnetically coupled to RFID chip

In addition, he has also presented a frequency doubling RFID tag inkjet-printed on the paper substrate for harmonic radar. This structure exploited two dipoles in a crossed configuration and four diodes in a bridge configuration to form a balanced multiplier. The reflected frequency, doubled with respect to transmitted frequency, could easily be detected by microwave receiver without being masked by reflections from the surroundings. [Alimenti 2010]

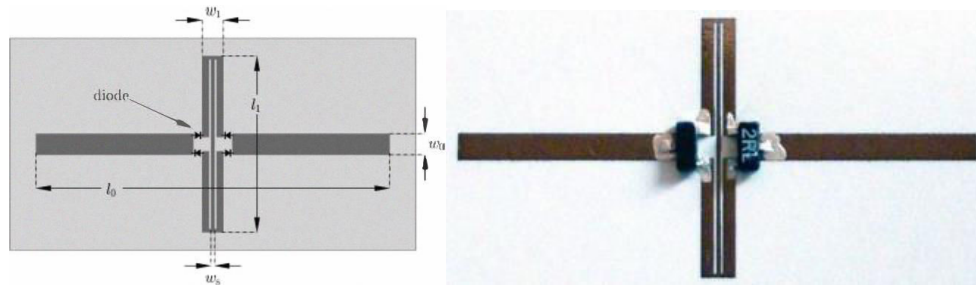


Figure 1-24: Layout [L] and paper-based prototype [R] of the frequency doubling tag

Orecchini has proposed another configuration of passive inkjet-printed UHF RFID tag with dual-radiating-body antenna featuring high directivity and increased read range. The radiation pattern had a dumbbell shape and the gain achieved at 915 MHz was 5.03 dBi. [Orecchini 2010]

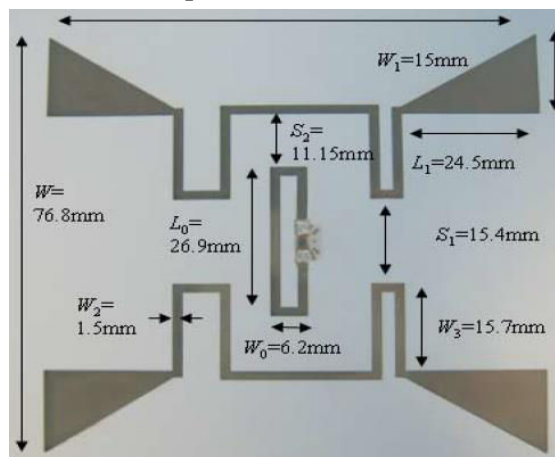


Figure 1-25: Dual-radiating-body RFID antenna inkjet-printed on paper

Clearly, the demonstration of these three RFID antennas of University of Perugia shows the feasibility of realization of "green" and flexible electronics on paper in the area of UHF RFID.

b/ Other printing methods

Merilampi et al. have characterized the conductive silver ink patterns screen-printed on the paper substrate in order to evaluate the mechanical and electrical performance of commercial silver inks and the possibilities of manufacturing novel flexible electronics by using this printing technique [Merilampi 2009]. She has also developed many bow-tie RFID tag antennas screen-printed on various paper substrates using different silver inks. The maximum reliable read range in the air for printed tags was quite the same as the values reported for the copper tag on FR4 laminate and the aluminum tag on plastic foil [Merilampi 2007]. This means that screen-printed RFID tags are competitive solutions for the low-cost mass products in simple identification applications.

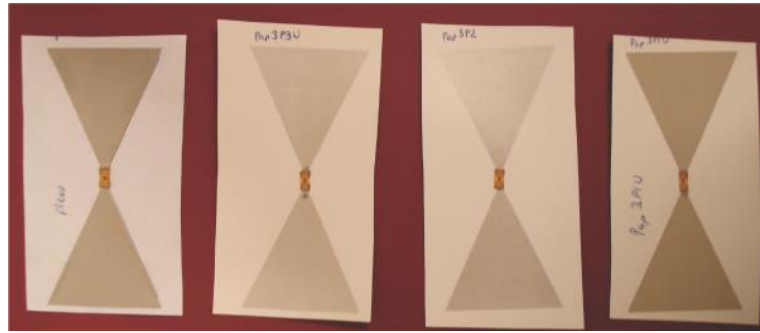


Figure 1-26: Screen-printed prototype of RFID bow-tie antennas on paper substrate

In another research, Amin et al. from KTH have investigated the bowtie antennas fabricated on various low-cost substrates (e.g. paper, Kapton, PET) using different printing technologies such as screen printing, rotary printing, dry phase patterning, and inkjet printing for the comparison of different substrates and printing processes. These bowtie antennas covered completely UHF RFID band (860–960 MHz). The normal bowties, as shown in Figure 1-27, had the radiation patterns nearly uniform (omnidirectional) at 915 MHz with a directivity around 2.1 dBi and a long reading range up to 9 m. [Amin 2012-1]

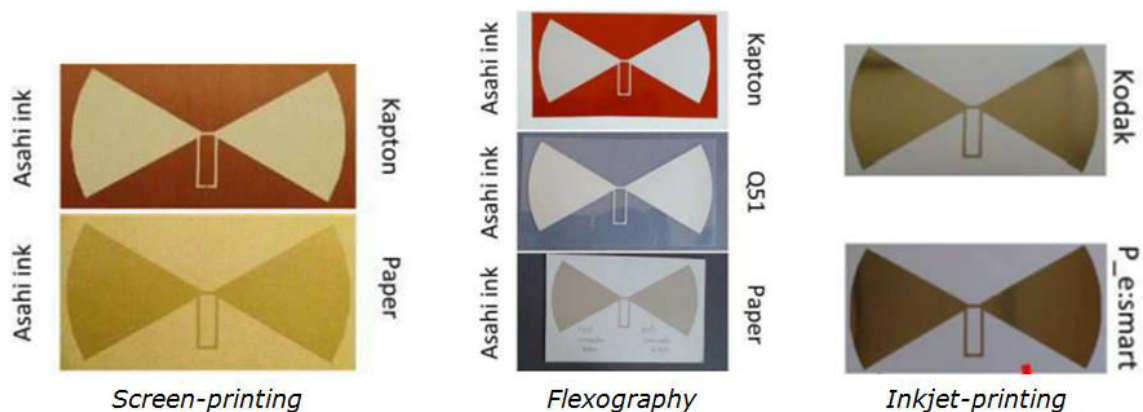


Figure 1-27: Prototypes of RFID tag bowtie antennas on different flexible substrates using different printing processes

And another quadrate bowtie antennas (*Figure 1-28*) with round corners exhibited many advantages of the smaller area ($9.2 \times 3.2 \text{ cm}^2$), better return loss in high frequency and higher gain (realized gain of 1.47 dBi). [Amin 2012-2]

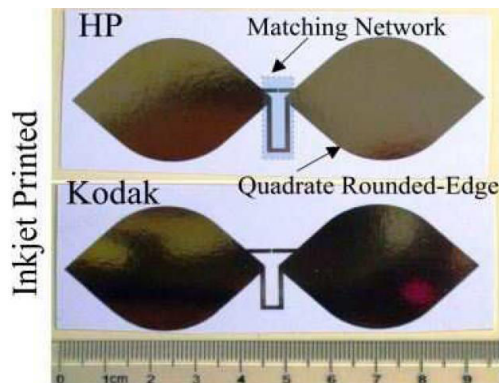


Figure 1-28: Inkjet-printed RFID quadrate bowtie antenna on HP and Kodak photopaper

Vena et al. from INP Grenoble have demonstrated for the first time a 19-bit chipless paper-based tag using flexography printing ($\sigma = 3 \times 10^5 \text{ S/m}$). It had a compact size ($7 \times 3 \text{ cm}^2$) and could be read remotely at 50 cm or farther with 0 dBm transmitting power. This chipless tag showed a very low-cost solution in comparison with commercial RFID chip tag for identification applications and proved that the flexography printing could be applied for the fabrication of RF components on paper substrates. [Vena 2013]

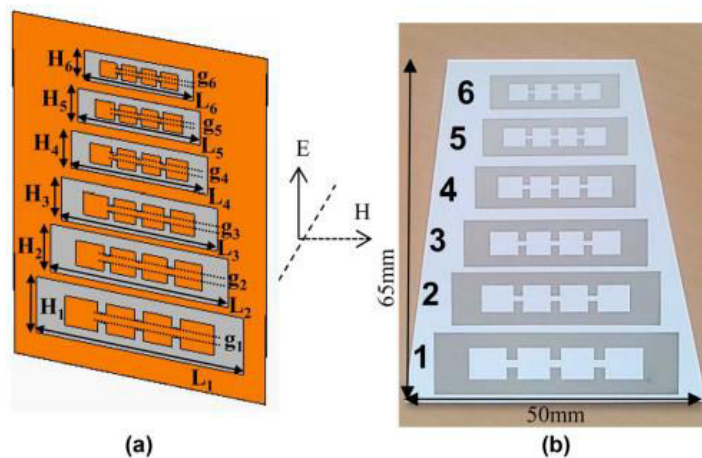


Figure 1-29: (a) Chipless RFID tag based on multiple 3-gap loop resonators; (b) Tag prototype printed on glossy paper by flexography

c/ Other fabrication methods

Ramade et al. have demonstrated for the first time the fabrication of an HF RFID transponder (tag) deposited on a paper substrate using thermal evaporation. Despite the low thickness of the antenna metal layer ($\leq 1 \mu\text{m}$), the good conductivity of aluminum ($\sigma = 2.8 \times 10^7 \text{ S/m}$) is sufficient for operation at 14 MHz. It exhibited a maximum read range of 4 cm. With the use of paper and low amount of metal, this process permitted a cost reduction estimated to 20% compared to equivalent commercial tag. [Ramade 2012]

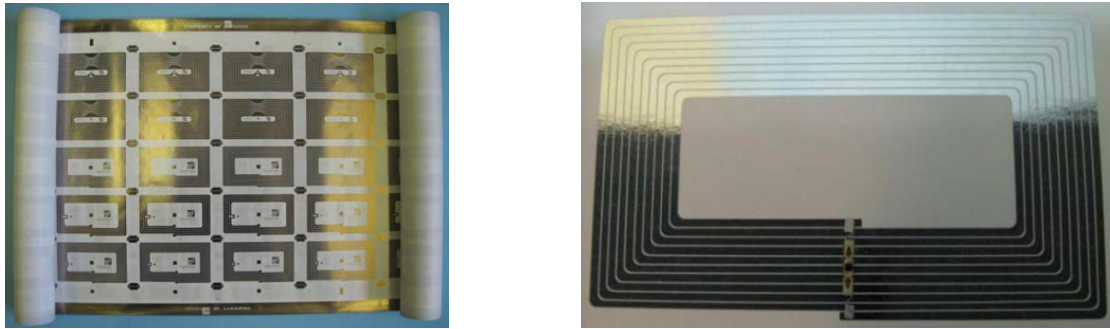


Figure 1-30: HF RFID antenna roll produced industrially with a metallizer [L]; HF tag prototype fabricated on paper substrate ($85.6 \times 53.98 \text{ mm}^2$ with $1 \mu\text{m}$ aluminum thickness) [R]

In general, the RFID applications do not require very high radiation efficiency of the antennas, so the dielectric losses of the paper substrate and the metallic losses of the conductive deposit do not affect much. Thence, the researchers have tested the diverse antenna structures and developed the different fabrication method on the paper substrate for the ultra-low-cost antenna. Obviously, the cost advantage for mass-production printing is the most important targeted purpose of these research works to reduce tag prices.

1.3.2.2 Wireless Local Area Network (WLAN)

In our research work, the Wireless Local Area Network is one of the required applications of the set-top-box. Therefore, the realization of the WLAN antenna on paper substrate in the bibliography is an important reference.

Konstas has presented in 2009 a "green" Z-shaped inkjet-printed monopole antenna topology on a flexible, low-cost photo paper substrate for UHF RFID tags. The paper substrate had thickness of 0.254 mm, a relative permittivity of 3.4 and a loss tangent of 0.08 with overall dimensions 75mm x 100mm, including the feed line. Monopole antenna type was utilized in his research work thank to its broadband characteristics and the use of a ground plane as an extra shield for other electronic components (sensors, power sources, IC) in the system, alleviating the cross-coupling and interference. In order to evaluate the inkjet printing technique, the same antenna was also fabricated with thin adhesive copper tape glued on the paper. Both prototypes (inkjet-printed and copper tape fabricated) showed similar resonant frequency around 900 MHz with a slight difference in bandwidth. The directivity of the inkjet-printed antenna was found 0.2dBi in the simulation. [Konstas 2009]

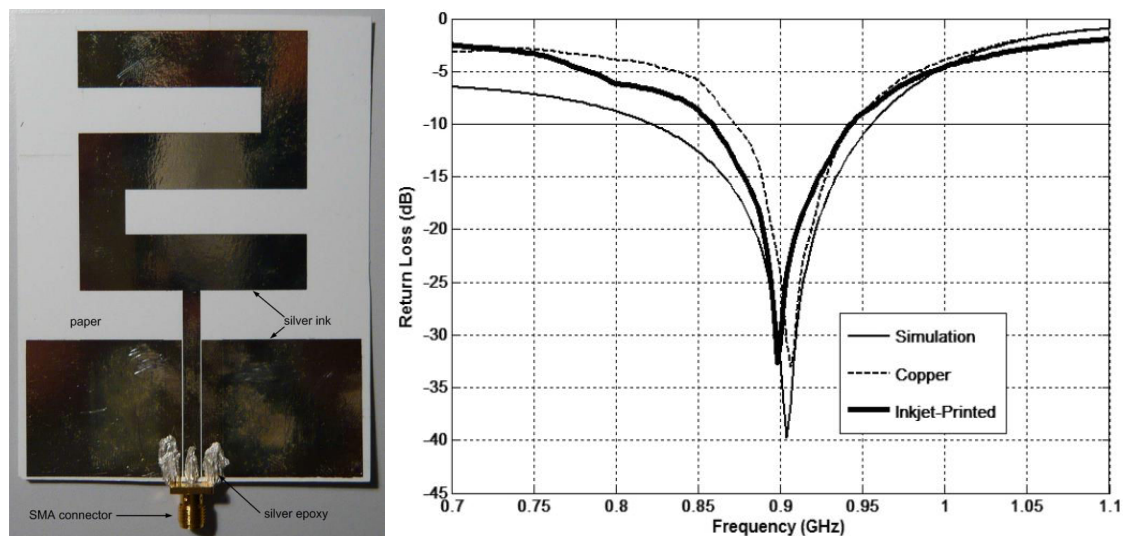


Figure 1-31: Prototype of the Z-shaped CPW-fed inkjet-printed monopole antenna on paper substrate with attached SMA connector [L]. The simulated and measured return loss of the inkjet-printed and copper-tape fabricated monopole [R]

Then, Anagnostou et al. from South Dakota School have proposed in 2010 a flexible inkjet-printed inverted-F antenna (PIFA) operating at 2.45GHz on an ultra-low-cost photographic paper substrate for WLAN and flexible display applications [Anagnostou 2010]. According to the author, although paper substrates exhibited relatively high dielectric losses ($\tan\delta \sim 0.07$), the maximum gain achieved of the fabricated antenna was 1.2 dBi and its total simulated efficiency was approximately 82% at the resonance frequency. He has also tested the flexibility of this PIFA by using cylindrical tubes with radius $R_1 = 1.25$ cm and $R_2 = 2.7$ cm both on the front side (as shown in Figure 1-33) as well as the reverse side. It was also flexed more than a thousand times in the air, for repeatability testing without failure. So, the demonstrated antenna can be easily integrated into a flexible display of a portable computer or even mobile phone. However, the limits of the flexibility and the difficulties in the realization (e.g. problem of micro-cracking during bending due to the break of the bond between the metallic nanoparticles in the ink deposit) have not been mentioned. This is considered to be the greatest difficulty for the application of printing technology in the manufacture of 3D structures and circuits on paper substrates. Therefore, there is a need to find solutions to overcome this difficulty, such as technology and material improvement, printing after folding/bending or another technical breakthrough ...

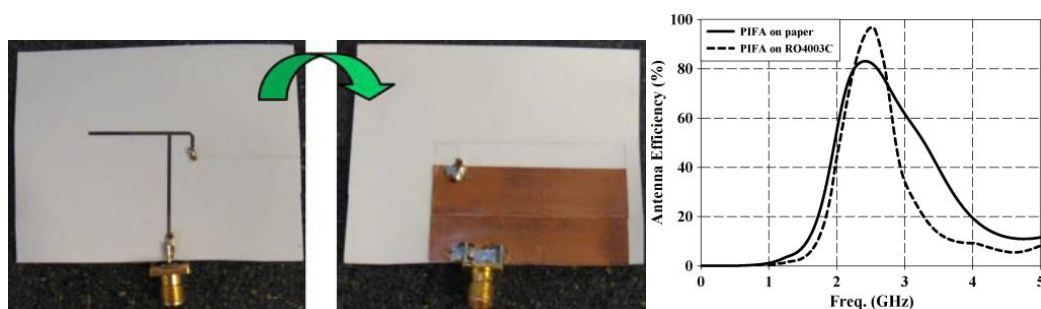


Figure 1-32: Fabricated PIFA antenna prototype on organic paper-based substrate [L]; Simulated total efficiency comparison of the antenna on paper (82%) and the antenna on a high-frequency laminate (95%) [R]

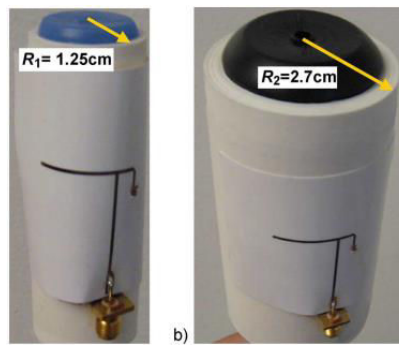


Figure 1-33: Inkjet-printed antenna on paper bent around cylindrical structures with different radii. It showed no sign of permanent deformation, conductivity deterioration (i.e. cracks) or ink detachment after extensive and repeated bending

Next, Cook et al. from Georgia Tech have developed in 2013 a 2.4 GHz meander monopole antenna on Teslin[®] paper. The meandered inductive load was used in order to shorten the overall antenna size (28% reduction in length over a standard $\lambda/4$ monopole). The two fabrication process: catalyst-based Cu deposition and inkjet printing of Ag nanoparticle ink were applied for comparison of antenna performance. Reasonably good agreement was obtained between the simulated and measured values for the fabricated Cu and Ag antennas. The demonstrated monopoles proved the feasibility of catalyst-based Cu deposition process in fabricating a variety of microwave components on flexible, paper-based substrates. [Cook 2013-1]

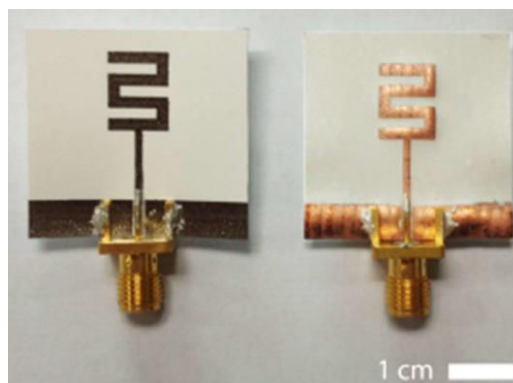


Figure 1-34: 2.4 GHz meander monopole on Teslin[®] paper fabricated by Ag inkjet printing [L] and electroless Cu deposition [R]

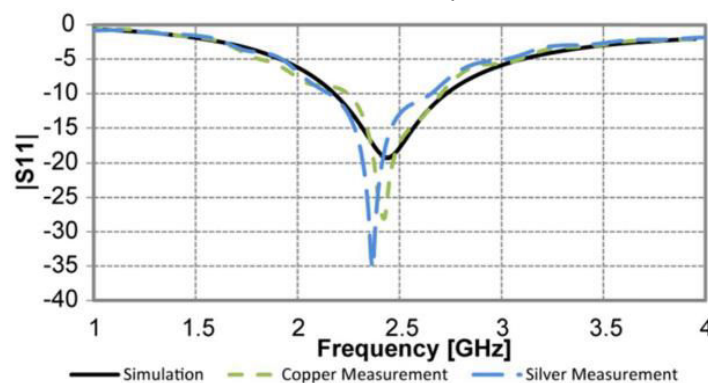


Figure 1-35: Simulated and measured insertion losses (S_{11} , dB) of the meander monopoles

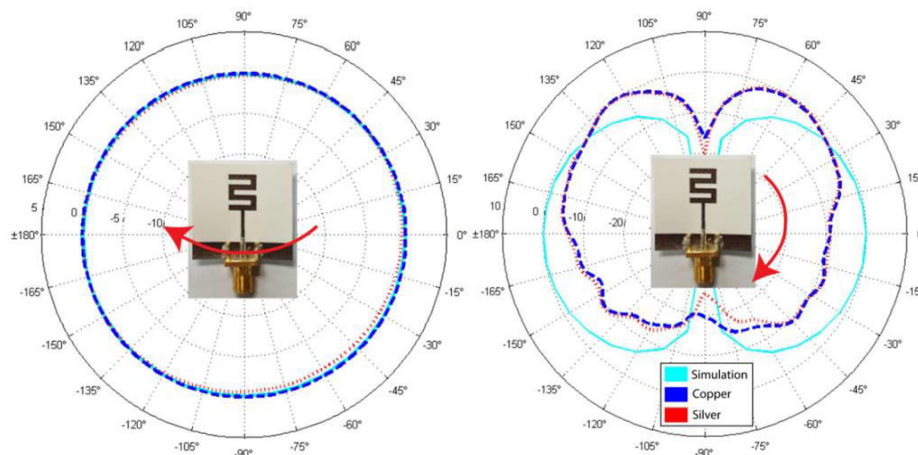


Figure 1-36: H-plane and E-plane radiation pattern obtained from simulation and measurement of the Cu and Ag monopole antennas

1.3.2.3 Ultra-wide-band or multi-frequency antenna

Multi-frequency or ultra-wide-band is an obligatory characteristic of our antenna design in order to ensure the operation of multi-standard and multi-application. Thus, some of the designs below give us ideas to implement our own antenna system.

Shaker et al. from University of Waterloo have demonstrated in 2011 a planar ultra-wideband (UWB) monopole through ink-jetting of conductive inks ($3\text{ }\mu\text{m}$ ink thickness, $\sigma = 9 \times 10^6 - 1.1 \times 10^7\text{ S/m}$) on commercially available paper sheets ($254\text{ }\mu\text{m}$ thickness, $\tan\delta = 0.06 - 0.07$) up to frequencies above 10 GHz (3-10.5 GHz). The measured pattern was almost uniform (omnidirectional) for the selected frequencies, which is ideal for many UWB applications. The antenna efficiency was better than 80% throughout the whole band. This work was expected to pave the way toward the next-generation of low-cost, environment-friendly ubiquitous UWB sensor networks. [Shaker 2011]

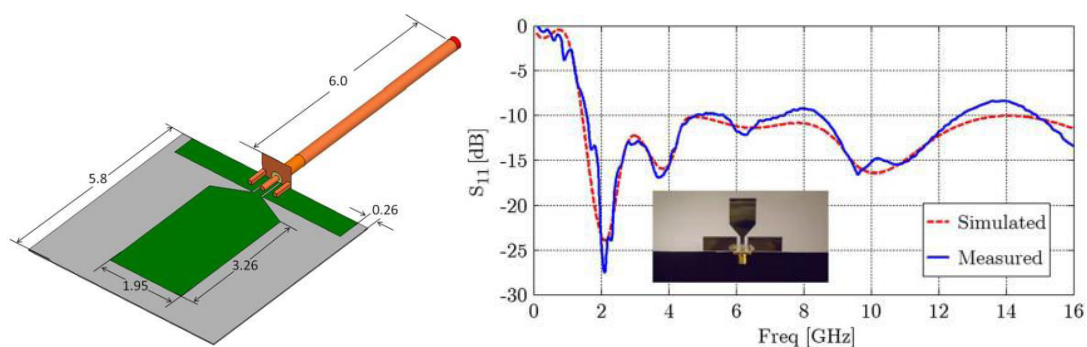


Figure 1-37: Model of the UWB monopole [L] and Simulated and measured S_{11} performance of the inkjet-printed antenna prototype [R]

Cook et al. from KAUST have developed in 2012 an UWB antipodal Vivaldi antenna (1-11 GHz), inkjet-printed ($\sigma = 1.2 \times 10^7\text{ S/m}$) on lossy paper substrate (loss tangent about 0.06). This antenna exhibited a significantly higher gain up to 7.8 dBi as compared to the others inkjet-printed antennas. His work laid a strong foundation for the fabrication of low-cost, high-gain and wideband antenna on environmentally friendly substrates using the inkjet printing process. [Cook 2012-1]

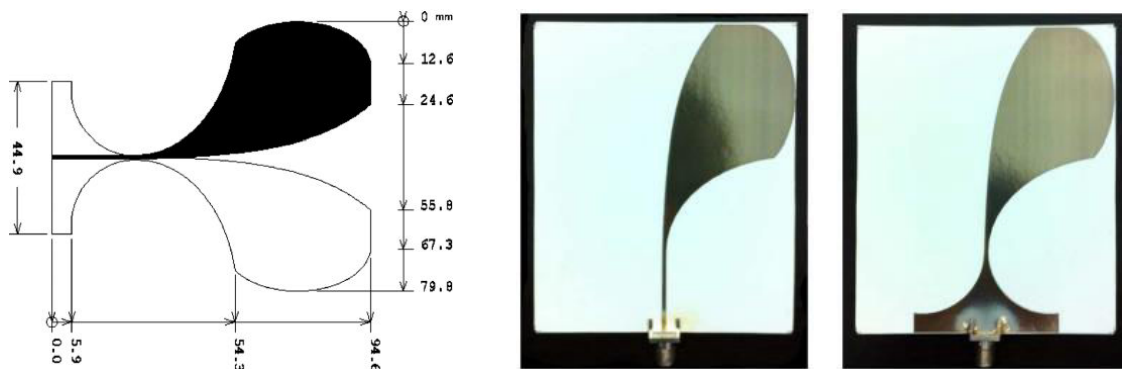


Figure 1-38: Antipodal Vivaldi design [L] and prototype fabrication on paper [R]

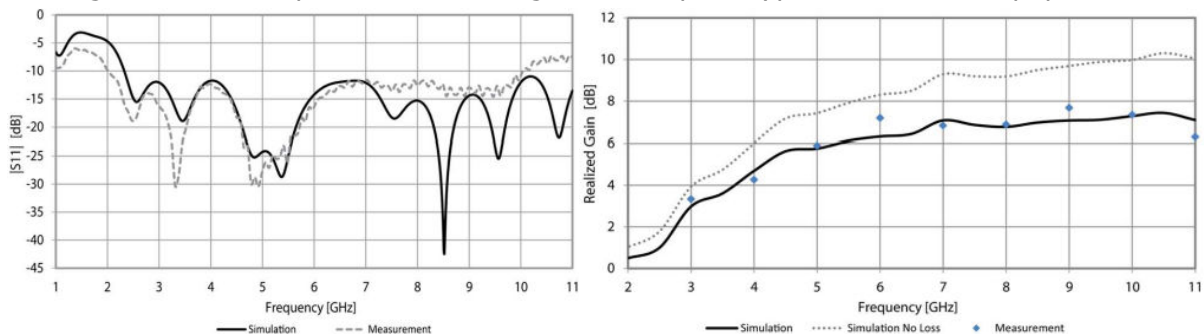


Figure 1-39: Measurement of the antipodal Vivaldi antenna with: (a) S_{11} ; (b) gain versus frequency

However, in general, these antennas have a very large size and do not meet the compact requirements in order to be integrated into our set-top-box.

Meanwhile, Abutarboush has concentrated on the development of inkjet-printed multi-frequency monopoles on paper substrate with different configurations. These antennas had almost low profile, compact size, light weight and low cost in order to integrate into small and slim wireless devices.

He has first presented a U-slot tri-band monopole antenna on a low-cost paper substrate using inkjet-printing technology with silver nanoparticle ink ($\sigma = 1.2 \times 10^7$ S/m). This compact size ($12 \times 37.3 \times 0.44$ mm³) antenna had a tri-band operation of 1.57, 3.2, and 5 GHz with measured impedance bandwidths of 3.21%, 28.1%, and 36%, respectively enough to cover the GPS, WiMAX, HiperLAN/2, and WLAN bands. The simulated radiation efficiencies were about 55%, 79%, and 71% in the 1.57, 3.2, and 5 GHz bands, respectively. The operating principle is very simple: it has three radiator branches for three resonance frequency and each branch could have a meander line configuration for the miniature purpose. [Abutarboush 2012]

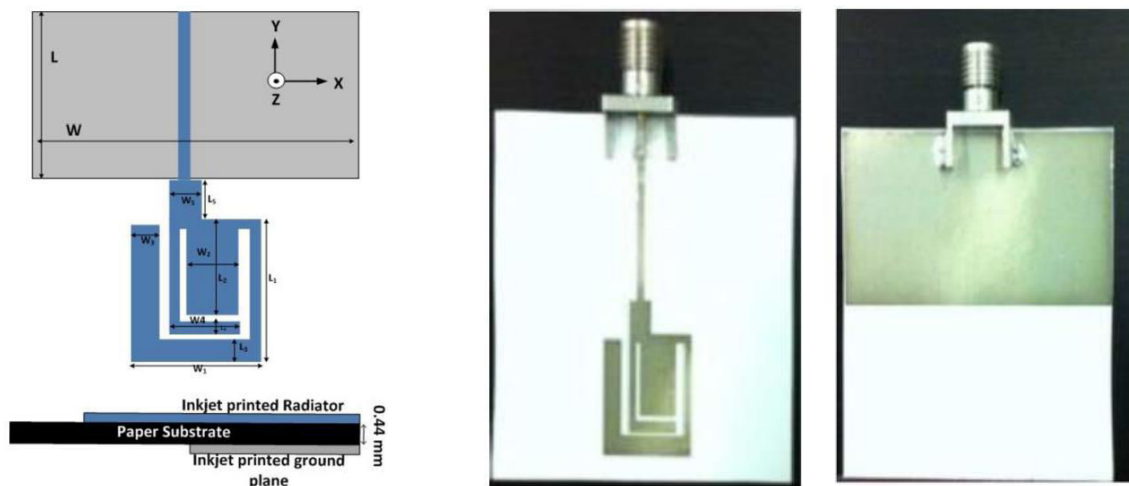


Figure 1-40: Layout [L] and inkjet-printed prototype [R] of U-slot tri-band monopole antenna

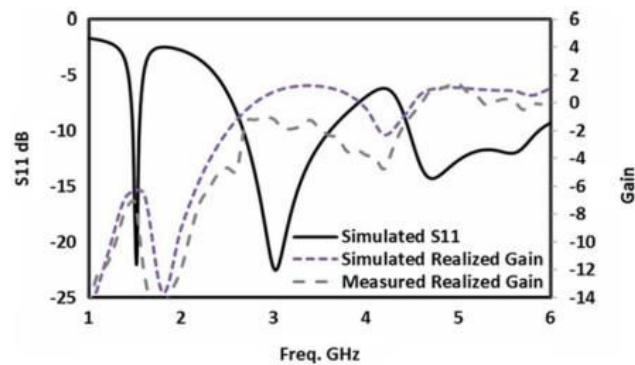


Figure 1-41: Simulated and measured S_{11} and realized gain of the proposed antenna

Then, he has proposed another wide frequency independently controlled dual-band inkjet-printed monopole for WLAN and WiMAX applications. Its operating principle is similar to the antenna above. The measured impedance bandwidths for the 2.4 and 3.4 GHz were 15.2 and 23.7%, respectively. According to the author, this was the widest independently controlled antenna in terms of bandwidth reported in the literature (148.83%). The simulated gain and efficiency of the proposed antenna were 0.5dBi and 65% at 2.4 GHz, 1.5 dBi and 80% at 3.4 GHz, respectively. [Abutarboush 2014]

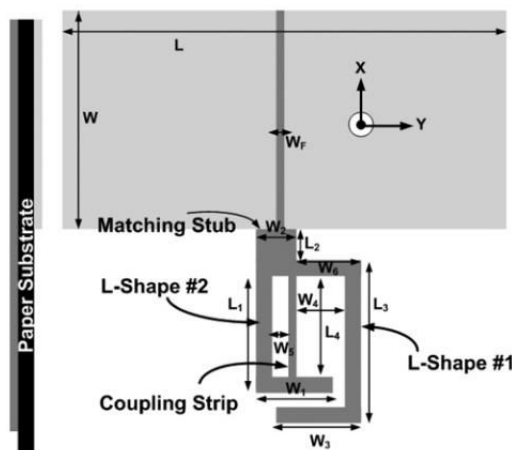


Figure 1-42: Layout of proposed wide frequency independently controlled monopole

Overall, these antennas have a simple structure and a compact size with meander line configuration. So, this kind of antenna could be stuck easily on the sidewall of our set-top-box for the wireless multimedia applications. In addition, they also feature independently controlled multi-band characteristic by tuning the dimensions of each branch.

Finally, Abutarboush has demonstrated a fabrication process for curving his inkjet-printed multi-frequency monopole, as illustrated in Figure 1-43. In order to avoid any cracking, the printed antenna was sintered after bending it to the required curvature. [Abutarboush 2015]

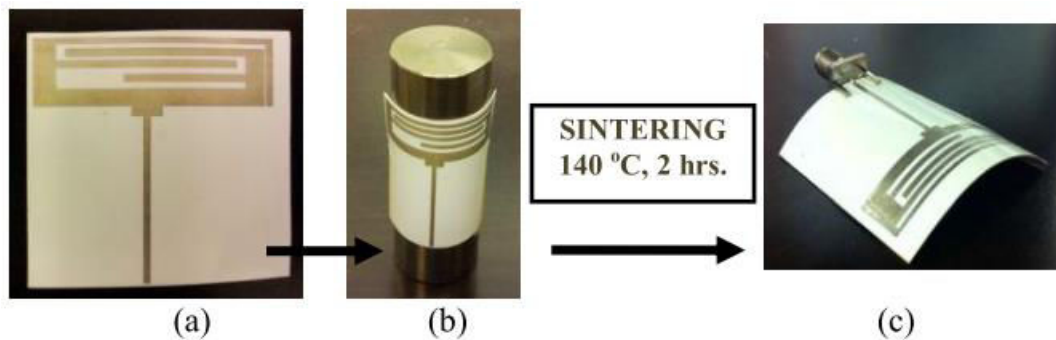


Figure 1-43: Fabrication process for the curved prototype: flat monopole was mounted on a cylindrical surface and was sintered

The author has then compared the antenna performance in two states: flat and bent. When the antenna was bent, the bandwidth was increased but the gain was dropped, meanwhile, the radiation patterns did not change much (cf. Table 1-5, Figure 1-44 and Figure 1-45).

Antenna Type	Low frequency bands	Middle frequency band	High frequency bands
Flat	Wideband 1.71–3.03 GHz	Narrow band 3.37–3.66 GHz	Wideband 4.51–5.5 GHz
Curved : 27.5 radius	Wideband 1.70–3.25 GHz	--	Wideband 4.05–6 GHz
Curved: 37.5 radius	Dual-band (1.68–2.16 GHz) (2.4–3.01 GHz)	--	Wideband 4.39–6.1 GHz

Table 1-5: Bandwidth of flat and curved antenna for $S_{11} < -10$ dB

All the results at three frequencies of 1.9, 2.4, and 5 GHz (cf. Figure 1-44) showed a monopole-shaped radiation pattern in the E-plane and an omnidirectional pattern in the H-plane. There was good agreement between the simulated and measured patterns for the flat antenna. The measured patterns for the curved antennas were quite similar to the flat case. This indicates that bending the antenna does not affect much the radiation patterns. Figure 1-45 showed that the measured peak gains of the flat and curved antennas follow the same trend. The measured efficiency of the flat antenna ranged between 45% and 58% but dropped to approximately 8% when the antenna was curved. According to the author, the curved structure in horizontal direction affects the electrical length of the resonance element in this monopole antenna, thereby slightly changing the return loss,

impedance bandwidth and gain, but the shape of the radiation pattern remains almost constant.

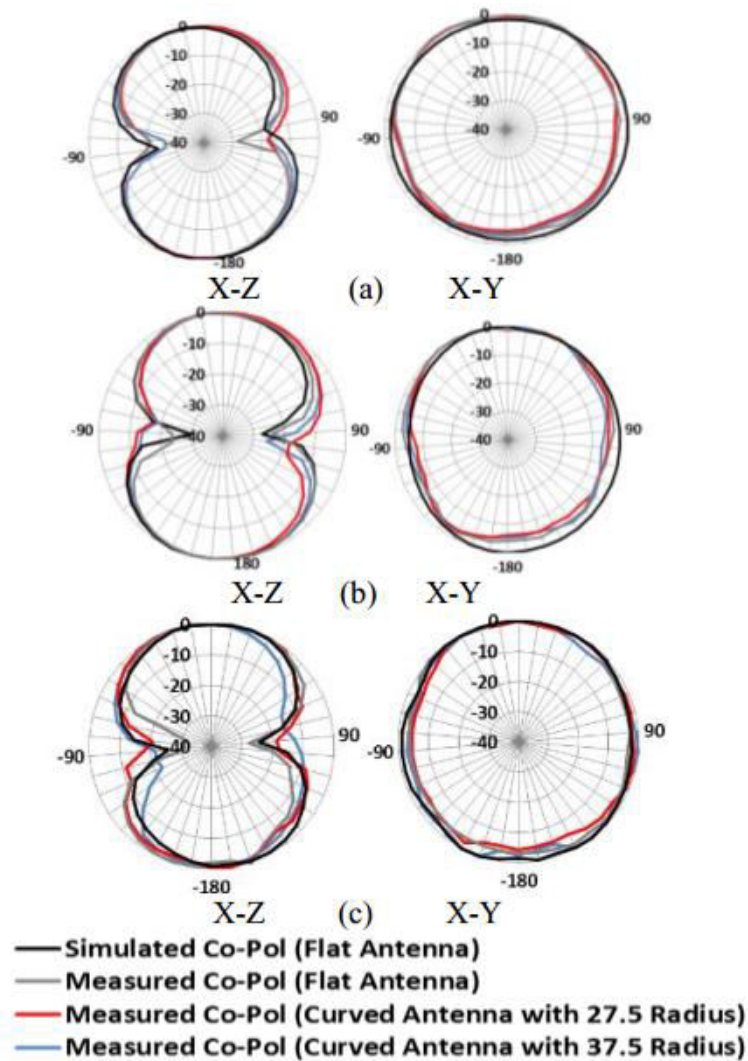


Figure 1-44: Simulated and measured co-polarization in X-Z and X-Y directions at (a) 1.9 GHz, (b) 2.4 GHz and (c) 5 GHz for flat and curved antenna

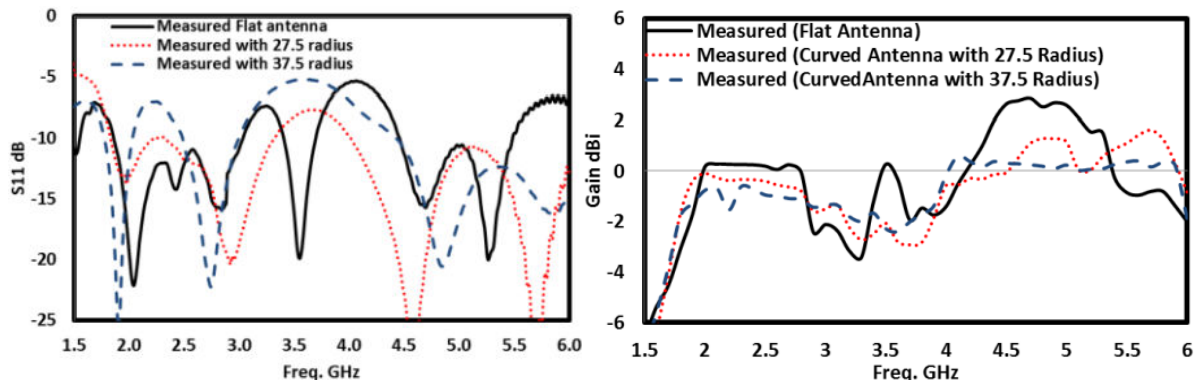


Figure 1-45: Measured S_{11} [L] and peak gain [R] for flat and curved monopole

These details about the conformal performance are quite interesting for the perspective of our research work. As we have mentioned in the context and objective, the antennas are stuck on the sidewall of the set-top-box. So, if it has a

non-planar form factor like round, oval, cylindrical ..., the antennas will be bent and operate in this curved state.

1.3.2.4 3D antenna

For miniaturization purpose, one of the most commonly proposed ideas is the implementation of 3D configurations. Thus, the antenna design could significantly reduce the occupied space in order to be integrated into the electronic box. In addition, some 3D antennas are realized to create an almost omnidirectional radiation pattern.

Monti et al. from University of Salento have presented a novel fully 3D UHF RFID reader antenna on cheap and eco-friendly substrates featuring compact dimensions, circular polarization and almost omnidirectional radiation. It consisted of four patch antennas placed on the lateral faces of a 3mm-thick cardboard cube by using adhesive copper. The ground plane on the back of the antenna worked as an electromagnetic shield for the inner volume of the cube. The diagonal slots were adopted to reduce the volume occupied by the antennas and result in a circular polarization. [Monti 2012]

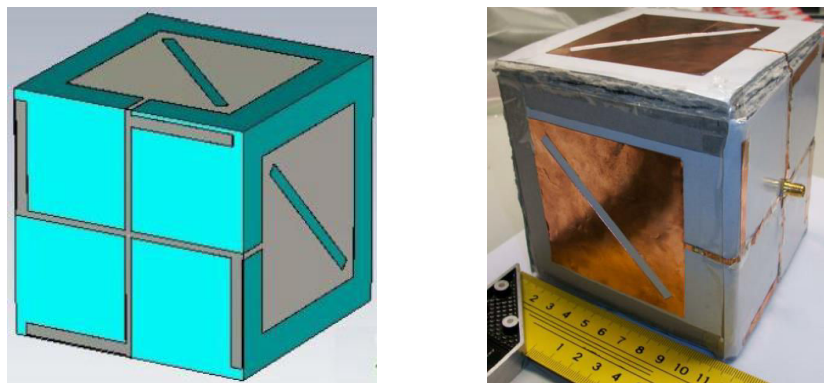


Figure 1-46: Model [L] and realized prototype [R] of cubic RFID antenna

Rida et al. from Georgia Tech have proposed a miniaturized three dimensional cubic RFID antenna to create an almost omnidirectional radiation pattern for the Real-Time Locating of automotive as well as deployment of Wireless Sensing Network (WSN) [Rida 2008]. Miniaturization was achieved by utilizing all sides of the cube and by using two dipole antennas each occupying three sides. The dipoles were inkjet-printed on a paper substrate and then were folded into a cube to realize a very small low-cost cubic RFID tag $32 \times 32 \times 32 \text{ mm}^3$. This suggests that one of the ideas for miniaturizing the antenna (in the condition that the dielectric constant of paper is hardly changeable) is the combination of meandered lines and 3D structure.



Figure 1-47: 3D RFID antenna using meander line configuration

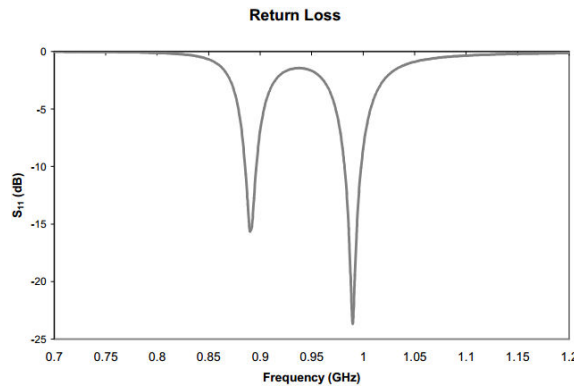


Figure 1-48: S_{11} vs. frequency for this 3D RFID antenna

Since 2014, the researchers from Florida International University have presented many 3D reconfigurable antennas on the paper substrate. Based on an origami antenna, frequency reconfigurability with multi-functionality and multi-band operation could be achieved by changing the antenna's appearance, and a more compact volume could be achieved by folding the origami antenna to save space.

Liu et al. have presented a reconfigurable axial mode helical antenna, constructed with copper foil on stretchable and lightweight paper base, which could be folded and unfolded using rigidly foldable origami structure to work at different resonant frequencies or varied purposes of wireless communications. This antenna could successfully achieve a frequency reconfigurability of 1.28 GHz with considerable gain differences. It operated at 860 MHz when unfolded and at 1.82 GHz and 2.14 GHz when folded with its height reduced by 83%. [Liu 2014-2]



Figure 1-49: Simulated model [L] and manufactured prototype [R] of the 18-steps origami helical antenna

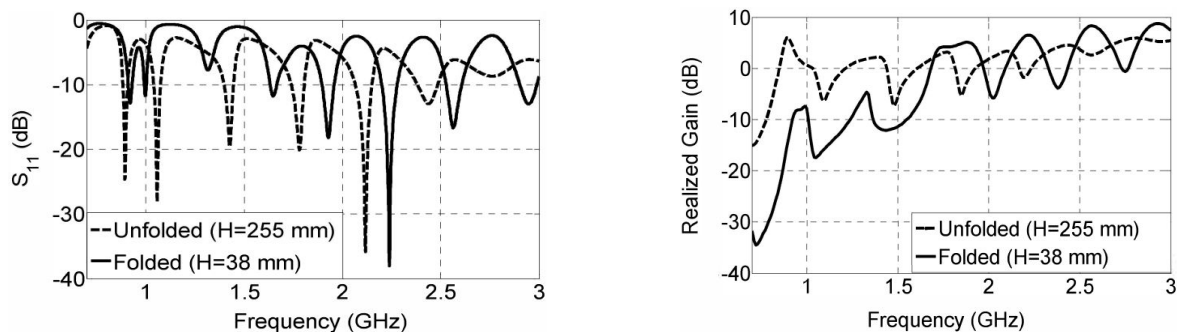


Figure 1-50: Simulated S_{11} [L] and realized gain at the axial direction [R] of folded and unfolded states

Yao et al. have proposed an origami accordion antenna structure [Yao 2014-1] and spring antenna structure [Yao 2014-2] on paper base with copper tape, which can be expanded and collapsed. So, its operating frequency could be changed based on its height.

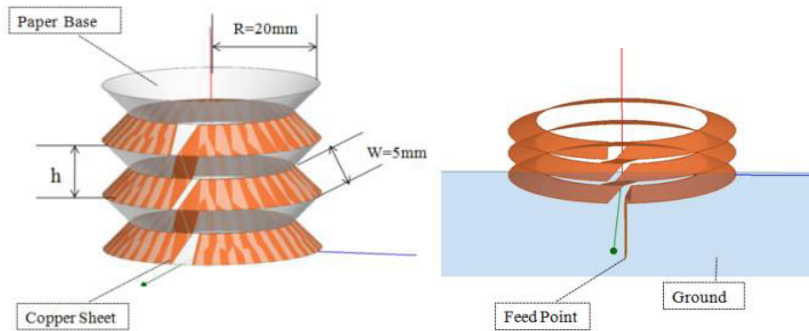


Figure 1-51: Designed origami accordion antenna [L] and its simulation model [R]

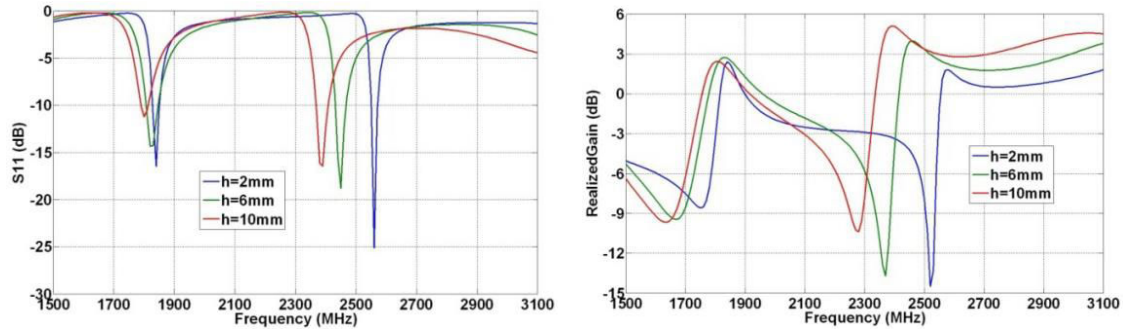


Figure 1-52: Simulated return loss [L] and realized gain [R] for different heights of accordion

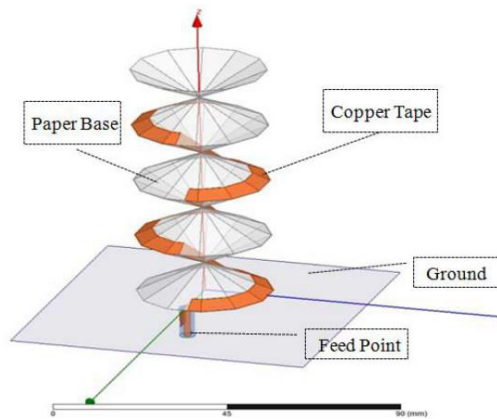


Figure 1-53: Origami spring antenna

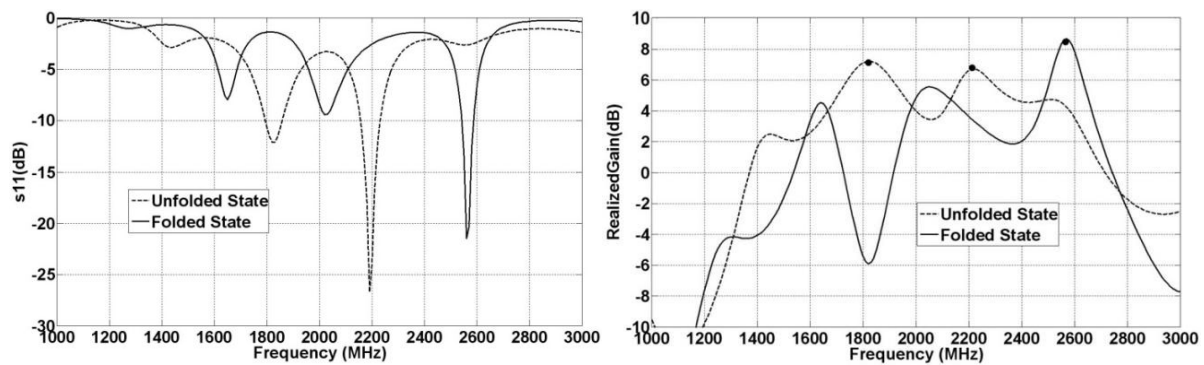


Figure 1-54: Simulated return loss [L] and realized gain [R] for unfolded and folded states

The researchers from Florida International University have not mentioned about the fabrication cost and realization time of these antennas. They have just presented their ideas about the implementation of the 3D reconfigurable antennas on flexible substrates such as paper.

In general, to perform 3D configuration, the researchers have realized the antenna in a 2D flat state, then they have folded or bent to create the new form factor. The treatment of cracks during bending, especially for the printed patterns using conductive ink, is the most difficult problem as presented in the research work of KAUST. The use of adhesive copper is not affected by this restriction, but this fabrication method can just be applied in laboratory scale to create some test prototypes and cannot be extended to mass production in industry.

1.3.2.5 Wireless sensor nodes

In this subsection, the demonstrated circuit structure is more complex, and the antenna is combined with others components in order to create the completely integrated modules on the paper substrate. Integrating sensors in the RFID tags renders the whole system capable of not only tracking but also providing real-time information about the environment. The ultimate goal is to create an easily deployable intelligent network of RFID-enabled sensors with as low-cost as possible.

Since 2006, the realization of the first highly integrated RFID-enabled wireless sensors on ultimate low-cost synthetic material such as photocopy papers has also been addressed by Vyas et al. from Georgia Tech [Vyas 2008]. The general system level design for this wireless transmitter, which used a dipole antenna for an operation of ISM (Industrial, Scientific, and Medical) frequency band at 904.4 MHz, is presented in Figure 1-55a. The complete wireless sensor system comprised a Microcontroller Unit (MCU), Phase Lock Loop (PLL) module, Power Amplifier (PA), an external crystal oscillator, a temperature sensor and a battery cell for "stand-alone" autonomous operation.

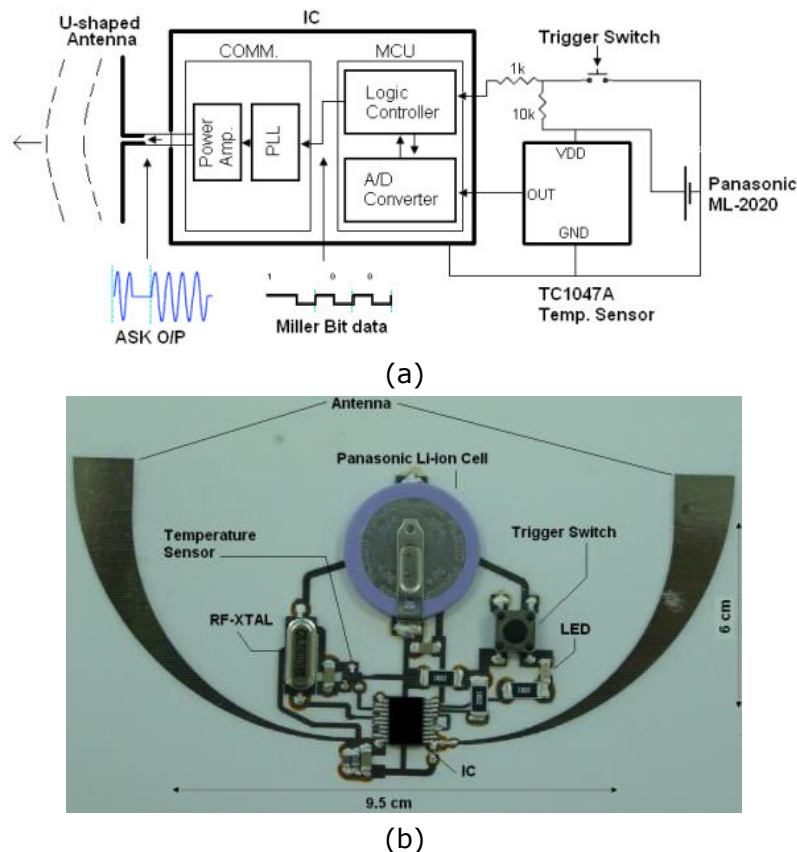


Figure 1-55: (a) System level diagram of the wireless sensor module; (b) RFID-enabled dipole-based wireless sensor transmitter using inkjet-printing on paper

This wireless sensor module prototype, as illustrated in Figure 1-55b, was printed on a 2D single-layer photo-paper (9.5 x 6 cm²). A tapering U-shaped half wavelength dipole structure was chosen for the antenna thanks to compact size and wide bandwidth. This dipole antenna and the circuit layout were inkjet-printed and cured on paper using silver ink (12 μ m ink thickness). The simulated results of the dipole antenna showed a -10dB bandwidth of 60 MHz and a maximum directivity of 1.54 dBi. All the discrete components including the IC, crystal oscillator, temperature sensor, and battery cell were assembled on the inkjet-printed traces. According to the author, the assembly process proved to be the most challenging aspect. Given the low-temperature tolerance of the paper substrate, the electronic components used, and the relatively weak adhesion of printed silver pads on paper, soldering cannot be applied. Therefore, multiple assembly methods were experimented in order to find a reliable alternative for mounting components: using of silver epoxies and conductive tapes.

Another configuration using double-layer monopole antenna of this wireless sensor transmitter module was also presented, as shown in Figure 1-56, in order to eliminate many drawbacks of the dipole-based module [Vyas 2009]. The monopole used its ground planes as a radiating surface, which could also be used to shield any circuitry behind it. The monopole antenna also did not require a differentially fed input signal like the dipole, which was more compatible with the Power Amplifier since its output was single-ended. The circuit for the monopole structure was laid out on two layers, which helped minimize the size of the circuit topology and avoid the long power supply traces used on the single-layer dipole-based

module. The top layer contained the printed antenna and most of the circuit components for the module. The bottom layer contained a battery cell and the power supply traces, which were routed to the top layer through drilled vias.

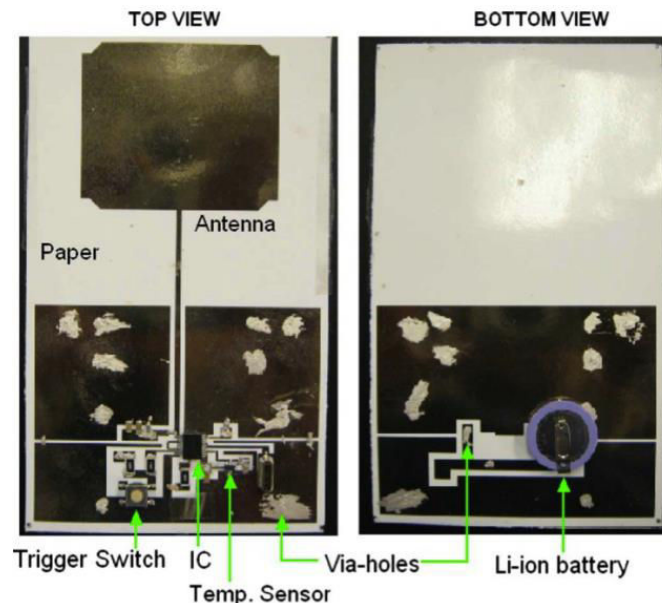


Figure 1-56: Monopole-based wireless sensor module (two layers)

The simulated return loss for the entire structure showed good wideband resonance of about 220 MHz around the design frequency of 904.4 MHz. The maximum simulated directivity obtained was 2.6 dBi. The effective isotropic radiated power (PEIRP) from the wireless sensor circuit was determined to be 4.91 dBm, which translates into a radiation efficiency of 61% for the silver nano-particle based antenna. In comparison with the previous dipole-based module, this monopole-based structure offered more wideband performance and longer read range.

According to Tentzeris, these wireless sensor modules prove the potential to be extended to a 3D multilayer paper-on-paper RFID and sensor module by laminating multi-paper sheets. This is expected to reduce significantly the cost of the sensor nodes with the increased functionality of communicating, sensing, and even information processing.

Orecchini et al. from University of Perugia have proposed in 2011 a shoe-mounted RFID tag with logo antenna operating at 433 MHz for walking energy scavenging [Orecchini 2011-1]. The extraction of electrical energy from human body movement was obtained by a piezoelectric energy scavenger which then powered up the RFID tag enough to transmit the packets of information bits to the RFID reader. The author has paid attention to both the performance and the aesthetic appearance of the antenna due to the requirement of wearable electronics. All the circuit and antenna were inkjet-printed together on a hydrophobic paper substrate and a silver epoxy was applied to fix the discrete components. This logo dipole was then bent and was stuck on the shoe. The effect of the human foot on the return loss and far-field radiation pattern of the logo antenna was also studied. The presence of the human tissue mainly caused a lower shift in the resonance frequency from around 430 MHz to 400 MHz because the tissue works partially as a dielectric substrate for the antenna [Orecchini 2011-2]. As a proof-of-concept, this autonomous inkjet-printed RFID system proved to the flexibility and reliability of the circuit realized on the paper substrate.

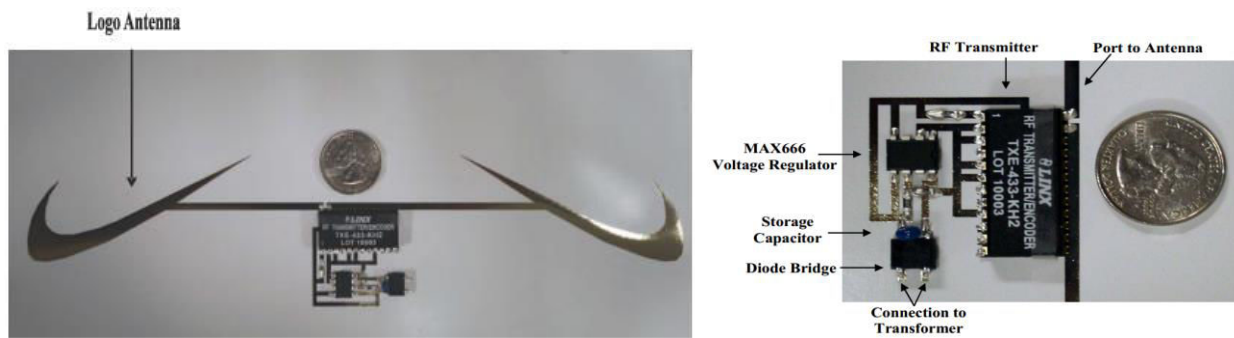


Figure 1-57: Assembled prototype showing the key components of the RFID tag packaged on a flexible paper substrate



Figure 1-58: Self-powered RFID shoe with mounted electronics

Then, Cooper has presented in 2012 a novel topology of isotropically radiating "smart cubes" for wireless sensors. He has used 3D frequency selective surfaces both for creating the desired radiation pattern and for creating a core which was electrically isolated from the antenna at the operation frequency of 900 MHz. The core allows embedding inside power source, processor, amplifier, and secondary antenna without interfering with the operation of the outside radiator. The demonstrated prototype was inkjet-printed on glossy paper using silver nanoparticles ink. The measured radiation pattern of this cube showed a quasi-isotropic radiator with less than 3 dB variance between the direction of maximum power transmission and any other direction. [Cooper 2012-2]

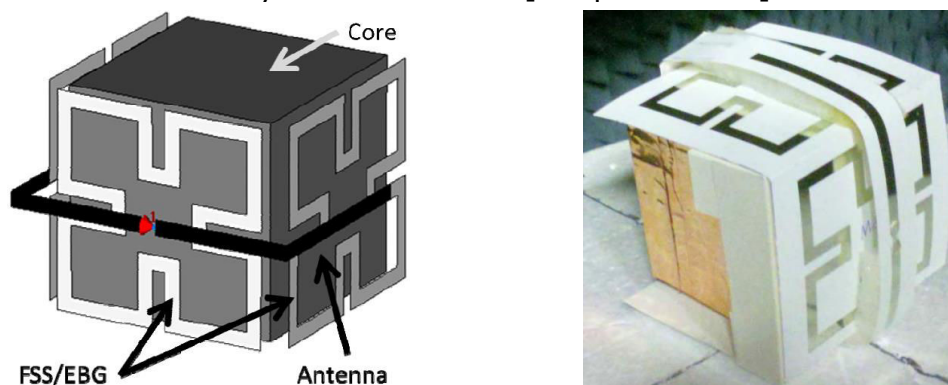


Figure 1-59: 3D RFID tag cube for wireless sensing [L] and fully fabricated prototype [R]

Farooqui et al. from KAUST have presented a 3-D (cube-shaped) sensor, inkjet printed on a paper substrate. This sensor comprised a transmitter chip and a microcontroller completely embedded in the cube, along with a dipole (operating at 2.4 GHz) implemented on all the faces of the cube to achieve a near isotropic radiation pattern. It was designed to operate both in the air as well as water (half

immersed) for real-time flood monitoring. The dipole was first inkjet-printed in 2D on Kodak photo paper using silver nanoparticle ink and then was folded in its 3D form. The printed structure was sintered after the folding and perforations using laser were realized along the crease of the cube to reduce the cracks. Then, conductive epoxy is used to fill in the cracked tracks. The 3D antennas had a maximum simulated gain of -1 dBi and the radiation pattern is near isotropic with a maximum variation of around 7 dB in the air. The measurement results confirmed that it can communicate up to 100 m in the air and up to 50 m in water with a receiver of -100 dBm sensitivity. This demonstrator was considered as a first step toward realizing all inkjet-printed, paper-based 3D electronics. [Farooqui 2014-2]

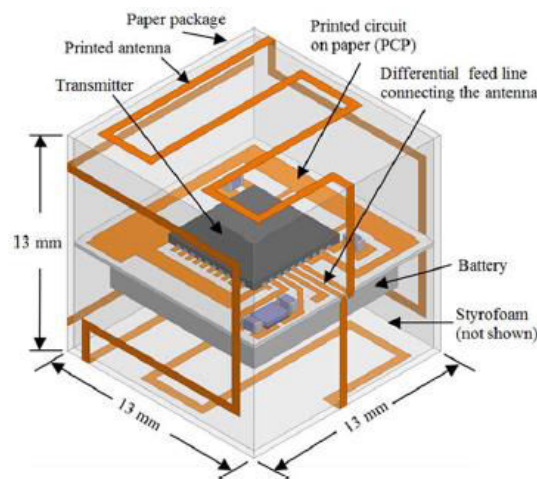


Figure 1-60: Proposed 3D sensor model inkjet-printed on paper

Next, a low-cost inkjet-printed sensor platform for agricultural application, called as SenSprout, was also proposed by Kim in 2013 in order to detect the humidity of the ambient environment, the water content in the soil and the rainfall [Kim 2013-2]. Its system level block diagram is shown in Figure 1-61a. It consisted of a leaf sensor, a soil moisture sensor, a microcontroller unit, and an antenna. The capacitances of the leaf sensor and soil moisture sensor varied depending on the humidity and water contents of the soil or near environment of the sensor platform. The microcontroller detected these capacitance variations, processed the collected data from the sensors, and broadcasted the information through the antenna. The antenna and microcontroller could also collect ambient power in order to reduce the battery usage. Whole passive components were inkjet-printed on a paper substrate, as illustrated in Figure 1-61b. The soil moisture sensor was buried in the ground to detect surface soil moisture. The leaf sensor, the microcontroller, and the antenna were exposed to the exterior environment.

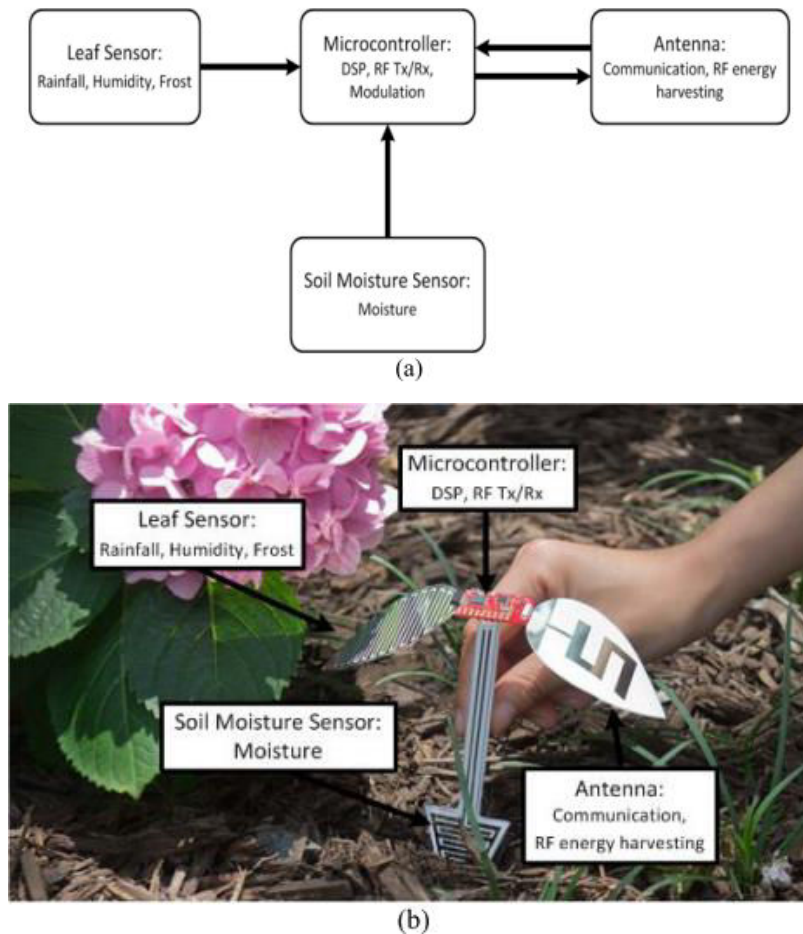


Figure 1-61: Inkjet-printed sensor platform for SenSprout agriculture application: (a) block diagram, (b) proposed design

Some of the demonstrators above like 3D "smart cubes" of Cooper or SenSprout of Kim are out of the subject of this thesis work. However, they show that a lot of complex RF circuits and systems have been studied and could be implemented on the low-cost flexible paper substrate.

1.3.2.6 Radar system

Finally, the radar application is presented as the most sophisticated system that could be realized by the researchers all over the world. Obviously, it has no relation to our research work, but I would like to show how complex the system on paper could be and the highest frequency that it could attain.

Alimenti et al. from University of Perugia have demonstrated for the first time a 24GHz Continuous Wave (CW) radar front-end, entirely realized on Mitsubishi-Electric photo-paper substrate. The whole circuit, consisting of a patch antenna array and several microstrip structures, was fabricated using a copper adhesive laminate on a single layer. The antenna array had a gain of 7 dBi and featured a half-power beam width of 42 degrees. Its efficiency was 25%, including the 1 cm long microstrip feed line. In Doppler mode, this radar was able to detect a small fan (e.g. the movement of its rotor) at 1m distance from the antenna. This contribution proves that circuits on cellulose are capable to operate up to the very high

frequency, for example herein 24 GHz, the boundary between microwave and millimeter-waves. [Alimenti 2015-1]

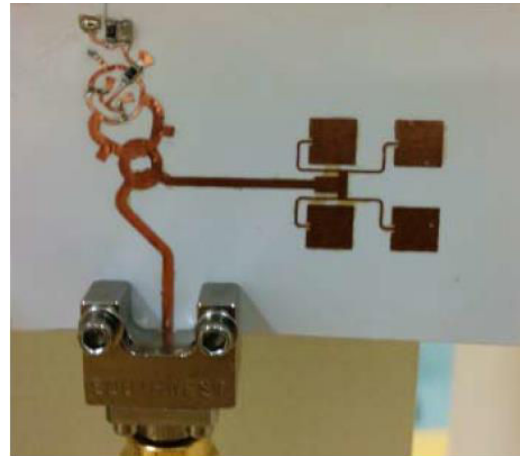
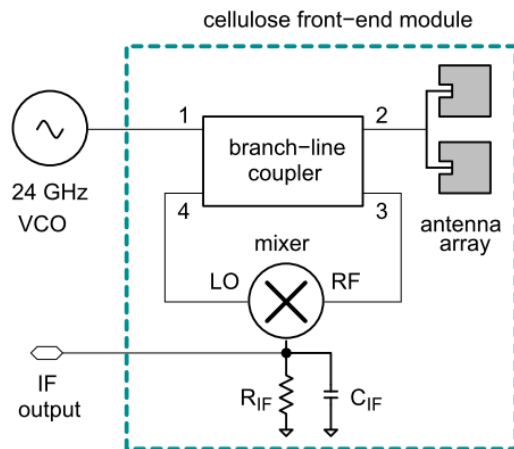


Figure 1-62: Block diagram [L] and prototype fabricated by copper adhesive on paper [R] of the 24GHz CW radar front-end

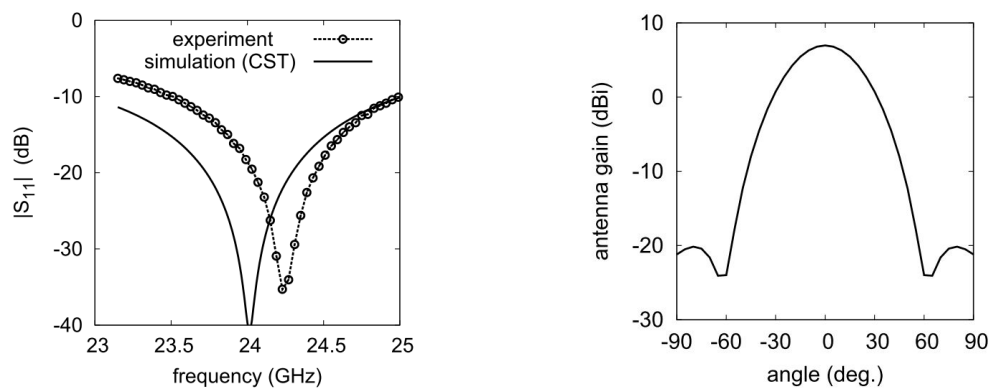


Figure 1-63: Return loss [L] and simulated radiation pattern [R] of the fabricated patch array antenna

Traille et al. from University of Toulouse have presented, in 2014, a first conformal and rollable FMCW Ground Penetrating Radar (GPR) system (at U/VHF bands) in which the passives, active components and antennas shared the same flexible substrate utilizing inkjet-printed technologies. The typical GPR systems are too bulky for backpack transportation and simple deployment during the manual wide-area measurements. Therefore, she would like to develop a new flexible radar platform providing the mechanical versatility that would facilitate geophysical studies (particularly in rugged environments such as the arctic, desert, uneven mountainous terrains). The ultra-low-cost system integration, packaging, and measurements of the entire system were also presented. It featured an almost identical and flex-independent performance for rolled and unrolled states of radar module. According to Traille, the simplicity, as well as the multilayer and multi-material capability of the additive printing process could enable the realization of highly flexible systems for wearable, biomonitoring, smart skins and geo-detection applications. The next major step is to design inkjet-printed UWB origami-based reconfigurable "accordion-shaped" antenna for this portable radar system for the purpose of size miniaturization. [Traille 2014]

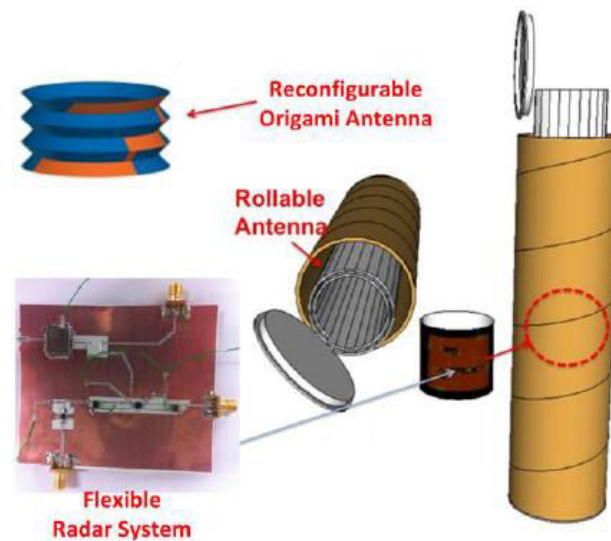


Figure 1-64: Concept of printed rollable GPR radar system

1.4 Conclusion about the state of the art and positioning of this thesis

The state-of-the-art of RF components and microwave circuits designed using paper substrates shows us that the technologies are just emerging with the last recent papers reporting on research activities and results published only about 10 years ago. We notice that paper, which holds one of the biggest market shares in the world, can potentially revolutionize the electronics market and eventually take the first step in creating an environmentally friendly first generation of truly "green" RF electronics and modules. However, all of the current ideas just stop at the design of single antenna or module integration, mostly for RFID tag and sensor applications. The key problem of interconnection to the PCB main board, as usual met when designing a whole electronic device, has never been mentioned. From the state of the art and the goal of the subject, I have determined the positioning of this thesis work as described below.

Firstly, this antenna system is mounted in a complex environment with the presence of a set-top-box, plastic sidewalls, and metallic PCB ground plane. In reality, the environment is much more complex and is highly disturbed by nearby parasitic metal parts (e.g. hard disk drive, shielding covers, heat-sinks, Ethernet/USB/HDMI/SATA connectors, cables etc.) which can impair the antennas performance. In addition, the coupling between the antennas in the system must be investigated in order to isolate them.

Secondly, the appropriate solutions are chosen for antenna structures. These antennas have a compact size in order to be easily integrated inside the set-top-box. They are also realized on paper substrate taking the advantages of low-cost, flexible, environmentally friendly properties and are fabricated by a low-cost printing process using conductive ink. These radiating elements, which exhibit multi-frequency feature (specifically dual-band antenna), have a configuration as simple as possible to be easily manufactured with the currently available technology.

Finally, the innovative flexible interconnection between antennas, feed lines, and PCB mainboard is also the key problem for the antenna integration in this electronic box. So, one of the most difficult challenges addressed in this thesis work is the implementation of low-cost low-loss feeding networks for antennas systems on flexible supports. In the configuration of RF sticker, antenna systems along with their feed lines are printed on the same paper sheet for low cost and flexible purpose. And the breakthrough solution for direct interconnection to the PCB mainboard without using the expensive coaxial cable is presented as one of the originalities of this thesis work.

Comparing with the state of the art above, it is obvious to see that such a demonstrator with all of these points has not yet existed in the literature and has never been developed. So, this is the originality of the thesis work that I have pursued.

In summary, the key points of my thesis are:

- Development of a "metallized paper" technology.
- Validation/ utilization of this technology through basic radiating elements.
- Extension to the integration of complete antenna systems.

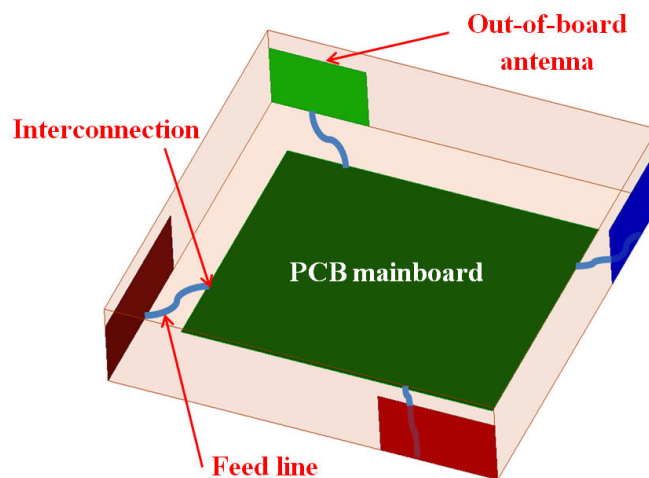


Figure 1-65: Illustration of antenna systems having direct interconnections with the PCB mainboard

Chapter 2: Characterization of flexible substrate and conductive layer

Principal content

2.1	Introduction.....	52
2.2	Dielectric characterization of flexible substrate	52
2.2.1	State of the art.....	52
2.2.2	Realized method	65
2.2.3	Discussion	73
2.2.4	E4D paper.....	75
2.3	Characterization of conductive layer.....	76
2.3.1	SEM image of ink deposit surface.....	77
2.3.2	Printing process on paper	79
2.3.3	Measurement of thickness and conductivity of ink deposit.....	86
2.4	Conclusion of chapter 2	88

2.1 Introduction

The flexible materials such as paper or polymer, which are produced in the commercial market, are not intended for use in radiofrequency applications. So, it is easy to understand that the performance of RF components and circuits fabricated on these flexible substrates will not be as perfect as on traditional substrates like FR4[®], Rogers[®] ... However, due to the new trend of electronic devices as well as the tastes of consumers, nowadays, they are being researched and developed more and more to create a new generation of smaller, lighter and more compact products. In order to design and manufacture the RF components (antenna, filter ...) and circuits on these special and unusual substrates, it is necessary to understand their electromagnetic properties. Therefore, firstly, the characterization of the material, as well as the associated metallization, becomes a must to have the thorough knowledge about their characteristics.

In this chapter, I will present the characterization process of the flexible substrate like paper along with the associated conductive layer. First, a state of the art of the dielectric characterization method will be introduced. Then, the method that we have applied will be described in detail. Next, I will talk about the printing method that we have adopted for the metallization. Finally, the measurement of thickness and conductivity of the ink deposit will be also mentioned.

2.2 Dielectric characterization of flexible substrate

There are many different paper and polymer materials available on the commercial market. Their electrical properties vary to a large extent, depending on density, coating, thickness, composition, texture. Each has its own RF characteristics: relative dielectric constant and loss tangent. Therefore, for an optimal RF performance of electronic components such as antennas, filters ... fabricated on these special and unusual substrates, we need to know as precisely as possible their properties. And thus, substrate material characterization through the measurement of dielectric constant and dielectric loss is the critical step that must be qualified for utilization of new material in a wide range of frequency domain application.

2.2.1 State of the art

The characterization of a very thin, soft and flexible substrate such as paper is not easy because it is too thin to insert into measurement systems (thickness of about several hundred of micrometers) and the accuracy of the results is also a critical problem. Therefore, just a few of the classical methods that are suitable for flexible paper substrate have been used in the literature. These characterization methods can be classified into two main kinds: non-resonant (two planar transmission lines) and resonant (ring resonator, T-resonator, cavity resonator). Each method has its own advantages and limitations, as presented hereafter.

2.2.1.1 Two planar transmission lines

This method was applied by Saghlatoon at University of Tampere to extract the high-frequency properties of the cardboard substrate [Saghlatoon 2014]. In this method, two identical 50 Ω microstrip lines with different lengths are implemented on the same test substrate. The effective permittivity (ϵ_{eff}) of the substrate can be

obtained from the phase difference of the signals, and the loss tangent is acquired from the insertion loss. It is not necessary to de-embed the effect of SMA connectors and junctions because all the calculations are based on the transmission line length difference, which effectively removes these parasitic effects. Using (2-1) and (2-2), the effective permittivity and total loss can be calculated, respectively:

$$\epsilon_{eff} = \left(\frac{\Delta\theta \times c}{2\pi f \times \Delta l} \right)^2 \quad (2-1)$$

$$\alpha [dB/m] = \frac{|S_{21}^{long}| [dB] - |S_{21}^{short}| [dB]}{\Delta l} \quad (2-2)$$

where c is the free-space speed of light, $\Delta\theta$ is the phase difference of the output signals for the long and the short lines, f is the frequency, and Δl is the length difference between the two microstrip lines.

The total losses are the sum of dielectric losses, conductor losses, and radiation losses. The radiation losses are very low and can be neglected from the calculations because there are no discontinuities on the short and straight transmission line. Therefore, by knowing the total losses and conductor losses, the dielectric losses and then the loss tangent can be determined.

The conductor losses of a transmission line can be obtained using:

$$R_s = \sqrt{\frac{\omega\mu_0}{2\sigma}} \quad (2-3)$$

$$\alpha_c = \frac{R_s}{Z_0 w} \quad (2-4)$$

where ω is the angular frequency, σ is the conductivity of the conductor, Z_0 is the characteristic impedance of the line, and w is the width of the microstrip line. Then, the loss tangent can be obtained using (2-5) which is valid for microstrip lines:

$$\tan \delta = \frac{\alpha_d \times 2\sqrt{\epsilon_{eff}} (\epsilon_r - 1)}{K_0 \epsilon_r (\epsilon_{eff} - 1)} \quad (2-5) \quad [\text{Saghlatoon 2014}]$$

where α_d is the dielectric losses, ϵ_r is the relative permittivity of the substrate, ϵ_{eff} is the effective relative permittivity of the substrate, and K_0 is the phase constant in free space:

$$K_0 = \frac{2\pi}{\lambda_0} = \frac{2\pi}{\lambda_g \sqrt{\epsilon_{eff}}} \quad (2-6)$$

Three 50Ω microstrip lines with 15-, 10-, and 5-cm lengths were realized on the surface of Stora Enso cardboard utilizing a 50-μm-thick and 2-mm-wide copper tape with bulk conductivity of 5.8×10^7 S/m for dielectric characterization from 500 MHz to 3 GHz. For higher measurement reliability, S-parameters for the three different lengths were compared one by one utilizing a two-port vector network analyzer (VNA).

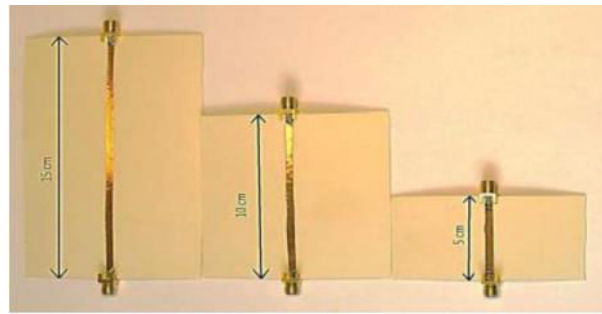


Figure 2-1: Implemented copper-tape microstrip lines on cardboard

The results for the average permittivity and loss tangent of the substrate were depicted in Figure 2-2 below. Saghlatoon has also measured the relative permittivity and loss tangent using Agilent 85070 Dielectric Probe Kit in the same frequency interval for comparison (This non-destructive method is one of the frequently used technique to measure lossy materials at high frequencies, but it shows some deflection for the low permittivity materials and the errors, which can be caused by air gaps formed between the probe and the tested material). The results were in a sufficiently good agreement between two characterization methods.

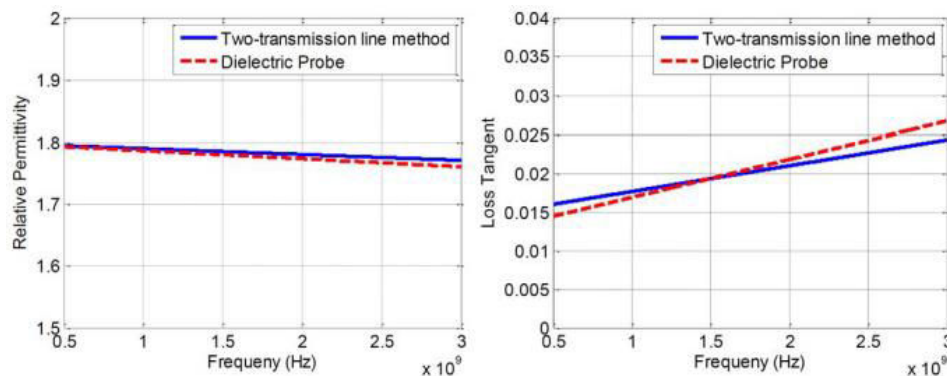


Figure 2-2: Measured properties of cardboard: (a) Relative permittivity, (b) Loss tangent

This method using two transmission lines is simple to measure thin materials. But if there are impedance mismatches due to discontinuities between the microstrip line and two connectors at both ends, the application of this method will give the incorrect results. Its accuracy depends also on the phase difference $\Delta\theta$ of the signals, the length difference Δl and the influence of the adhesive layer in copper tape. According to [Riedell 1989], this method gives an error of about 10% for ϵ_r and 25% for $\tan\delta$ in the frequency band 200 MHz - 2 GHz when tested on FR4 materials.

2.2.1.2 Microstrip ring resonator

This method was initially proposed by Georgia Tech in [Yang 2007-1] for determining RF characteristics of a hydrophobic coating paper (thickness of a single sheet: $260 \pm 3 \mu\text{m}$). The ring resonator produces S_{21} results with periodic frequency resonances. In this method, relative permittivity ϵ_r can be extracted from the location of the resonances of a given radius ring resonator, while loss tangent $\tan\delta$ is extracted from the quality factor at the resonance peak positions along with the theoretical calculations of the conductor losses.

ε_{eff} is a function of the ring radius r_m , the n th resonant frequency $f_{0,n}$ obtained from measurement of the insertion loss, and the speed of light in vacuum c , as defined in (2-7) as follows:

$$\varepsilon_{eff,n} = \left(\frac{n \times c}{2\pi \times r_m \times f_{0,n}} \right)^2 \quad (2-7) \quad [\text{Yang 2007-1}]$$

Then, the relative permittivity ε_r can be extracted from the effective relative permittivity ε_{eff} and the dimensions of the microstrip.

With a weak coupling achieved by the air gaps between the microstrip ring resonator and their feed lines, the unloaded quality factor Q_0 is calculated from the insertion loss (LA) and the -3dB bandwidth measured at the resonant frequency f_0 using (2-8) as follows:

$$Q_0 = \frac{f_0}{BW_{-3dB} \times (1 - 10^{-L_A/20})} \quad (2-8)$$

The total attenuation in the resonator is obtained from its unloaded quality factor Q_0 given in (2-9) as follows:

$$\alpha_{total,n} = \frac{\pi \sqrt{\varepsilon_{eff,n}}}{Q_0 \lambda_{0,n}} \quad (2-9)$$

Then, the attenuation due to the dielectric α_d was extracted by subtracting the attenuation due to the conductor α_c and radiation α_r from the total attenuation α_{total} that occurs in the structure at the resonant frequencies. According to the author, the ring attenuation due to radiation, calculated using [Pauw 1977] and [Abouzahra 1979], was found to be negligible, and therefore ignored in this computation. And, the attenuation in the rings due to conductor losses was computed using formulas given in [Zou 2002].

The loss tangent of the paper substrate is a function of only the attenuation due to the dielectric α_d at the resonant frequency and is computed using (2-10) as follows:

$$\tan \delta = \frac{\alpha_{d,n} \times \lambda_{0,n} \times \sqrt{\varepsilon_{eff,n}} (\varepsilon_{r,n} - 1)}{8.686 \times \pi \times \varepsilon_{r,n} (\varepsilon_{eff,n} - 1)} \quad (2-10) \quad [\text{Yang 2007-1}]$$

where λ_0 is the wavelength of the free-space radiation from the rings at the resonant frequencies, α_d was extracted by subtracting the attenuation due to the conductor α_c and radiation α_r from the total attenuation α_{total} that occurs in the structure at the resonant frequencies.

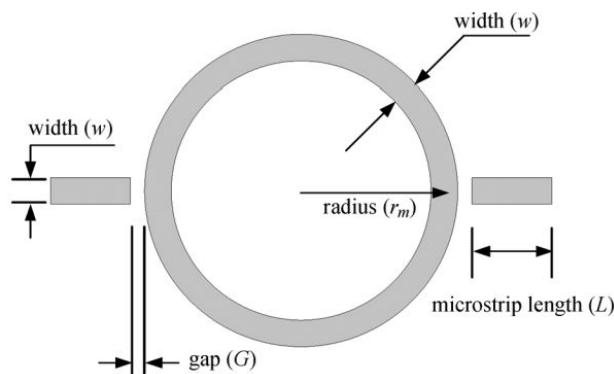
With the aim of verifying the loss tangent values, Yang has also utilized a transmission line (TL) method. A 50Ω microstrip line was fabricated on the same paper material. Simulation results for conductor and radiation losses α_c and α_r , respectively, of the microstrip lines were subtracted from the total losses α_{total} . This

was done by simulating a microstrip line with no dielectric losses in HFSS and extracting α_c and α_r , then subtracting these effects from the total measured losses.

The layout of the microstrip ring resonator is shown in *Figure 2-3*. In order to avoid a significant influence of curing temperature and duration time on the conductivity of the ink deposit and to de-embed the conductive losses of the microstrip circuit, a copper foil was selected as the metallic material heat-bonded on both sides of the paper substrate following by etching process.

Two microstrip ring resonators (Ring A & Ring B) were designed and fabricated on three and nine sheets of the paper substrate, respectively to investigate the sensitivity of the results to the paper thickness.

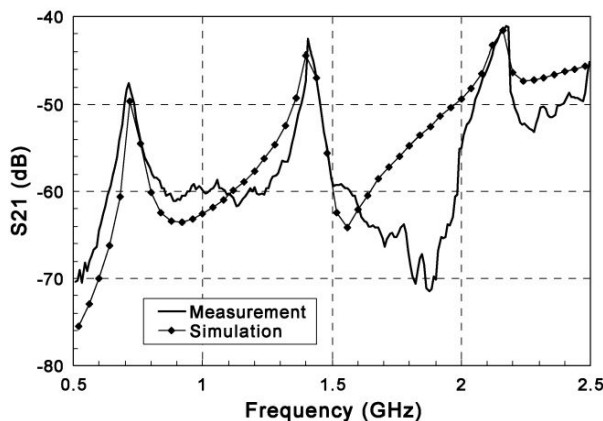
The effects of the input and output feed lines were de-embedded using the thru-reflect-line (TRL) calibration on the TRL lines that were designed to be a quarter-wavelength long at different frequencies over the range of measurement 0.5 – 5GHz. A reference plane was set at the edge of the coupling gap to the resonator. Therefore, only the response of the resonating ring element was effectively measured.



	Ring A	Ring B
Radius of Ring (r_m)	40 mm	39.7 mm
Line Width (w)	7.46 mm	1.6 mm
TRL 1	11.467cm	6.515 cm
TRL 2	9.429cm	4.886 cm
TRL 3	6.288cm	2.44 cm
TRL 4	5.257cm	1.626 cm
TRL 5	3.568cm	1.218 cm
TRL Open	1.58cm	1.03 cm
TRL Short	3.26cm	2.06 cm

Figure 2-3: Microstrip ring resonator configuration diagram [Yang 2007-1]

The peak positions, 3-dB bandwidth, and insertion loss at the resonant frequencies were shown in *Figure 2-4*.



	Resonant Modes	Resonating Freq. (MHz)	BW _{-3dB} (MHz)	Insertion Loss (dB)
Ring A	N=1	711.5	42.4	47.1
	N=2	1408	27.29	42.5
	N=3	2173	64.8	41.1
Ring B	N=1	736.3	56.97	63.2
	N=2	1490	93.92	57.2
	N=3	2243.7	153.3	64.5

Figure 2-4: Measured and simulated S_{21} of the ring resonator configuration A. Peak positions and -3dB bandwidth at the three resonant frequencies were used to extract the relative permittivity and the loss tangent of the paper substrate

The values of the relative permittivity extracted at the three resonating modes' frequencies for each ring resonator were shown in *Figure 2-5a*. The lowest value

obtained was 3.2 and the highest was 3.5 in the range of 0.5–2.5 GHz with a slight decrease with increasing frequency. Lower ϵ_r is expected at a higher frequency band, as verified by the cavity resonator measurements in [Yang 2007-2]. The uncertainty in ϵ_r comes from the errors in measurement of the ring resonator dimensions, sample thickness, and resonant frequency. Linear regression analysis was applied to estimate the confidence interval of results under the rule of least squares [Kutner 2005]. The corresponding error bar was also plotted in Figure 2-5a.

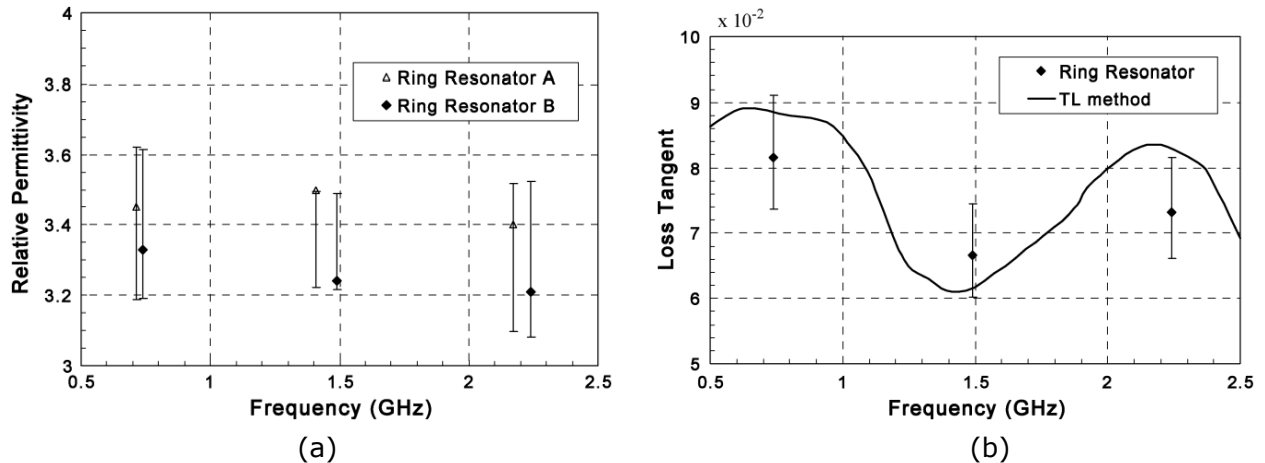


Figure 2-5: (a) Extracted relative permittivity of paper at the resonant frequencies; (b) Paper loss tangent versus frequency measured with the microstrip ring resonator method and TL method.

The loss tangent extracted from ring B at three different resonating frequencies was shown in Figure 2-5b above. It showed values between 6×10^{-2} and 8×10^{-2} . According to the author, the uncertainty of the measured quality factor Q_o is the major error source of loss tangent. If other uncertainties such as resonant frequency are neglected, the uncertainty in $\tan\delta$ can be calculated from the uncertainty in the measured Q_o . For these sets of measurements, a 10% uncertainty in measured Q_o was assumed. The calculated uncertainty in $\tan\delta$ was also shown in the error bar in Figure 2-5b.

The average values of the measured relative permittivity (3.2) and the loss tangent (7.7×10^{-2}) were then adopted in the full-wave HFSS simulation. A good agreement in terms of resonant peak positions between measured and simulated results is shown in Figure 2-4.

This method is relatively effective and accurate for characterization of flexible substrates like paper (error of $\epsilon_r < 9\%$ and error of $\tan\delta < 14\%$ in the frequency range of 0.5 – 2.5 GHz). However, there are some uncertainties in ϵ_r (due to errors of the ring resonator dimensions, sample thickness, and resonant frequency) and in $\tan\delta$ calculation (due to the measured quality factor Q_o and the ignoring of the radiation losses). In addition, the difficulty in the controlling of coupling gap in the ring resonator has not been mentioned.

2.2.1.3 T-resonator

This method was applied by Cook at KAUST and then at Georgia Tech to characterize a standard commercial photo paper [Cook 2012-1]. The microstrip T-

resonator is a transmission line with an open circuit stub, as shown in *Figure 2-6*. It has a null in the insertion loss when the reflected wave from the stub is 180° out of phase with the incident wave, which occurs when the value of the stub length corresponds to $\lambda_g/4$ (at the resonant frequency). The effective permittivity (ϵ_{eff}) of the substrate was determined by (2-11) below via the length of the open circuit stub and the resonance frequencies. [Latti 2007]

$$f_{r,n} = \frac{nc}{4(L + L_0)\sqrt{\epsilon_{eff,n}}} \quad (2-11) \quad [\text{Cook 2012-1}]$$

where n is the resonance mode (i.e. $n = 1, 3, 5 \dots$), c is the speed of light in free space, L is the length of the open circuit stub, L_0 is the correction factor for the fringing capacitance at the end of the stub.

This effective permittivity ϵ_{eff} can then be related to relative permittivity ϵ_r .

The loss tangent of the substrate, $\tan\delta$, was obtained from the quality factor Q , associated with the primary and higher order resonances. The loaded Q-factor, $Q_{l,n}$ (i.e. the Q obtained without removing the load due to connected measurement equipment), was calculated using (2-12).

$$Q_{l,n} = \frac{f_{r,n}}{BW_{-3dB,n}} \quad (2-12)$$

The $Q_{l,n}$ value was then converted to the unloaded Q-factor, $Q_{ul,n}$, using (2-13), where $BW_{-3dB,n}$ refers to the -3 dB bandwidth of the n th mode and L_a is the insertion losses (in dBs) at the corresponding resonance n . [Latti 2007]

$$Q_{ul,n} = \frac{Q_{l,n}}{\sqrt{1 - 2 \times 10^{L_a/10}}} \quad (2-13)$$

The unloaded Q-factor, $Q_{ul,n}$, was then inserted into (2-14) to obtain the total losses, $\alpha_{tot,n}$ (in dB/m).

$$\alpha_{tot,n} = \alpha_{c,n} + \alpha_{d,n} + \alpha_{r,n} = \frac{8.686\pi \times f_{r,n} \times \sqrt{\epsilon_{eff}}}{c \times Q_{ul,n}} \quad (2-14)$$

The value of dielectric losses, $\alpha_{d,n}$, was obtained by subtracting the value of the conductor losses, $\alpha_{c,n}$ (calculated through Agilent's Line-Calc software), from the total losses, $\alpha_{tot,n}$, and ignoring the radiation losses, $\alpha_{r,n}$ (which should be quite small over the measured frequency range [Markovic 2007]). The value of the loss tangent, $\tan\delta$, was then calculated from (2-10) at each resonance frequency $f_{r,n}$.

This T-Resonator was fabricated on a cellulosic substrate formed by two layers of paper bonded together using an Ingstrom at 80°C and 300 N. The increase of substrate thickness allowed for an enhanced precision of permittivity and loss tangent extraction because wider microstrip lines were required to produce 50Ω impedance hence the edge roughness effect was minimized. Then, the T-Resonators were inkjet-printed using five layers of ink to ensure high conductivity (each ink layer was laser sintered before printing the next layer). SMA connectors

were mounted using a conductive silver epoxy. To de-embed the effects of the mounted connectors, thru-reflect-line (TRL) calibration microstrip lines were fabricated using the same parameters as the T-Resonator.

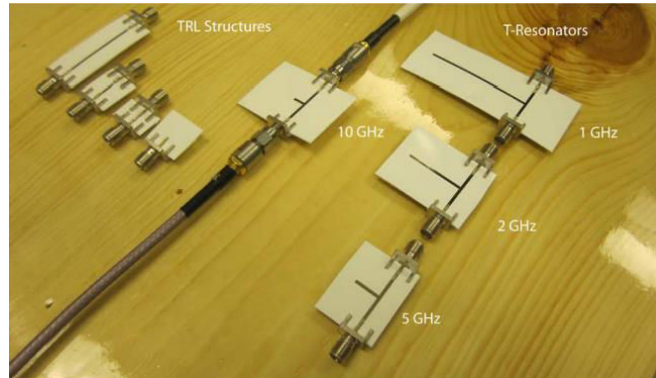


Figure 2-6: Fabricated T-Resonators and TRL calibration lines [Cook 2012-1]

The results yielded a relative permittivity of near 3.3 at 1 GHz which decreased to 2.8 near 10 GHz, as shown in Figure 2-8a. The loss tangent, which was shown in Figure 2-8b, had average value of 0.06 over the frequency range.

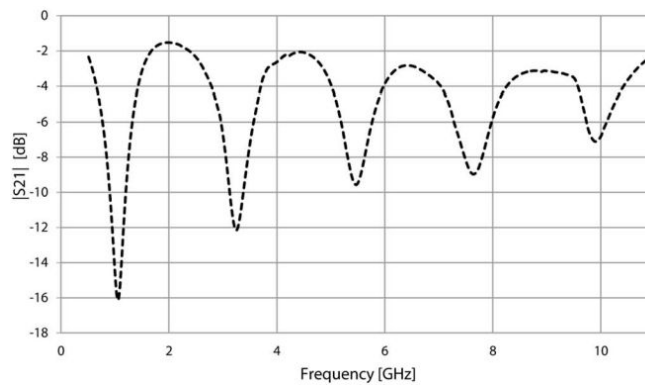


Figure 2-7: Measured S_{21} of the 1 GHz T-Resonator

To validate the 1 GHz T-Resonator measurements, resonators for 2, 5, 10, and 12.5 GHz were printed as well and the first resonance of each resonator was used to compare the extracted permittivity with that of the 1 GHz T-Resonator. The results were displayed along with the results from the 1 GHz resonator in Figure 2-8a. As shown, the first resonant modes of the 2, 5, 10, and 12.5 GHz resonators revealed the permittivity values very close to those given by the n th resonant mode of the 1 GHz resonator.

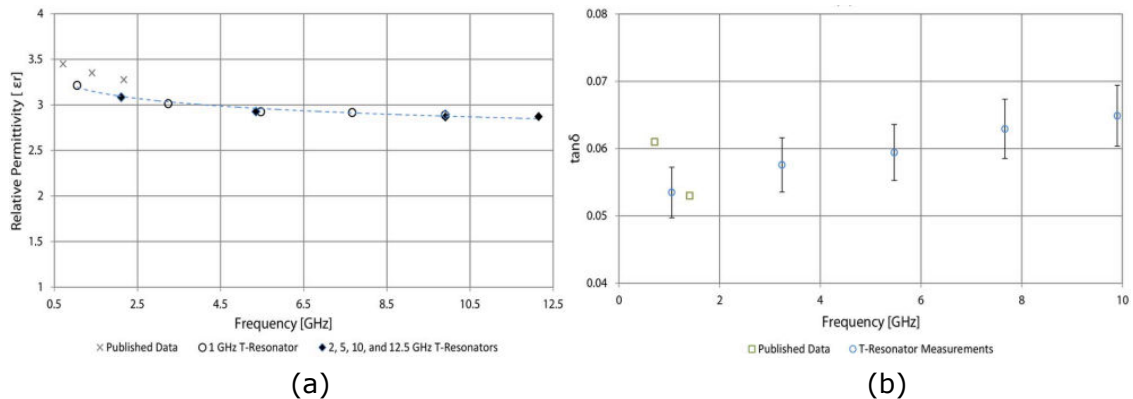


Figure 2-8: (a) Extracted permittivity using 1–12.5 GHz T-Resonators and (b) extracted loss tangent data from the fabricated T-Resonator

This method is simpler than ring resonator method in terms of implementation because of no required coupling gap. And, it gives also relatively accurate results for characterization of flexible substrates (error of $\tan\delta < 8\%$). However, besides the uncertainty of the measured quality factor Q_0 and the ignoring of radiation losses, the inaccuracy of metal losses estimation also contributes to the uncertainty of loss tangent. Moreover, the two discontinuities at the open-end and T-junction make it more complicated and more errors in the determination of permittivity, cf. [Latti 2007].

2.2.1.4 Cavity resonator

The cavity resonator is a waveguide short-circuited at both ends by metallic walls. This disturbance method has been investigated by Yang in Georgia Tech since 2007 in order to study the RF characteristics of paper-based substrates [Yang 2007-2].

A split-cylinder resonator was fabricated with a circular-cylindrical cavity of radius 6.58mm and length 7.06mm, separated into two halves by a variable gap which could be adjustable to the thickness of the characterized paper substrate, as described in Figure 2-9a below. A TE_{011} resonant mode was excited in the cavity at f_{011} .

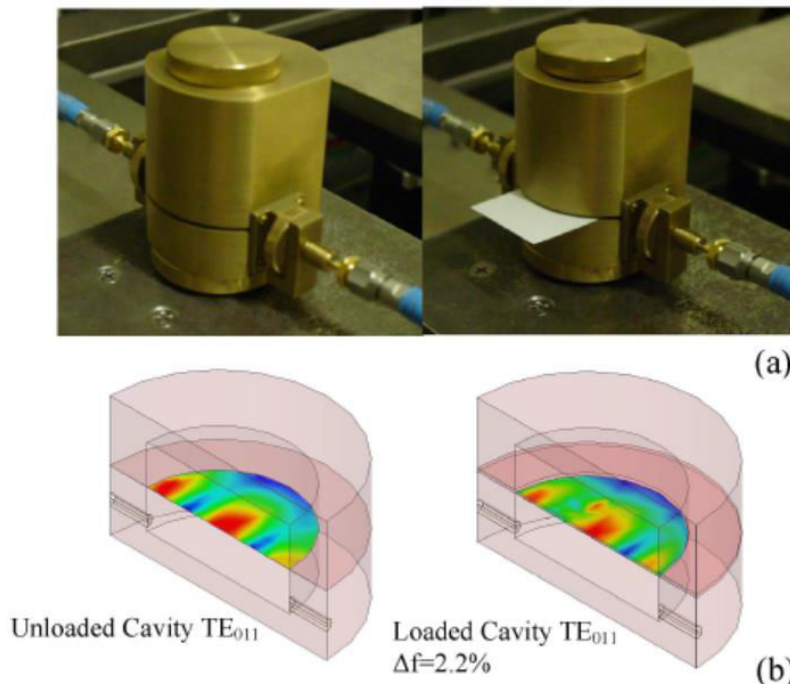


Figure 2-9: (a) Split-cylinder cavity in unloaded and loaded status; (b) Simulated field distributions at TE_{011} mode

A paper substrate was placed in the gap between the two cylindrical-cavity sections. The existence of the inserted substrate caused the shifting of the TE_{011} resonant mode. Using the resonance and boundary conditions for the electric and magnetic fields, the substrate's dielectric constant can be calculated from the shifting [Kent 1998]. The full-wave electromagnetic solver HFSS was also used to

assist identifying the correct position of the TE_{011} resonant peak, as shown in Figure 2-9b.

The measurement data of the resonant modes shifting was plotted in Figure 2-10. After the paper sample was inserted, the observed frequency at the dominant mode TE_{011} shifted down from 34.54GHz (for the empty cavity) to 33.78GHz (for the loaded cavity). By this way, the sample dielectric constant could be determined. [Yang 2007-2]

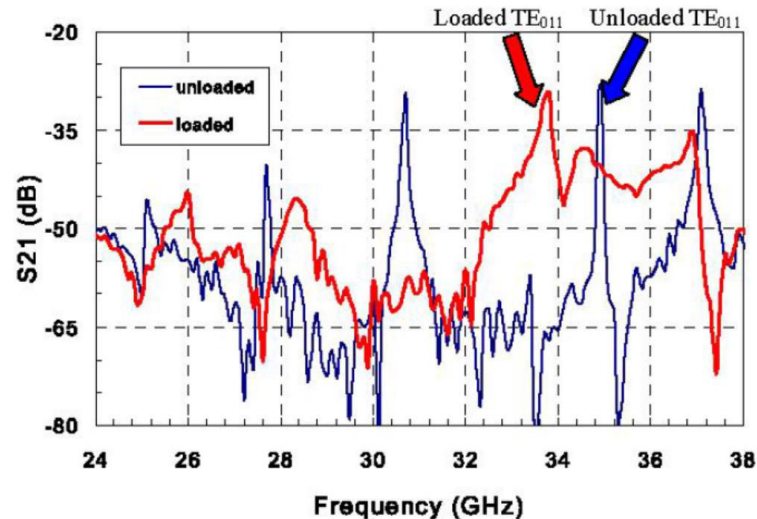


Figure 2-10: Measured modes shifting of the unloaded/loaded split-cylinder cavity

This method was also applied by XLIM Limoges for non-destructive characterization of thin and flexible dielectric materials such as paper substrate. The introduction of the sample into the cavity modified the resonance conditions of the cavity (modes TE_{012p+1} for the determination of ϵ and TE_{012p} for the determination of μ).

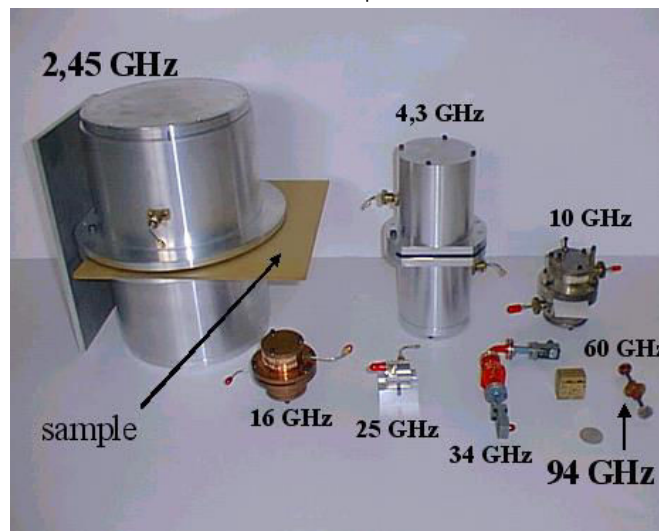


Figure 2-11: Loaded and empty cavities used by XLIM for characterization

In principle, for each cavity, three resonance modes could be exploited: TE_{011} , TE_{013} , TE_{015} and thus three complex permittivities at 3 different frequencies could be obtained. However, in the reality, depending on the samples and the thicknesses, the TE_{011} and TE_{015} modes were not usable because there is the presence of other parasitic modes which strongly disturb the measurement and make the characterization impossible.

An analytical electromagnetic model was developed to calculate the permittivity or permeability of the sample under test by an iterative process. This is not a method called as "low disturbance". The only simplifying assumption is that the gap must have a small size in comparison with the wavelength so as not to be seen by the field.

Cavity	Unloaded Frequency modes		Samples		
			a x b (mm x mm)		t thickness
	TE ₀₁₁ (GHz)	TE ₀₁₃ (GHz)	min	max	max (mm)
2,45 GHz	2	2.45	200 x 200 and more	opened slit	8
4.3GHz	4,3	4,7	100 x 100 and more	opened slit	6
10GHz	8,3	10,3	48 x 48 and more	51 x 51	1
16GHz	12,8	15,6	35 x 35 and more	51 x 51	1
25GHz	21,6	29,9	20 x 20 and more	opened slit	0.7
34GHz	26,5	35,8	18 x 18 and more	25 x 25	0.7
60GHz	48,6	60.6	10 x 10 and more	opened slit	0.5
90GHz	78.7	98.7	8 x 8 and more	9 x 9	0.3

Table 2-1: Sample dimensions and unloaded resonance frequency of each cavity at XLIM Limoges

The maximum distribution of the electric field in a cavity resonator at TE_{012p+1} modes concentrates around the half of the cavity radius (mid-height at the sample level). Therefore, the thickness of the sample was measured in the zones near this maximum of the field, as shown in Figure 2-12 below.

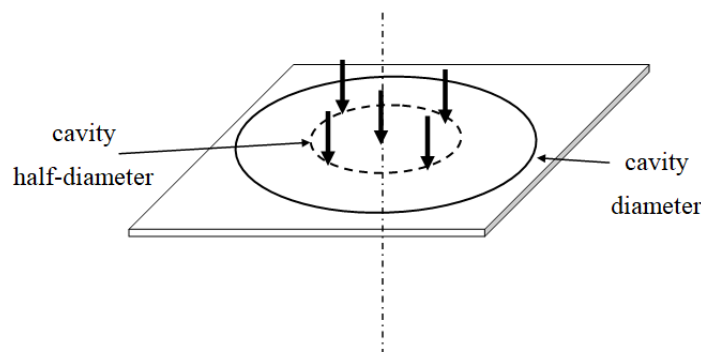


Figure 2-12: Required points for thickness measurements in order to obtain an average thickness of the sample

INPG Grenoble has also adopted the cavity resonator method for their characterization process, but they have used another type of cavity, as described in Figure 2-14 [Phan 2016]. In order to determine the dielectric properties, the resonance frequency and the -3dB bandwidth of the resonator were measured with and without the test sample at TM₀₁₀ mode. The introduction of the test sample into

the cavity resonator caused a disturbance which shifted the resonant frequency and reduced the quality factor of the resonator. Therefore, this disturbance method allows determining the complex permittivity of the test sample.

The dielectric properties of the test sample are determined by the following relationships:

$$\varepsilon_r = \varepsilon_r' = 1 + 0.539 \times \frac{V_{cavity} (f_{r0} - f_{r1})}{V_{sample} f_{r0}} \quad (2-15) \quad [\text{Phan 2016}]$$

$$\tan \delta = \frac{\varepsilon_r''}{\varepsilon_r'} = \frac{0.539}{2\varepsilon_r'} \left(\frac{V_{cavity}}{V_{sample}} \right) \left(\frac{1}{Q_{empty}} - \frac{1}{Q_{load}} \right) \quad (2-16)$$

where f_{r0} is the resonant frequency of the empty cavity, f_{r1} is the resonant frequency of the cavity loaded by a test sample; V_{cavity} is the volume of the cavity, V_{sample} is the volume of the test sample loaded inside the cavity; Q_{empty} is the Q-factor of the empty cavity, Q_{loaded} is the Q-factor of the cavity loaded by a test sample.

Two cylindrical cavities operating at 2.5 GHz (with dimensions $\Phi = 92\text{mm}$, height = 40mm) and 925MHz (with dimensions $\Phi = 247.35\text{mm}$, height = 39.7mm) were used. The cavity resonator, the measurement bench and the insertion of a test sample into the cavity were presented in Figure 2-13 and Figure 2-14.



Figure 2-13: Open cavity

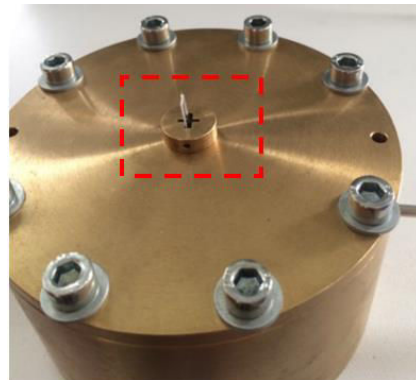
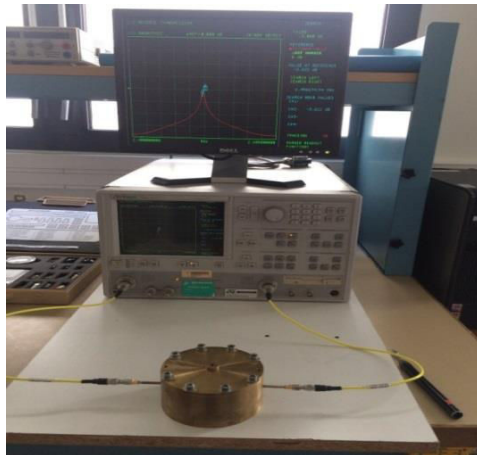


Figure 2-14: Measurement bench with the insertion of a test sample into the cavity

The dimensions of the test samples were chosen so that they can be inserted into the slot of the cavity resonators. At 925 MHz, the only dimension of 9 mm width of the test sample was applied. At 2.5 GHz, the measurement was realized with two dimensions for each sample (5 mm and 6 mm width, respectively) in order to compare the characterized results.

In general, the advantage of the cavity resonator method is noticed that the sample is kept non-destructive. So, it allows characterizing directly the material under test without considering the influence of the metallization layer. But this characterization approach is just validated in a very narrow band at the frequencies around the resonant frequency of the cavity. Therefore, when we work on the wide range of frequency, we cannot estimate the dispersion of the characterized dielectric properties in function of frequency. In this case, we need a lot of resonance cavity at different frequencies, which depends on the equipment availability of the laboratory. The second problem is the uncertainty in the estimation of the thickness of the thin flexible substrate, especially with paper or others cellulosic materials, because paper is an elastic substrate (very difficult to measure accurately the thickness) and can be easily compressed when inserting into the cavity. That can introduce the inaccuracy in the determination of dielectric constant and loss tangent. In addition, the filling conditions to have low disturbance and the size limitation of the sample must be executed. According to [Janezic 1999], this method exhibits an average error of 4% for dielectric constant and 25% for loss tangent when tested on different thin materials.

All presented dielectric characterization methods for paper substrates are summarized in *Table 2-2* below. It can be easily seen that each method has its own advantages and limitations. Therefore, the choice of method depends on the condition and equipment availability of the laboratory as well as the application and the frequency range of the RF components.

Method	Type	Advantage	Disadvantage
<i>Two planar transmission lines</i>	non-resonant	Simple realization	Requirement of the impedance matching. Accuracy depends on the phase difference $\Delta\theta$, the length difference Δl and the influence of the adhesive layer.
<i>Microstrip ring resonator</i>	resonant	Relatively accurate characterization method	Uncertainties in ϵ_r (due to the resonator dimensions, sample thickness, and resonant frequency) and in $\tan\delta$ (due to the quality factor Q_0 and the radiation losses). Difficulty in the controlling of coupling gap.
<i>T-resonator</i>	resonant	Relatively accurate characterization method. Simpler than ring resonator method in	Uncertainties in ϵ_r due to the two discontinuities at the open-end and T-junction. Uncertainties in $\tan\delta$ due to the measured quality factor, the

		terms of implementation	ignoring of radiation losses, and the inaccuracy of metallic losses
<i>Cavity resonator</i>	resonant	Non-destructive method. Characterizing directly the material under test without considering the influence of the metallization layer.	Just validated in very narrow band around the resonant frequency. Uncertainties due to the estimation of paper thickness.

Table 2-2: Summary of some basic dielectric characterization methods for paper substrates

2.2.2 Realized method

The most precise methods for determination of the substrate dielectric properties are resonator methods, such as cavity resonators (characterizing directly the material under test and not depending on metallization layer), but they are just precise in a narrow band. So, we choose the method based on microstrip transmission line resonator in order to exploit the stationary phenomena over an ultra-wide frequency band (for example 0-20 GHz). Its structure is also very simple, very easy to fabricate and does not require any complex technique. The drawback is focused mainly on the determination of loss tangent because we must consider simultaneously the dielectric losses with the metallic losses. The uncertainty in the estimation of the metallic losses of the conductive deposit can introduce the inaccuracy in the determination of loss tangent. Additionally, the connector losses also influence in the calculation of dielectric losses when we use an OSLT (Open-Short-Load-Thru) type calibration.

2.2.2.1 First tests

We have started with the simplest metallization method: using an adhesive copper tape, whose main advantage is a rapid, ultra-low-cost prototyping method with a very good conductivity despite the limited resolution due to manual cutting process. This method can be realized quickly at laboratory stage. However, two thin adhesive layers (with 25 μm thickness), that we have not known their dielectric properties, are interposed between each copper layer and the substrate. That can influence the accuracy in the characterization of the dielectric properties.

As we have mentioned above, with transmission lines characterization method, exploiting OSLT (Open-Short-Load-Thru) type calibration, connector losses are observed in measurement due to non-ideal interconnection performance between the coaxial cables input-output and the microstrip transmission line. To specify this problem, we have realized two transmission lines of different lengths in order to evaluate these connector losses.

First, two microstrip transmission lines have been realized on a 254 μm thick Teflon glass substrate, a reference substrate which has a very low loss tangent, by using copper etched metallization. Then, their S_{21} parameters have been measured and compared as illustrated in *Figure 2-15* in order to determine the linear losses of the microstrip lines and thus estimate the connector losses:

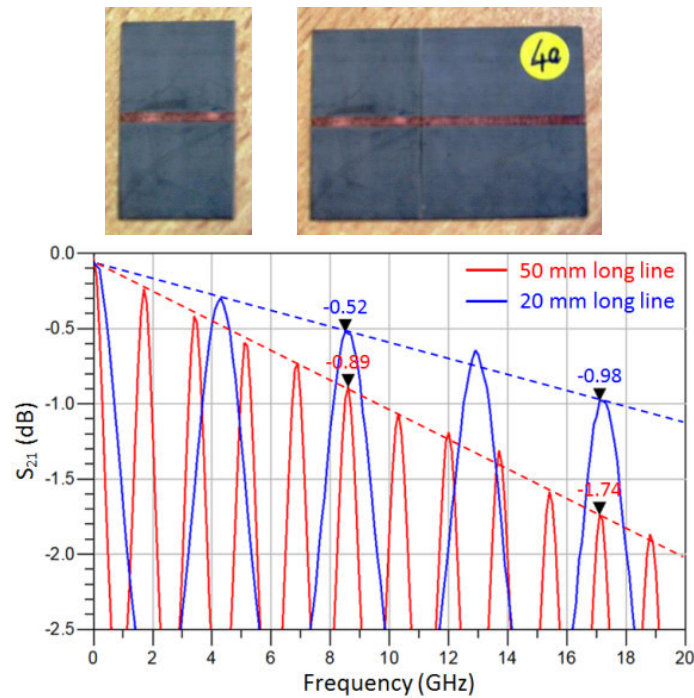


Figure 2-15: (a) Prototypes and (b) measured S_{21} parameter of the two transmission lines (20 mm and 50 mm of length) fabricated using copper etched on Teflon substrate.

Frequency	Insertion loss difference [dB]	Linear losses [dB/cm]	Connector losses [dB]
8.3 GHz	$0.89 - 0.52 = 0.37$	$0.37/\Delta l = 0.123$	$0.52 - 0.123 \times 2 = 0.273$
17.1 GHz	$1.74 - 0.98 = 0.76$	$0.76/\Delta l = 0.253$	$0.98 - 0.253 \times 2 = 0.473$

Table 2-3: Estimation of the connector losses through two different transmission lines

The connector losses have been calculated easily: -0.273 dB and -0.473 dB for two connectors respectively at 8.5 GHz and 17.1 GHz.

Second, in order to study the dielectric properties of these adhesive layers of copper tape, a microstrip transmission line with a 2 mm width and a 50 mm length was realized using an adhesive copper tape (40 μm copper thickness with 25 μm adhesive layer thickness) laminated on the same Teflon glass substrate above. The conductivity value of the copper tape measured at DC value using a four-point method is about $\sigma = 3.94 \times 10^7$ S/m. The dielectric properties of Teflon glass substrate given by the manufacturer are $\epsilon_r = 3.5$ and $\tan\delta = 0.003$ at 1 GHz. Therefore, by comparing the concordance between simulation and measurement results, the dielectric properties of the adhesive layer of the copper tape are determined as $\epsilon_r = 1.9$ and $\tan\delta = 0.01$, cf. Figure 2-17. Of course, the comparison between measurement and simulation has taken into account the connector losses.

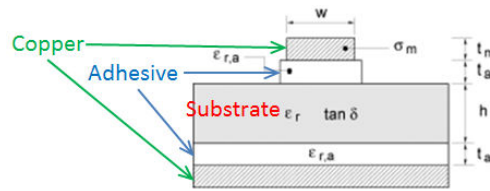


Figure 2-16: Model of transmission line fabricated by using an adhesive copper tape

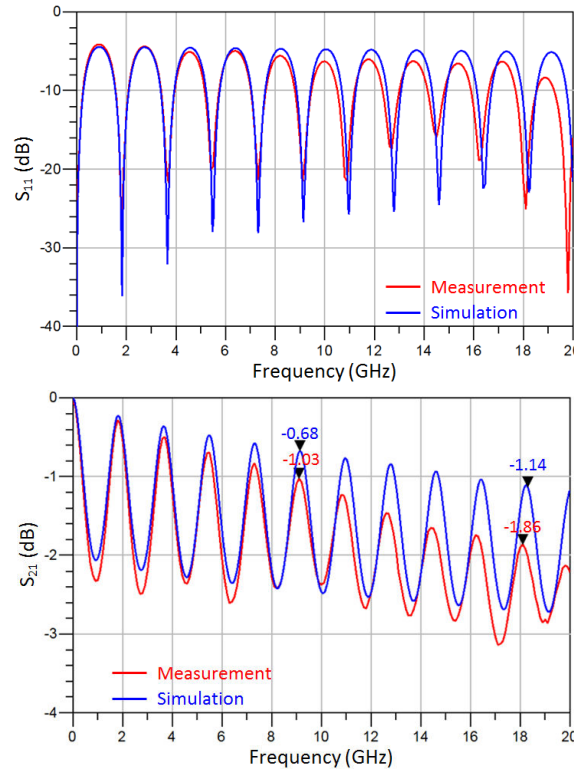


Figure 2-17: Measured and simulated S_{ij} -parameters of a 2 mm width transmission line fabricated on Teflon glass by using an adhesive copper tape.

Finally, the dielectric properties of any flexible substrate can be now estimated based on the following principle. By taking into account the insertion losses related to connectors (with OSLT type calibration), we have determined the values of relative permittivity ϵ_r and loss tangent $\tan \delta$ so that the retro-simulation, using Momentum simulator, has the best agreement with the measurement over the whole selected frequency band 0 – 20 GHz.

For example, Teslin paper, a paper substrate which has the lowest loss tangent value in comparison with the state-of-art [Cook 2013], has been investigated below for dielectric characterization. A microstrip transmission line was fabricated using the adhesive copper tape mentioned above (40 μm copper thickness with 25 μm adhesive layer thickness, $\epsilon_r = 1.9$ and $\tan \delta = 0.01$ at 2 GHz), laminated on a 250 μm thick Teslin paper substrate. Using the determination principle indicated above and taking into account the connector losses, the experimental dielectric properties of Teslin paper substrate are $\epsilon_r = 2.26$ and $\tan \delta = 0.051$ at 2 GHz, cf. Figure 2-18. And these values are also approximate with the characterized results reported by Cook ($\epsilon_r = 2.16 \pm 0.03$ and $\tan \delta = 0.012\text{--}0.024$) in 2013. [Cook 2013]

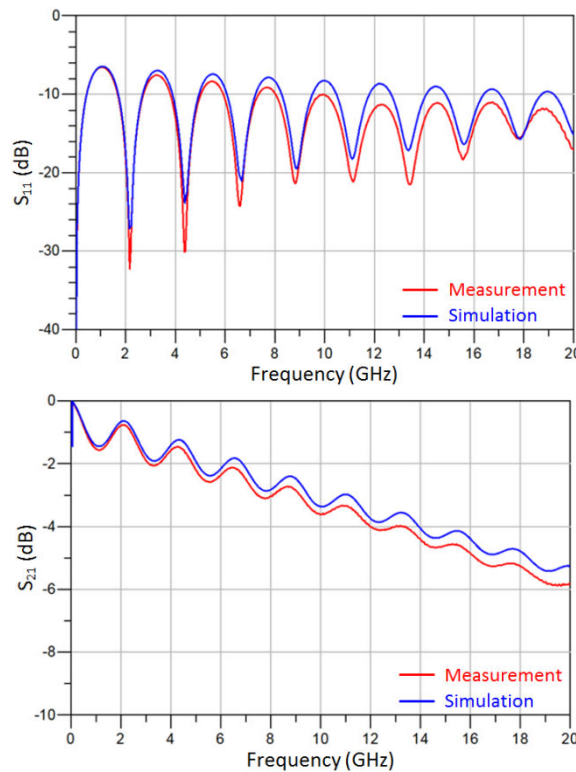


Figure 2-18: Measured and simulated S_{ij} -parameters of a 2 mm width transmission line fabricated on Teslin paper by using an adhesive copper tape

Overall, a very good agreement between measured and simulated results was observed over an ultra-large frequency band of interest. Experimental results show an insertion loss of about 1.16 dB /cm for 2 mm width adhesive copper tape line on Teslin paper at 20 GHz.

By applying the method described above, we have also determined the dielectric properties of the other several paper substrates. In fact, we have realized many microstrip transmission lines using adhesive copper on various different paper substrates, e.g. cardboard, Silver Image Laser paper, photo paper, Teslin paper, etc. to characterize them. The results of dielectric properties of all characterized flexible paper substrates are summarized in *Table 2-4* below. Herein, the results at the first resonance frequency (around 2 GHz) are presented. Of course, there are always some dispersions of ϵ_r and $\tan\delta$ values over an ultra-large frequency band up to 20 GHz.

Paper substrates	Thickness (μm)	ϵ_r	$\tan\delta$
Teslin	250	2.26	0.051
Kodak Polycontrast	245	2.95	0.056
Kodak Polymax	245	2.95	0.062
Couverture magazine	245	3.67	0.065
Ilford	250	3.05	0.067
Silver Image Laser	250	3	0.085
Carton blanc	265	2.85	0.093
PWC	230	2.82	0.069
PRP60	75	3.7	0.093
PRJ	60	4.4	0.098
BL200	245	3.25	0.108
PRC	60	5.3	0.111
SP3	330	2.55	0.065
E4D_75	330	2.68	0.066
FS2	170	3.2	0.081

Table 2-4: Dielectric properties results of characterized paper substrates at 2 GHz

In general, using this simple method, we can determine the dielectric properties of any flexible substrate with relatively good accuracy. The errors in the selection of dielectric property values, so that the retro-simulation has the best agreement with the measurement over the whole frequency band 0 – 20 GHz, are $\Delta\epsilon_r = \pm 0.01$ and $\Delta\tan\delta = \pm 0.001$. More specifically, the simulations have run repeatedly many times with the step of 0.01 for $\Delta\epsilon_r$ and 0.001 for $\Delta\tan\delta$ around the supposed values of ϵ_r and $\tan\delta$ until the simulated resonance frequency and simulated S_{21} value at this resonance frequency have the best matching with the measured results. But the uncertainty of dielectric properties of the adhesive layer of copper tape introduces the inaccuracy of the dielectric properties. In addition, the uncertainty of ϵ_r depends on the accuracy of transmission line dimensions; and the uncertainty of $\tan\delta$ comes from the uncertainties in the estimation of connector losses and the conductivity of the metallization deposit.

This determination principle shows some advantages that are simple, no need to apply the electromagnetic formulas and based on a visual comparison between the measurement and simulation. And more importantly, it allows calculating the dielectric properties of the thin flexible materials over the ultra-wide frequency band, for example up to 20 GHz, as well as showing the dispersion in function of frequency. However, it takes a lot of time to run the simulation repeatedly until selecting the closest values at each resonance frequency. In addition, it is very difficult to accurately determine the error of this estimation principle based on simulation.

2.2.2.2 Dielectric characterization

After the first successful tests, in order to eliminate the influence of adhesive layer of copper tape, we have used the direct metallization process like silver ink screen printing on paper or aluminum etching on PET.

a/ Relative permittivity

Besides the determination method based on simulation as presented above, we have also developed the microstrip transmission line resonator method in term of analytical calculation in order to compare and collate between these two approaches. We have recognized that a transmission line with characteristic impedance different from 50Ω , realized on the characterized dielectric substrate, plays a role as a microstrip resonator placed between two 50Ω connectors, as depicted in *Figure 2-19* (multi $\lambda_g/2$ resonator).

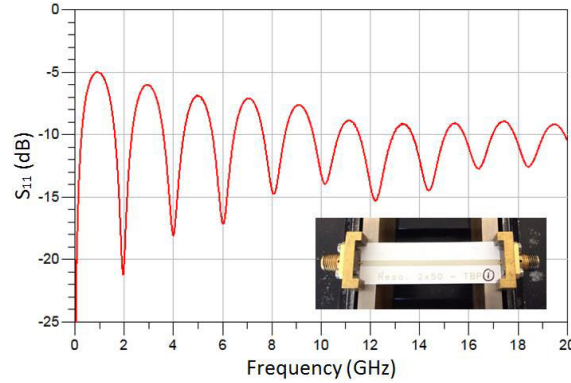


Figure 2-19: Measured S_{11} of a microstrip transmission line (2 mm width, 50 mm length, and $7.6\mu\text{m}$ ink thickness) screen-printed using silver ink on E4D-240 μm paper

So, the effective permittivity (ϵ_{eff}) can be determined by (2-17) below via the length of the transmission line and the resonance frequencies. This equation is developed from the formula of the classical quarter-wave resonator. [Latti 2005]

$$f_{r,n} = \frac{nc}{2L\sqrt{\epsilon_{\text{eff},n}}} \quad (2-17)$$

where n is the resonance mode (i.e. $n = 1, 2, 3 \dots$), c is the speed of light in free space, L is the length of the transmission line and $f_{r,n}$ is the resonant frequency at mode n .

This effective permittivity ϵ_{eff} can then be related to relative permittivity ϵ_r of the substrate using (2-18) with h and w referring respectively to the thickness of the substrate and the width of the transmission line (in our case $w > h$).

$$\epsilon_{\text{eff},n} = \frac{\epsilon_{r,n} + 1}{2} + \frac{\epsilon_{r,n} - 1}{2} \times \left(1 + 12 \times \frac{h}{w}\right)^{-0.5} \left(\frac{w}{h} > 1\right) \quad (2-18)$$

By this way, the characterization of dielectric constant is very accurate because the errors in L , w , h dimensions measured with microscope and thickness meter, and the error in resonant frequencies ($f_{r,n}$) measured using Vector Network Analyzer (VNA) are very small. And, it is entirely possible to establish the function for calculating the error from the formula (2-17) and (2-18) above.

$$\text{From (2-17): } \ln(\epsilon_{\text{eff},n}) = -2 \times \ln(L) - 2 \times \ln(f_{r,n})$$

$$\Leftrightarrow d[\ln(\epsilon_{\text{eff},n})] = -2 \times d[\ln(L) + \ln(f_{r,n})]$$

$$\Leftrightarrow \frac{d\varepsilon_{eff,n}}{\varepsilon_{eff,n}} = -2 \times \left(\frac{dL}{L} + \frac{df_{r,n}}{f_{r,n}} \right)$$

$$\Leftrightarrow \frac{\Delta\varepsilon_{eff,n}}{\varepsilon_{eff,n}} = 2 \times \left(\frac{\Delta L}{L} + \frac{\Delta f_{r,n}}{f_{r,n}} \right) \quad (2-19)$$

So, if $\Delta L/L = 0.5\%$ and $\Delta f_{r,n}/f_{r,n} = 3\%$, $\Delta\varepsilon_{eff,n}/\varepsilon_{eff,n}$ is 7% .

Furthermore, it enables faster computation of relative permittivity at each resonance frequency instead of run repeatedly too many simulations. We can see clearly the dispersion of relative dielectric constant ε_r in function of frequency (cf. *Table 2-5* and *Table 2-6*).

b/ Loss tangent

The loss tangent $\tan\delta$ is determined by the same method based on Momentum retro-simulation as described in the *section 2.2.2.1*. By taking into account the insertion losses related to connectors (with OSLT type calibration), the values of $\tan\delta$ are chosen so that the retro-simulation has the best agreement with the measurement. For showing the dispersion of $\tan\delta$ in function of frequency, the loss tangent values have been also extracted at each resonance frequency over the whole frequency band 0 – 20 GHz. The error in this determination of $\tan\delta$ varies from 7% to 10% (depending on the material) if the error in the measurement of S_{21} values is supposed about 5%.

In general, this characterization method based on the microstrip transmission line is quite accurate, especially in term of relative dielectric constant because the errors in L , w , h dimensions measured with microscope and thickness meter, and the error in resonant frequencies ($f_{r,n}$) measured using Vector Network Analyzer (VNA) are very small. About the characterization of loss tangent, there are some uncertainties due to the estimation of metallic losses and connector losses. Even so, the characterization results are still quite reasonable when applied to antenna design.

For example, by using our proposed method, two microstrip transmission lines with 2 mm width and 50 mm length were fabricated using silver ink screen printing and aluminum etching respectively on E4D_240 μ m paper (240 μ m thickness) and PET film (130 μ m thickness) for dielectric characterization. The characterized results of these two flexible substrates are presented in *Table 2-5* and *Table 2-6* below. It is clear to see the dispersion of both relative dielectric constant and loss tangent values in function of frequency. Dielectric properties are particularly stable at high frequencies. The determination of loss tangent of PET is more accurate than that of E4D paper, mainly because of the better quality of the conductive deposit that will be mentioned in the *section 2.3.1* below.

E4D_240μm paper									
Resonance mode	1	2	3	4	5	6	7	8	9
f (GHz)	1.95	4	6.02	8.08	10.17	12.22	14.37	16.39	18.44
ϵ_r	2.68	2.53	2.51	2.47	2.43	2.43	2.39	2.4	2.4
$\tan\delta$	0.056	0.05	0.049	0.048	0.046	0.046	0.043	0.045	0.043

Table 2-5: Dielectric properties results of E4D_240 μ m paper substrate in function of frequency

PET film											
Resonance mode	1	2	3	4	5	6	7	8	9	10	11
f (GHz)	1.77	3.56	5.36	7.14	8.94	10.74	12.53	14.34	16.11	17.9	19.69
ϵ_r	2.91	2.89	2.86	2.86	2.85	2.85	2.85	2.84	2.85	2.85	2.85
$\tan\delta$	0.013	0.01	0.009	0.01	0.009	0.009	0.01	0.008	0.01	0.009	0.01

Table 2-6: Dielectric properties results of PET substrate in function of frequency

We have also applied the average values of dielectric properties into Momentum retro-simulations to verify the characterized results above:

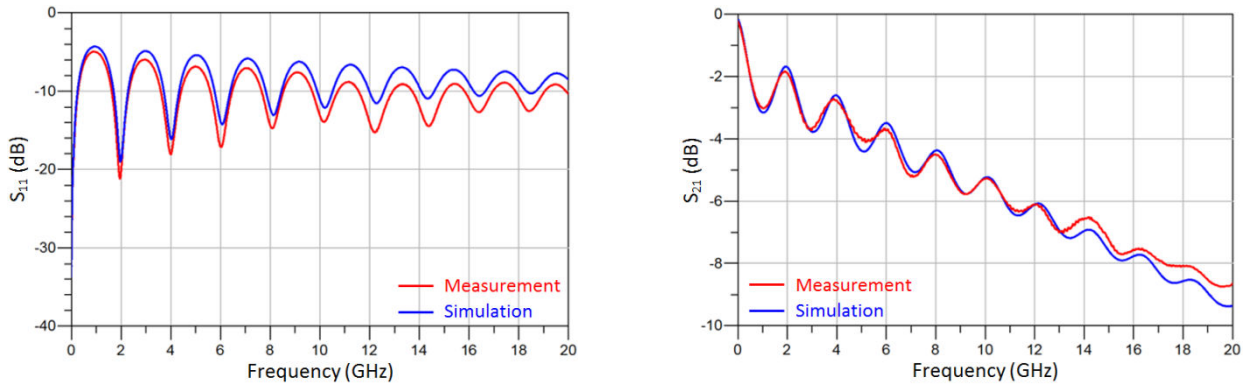


Figure 2-20: Measured and simulated S_{ij} -parameters of a 2 mm width transmission line screen-printed on E4D paper by using silver ink: $\epsilon_r = 2.54$ & $\tan\delta = 0.05$

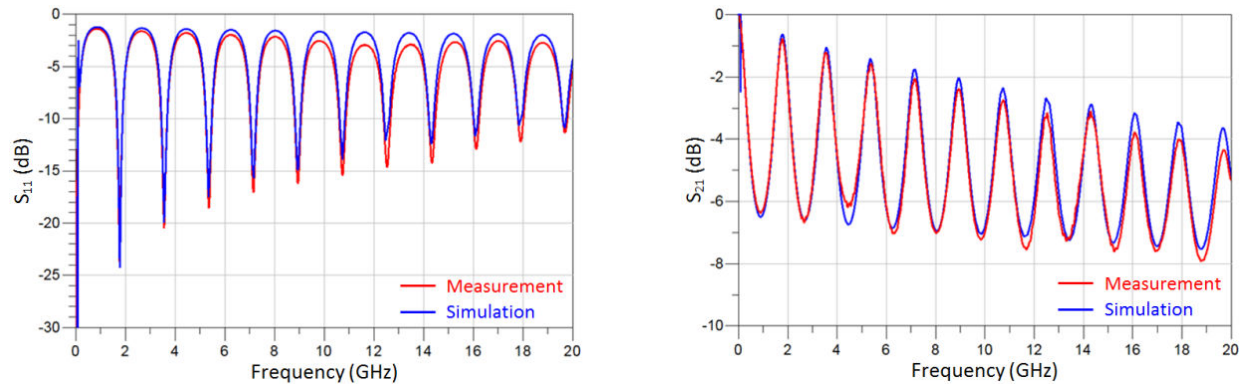


Figure 2-21: Measured and simulated S_{ij} -parameters of a 2 mm width transmission line fabricated on PET film by using aluminum etched: $\epsilon_r = 2.85$ & $\tan\delta = 0.009$

Overall, a very good agreement was observed over the ultra-large frequency band. The dispersion of dielectric properties of PET in function of frequency is very low, as described in *Table 2-6* above. Therefore, in the case of aluminum etched transmission line on PET, we have recognized obviously an almost perfect agreement over the entire frequency band 0 – 20 GHz by using an average value. Meanwhile, for paper substrates, the dispersion is quite high, especially the loss tangent. By using the average value of loss tangent ($\tan\delta = 0.05$) in the retro-simulation, it could be seen that the simulation line (blue) of S_{21} is superior to the measurement line (red) of S_{21} at low frequency, but inferior to the measurement line at high frequency, cf *Figure 2-20*.

These experimental results prove a high precision of our dielectric characterization method on any flexible substrate with any metallization technology. And, we have also noted that the dispersion in dielectric characteristics is not the same between different substrates.

2.2.3 Discussion

We have sent some paper samples to XLIM Limoges and INP Grenoble for dielectric characterization and for result comparison. They have used a cavity resonator method whose characterization principle is described in *section 2.2.1.4*.

XLIM Limoges has used 3 cavity resonators at 2.4, 4.5 and 10.2 GHz, as shown in *Figure 2-11*, to characterize some paper substrates (Silver Image Laser paper, magazine cover, Kodak photo paper) at TE_{013} mode.

The dielectric property results of these paper substrates are reported in *Table 2-7* below.

Substrate	f (GHz)	ϵ_r	$\pm\Delta\epsilon_r / \epsilon_r$	$\tan\delta$	$\pm\Delta\tan\delta / \tan\delta$	Average thickness
Silver Image Laser Paper	2.4	3.19	12%	9.2E-2	21.2%	242 ± 20 μm
	4.5	3.13	8.5%	8.2E-2	17.9%	
	10.2	2.93	13.5%	7.8E-2	22.2%	
Magazine Cover	2.4	3.86	11.9%	7.3E-2	21.2%	244.5 ± 20 μm
	4.5	3.77	8.6%	5.8E-2	18.1%	
	10.2	3.67	9.5%	4.4E-2	18.0%	
Kodak Photo Paper	4.5	3.26	9%	8.3E-2	18.5%	243 ± 20 μm
	10.2	2.94	10.7%	5.3E-2	19.6%	

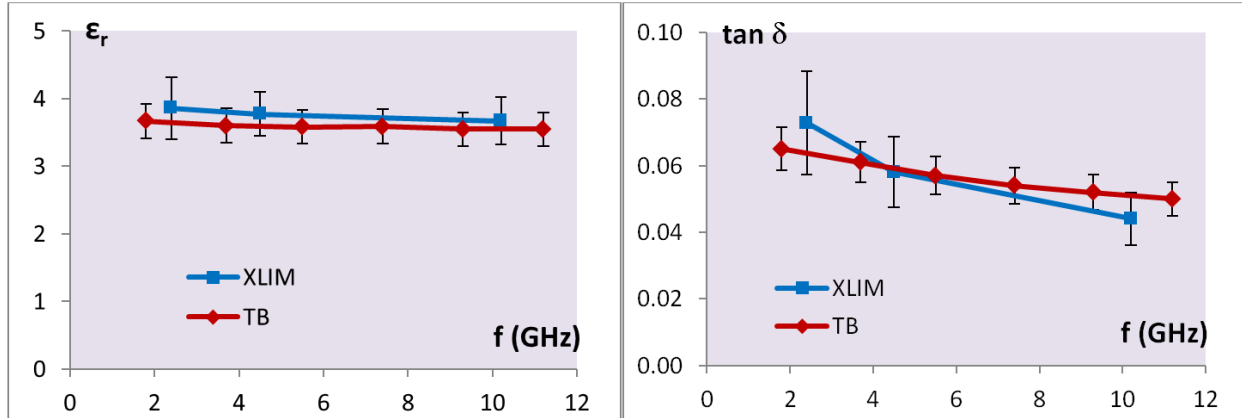
Table 2-7: Dielectric property results of some paper substrates realized by XLIM Limoges using cavity resonator method

The error in XLIM characterization is relatively high, about 10% and 20% respectively for ϵ_r and $\tan\delta$. It is mainly due to the uncertainty in substrate thickness measurement. Specifically, the percentage error in the paper thickness measurement is approximately equal to the percentage error of the permittivity of the paper substrate.

If we compare them with IMT (TB) characterized results, presented in *section 2.2.2.1* above, through the microstrip transmission line method using adhesive

copper tape, we can notice that the characteristic curves of ϵ_r and $\tan\delta$ of XLIM tend to converge toward IMT (TB) characterized values at high frequencies, cf. *Figure 2-22*. Thus, these experimental results realized by two different research groups show the consistency between two totally different methods.

Glossy Paper



Laser Printing Paper

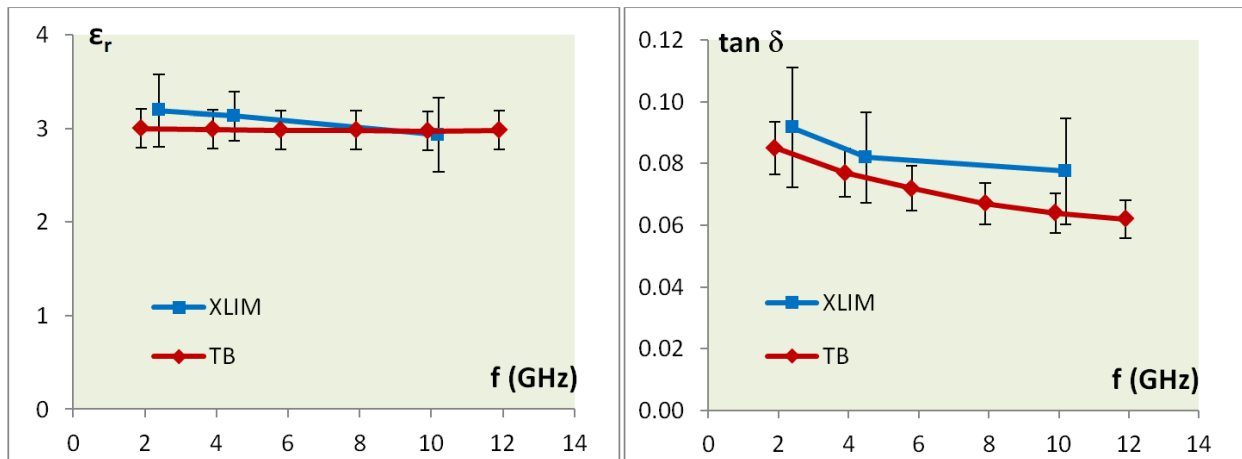


Photo Paper

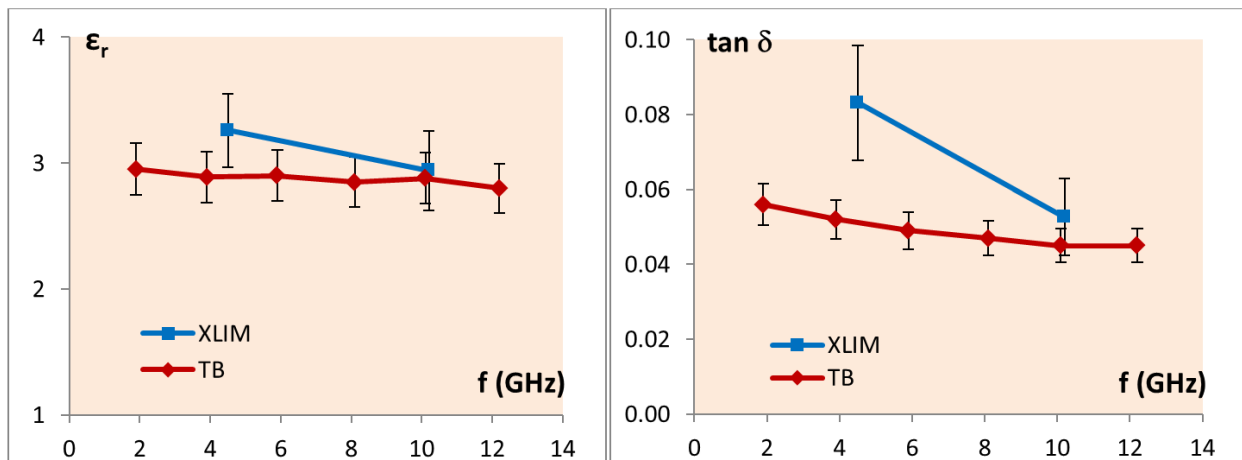


Figure 2-22: Comparison between the characterized dielectric properties of some paper substrates realized by XLIM and IMT: (a) Magazine cover, (b) Silver Image Laser paper, (c) Kodak photo paper

INP Grenoble has used 2 cavity resonators at 925 MHz and 2.5 GHz for characterization, as presented in *section 2.2.1.4*. The characterized results of some paper substrates are shown in *Table 2-8* below.

Substrate	Thickness	Frequency	ϵ_r	$\tan\delta$
Teslin Paper	254 μ m	925 MHz	2.83	0.033
		2.5 GHz	2.34	0.037
Silver Image Laser Paper	245 μ m	925 MHz	2.58	0.123
		2.5 GHz	2.71	0.159
PWC Paper	230 μ m	925 MHz	2.69	0.107
		2.5 GHz	3.22	0.122
BL200 Paper	240 μ m	925 MHz	3.75	0.148
		2.5 GHz	3.13	0.141

Table 2-8: Dielectric property results of some paper substrates realized by INP Grenoble using cavity resonator method

The results of relative dielectric constant ϵ_r at 2.5 GHz are approximate to our characterized dielectric properties reported in *Table 2-4*. But, the loss tangent $\tan\delta$ is overestimated. And, the error in INPG characterization process seems to be relatively high. By comparing with IMT (TB) and XLIM results, for example in the case of Silver Image Laser paper, INPG characterized dielectric properties show more discrepancies.

2.2.4 E4D paper

Among the critical needs for the selection of the appropriate type of paper for electronic applications are the lowest dielectric losses, surface planarity, water repelling, double-side printability, via-forming ability, lamination capability for future 2.5D development, and processability with low-cost manufacturing. So, the choice of correct paper material for use as a substrate requires careful selection.

A dozen of cellulosic substrate types, which are compatible with the printing process such as PRC, PRJ, PRP-60, FS2, PWC, BL200, E4D ... have been characterized to choose the best flexible paper substrate. The characteristics of these papers were also presented in *Table 2-4*. And, E4D paper is finally selected for some important reasons. It is printable double-sided and has the lowest loss tangent among all tested papers which can be printed on two sides (recto-verso).

E4D papers have many different thicknesses such as 100 μ m, 200 μ m, 300 μ m ... The 300 μ m thickness type is too thick to use because it is too stiff to be bent and the printed patterns will be completely fractured, so we just take into consideration herein the two other types. Their dielectric properties at 5 GHz are slightly different and are presented in *Table 2-9* below.

The E4D-100 paper is very flexible thanks to its very thin thickness (106 μ m), so it is very easy to bend or fold. But its loss tangent is too high (0.06 at 5 GHz), so the insertion losses of the 50 Ω feed line are extremely high, about 1.1 dB/cm at 2.4 GHz and about 1.6 dB/cm at 5.5 GHz.

The E4D-200 paper have slightly lower loss tangent (0.05 at 5 GHz). In addition to the lower dielectric losses, the wider 50Ω feed line also allows reducing the metallic losses. Therefore, the insertion losses of the 50Ω feed line are significantly reduced, about 0.49 dB/cm at 2.4 GHz and about 0.76 dB/cm at 5.5 GHz. As shown in *Figure 2-23*, the 50Ω line screen-printed on E4D_200 paper has much fewer losses than that printed on E4D_100 paper; of course, its performance is still far from being compared with that of the line realized with adhesive copper. However, due to a double thickness (204μm), its flexibility is a question to experimentally verify, especially in bending and folding the printed lines and patterns.

At the beginning of the research work, we have begun with the lines and antennas on E4D-100 paper, expecting to exploit its tremendous flexibility in bending or folding to create 3D structures for the final demonstrator. However, we have quickly realized that the insertion losses on the 50Ω feed line are too great if using this kind of too thin paper. This greatly increases the insertion losses (so decreases the transmitted power) in the feed line, especially when we will need to connect with a PCB mainboard by a long interconnection line in order to create the final demonstrator. Therefore, we have decided to change into E4D-200, a thicker paper substrate, in the final stage in order to reduce these unwanted losses.

Paper substrate	Thickness (μm)	ϵ_r	$\tan\delta$
E4D-100	106	2.85	0.06
E4D-200	204	2.57	0.05

Table 2-9: Dielectric properties of E4D type papers at 5 GHz

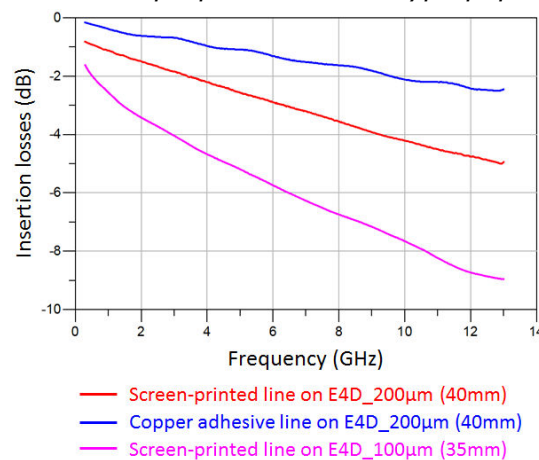


Figure 2-23: Comparison of the insertion losses between different 50Ω lines on E4D paper substrates

In short, as we have mentioned before, the paper substrates have a very high dielectric loss and a very rough surface state. What makes it attractive is the extremely low cost, great flexibility and environmentally friendly purpose. Therefore, it is evident that the performance of printed patterns on paper will not be perfect. So, we have to select an almost perfect substrate for comparison. PET ($\epsilon_r = 2.85$), the cheapest polymer material, is thence chosen as a reference substrate to compare. It has also a significantly lower loss tangent (0.009 at 5 GHz) and a much better surface quality than the paper substrate.

2.3 Characterization of conductive layer

In addition to the dielectric characterization of the utilized flexible substrate, the conductive layer characterization is also very important for antenna and circuit design, e.g. thickness and conductivity of the deposit. It will help us to accurately estimate losses on the feed line and in the antenna, and to model most precisely as possible these circuits.

2.3.1 SEM image of ink deposit surface

Before proceeding to determine quantitatively the parameters such as thickness and conductivity of the deposit, we have investigated its qualitative surface to have a first look at the difficulties of printing conductive lines and patterns on a flexible substrate like paper. More specifically, in this section, the SEM (Scanning Electron Microscopy) images of the surface of two different types of conductive deposits are presented in order to help us better understand their characteristics.

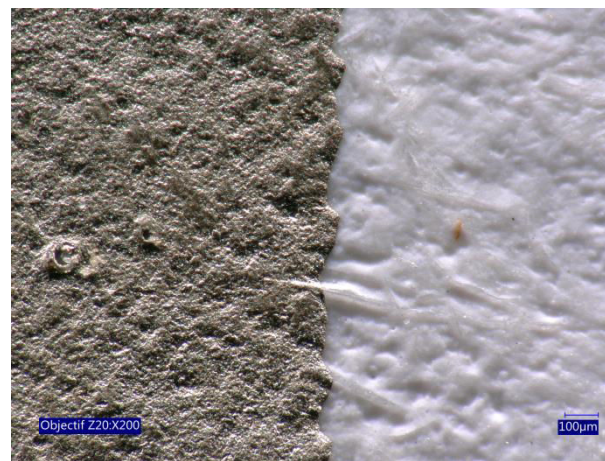


Figure 2-24: Perspective view of a screen-printed pattern on paper substrate using silver ink. First, with a 500µm scale, the general view in *Figure 2-25* along the screen-printed deposit on the E4D paper substrate gives us first impressions. The edge of the silver ink deposit is not straight but in sawtooth form. So, the dimensions of the pattern are difficult to be determined exactly. The paper surface is very rough with many pinholes, small holes and microfibers. The silver ink deposit surface is very rough too. That explains why the mechanical profilometer, which simultaneously measures the screen-printed deposit and paper substrate, cannot give the accurate results of thickness, *cf. section 2.3.3*.

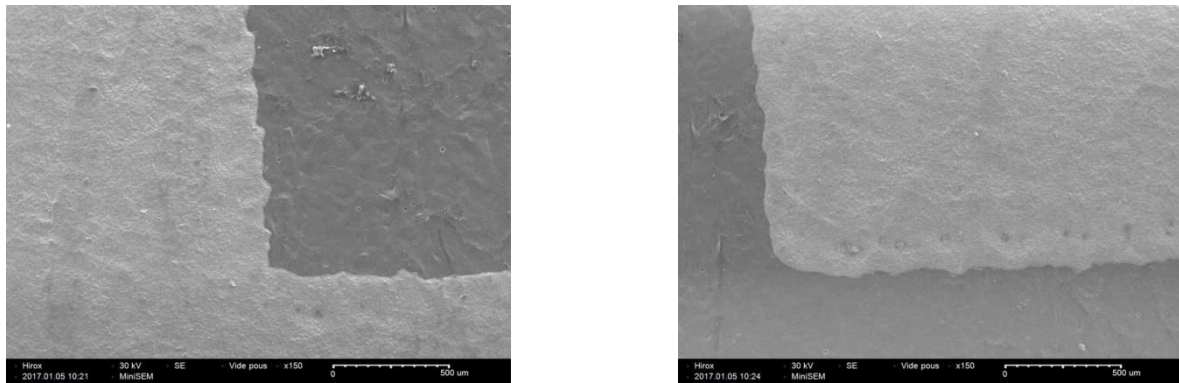


Figure 2-25: SEM image of the silver ink deposit surface at 500µm scale

Then, with the smaller scale of 20µm and 10µm, it can be seen that the silver ink deposit is formed by the chaotic stacking of numerous submicron silver particles in a random way. A lot of air gaps appear between them, which significantly reduce the conductivity of the metallic deposit. So, this deposit quality is very far from the retro-simulation model which has a rectangular solid block shape. That explains why there are always small differences between simulation and measurement even if the equivalent values of average thickness, roughness and conductivity of the silver ink deposit have already been taken into account.

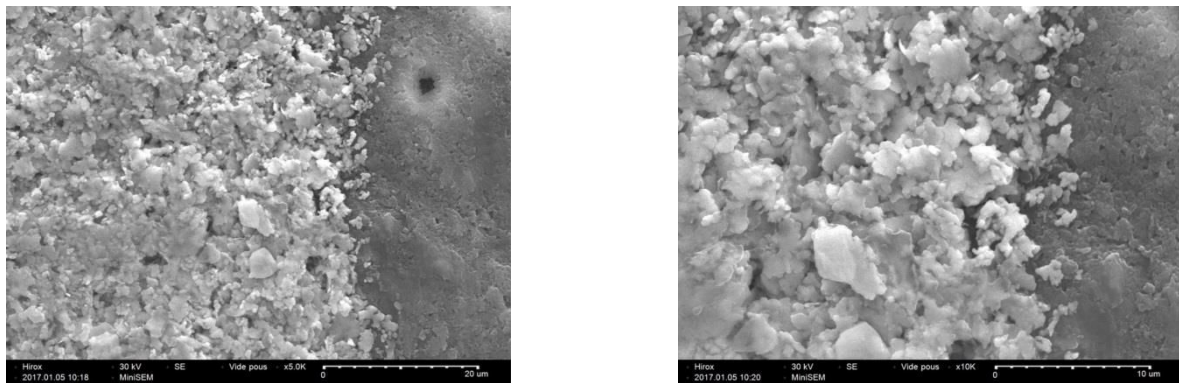


Figure 2-26: SEM image of the silver ink deposit surface at 20µm [L] and 10µm [R] scale

In contrast, the SEM images of aluminum etched deposit on PET are completely different. By comparing with the screen-printed deposit, the edge of the aluminum etched deposit is much straighter, so easier to measure the dimensions. The surface state of PET is also much more planar than that of paper with very rare pinholes. Therefore, that is the reason why the thickness measurement of the aluminum etched deposit on PET using mechanical profilometer is very clear, visual and gives accurate results, as shown in Figure 2-47.

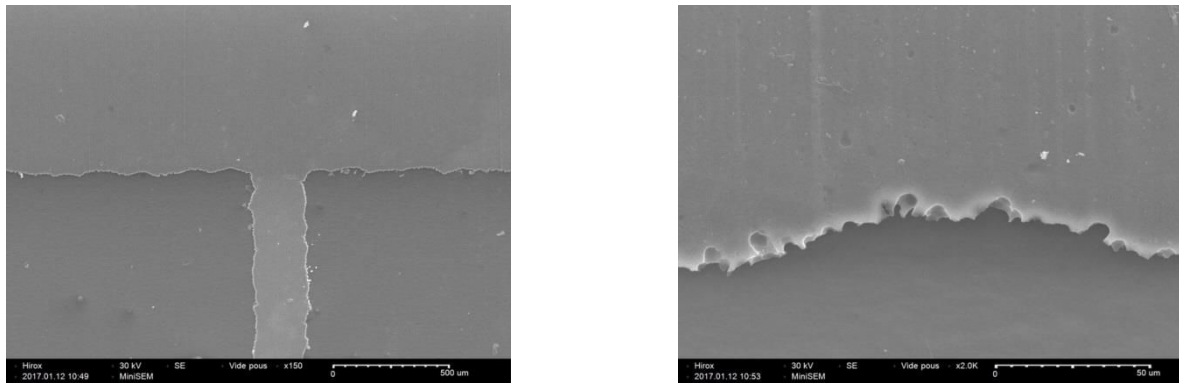


Figure 2-27: SEM image of the aluminum etched deposit surface at 500μm [L] and 50μm [R] scale

With the smaller scale 20μm and 10μm, we found that the aluminum etched deposit is a unified and planar block. There are almost no air gaps in the conductor. This explains why its conductivity is much higher than silver ink deposit. And thus, the simulations of aluminum etched lines and antennas are perfectly in agreement with the measurements, as presented in Figure 2-21.

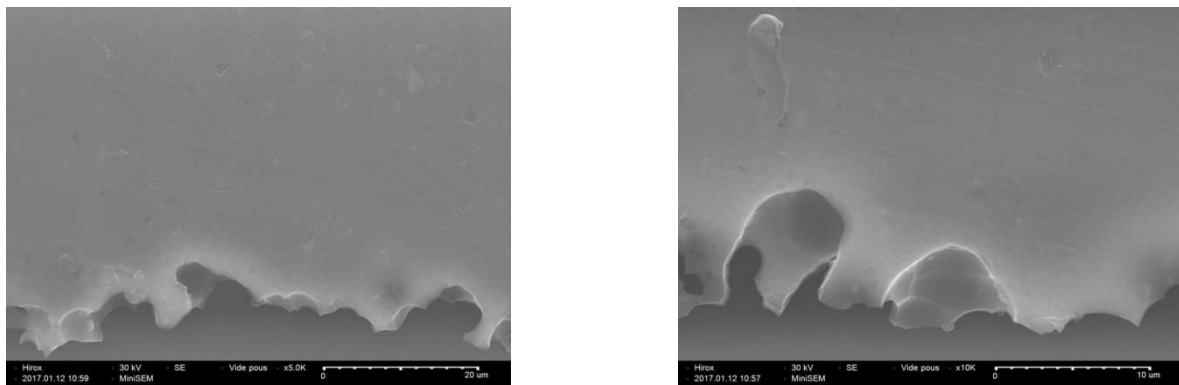


Figure 2-28: SEM image of the aluminum etched deposit surface at 20μm [L] and 10μm [R] scale

In general, we have to imagine that silver ink deposit on paper substrate is a chaotic block formed by the stacking of numerous submicron silver particles in a random way with a great roughness (due to the roughness of the printed layer plus the roughness of the paper). Therefore, it does not have the rectangular and flat shape similar to that in the simulation. Even if in the retro-simulations, we have taken into account the roughness of the deposit, the simulator has just recalculated by reducing its conductivity a little. Thus, this phenomenon cannot be simulated completely and accurately. This leads to difficulties in modelling circuits on the paper substrate. In addition, the accurate measurements of thickness, conductivity, and dimensions of the ink deposit are extremely difficult because these values vary randomly at each position on the pattern.

2.3.2 Printing process on paper

As we have presented in the state of the art in *chapter 1*, there are many metallization processes for fabricating antennas on a flexible substrate such as

paper. Of course, each method has its own advantages and disadvantages. However, we have chosen a manufacturing technique that is not expensive and most suitable for the paper substrate as well as available equipment facilities: printing process. The aluminum etching on PET has been also utilized as reference technology to compare.

For conductive ink material, different possible metal nanoparticle solutions can be applied. But gold is too expensive for mass production; whereas copper encounters a problem of oxidation in the sintering process. Therefore, silver which has the highest electrical conductivity among all of the metals is the most suitable. In this thesis, we have used a conductive ink consisting of silver nanoparticles and water solvent for "green" solution in the circuit fabrication on the paper substrate.

In the condition of facilities and equipment available, we have tested two approaches: flexography printing and screen-printing, as depicted in *Figure 2-29* below. Their performances are presented below for comparison.

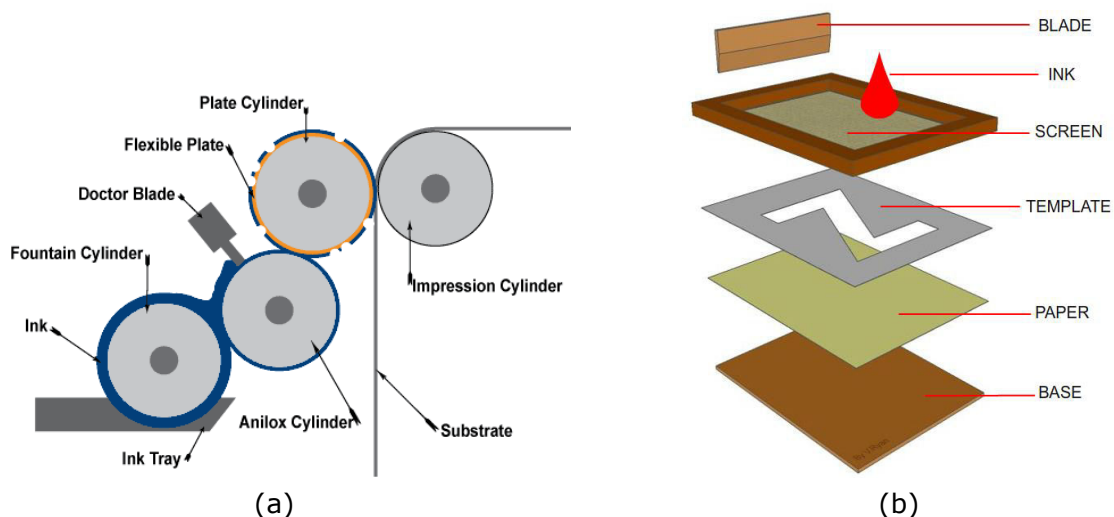


Figure 2-29: Schematic of: (a) Flexography printing and (b) Screen-printing

2.3.2.1 Flexography printing

The microscope image reveals that the printing quality of flexography is not good. There is a lack of silver ink deposition at the edge of the pattern, as shown in *Figure 2-30*, which can influence the performance of the circuit (ex: shift of resonant frequency, degradation of S_{11} ...).

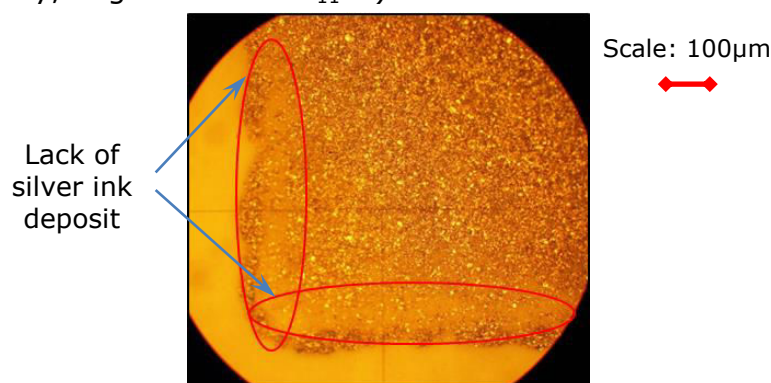


Figure 2-30: Microscope image of a flexography printed pattern on E4D paper

The average deposit thickness at a cross section measured with a mechanical profilometer is about $2.25 \pm 1.347 \mu\text{m}$ (RMS error $\sim 59.87\%$), cf. *Figure 2-31*.

The skin depth δ_n at frequency f can be calculated from the DC conductivity σ of the conductive layer by the following equation:

$$\delta_n = \frac{1}{\sqrt{\pi\mu_0\sigma f}} \quad (2-20)$$

According to the formula (2-20), the required thickness must be greater than $11.7\mu\text{m}$ for a good operation at 2.4 GHz ($\sigma = 7.7 \times 10^5 \text{ S/m}$). So, the conductor deposit in this case is too thin, just about $2.25\mu\text{m}$. This measurement also shows that the roughness of the deposit is very high in comparison with the surface state of the aluminum etched deposit on PET, as presented in *Figure 2-47*.

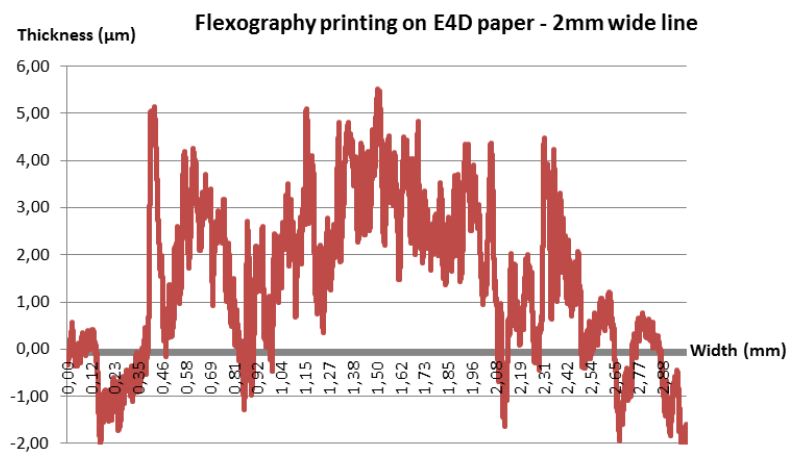


Figure 2-31: Thickness measurement of the flexography printed deposit on E4D paper

The DC conductivity value of the flexography printed silver ink measured with a four-point method is about $\sigma = (7.73 \pm 5.35) \times 10^5 \text{ S/m}$ (error 69.23%). The DC conductivity is clearly too low, less than 10^6 S/m . That will introduce too many losses in the feed lines and antennas.

We have noticed a fairly good repeatability of lines and patch antennas printed by flexography in *Figure 2-32* and *Figure 2-33* even if its printing quality is not good.

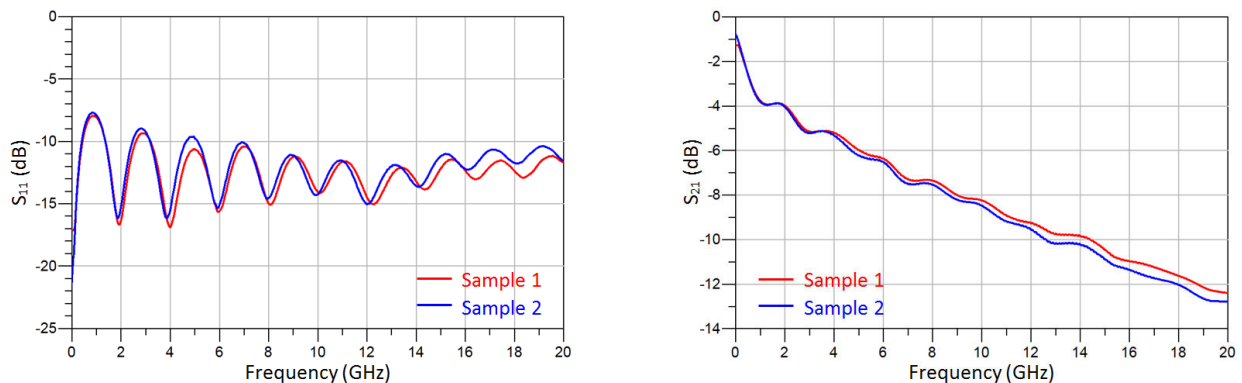


Figure 2-32: Measured S_{ij} -parameters of two samples of 2 mm width transmission line flexography-printed on E4D paper

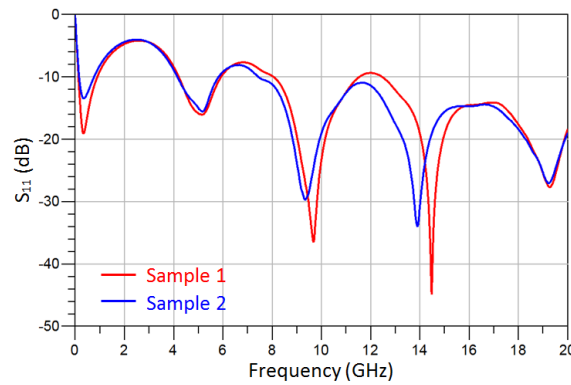


Figure 2-33: Measured S_{11} of two samples of patch antenna flexography-printed on E4D paper

However, the simulation and measurement of the patch antenna are not in agreement, cf. Figure 2-35. Specifically, from the measurement and simulation results of the printed transmission line, we have determined the dielectric properties (ϵ_r , $\tan\delta$) of the E4D paper according to the method described in section 2.2.2.2 above.

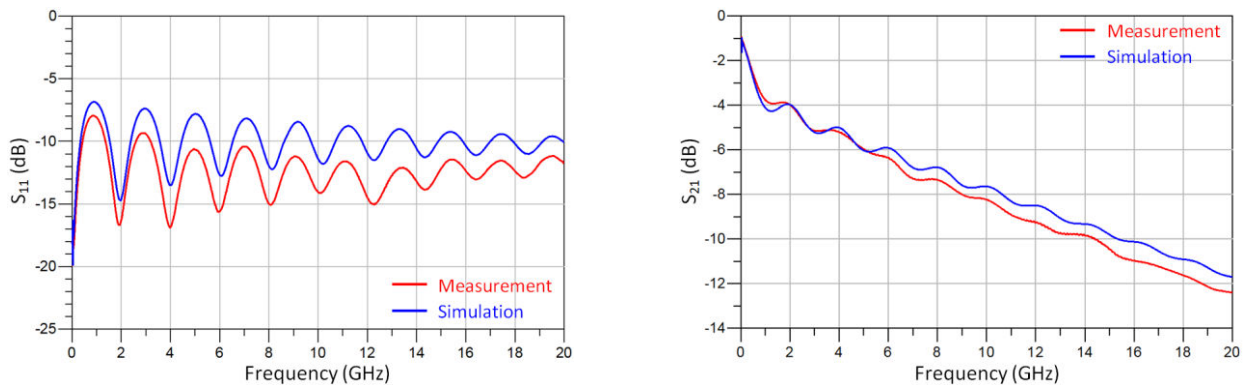


Figure 2-34: Determination of dielectric properties of E4D-290 μ m paper through a 2 mm width transmission line flexography printed: $\epsilon_r = 2.75$ & $\tan\delta = 0.05$ at 5 GHz

Then, these dielectric characteristics were incorporated into the retro-simulation of the patch antenna. We see obviously a degradation of the measured S_{11} level by comparing with the Momentum simulation even though the positions of the resonant frequencies are still quite accurate. The difference between the simulation and the measurement results in Figure 2-35 of this patch antenna can be explained by a very high roughness of the too thin ink deposit (the roughness is approximately half of the thickness). As mentioned in section 2.3.1, the silver ink deposit, in reality, does not have the rectangular and flat shape similar to that in the simulation. Thus, the conductor profile cannot be modelled accurately. And it is normal that this phenomenon cannot be simulated completely.

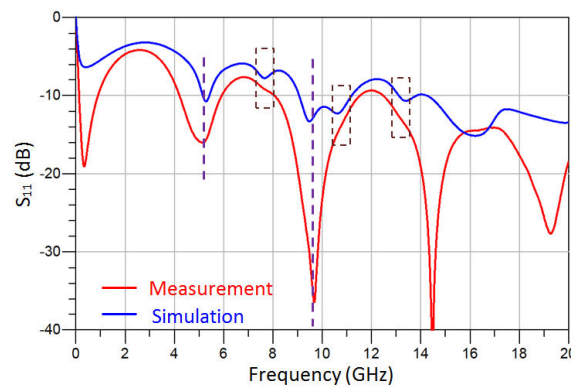


Figure 2-35: Measured and simulated S_{11} of a patch antenna flexography-printed on E4D paper

In general, this technology shows too many disadvantages and is not applicable for the realization of antennas on paper with an acceptable level of performance: especially, the ink thickness is too thin by comparing to the required skin depth and the conductivity is extremely low. And at this moment, we have not found a way to improve this technology.

2.3.2.2 Screen-printing

Under microscope image, the edge of the conductor deposit is in sawtooth form, as shown in Figure 2-36. This causes many difficulties in accurately measuring the dimensions.

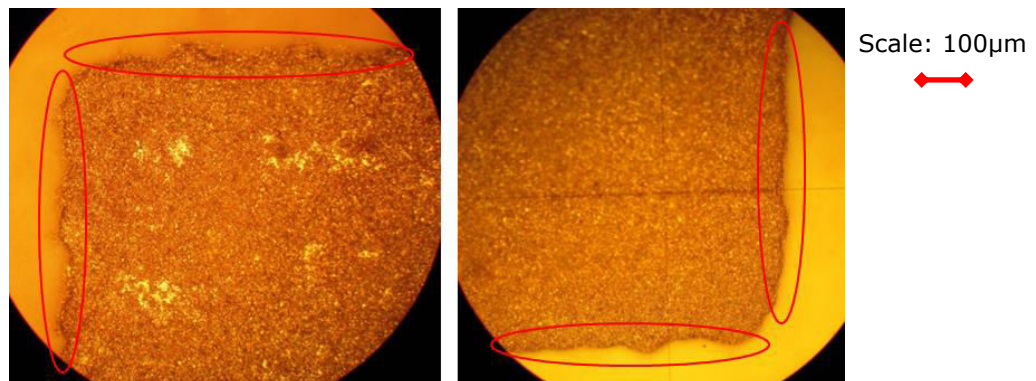


Figure 2-36: Microscope image of a screen-printed pattern on E4D paper

The average deposit thickness at a cross section measured with a mechanical profilometer is about $6.58 \pm 1.37 \mu\text{m}$ (RMS error 20.82%), cf. Figure 2-37. So, the roughness of the deposit is also very high in comparison with the aluminum etched deposit on PET (shown in Figure 2-47), but the conductor deposit is much thicker than flexography printed deposit. According to the formula (2-20), the required skin depth is about $8.4 \mu\text{m}$ for the operation at 2.4 GHz; and the average thickness of the ink layer ($7.6 \mu\text{m}$) is approximately equal to this value. This ensures a better performance of the antennas and circuits in comparison with the flexography printing.

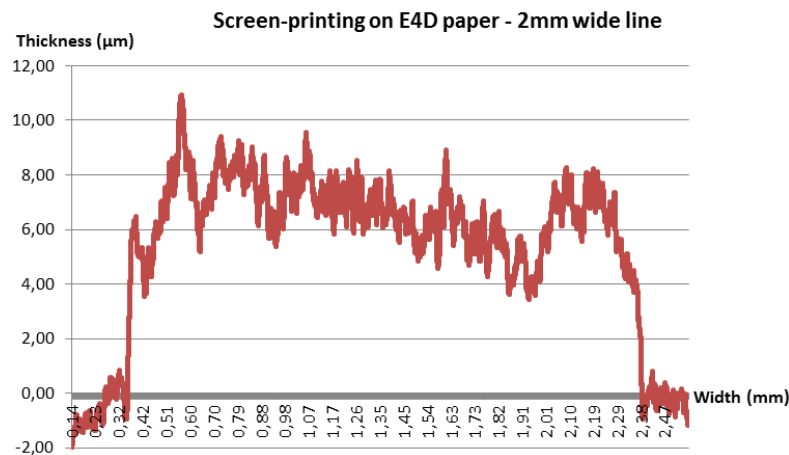


Figure 2-37: Thickness measurement of the screen-printed deposit on E4D paper

The DC conductivity value of the screen-printed silver ink measured with a four-point method is about $\sigma = (1.51 \pm 0.45) \times 10^6$ S/m (error 29.8%). So, its conductivity is about two times higher than flexography conductivity. By comparing two identical 2mmx5cm transmission lines fabricated on the same E4D paper substrate using flexography printing and screen-printing, we have easily noticed that the second one has much fewer losses, as shown in Figure 2-38 below.

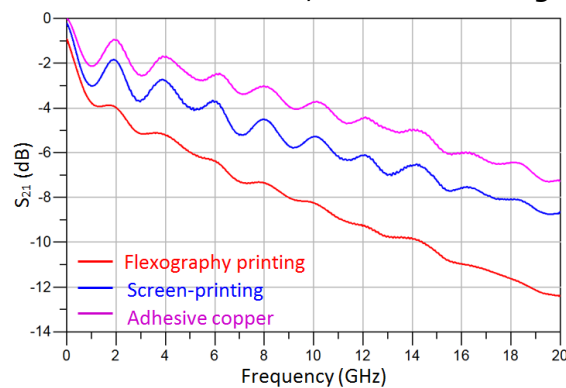


Figure 2-38: Performance comparison of three identical 2mmx5cm transmission lines fabricated using various metallization technologies like adhesive copper tape, screen printing and flexography printing on the same E4D paper substrate

We have also recognized a fairly good repeatability of different tested samples of screen-printed lines and patch antennas in Figure 2-39 and Figure 2-40.

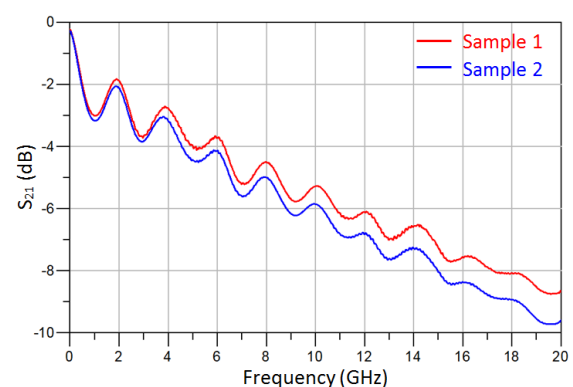
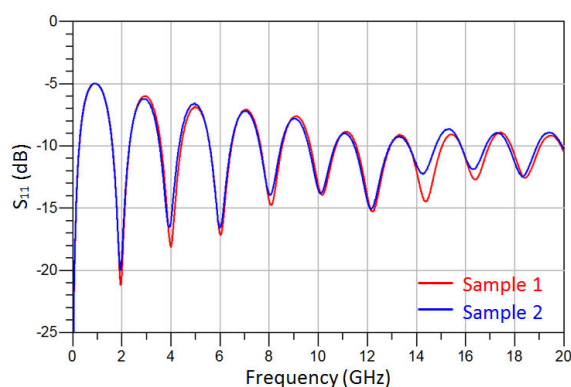


Figure 2-39: Measured S_{ij} -parameters of two samples of 2 mm width transmission line screen-printed on E4D paper

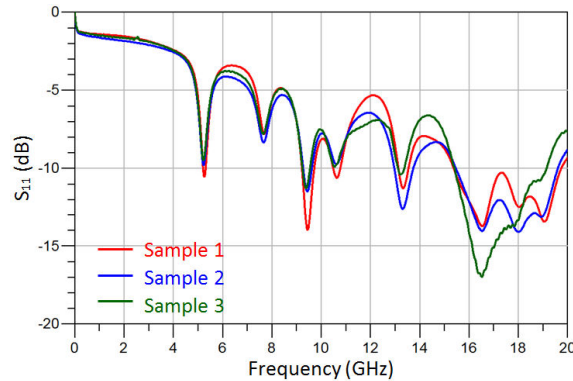


Figure 2-40: Measured S_{11} of three samples of patch antenna screen-printed on E4D paper

Moreover, the simulation and measurement of the patch antenna are in very good agreement over the whole frequency band chosen, from 0 to 20 GHz, as depicted in Figure 2-42. We have done the same process like with flexography: the dielectric characteristics of E4D paper were incorporated into the retro-simulation of the patch antenna. But in this case, a very good concordance was obtained. This greatly improved performance can be explained mainly because the thickness of the ink deposit has been increased significantly (the roughness is still very high, but only about 1/5 the ink thickness). That allows the simulation to be more accurate in comparison with the measurement results.

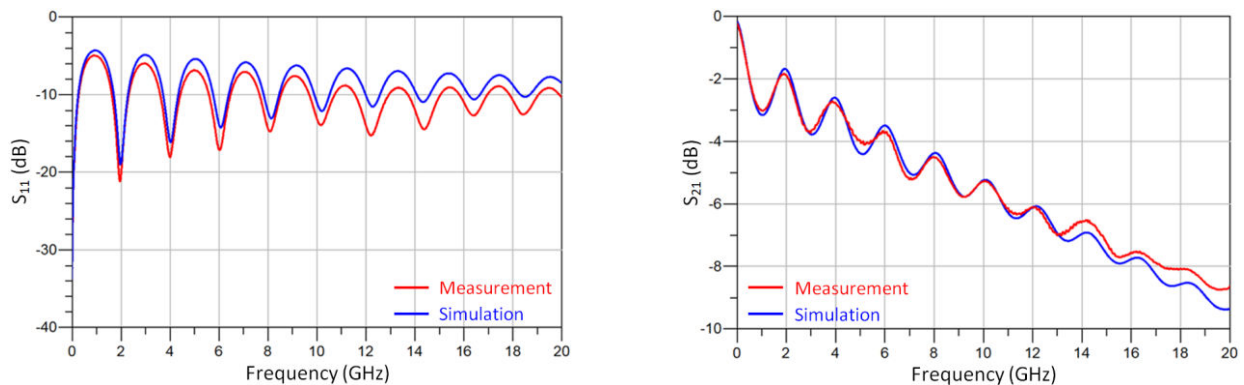


Figure 2-41: Determination of dielectric properties of E4D-240μm paper through a 2 mm width transmission line screen-printed: $\epsilon_r = 2.54$ & $\tan\delta = 0.05$ at 5GHz

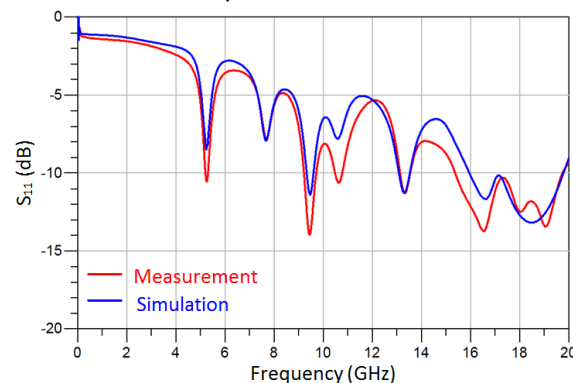


Figure 2-42: Measured and simulated S_{11} of a patch antenna screen-printed on E4D paper

Looking at the better quality of the deposit, the higher conductivity, the good repeatability and the better performance of screen-printing process, we have decided to use it as the definitive choice in this thesis work.

2.3.3 Measurement of thickness and conductivity of ink deposit

For thickness measurement of ink deposit, we have used a mechanical profilometer, as depicted in *Figure 2-43* below.

In fact, we have realized many measurements in the arrow directions, as shown in *Figure 2-43*, namely as follows:

- (1) Measurement of the paper roughness
- (2) Measurement of the ink deposit roughness
- (3) Measurement of the ink deposit thickness

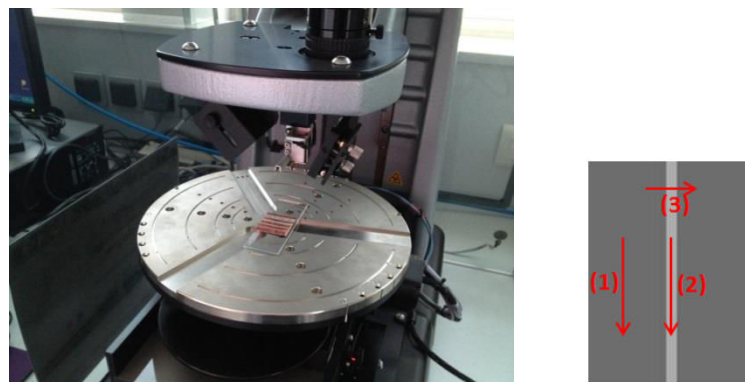


Figure 2-43: Measurement of the deposit thickness with a Veeco mechanical profilometer at UBO

For paper roughness measurement, we have measured at 9 different positions on the paper surface and have calculated the average value: $3.02 \pm 0.351 \mu\text{m}$. We can easily notice that the roughness of E4D paper is extremely high.

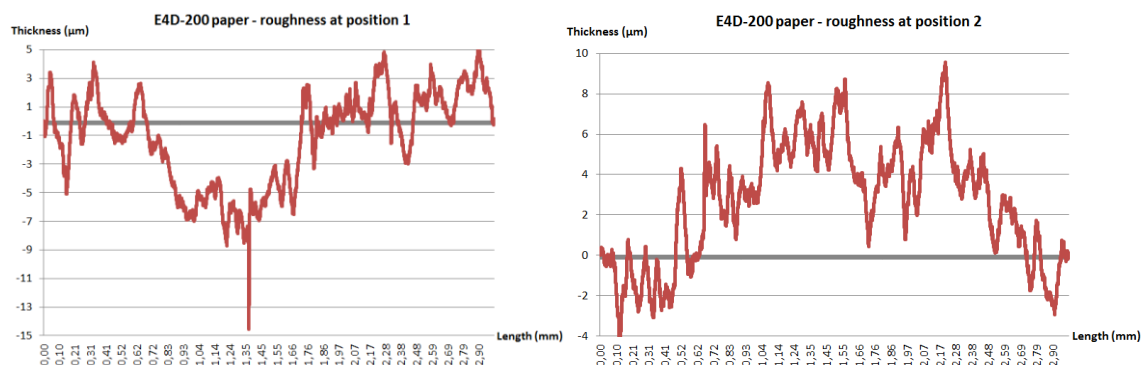


Figure 2-44: Measurement of the paper roughness at two different positions on E4D paper

For ink deposit roughness measurement, we have measured at 11 different positions along the screen-printed line and have calculated the average value: $2.846 \pm 0.657 \mu\text{m}$. Obviously, the roughness of the screen-printed deposit is also extremely high.

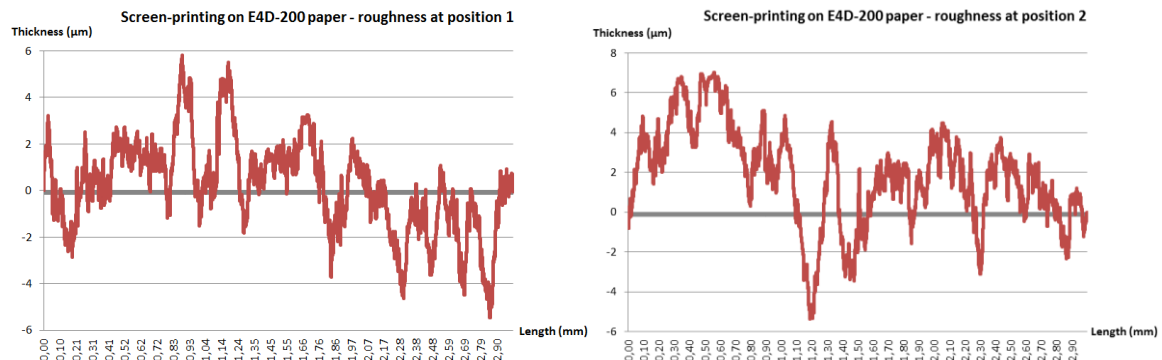


Figure 2-45: Measurement of the ink deposit roughness at two different positions on screen-printed line

Finally, we have measured at 19 cross-sections on a same line 2mm x 4cm to estimate the average thickness of the screen-printed ink deposit: $7.604 \pm 2.068 \mu\text{m}$.

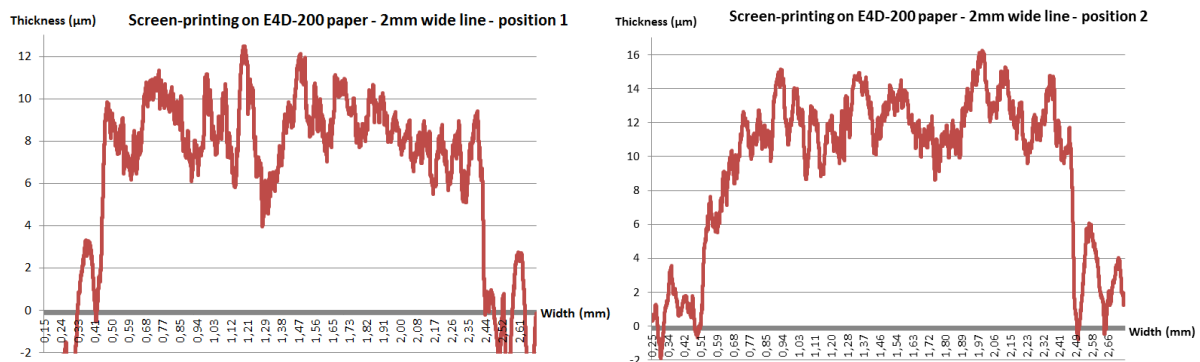


Figure 2-46: Measurement of the ink deposit thickness at two different cross-sections on the 2mmx4cm screen-printed line

We have easily noticed that the margins of the ink deposit are not clear because of the extremely high roughness of the E4D paper and of the screen-printed deposit. That greatly affects the precision of the thickness measuring of the ink deposit. This is the reason why the ink thickness measurement is really very difficult and not totally precise. And the mechanical profilometer, which measures simultaneously the quality of the ink deposit & the paper sheet, is not an appropriate instrument for accurately measuring the thickness of the pattern printed on a paper substrate. That is also the constraint of this mechanical profilometer.

We have also measured the thickness of aluminum etched deposit for comparison. And we can easily see the difference. The average deposit thickness at a cross section measured with the same mechanical profilometer is about $6.76 \pm 0.439 \mu\text{m}$ (RMS error 6.49%), cf. Figure 2-47. The surface quality of the aluminum etched deposit is much smoother, and therefore the thickness measurement is simpler and more accurate.

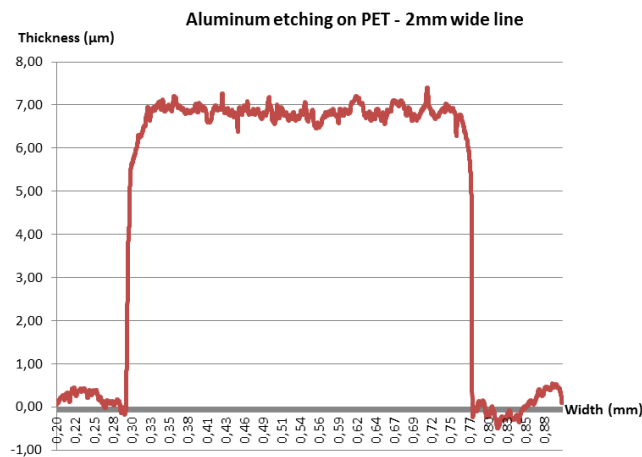


Figure 2-47: Thickness measurement of the aluminum etched deposit on PET

In order to measure the DC conductivity, we have used a 4-point method. This method is described in detail in ANNEX A. It is normally used to measure sheet resistance of thin films.

The average DC conductivity calculated is $(1.51 \pm 0.45) \times 10^6$ [S/m] (error 29.8%) for recto layer and $(1.49 \pm 0.41) \times 10^6$ [S/m] (error 27.5%) for verso layer. The DC conductivity of aluminum etched deposit, measured by the same method, is $\sigma_{\text{Alu}} = (3.59 \pm 0.29) \times 10^7$ [S/m] (error 8.1%).

Obviously, the conductivity of screen-printed ink deposit, just about 1.5×10^6 S/m, is much lower than aluminum etching (more than 20 times). This is completely understandable and reasonable, as we have observed in section 2.3.1. The silver ink deposit is formed by the chaotic stacking of numerous submicron silver particles along with a lot of air gaps between them. Therefore, the quality of the metallic connections cannot be compared to aluminum bulk, which is a unified block. The relative error of about 30% is also much higher, mainly due to error in the thickness measurement of the silver ink deposit.

The low conductivity will lead to significant metal losses of the feed lines and result in a decreased performance of the antennas (gain, efficiency) and RF circuits. This contributes to the main difficulties for designing an antenna system on a flexible paper substrate beside the very high dielectric losses of paper. For the perspective, in order to improve the conductivity problem, we need to study furthermore about the printing and sintering process or use the silver ink having a better quality.

2.4 Conclusion of chapter 2

In this chapter, we have presented a characterization method using microstrip transmission line resonator on the flexible substrate as well as the characterization of the silver ink layer. All of the results show the good agreement between measurements and simulations over the ultra-wide frequency band 0-20 GHz. These experimental results prove a high precision of our dielectric characterization method on any flexible substrate.

In general, all paper substrates show very high dielectric losses ($\tan\delta > 0.04$, more than 10 times greater than the $\tan\delta$ of Rogers®). Therefore, for antenna design on paper substrate, we must choose antenna types mostly monopole or dipole in order to limit the influence of its dielectric losses to the antenna performance because the

monopole and dipole antennas only consider the paper support (which having a thin thickness) as a very small portion of the surrounding environment and the electromagnetic field is not restricted in the substrate between the pattern and the ground plane as in the case of patch antenna. In addition, the paper substrate and the silver ink deposit on it have an extremely high roughness ($\Delta = 3 \mu\text{m}$). The associated screen-printing metallization is a random deposition of silver ink particles ($\Delta = 2.8 \mu\text{m}$) with a limited thickness of the deposit ($t = 7.6 \mu\text{m}$). Moreover, this silver ink metallization has too many metallic losses due to the very low conductivity σ (approximately $1.5 \times 10^6 \text{ S/m}$, over 30 times lower than the copper bulk conductivity). That has a particularly significant impact on the losses of the designed antenna system. Therefore, for perspective, we must improve in future the printing process and the silver ink quality.

Meanwhile, a reference technology like aluminum etching on PET shows a much more superior performance. PET has much lower dielectric losses and better surface quality than paper. And aluminum etching metallization has also a much higher conductivity than screen-printing along with the more stable thickness.

However, we still choose the paper substrate for this thesis work thanks to its ultra-low-cost and environmentally friendly characteristics such as mentioned in *chapter 1*. E4D paper is finally chosen as a flexible substrate for the antenna system design after a characterization test of several paper types. And silver ink screen-printing is also chosen as the definitive fabrication technique, which is compatible with paper substrate and is most performing in the condition of our available equipment.

Chapter 3: Antenna realization on flexible substrate

Principal content

3.1	Introduction.....	91
3.2	Patch antenna.....	91
3.3	Planar monopole antenna	94
3.4	Dual-band Wi-Fi monopole antenna (2.4 GHz/5.5 GHz)	97
3.5	Planar dual-band dipole antenna (2.4 GHz/5.5 GHz)	104
3.6	Conclusion of chapter 3	112

3.1 Introduction

After the characterization of the flexible paper substrate and the conductive layer, we have tested the elementary antennas such as patch, monopole to validate the models established from the properties of the materials deduced in the previous chapter. Then, the antennas have been designed to satisfy the applications and the technical specification requirements given in *chapter 1*. These antennas will be investigated and characterized thoroughly for parameters such as return loss, radiation pattern, gain, efficiency in a stand-alone operation state. The difficulties in the design and implementation will also be presented. All potential radiation structures will be selected to build the antenna system for the final demonstrator.

3.2 Patch antenna

Firstly, we need to validate the electrical performance of the "printed paper" technology. A classic rectangular patch antenna with a microstrip feed line was tested in order to verify the characterization results of the dielectric properties of the flexible substrates, as presented in *chapter 2*. The layout and the prototype of the patch antenna screen-printed on E4D-240 μ m paper are shown in *Figure 3-1* below.

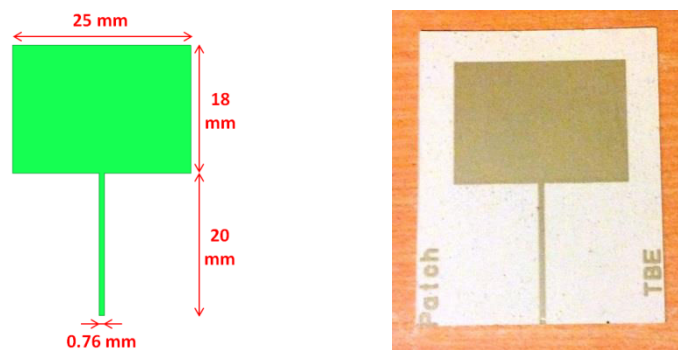


Figure 3-1: Design and prototype of the patch antenna, screen-printed on E4D-240 μ m paper

This patch antenna was initially designed to validate the dielectric properties of E4D paper substrate and prove that the characterization results are accurate. Therefore, a retro-simulation was deployed over the ultra-wide frequency band 0 – 20 GHz, as described in Figure 3-2. Overall, a very good agreement was observed over this entire frequency band.

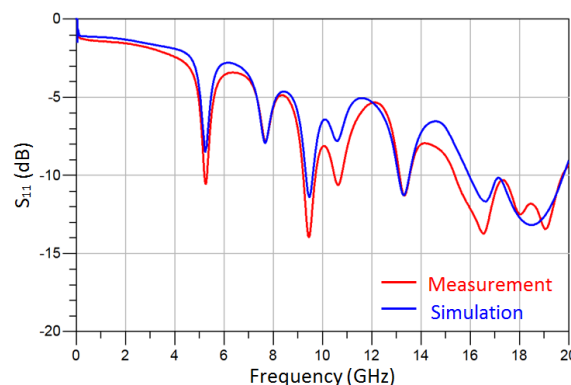


Figure 3-2: Measured and simulated return loss of a patch antenna screen-printed using silver ink on E4D paper

The return loss S_{11} yielded a resonance frequency of 5.2 GHz, as shown in *Figure 3-3*, but the impedance matching was not good and the -10dB impedance bandwidth is very narrow. The narrow bandwidth is normal with this patch antenna type.

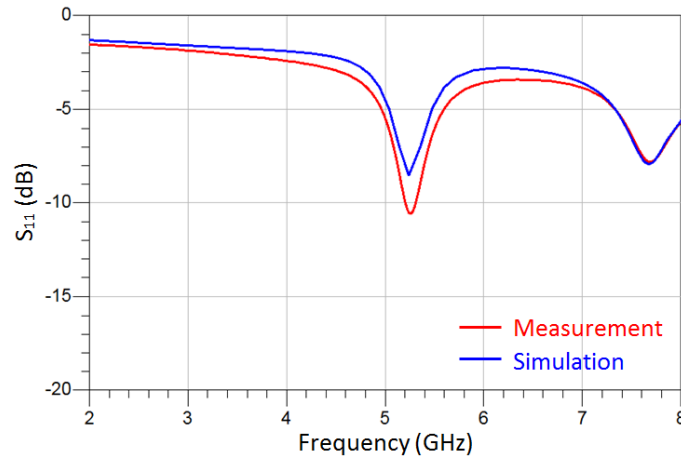


Figure 3-3: Return loss S_{11} of this patch antenna

The radiation pattern and gain at 5.2 GHz of this screen-printed patch antenna were also measured in the Stargate[®] SG-24 anechoic chamber at MVG, as shown in *Figure 3-4*. The tolerance of this MVG system is about 0.6 dB for gain values <10dB in the frequency range of 0.4 - 6 GHz.

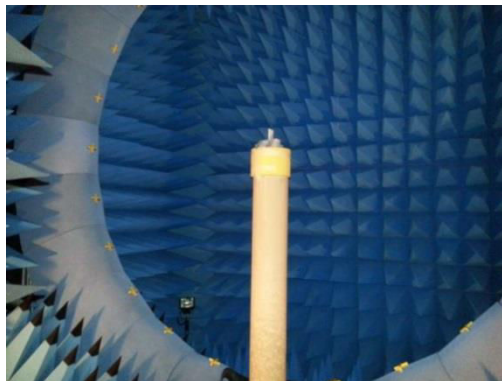


Figure 3-4: Setup of the antenna measurement in the MVG Stargate[®] system (SG-24)

The measurement results corresponded very well with the simulation as shown in *Figure 3-5*. The measured radiation pattern results of different patch antenna prototypes were also similar, which proved the good repeatability of the printing technology.

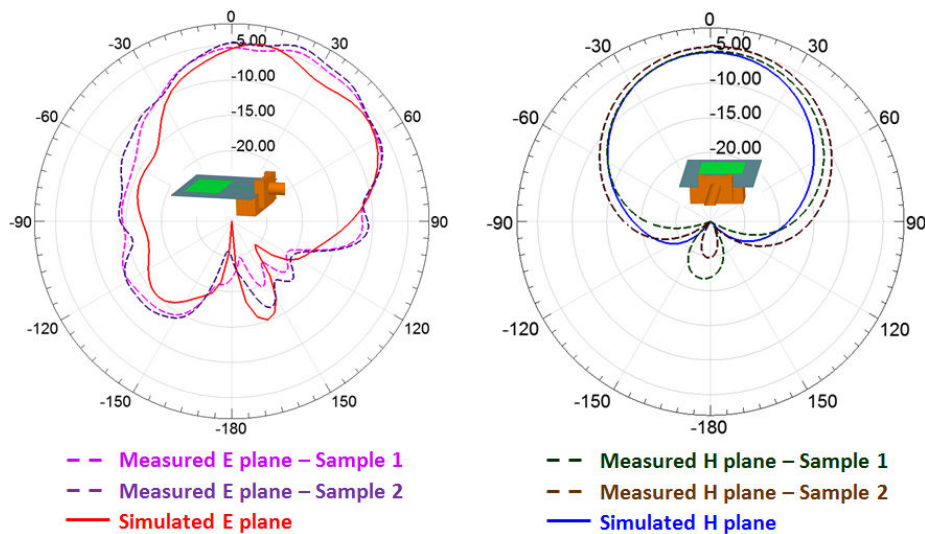


Figure 3-5: Radiation pattern in E-plane and H-plane at 5.2 GHz of the patch antenna screen-printed on E4D-240 μ m paper

At 5.2 GHz, the simulated and measured max realized gains were -4.23 dBi and -3.47 dBi respectively (excluding insertion losses in the 20 mm feed line: -1.4 dB at 5.2 GHz).

The simulated and measured total efficiencies at 5.2 GHz were just 6.1% and 7.3% respectively. Obviously, the efficiency of this patch antenna is very low. In order to analyze the cause of the very low efficiency, we have examined the ideal model of this patch antenna to compare with the actual model. The values of loss tangent of the substrate or/and of the conductivity of the metallization were tested while the dimensions of the antenna were kept unchanged.

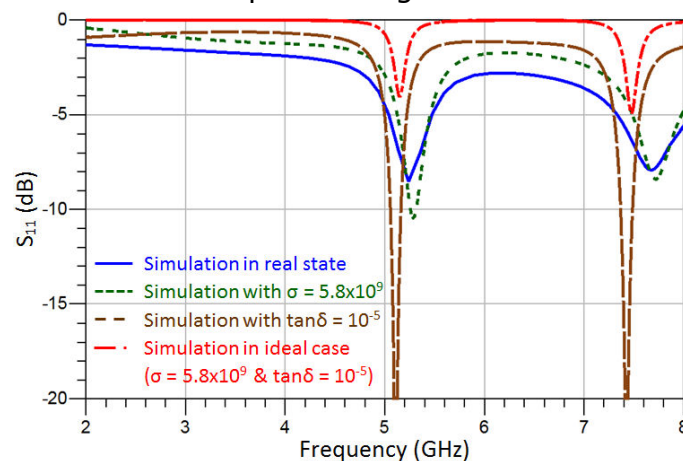


Figure 3-6: Return loss S_{11} of this patch antenna in various test cases

Case	$\tan\delta$	σ (S/m)	Realized gain (dB)	Total efficiency (%)	Radiation efficiency *
Actual	0.05	1.6×10^6	-4.23 dB	6.1%	6.9%
Perfect conductivity	0.05	5.8×10^9	-1.05 dB	12.7%	13.3%
Perfect dielectric	0.00001	1.6×10^6	-0.21 dB	15.2%	15.4%

<i>Ideal model</i>	0.00001	5.8×10^9	5.26 dB	54.2%	98%
--------------------	---------	-------------------	---------	-------	-----

Table 3-1: Performance comparison of this patch antenna in various test cases

(Radiation efficiency *: Efficiency in the case of optimal impedance matching)

By changing the characteristics of the materials (paper, silver ink), the impedance matching would also be affected accordingly, as seen in *Figure 3-6*. However, considering the radiation efficiency, we can see in the above comparison table that the efficiency of this patch antenna is very low due to both metallic losses and dielectric losses. In the ideal case with perfect dielectric and perfect conductivity, the radiation efficiency could be up to near 100%. But, if we have simulated with the real dielectric losses or the real metallic losses, the radiation efficiency was only about 13-15%. And worst of all, when combining these two loss elements in the actual model, it was just 7%.

This can be explained as follows. In terms of dielectric losses, the entire electromagnetic field, confined between the patch and the ground plane, is weakened by a dielectric substrate having too many losses ($\tan\delta = 0.05$ at 5 GHz). About the metallic losses, the large surface of patch introduces also a great number of ohmic losses due to the very low conductivity of the silver ink.

In general, the patch antenna screen-printed on paper substrate using silver ink shows the gain and efficiency very low. Moreover, the bandwidth of this kind of antenna is very narrow. Therefore, this type of antenna cannot be used for the demonstrator, but the idea herein is to validate the simple models based on the properties of the materials deduced from the characterization stage and validate also the electrical characteristics of the "printed paper" technology.

3.3 Planar monopole antenna

To overcome the disadvantages of patch antennas on paper, we have experimented another type of antenna aiming to expand the bandwidth and increase the efficiency: monopole type antenna. This kind of antenna only considers the paper support (having a thin thickness) as a very small portion of the surrounding environment. Therefore, the influence of the dielectric losses on the performance of the antenna will be reduced significantly.

In fact, a classic monopole antenna operating at 5GHz was screen-printed on the E4D-100 μ m paper (106 μ m thickness), as depicted in *Figure 3-7*. Its structure is extremely simple including a straight strip along with a small rectangular ground plane at the back side. (In this time, the antenna designs were tested on E4D-100 μ m paper before realizing that the insertion losses of the 50 Ω feed line on this flexible substrate are extremely high.)



Figure 3-7: Layout and prototype of the 5GHz monopole antenna, screen-printed on E4D-100 μ m paper

A small metallic support (10x30x10 mm³) was screwed to attach the SMA connector to the antenna for measurement. The dielectric properties of E4D-100 μ m paper ($\epsilon_r = 2.9$ and $\tan\delta = 0.06$ at 5 GHz), as well as the characteristics of the silver ink deposit (width, thickness, roughness, conductivity σ), were also incorporated into HFSS simulation in order to compare with the simulation.

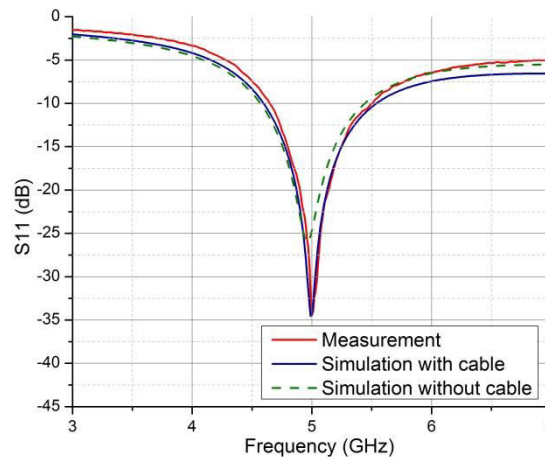


Figure 3-8: Return loss S_{11} of the classic monopole antenna screen-printed on E4D-100 μ m paper

A very good agreement between the measurement and the HFSS simulation of S_{11} was observed, cf. Figure 3-8 above. The measured return loss yielded a resonance frequency of 5 GHz with an -10 dB impedance bandwidth of 0.86 GHz (between 4.65 and 5.51 GHz) or 17.2%.

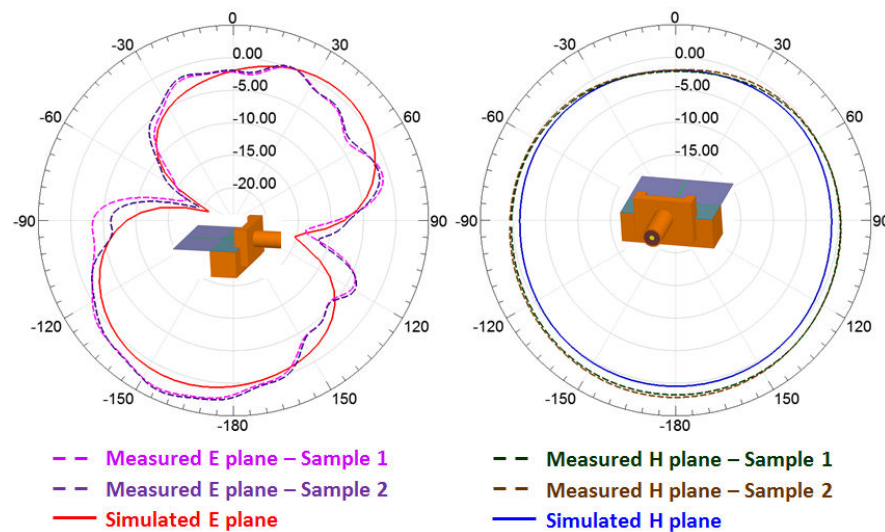


Figure 3-9: Radiation pattern in E-plane and H-plane at 5 GHz of this classic monopole antenna

The radiation pattern measured at MVG Stargate[®] (SG-24) (Figure 3-9) showed a good agreement with the HFSS simulation. The simulated and measured results exhibited a bi-directional monopole-shape radiation pattern in the E-plane and an almost omnidirectional radiation pattern in the H-plane. The E-plane graph was slightly tilted to the right and the H-plane graph was slightly shifted to the bottom due to the influence of the attached connector along with the metallic support at the back side, as depicted in Figure 3-9. However, in general, the monopole behavior like in theory has been obtained. The radiation patterns of two different tested samples were also similar, which proved the good repeatability of the printing technology and its relative sensitivity to the tolerances of the printing process.

The simulated and measured max realized gains of this antenna were 1.29dBi and 3.25dBi at 5 GHz, respectively (excluding insertion losses in the 10 mm feed line: -1.45 dB at 5 GHz). The simulated and measured total efficiencies were 81% and 91.9% at 5 GHz (0.55 dB difference) respectively. These performances are reasonable when considering a paper substrate with many losses, and a printing technology that introduces a very low conductivity ($\sigma = 1.5 \times 10^{-6}$). The difference between the measured and simulated gain, and thence between the measured and simulated efficiency, can be explained by the difference between the measured and simulated radiation patterns. So, the effect of the attached connector and metallic support in the real measurement cannot be fully simulated, namely the ripples as seen in Figure 3-9.

In general, these obtained results not only validate the measured characteristics of the E4D-100 paper substrate with the associated screen-printing metallization but also show the better performance of the monopole type antenna on the paper substrate in comparison with the patch antenna above. The antenna efficiency has increased considerably due to the weaker interaction between the guided fields and the dielectric substrate. This type of antenna (monopole or dipole) therefore seems more appropriate in terms of wider -10dB impedance bandwidth, quasi-omnidirectional radiation pattern and improved efficiency (efficiency > 60%) to construct the final antenna system. Multi-frequency or ultra-wideband antenna solutions can be thence applied to satisfy multi-standard, multi-band

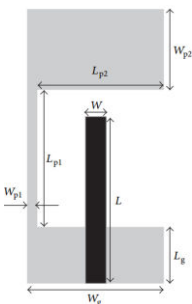
communication requirements. However, in order to avoid the risks of electromagnetic pollution, the multi-frequency solution is more preferred.

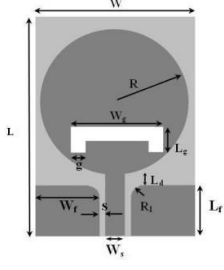
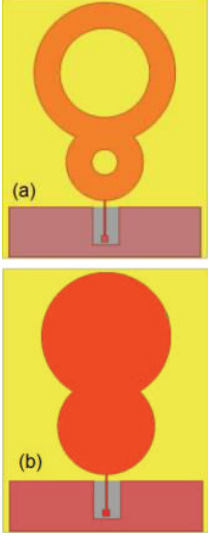
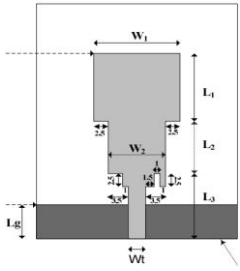
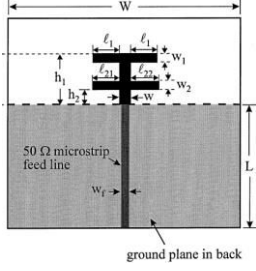
3.4 Dual-band Wi-Fi monopole antenna (2.4 GHz/5.5 GHz)

As mentioned in the previous section, we have developed the monopole or dipole type antenna with multi-frequencies performances in order to satisfy the multi-standard communication requirements of advanced multimedia set-top-boxes given at the beginning of this thesis. The proposed antenna must cover at least two frequency bands 2.4 – 2.5 GHz and 5.15 – 5.85 GHz, with omnidirectional radiation pattern and minimum 60% radiation efficiency. Of course, manufacturing constraints are to be considered regarding the available fabrication technology of our partner. So, the antenna has a simple configuration for easy and robust realization. And most importantly, the antenna size is very limited to permit its integration into a set-top-box by sticking it on plastic sidewalls of the casing. Specifically, the length of the radiator and ground should not exceed 3cm (height of the electronic box). So, the designed antenna must be very compact.

Many solutions of planar dual-band monopole have been reported in the literature for wireless applications, as summarized in *Table 3-2*. All these antennas have two frequency bands which can be controlled independently. However, many of them have a quite large size not compatible with the required compactness feature. Therefore, we have chosen a folded antenna, inspired from the 9-shaped folded monopole in [Jyoti 2011], to implement our dual-band monopole structure. The expected bandwidths for WLAN applications can be reached, considering also miniaturization criterias (by utilizing the meandered lines) with simple geometry. The main drawback is probably its non-ideal monopole-like radiation pattern at 5.5 GHz due to the influence of the long C branch.

We have also noticed that a lot of monopole antennas in the literature use the coplanar waveguide (CPW) structure instead of microstrip structure for the feed line. This will help the electromagnetic field to propagate significantly less in the lossy substrate. In addition, the wider central signal line permits to reduce the ohmic (metallic) losses. However, in our reality case, the gaps between the central signal line and the ground planes on both sides will be very small: just about 0.08 mm (if the central signal line is 3mm on 106 μm thick E4D-100 paper). This is not compatible with our printing technology when the error tolerance of dimension is about ± 0.05 mm. Therefore, we have still designed our monopole antenna with microstrip feed line structure even though its quite great losses.

Antenna	Shape	Substrate	Advantage	Disadvantage
Monopole with an extended ground plane [Ayman 2016]		FR4 (1.6 mm thick, $\epsilon_r=4.4$)	Compact size (25×10 mm ²). Two frequency bands can be controlled independently by the inverted-L parasitic resonator and the length of	The impedance matching at low-frequency band is not good. The gains at low frequency band are reduced due to the loss of

			the straight strip.	coupling with the parasitic resonator.
<i>Circular monopole with U-slot</i> [Yuan Zhu 2016]		FR4 (1.5 mm thick, $\epsilon_r=4.4$, $\tan\delta=0.019$)	Two frequency bands can be controlled independently by circular patch size and U-shaped slot.	Its size ($28 \times 26 \text{ mm}^2$) is relatively large. The H-plane radiation pattern at 5.5 GHz is slightly distorted.
<i>Cascaded annular ring or Cascaded disk</i> [Lo Hine Tong 2016]		PET (130 μm thick, $\epsilon_r=2.85$, $\tan\delta=0.009$)	Two frequency bands can be controlled independently by the radius of the two rings/disks. Omnidirectional radiation pattern at the two resonance frequencies.	Its size ($33 \times 22 \text{ mm}^2$) is relatively large.
<i>Dual-Band (2.4/5.2GHz) Monopole</i> [Rathore 2010]		FR4 (1.57 mm thick, $\epsilon_r=4.4$)	Two frequency bands can be controlled independently. Almost omnidirectional radiation pattern at the two resonance frequencies.	Its size ($29 \times 15 \text{ mm}^2$) is relatively large.
<i>Double-T monopole</i> [Yen-Liang 2003]		FR4 (0.8 mm thick, $\epsilon_r=4.4$)	Compact size ($16.5 \times 18 \text{ mm}^2$). Two frequency bands can be controlled independently by the two T-branches.	The impedance matching at low-frequency band is not good. The bandwidth at high-frequency band is very narrow.

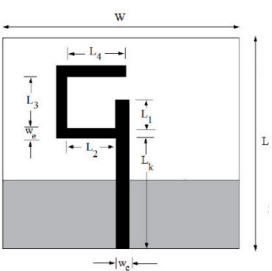
<p>9-shaped folded monopole [Jyoti 2011]</p>		<p>FR4 (1.6 mm thick, $\epsilon_r=4.4$)</p>	<p>Compact size ($18 \times 11 \text{ mm}^2$). Two frequency bands can be controlled independently by the lengths of the two branches.</p>	<p>The E-plane radiation pattern at 5.5 GHz is slightly distorted and does not show the ideal monopole behavior.</p>
--	---	--	---	--

Table 3-2: State of the art of the planar dual-band monopole for Wi-Fi application

In fact, a dual-band Wi-Fi monopole has been designed by parametric optimization for WLAN applications at two frequency band 2.4 - 2.5 GHz and 5.15 - 5.85 GHz. The layout and the prototype of this antenna, screen-printed on E4D-100 μm paper, are shown in *Figure 3-10* below. (In this time, the antenna designs were tested on E4D-100 μm paper before realizing that the insertion losses of the 50 Ω feed line on this flexible substrate are extremely high.)

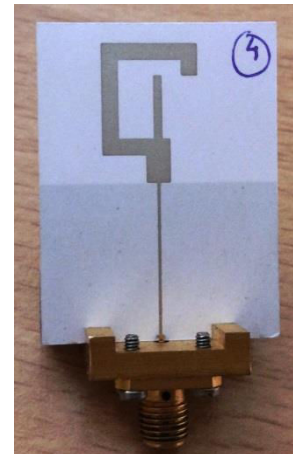
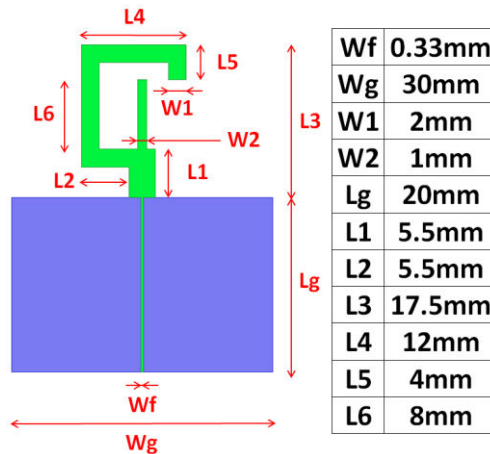


Figure 3-10: Layout and prototype of the dual-band Wi-Fi monopole antenna, screen-printed on E4D-100 μm paper

This monopole, with a compact size ($17.5 \times 12 \text{ mm}^2$), exhibits two resonance frequencies and two associated bandwidths that can be controlled independently. It has two radiating elements: a hook-shaped branch #1 for the low-frequency band and a straight branch #2 for high frequencies. Its structure is also simple, appropriate for the double-sided printing process on paper substrate, and there are no special technical requirements for antenna fabrication (no via holes realization, for example).

The behavior of the antenna has been also studied through the visualization of current distributions using HFSS EM-simulations in order to verify the independence of the two frequency bands (2.4 and 5.5 GHz), as shown in *Figure 3-11*. It can be seen that the hook-shape branch #1 has a high current density and appears to be "active" at 2.4 GHz (see *Figure 3-11a*). On the other hand, the straight branch #2 is more "active" at 5.5 GHz. It can be seen that the current is concentrated mostly around the straight branch #2 (see *Figure 3-11b*).

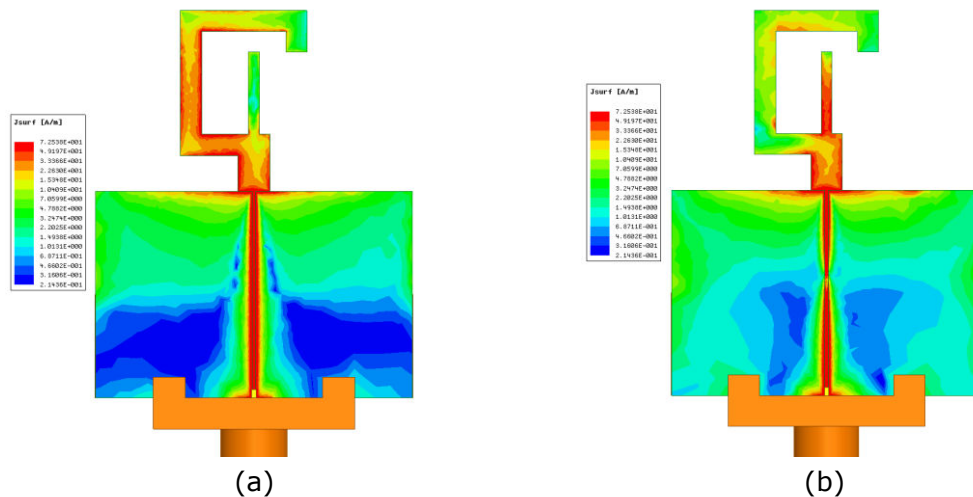


Figure 3-11: Simulated current distribution at: (a) 2.4 GHz and (b) 5.5 GHz

Since the two branches appear as quite independent in terms of electrical behavior in the two sub-bands, a parametric analysis has been carried out by varying one of the effective length parameters while keeping constant the other length parameter of the antenna to reach the optimized dimensions, as illustrated in Figure 3-12 and Figure 3-13.

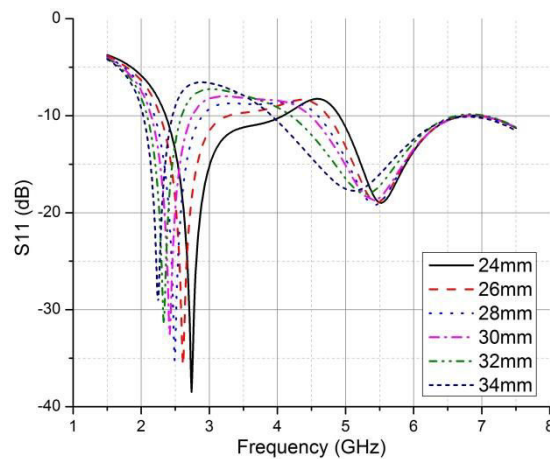


Figure 3-12: Effects of changing L_1 , length of the hook-shaped branch #1, on the 2.4 GHz frequency band

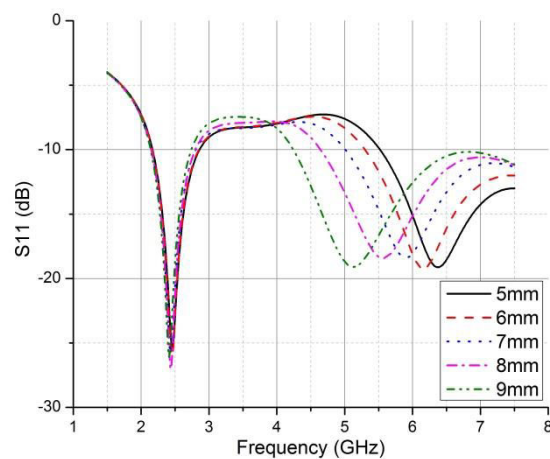


Figure 3-13: Effects of changing L_2 , length of the straight branch #2, on the 5.5 GHz frequency band

It can also be seen that the resonance frequencies, as well as the associated bandwidths of the antenna, are sensitive to the length of each branch. Hence, we can also notice that the performance of this antenna could be sensitive to the dimension tolerance of the fabrication process, specifically herein the length of two branches. However, considering the quite good printing technology accuracy (about ± 0.05 mm), a negligible impact has been observed.

The return loss S_{11} , radiation patterns and gains of this antenna at two resonance frequencies 2.4 GHz and 5.5 GHz were measured to compare with the HFSS simulations and to analyze its performance. A small metallic support ($10 \times 30 \times 10$ mm³) was screwed to attach the SMA connector to the antenna for measurement.

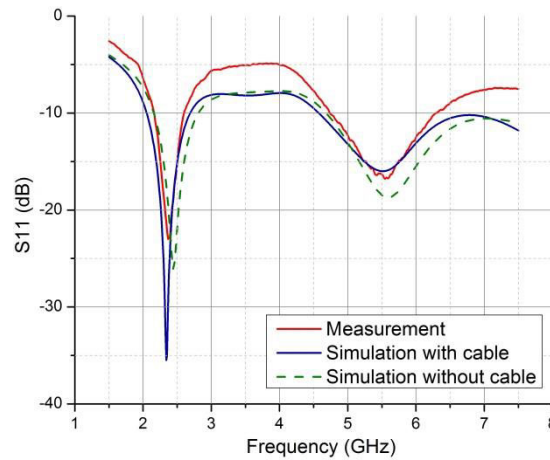


Figure 3-14: Return loss S_{11} of this dual-band Wi-Fi monopole antenna

A reasonably good concordance was obtained between the measurement and the HFSS simulation of S_{11} . Obviously, the simulation with connector and cable was more accurate in comparison with the measurement than simulation without connector and cable. The simulated return loss, displayed in Figure 3-14, yielded a 1st frequency of 2.4 GHz with an impedance bandwidth of 0.64 GHz and a 2nd frequency of 5.5 GHz with an impedance bandwidth of 2.22 GHz. Meanwhile, the measured -10dB impedance bandwidths are 0.44 GHz (18%) and 1.55 GHz (28.2%) at 2.4 and 5.5 GHz, respectively. They completely covered the two bands of IEEE.802.11a/b/g/n/ac WLAN standards. This indicates the suitability of the proposed antenna for the WLAN systems.

The radiation patterns measured at 2.4 GHz and 5.5 GHz with a MVG Stargate® system (SG-24) showed a good agreement with the HFSS simulations (cf. Figure 3-15a and Figure 3-15b). It can be observed that the H-plane radiation patterns were almost omnidirectional at both resonant frequencies 2.4 and 5.5 GHz. At 2.4 GHz, the simulated and measured results exhibited a bi-directional monopole-shape radiation pattern in the E-plane. The E-plane graph was slightly tilted to the right and slightly distorted due to the influence of the attached connector along with the metallic support at the back side, as depicted in Figure 3-15a. Meanwhile, at 5.5 GHz, we have no longer seen a bi-directional monopole behavior in the E-plane due to the influence of the hook-shaped branch #1 into the radiation pattern of the straight branch #2. Specifically, there was only one null toward the ground plane and the null toward the hook-shaped branch #1 has been lost.

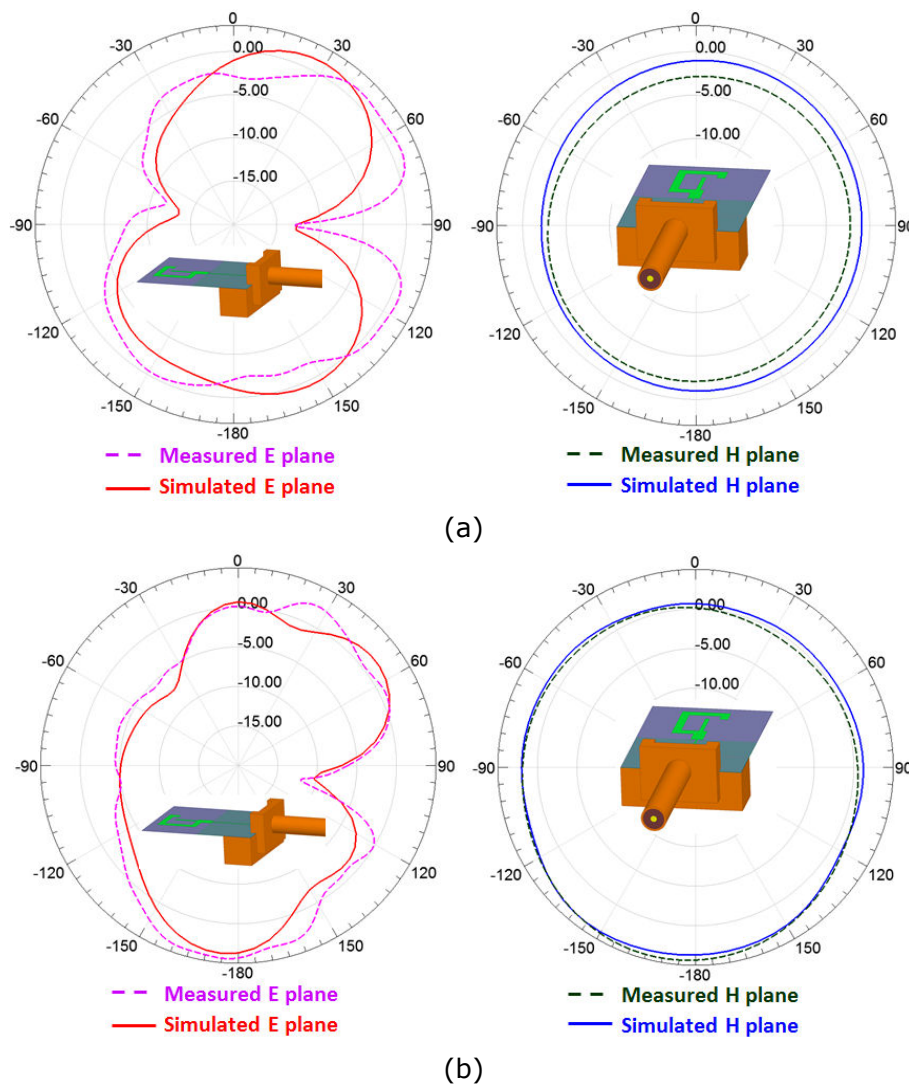


Figure 3-15: E-Plane and H-Plane radiation patterns obtained from simulation and from measurement of dual-band Wi-Fi monopole antenna at: (a) 2.4 GHz and (b) 5.5 GHz

The simulated and measured max realized gains versus frequency (Figure 3-16) are also fairly consistent: 1.3dBi and 1.87dBi at 2.4 GHz, 3.21dBi and 4.1dBi at 5.5 GHz, respectively (excluding insertion losses in the 20 mm feed line: -2.3 dB at 2.4 GHz and -3.1 dB at 5.5 GHz).

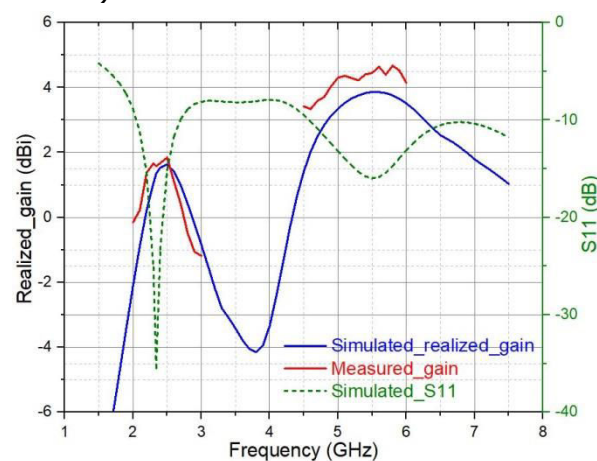


Figure 3-16: Simulated and measured realized gain of the antenna versus frequency

The simulated max realized gain and total efficiency are slightly different from measured values, as summarized in Table 3-3. Obviously, with relatively low gain antennas, the influence of cable, connector and metallic support in the measurement environment, which cannot be totally taken into account in the simulation, is significant to the measurement results. Moreover, the uncertainties in thickness and conductivity measurement of the ink deposit and in the $\tan\delta$ determination of the paper substrate also introduce the impact on the accuracy of the simulation.

The simulated and measured total efficiency was 80.4% and 64.5% at 2.4 GHz (0.96 dB difference) and 92.6% and 93.4% at 5.5 GHz (0.04 dB difference) respectively, excluding insertion losses in the 20mm feed line (estimated losses: -1.15 dB/cm at 2.4 GHz and -1.55 dB/cm at 5.5 GHz for 50 Ω feed line on E4D-100 μ m paper: $\epsilon_r = 2.9$, $\tan\delta = 0.06$ at 5.5 GHz). It can be seen that the efficiency at 2.4 GHz is lower than at 5 GHz because the ink thickness (7.6 μ m) is not enough if compared with the skin depth condition, which introduces more metallic losses. According to the formula (2-20), the required thickness must be greater than 8.4 μ m for a good operation at 2.4 GHz ($\sigma = 1.5 \times 10^6$ S/m). We have also noticed that even if the conductor thickness along with the roughness is incorporated into the simulation, HFSS simulator has just used them to recalculate the conductivity value. So, the skin depth phenomenon at 2.4 GHz is not fully modelled like in practice. That is the reason why the discrepancy between the simulated and measured efficiency at 2.5 GHz is greater than that at 5.5 GHz.

Comparison	Frequency (GHz)	Max realized gain (dBi)	Total efficiency (%)
Simulation	2.45 GHz	1.3 dBi	80.4% (-2.6 dB)
	5.5GHz	3.21 dBi	92.6% (-3.4 dB)
Measurement	2.45 GHz	1.87 dBi	64.5% (-4 dB)
	5.5GHz	4.1 dBi	93.4% (-2.5 dB)

Table 3-3: Simulation and measurement results of the proposed monopole

By comparing with other planar multi-band monopole in Table 3-4, all these performances are reasonable. The 9-shaped folded monopole, depicted in [Jyoti 2011], has a shape similar to our proposed antenna, but is fabricated with the classic technology (copper etching on FR4). So, it is understandable that this monopole has a better performance than our proposed antenna. Excluding insertion losses in the feed line, we can notice that the gain of our proposed antenna at 5.5 GHz is approximate to the gain of this reference monopole (3.21 dBi vs 3.29 dBi). However, at 2.45 GHz, the difference is greater (1.3 dBi vs 2.76 dBi) due to much more losses (mostly metallic losses related to the thin thickness of the conductive layer) on the long hook-shape branch #1. It should remember that our printing technology is also far from optimized (very low conductivity, $\sigma = 1.5 \times 10^6$ S/m, with respect to copper bulk, $\sigma_{Cu} = 5.85 \times 10^7$ S/m) and the paper substrate is very thin and introduces too many dielectric losses ($\tan\delta = 0.06$ at 5.5 GHz).

Meanwhile, the compact tri-band monopole, presented by Abutarboush in [Abutarboush 2012], does not show an impressive performance even though it is fabricated with a better printing technology. However, in the calculation of gain and efficiency, the author has taken into account the insertion losses in the 20 mm feed

lines. So, if we exclude these losses, his monopole will have the gain and efficiency a little more than our antenna performance. This is totally reasonable.

Antenna	Frequency (GHz)	Size (mm ²)	σ_{cond} (S/m)	$\tan\delta$	Paper thickness (μm)	Simulated gain (dBi)	Simulated efficiency (%)
9-shaped folded monopole [Jyoti 2011]	2.4 GHz & 5.5 GHz	18x11	5.8e7	0.002	1600	2.76 dBi, 3.29 dBi	
Tri-band monopole [Abutarboush 2012]	1.6 GHz, 3.2 GHz & 5GHz	12x17.3	0.9e7-1.1e7	0.05	440	-6 dBi, -1 dBi, 1 dBi	55%, 79%, 71%
Proposed dual-band Wi-Fi monopole	2.4 GHz & 5.5 GHz	17.5x12	1.5e6	0.06	106	1.3 dBi, 3.21 dBi	80.4%, 93%

Table 3-4: Performance comparison with the other planar multi-band monopole

In general, the screen-printed dual-band monopole prototype shows the good performances as in design simulations. It is very compact to be easily integrated into the set-top-box. It has two frequency bands that allow the operation of the WLAN applications. The radiation patterns in H-plane are almost omnidirectional at two resonance frequencies 2.4 GHz and 5.5 GHz. The efficiency is greater than 60% over both frequency bands if excluding the insertion losses in the feed line. Thus, it entirely fulfills all requirements set at the beginning of the thesis work for set-top-box applications.

3.5 Planar dual-band dipole antenna (2.4 GHz/5.5 GHz)

We have continued to design the dipole type antenna for another type of omnidirectional radiation pattern. The dipole antennas usually exhibit a wider impedance bandwidth than the monopole. We have consequently investigated a dual-band dipole prototype that is intended to be stuck on the sidewall of a set-top-box for WLAN applications (2.4 GHz and 5.5 GHz).

The basic geometries of a printed planar dipole are shown in *Figure 3-17*. Two types of integrated microstrip balun, the $\lambda/4$ open-stub structure (*Figure 3-17a*) or the via-hole structure (*Figure 3-17b*), act as an unbalance-to-balance transformer from the feed microstrip line to the two printed dipole strips. As indicated in this figure, the $\lambda/4$ open-stub or shorted via hole (at ②) renders the point ② to be shorted to the ground plane. This will let the feed point of a printed dipole arm to have the same phase as the point of the top microstrip (at ②). Since the point ① and ② of the top microstrip are very close, it can be considered to have the same phase. It is noted that the length of the dipole-arm and the microstrip balun are approximately a quarter-wavelength. [Chuang 2007]

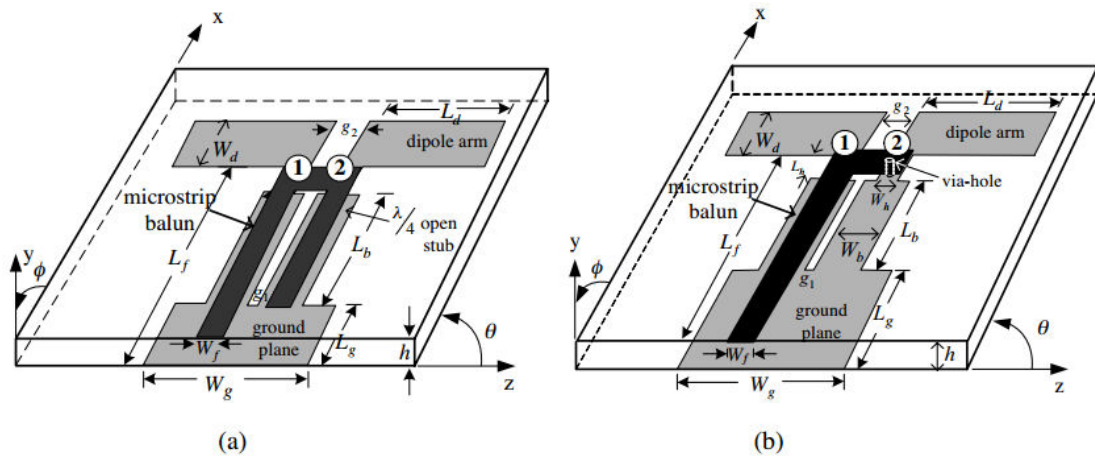


Figure 3-17: Geometry of printed dipole antennas with integrated microstrip balun: (a) open-stub structure, (b) via-hole structure.

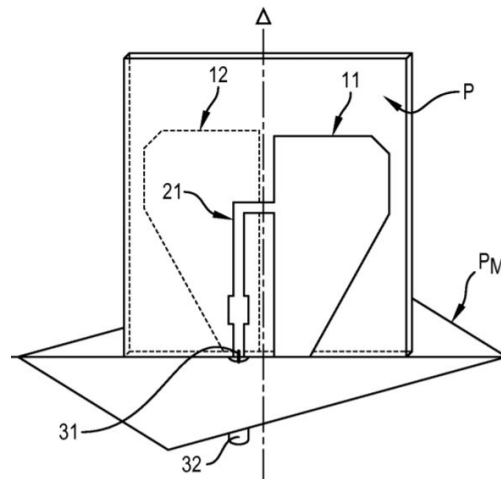


Figure 3-18: Dual fin antenna (patent at IMT Atlantique)

Firstly, a 5 GHz wideband dipole antenna with an integrated balun, inspired from the basic printed planar dipole above and the dual fin antenna (antenna patent invented in IMT Atlantique [Coupez 2012]) described in *Figure 3-18*, was tested on a 250 μ m thick Teslin paper substrate with adhesive copper tape. The determined dielectric properties of Teslin paper (presented in *Table 2-4* in *chapter 2*) along with adhesive layer inside copper tape were incorporated into the HFSS simulation for antenna design. The layout and prototype of this antenna are depicted in *Figure 3-19* below.



Figure 3-19: Layout and prototype of the ultra-wideband dipole antenna, fabricated with adhesive copper tape on Teslin-250 μ m paper

The measurement of S_{11} corresponded fairly well with the HFSS simulation, as shown in Figure 3-20, even if there are some uncertainties due to the dielectric properties of the adhesive layer. The measured return loss yielded a very wide -10dB impedance bandwidth of 3.1 GHz (or 62%): 4.06 - 7.16 GHz. It covered totally the second frequency band (5.15 - 5.85 GHz) of the WLAN application.

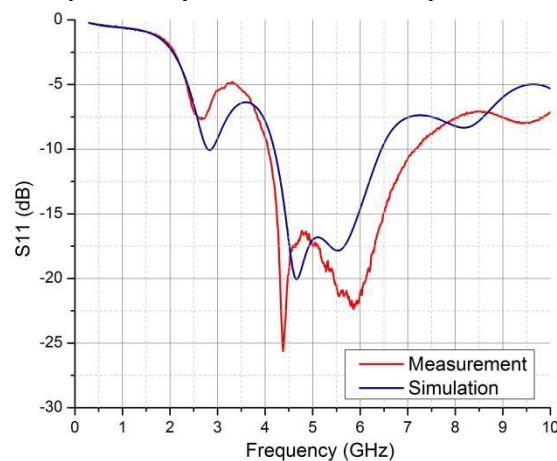


Figure 3-20: Return loss S_{11} of this ultra-wideband dipole antenna

The simulated radiation pattern in H-plane was very close to omnidirectional (Figure 3-21). The E-plane radiation pattern did not have an ideal dipole-like shape due to the influence of the large ground plane at the rear of the slot. The simulated total efficiency at 5 GHz is 97.1% (excluding insertion losses in the 47 mm feed line: -1.28 dB at 5 GHz). Apart from the lower loss tangent of Teslin paper ($\tan\delta = 0.046$ at 5 GHz), the principal reason for this high-efficiency value is thanks to the very good conductivity of adhesive copper ($\sigma = 3.94 \times 10^7$ S/m).

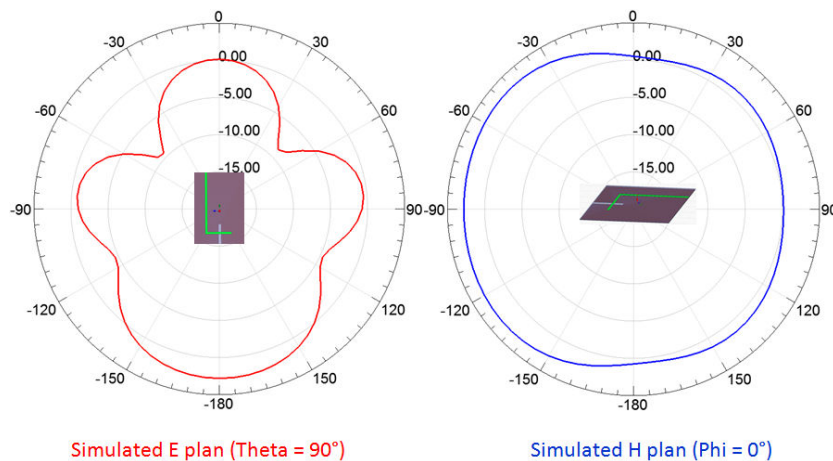


Figure 3-21: Radiation pattern in E-plane and H-plane at 5 GHz of this ultra-wideband dipole antenna

From these interesting results, we have developed a new model of the broadband dipole antenna, which was screen-printed on E4D-210 μ m paper. The form factor was modified, as depicted in Figure 3-22, to extend the -10dB impedance bandwidth while reducing the overall size.

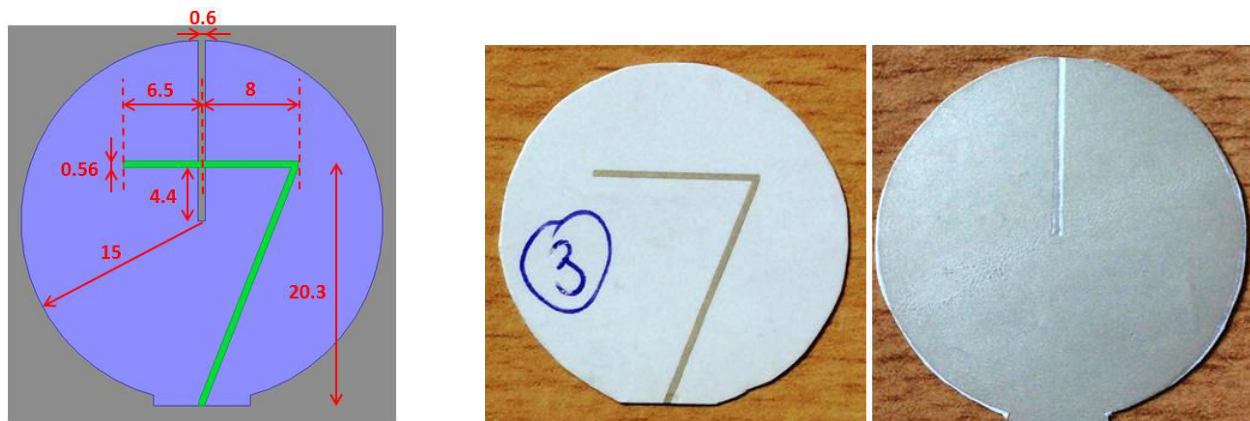


Figure 3-22: Layout and prototype of the modified ultra-wideband dipole antenna, screen-printed on E4D-200 μ m paper

The simulated return loss, displayed in Figure 3-23, showed a resonance frequency of 5.7 GHz with an impedance bandwidth of 4.27 – 6.86 GHz (2.59 GHz or 45.4%). A fairly good concordance was obtained between the measurement and the HFSS simulation of S_{11} . However, when this dipole was stuck on the ABS plastic ($\epsilon_r = 2.69 - 2.76$ in the frequency range of 2.2 – 6 GHz), its impedance matching was severely degraded due to the changing of the effective permittivity. So, the ultimate goal to stick this antenna onto the plastic sidewall of the set-top-box in order to construct the final antenna system will be unworkable. The dielectric properties and the characterization step of ABS plastic are presented in ANNEX B.

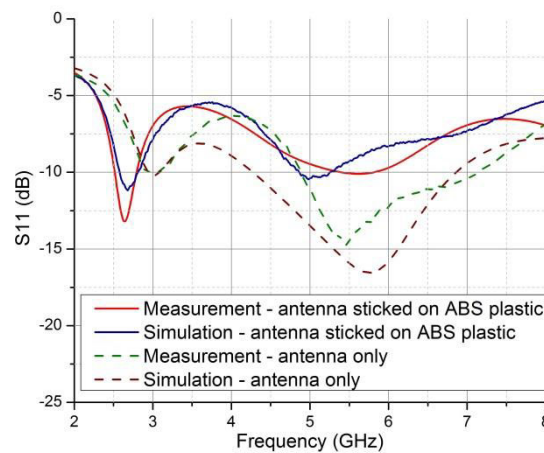


Figure 3-23: Return loss S_{11} of this modified ultra-wideband dipole antenna

We have measured the radiation pattern of this modified ultra-wideband dipole, stuck on ABS plastic, at MVG Stargate[®] (SG-24). The measurement results show a good agreement with the HFSS simulations (Figure 3-23). The simulated and measured max realized gain of this antenna is 2.41dBi and 3.73dBi at 5.7 GHz, respectively (excluding insertion losses in the 29 mm feed line on E4D_200 μ m paper ($\epsilon_r = 2.6$, $\tan\delta = 0.05$ at 5 GHz): about -1.73 dB at 2.4 GHz and -2.6 dB at 5.5 GHz). The simulated and measured total efficiency is 60.9% and 56.4% at 5.7 GHz (0.3 dB difference) respectively, excluding losses in the 29mm feed line. Besides the relatively bad impedance matching when it is stuck on the ABS plastic, another reason that makes the gain and efficiency of this dipole rather low, is because of metallic losses in the large screen-printed dipole surface.

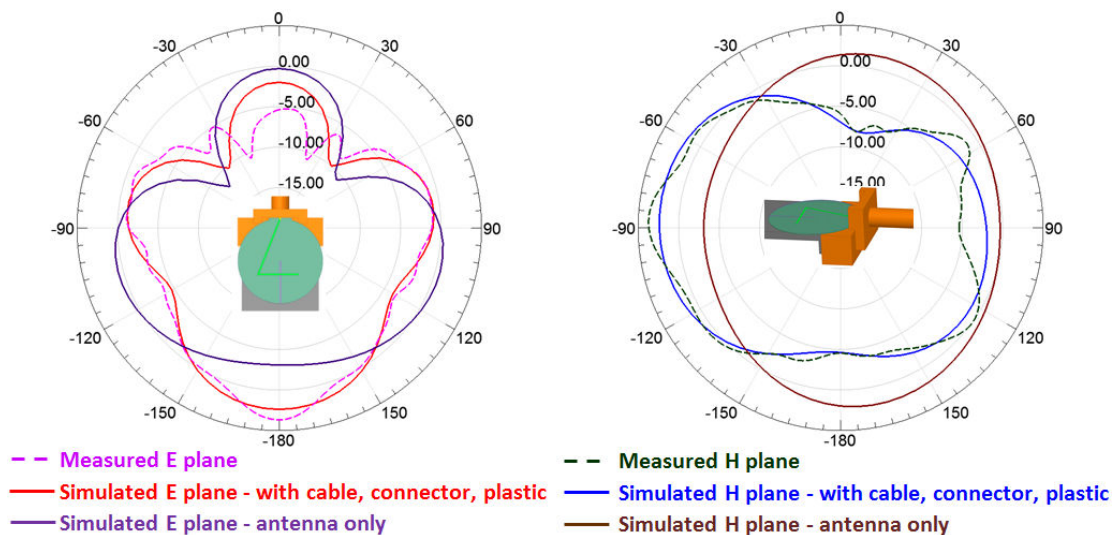


Figure 3-24: Radiation pattern in E-plane and H-plane at 5.7 GHz of this modified ultra-wideband dipole antenna

To overcome these disadvantages, the antenna structure was then adjusted to improve the impedance matching and add the second frequency band for the dual-band Wi-Fi dipole antenna. Two new slots were inserted to modify the current distribution and make a better impedance matching for the frequency band around

5.5GHz. The design process is presented in Figure 3-25 below. The circle ground plane was also truncated in *Ant 2* to reduce the overall size of the antenna and allow decreasing the length of the feed line to 21 mm (so, reduce the insertion losses in the feed line). However, the impedance matching of *Ant 2* at 5.5 GHz was degraded. Therefore, in *Ant 3*, two new slots were added in order to improve the impedance matching at 5.5 GHz. In fact, the second dipole is nested into the first one to create two dipole antennas (one operates at 2.45 GHz and the other at 5.5 GHz) on the same radiation structure.

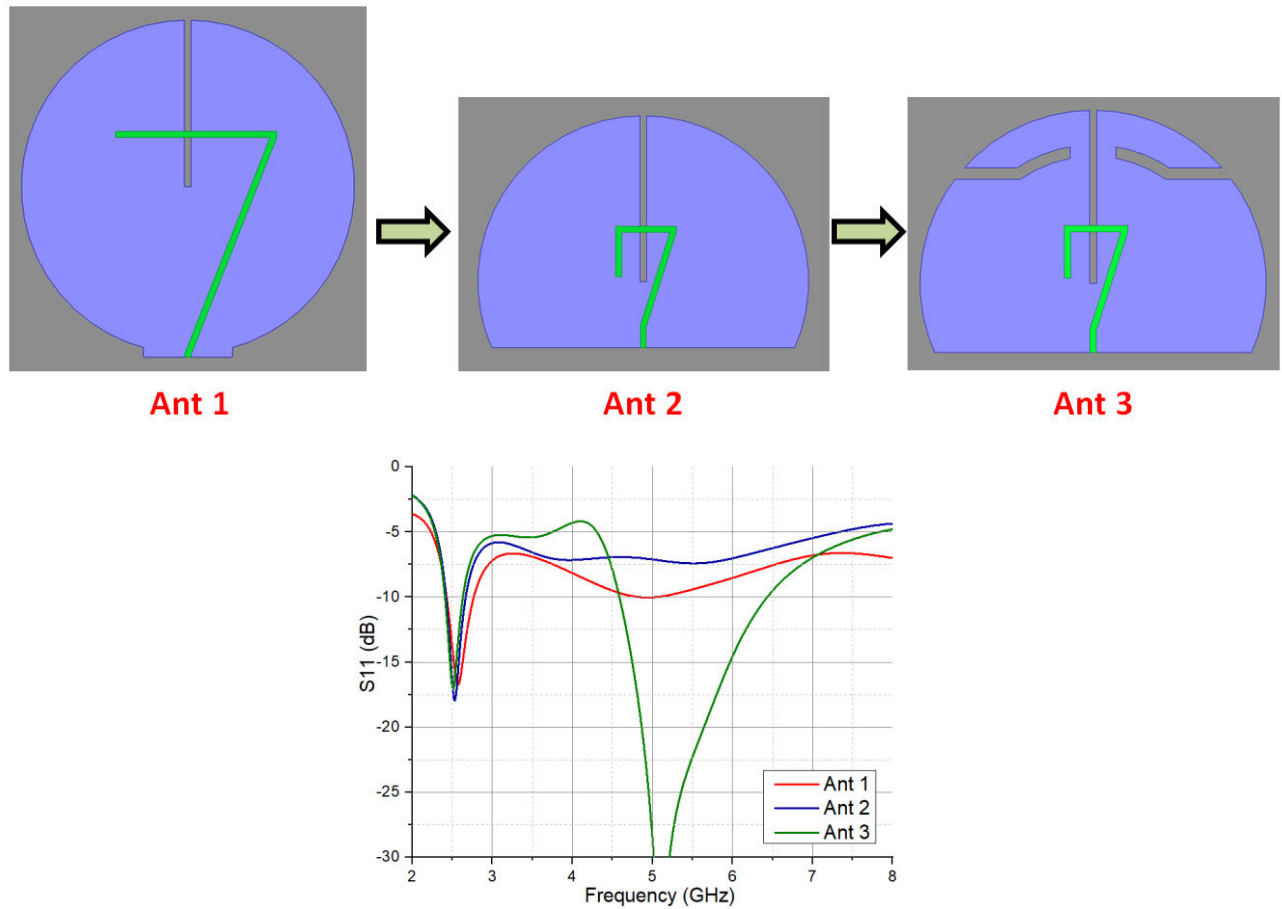


Figure 3-25: Design process of the dual-band dipole antenna

The layout and the prototype of this proposed dipole are shown in Figure 3-26.

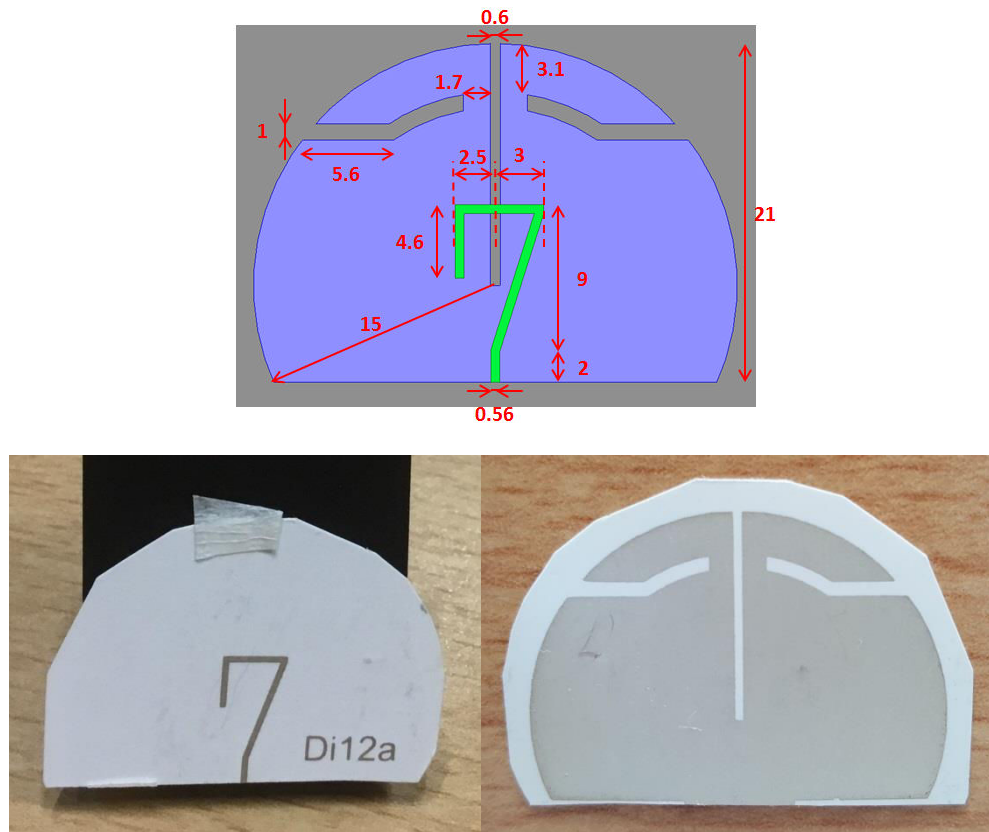


Figure 3-26: Layout and prototype of the proposed dual-band Wi-Fi dipole antenna, screen-printed on E4D-200 μ m paper

This dual-band Wi-Fi dipole, when being stuck on ABS plastic, had two simulated bandwidths of 2.4 - 2.63 GHz (0.23 GHz, or 9.2%) and 4.59 - 6.43 (1.84 GHz, or 36.1%) GHz, which corresponded to the two frequency bands of WLAN. A fairly good agreement was obtained between the measurement and the HFSS simulation of S_{11} .

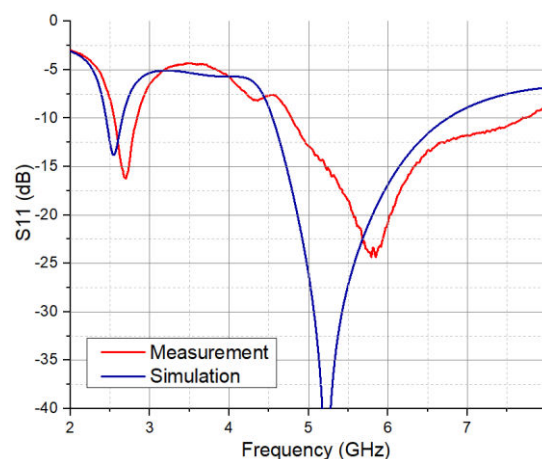


Figure 3-27: Return loss S_{11} of the proposed dual-band Wi-Fi dipole antenna

The current distribution at 2.5 GHz and 5.5 GHz in HFSS simulations is shown in Figure 3-28. Obviously, at 5.5 GHz, a high current density is concentrated mostly

around the small dipole part at the top. Meanwhile, at 2.5 GHz, the current distribution spreads all over the whole circle surface. Through the animation run, we have also noticed that at 2.5 GHz, a fairly great amount of energy is reflected in the transition from the microstrip feed line to the slot, which will reduce the radiation efficiency at this frequency. So, in order to improve the performance at 2.5 GHz, we must improve the matching from the microstrip feed line to the slot, for example, by prolonging the slot as well as the matching stub.

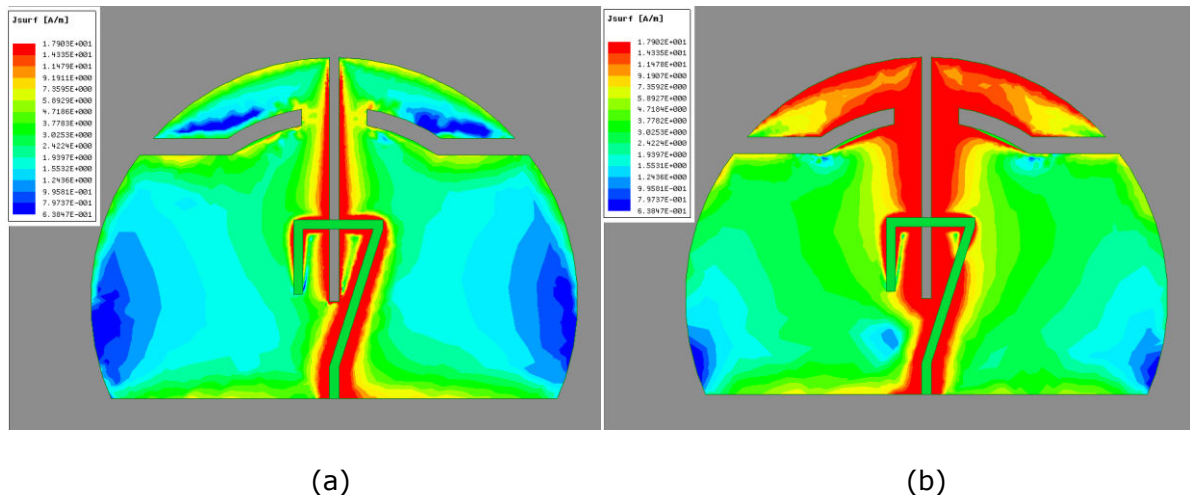


Figure 3-28: Simulated current distribution at: (a) 2.5 GHz and (b) 5.5 GHz

This dual-band Wi-Fi dipole was fabricated at the end of my thesis work, so, unfortunately, we have not yet measured its radiation pattern and efficiency in the anechoic chamber at MVG. That is the reason why we can only analyze with simulation results.

The simulated radiation pattern in E-plan and H-plan were shown in *Figure 3-29*. At 2.45 GHz, the proposed antenna showed a dipole-like radiation pattern similar to that in theory. At 5.5 GHz, it can be seen that the radiation pattern was truncated at the rear of the central slot because the large dipole surface, below 2 new added slots, plays the role of a reflector. That is the reason why the radiation pattern at 5.5 GHz is much more directional. However, this is not too serious because the rearward of the slots will be the direction of the PCB ground plane of the set-top-box. So, this is not the desired radiation direction.

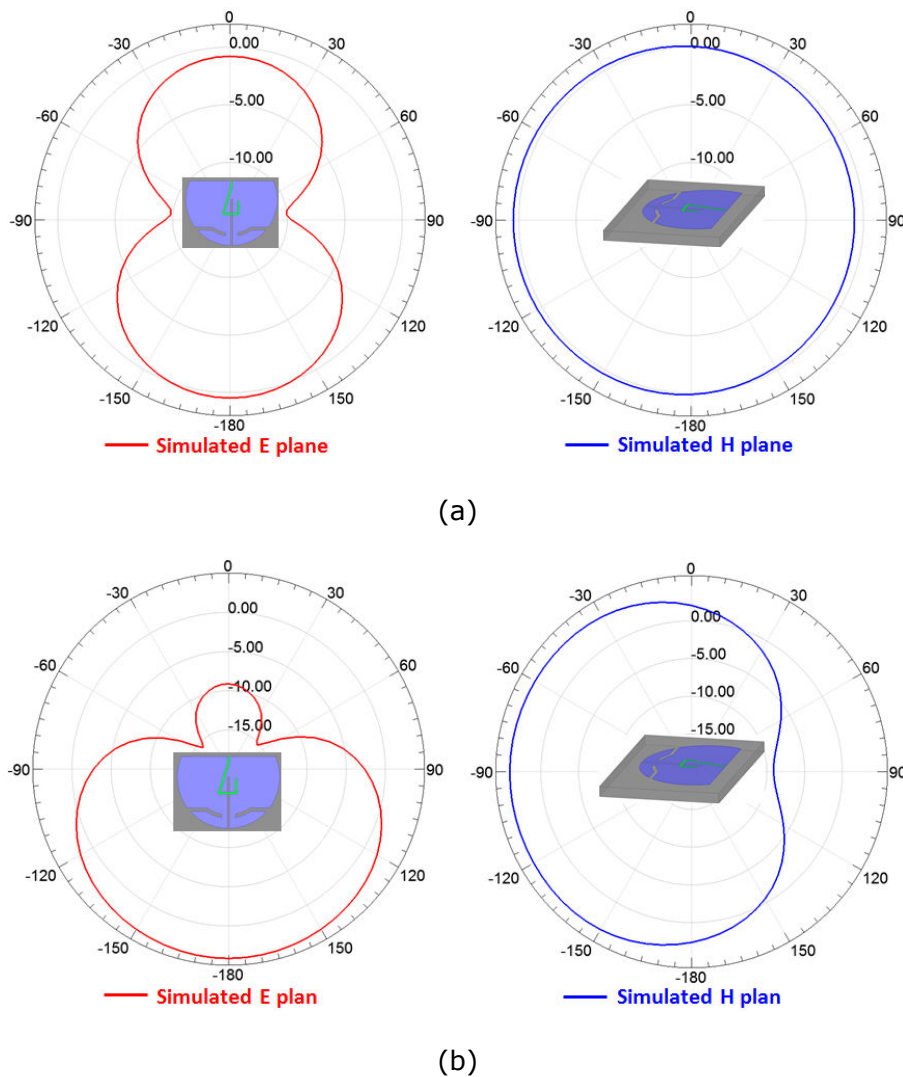


Figure 3-29: Radiation pattern of this dual-band Wi-Fi dipole antenna: (a) at 2.5 GHz; (b) at 5.5 GHz

The simulated max realized gain of this dipole was -0.23dBi at 2.5 GHz and 3.3dBi at 5.5 GHz, respectively. The simulated total efficiency was 54.8% at 2.5 GHz and 92.2% at 5.5 GHz respectively, excluding losses in the 21mm feed line. So, the performance of this antenna is improved in comparison with the previous configuration thanks to improving the impedance matching. The performance at 2.5 GHz is much lower than at 5GHz for two principal reasons: the transition from the microstrip feed line to the slot is not optimized at this frequency; and the ink thickness ($7.6 \mu\text{m}$) is not enough according to the skin depth condition (required skin depth $8.4 \mu\text{m}$), which leads to more metallic losses.

In short, the planar dual-band dipole which featured two frequency bands for an operation of WLAN applications at 2.45 GHz and 5.5 GHz were presented. It has just enough size to be integrated into the set-top-box. It shows also a good performance in terms of radiation pattern, gain and efficiency. Therefore, it proves to be a good solution the final antenna system.

3.6 Conclusion of chapter 3

The simulations are almost in good agreement with the measurement results; that allows validating the measured characteristics of the E4D paper substrate and of the associated screen-printing metallization. The measured results (return loss, radiation patterns, gain and efficiency) of different antenna prototypes were also similar, which proved the good repeatability of the printing technology. The currently used technology is sufficiently stable, satisfactory enough for the manufacture of RF circuits (not requiring, for example, critical technological steps: wide slots or very narrow patterns, the realization of metallized vias, ...)

In order to limit the influence of the very high dielectric losses of paper substrates to the antenna performance, the antenna types mostly monopole or dipole are preferred thanks to the weaker interaction between the guided fields and the dielectric substrate. Therefore, one monopole and one dipole antenna have been designed to cover both frequency bands 2.4 – 2.5 GHz and 5.15 – 5.85 GHz for WLAN applications.

Our antennas printed on paper prove its operation up to at least 6 GHz even if the used printing technology is far from optimized (very low conductivity), and our paper substrate introduces a lot of dielectric losses. Obviously, by excluding the insertion losses in the feed line, the radiation efficiency of these antennas are still fairly good (superior to 60%). However, the main problem of these antennas is the very high insertion losses on feed lines (equal to or greater than -1dB/cm at 5 GHz, if compared with the micro coaxial cable: -0.1 dB/cm at 5GHz), which reduce significantly their performance. Therefore, the interconnection/ feed lines must be shortened as much as possible.

These very encouraging results are important bases for constructing the final antenna system, which will be presented in the following chapter. Two selected antenna structures are dual-band monopole and dipole thanks to wide impedance bandwidth, almost omnidirectional radiation pattern, and most importantly, compact size enough to be easily integrated into the set-top-box environment.

Chapter 4: Antenna system integrated within the set-top-box environment

Principal content

4.1	Introduction.....	115
4.2	RF interconnection to PCB mainboard.....	115
4.2.1	Miniature coaxial cables – Available solutions and limitations.....	115
4.2.2	Identification of interconnection solutions compatible with paper & flex technologies - State of the art	117
4.2.3	Investigations: characterization of flexible interconnections using advanced ZIF connectors	126
4.2.4	Conclusion	136
4.3	Antenna system on flexible substrate.....	137
4.3.1	Three dual-band Wi-Fi monopole antenna	138
4.3.2	Three dual-band Wi-Fi dipole antenna	143
4.4	Conclusion of chapter 4	147

4.1 Introduction

To meet the multiple expectations in terms of communication capabilities of electronic boxes (multi-standards, coverage constraints), we need to develop antenna systems:

- having a large number of radiating elements distributed within the electronic box (choice of antennas with positions, orientations)
- realized by a technology allowing: the formatting of the radiating elements, their easy mounting within the global structure, and their RF interconnection with the PCB mainboard
- taking into account the disturbing effect of the environment (dielectric shielding, PCB mainboard, battery,...)

In this last chapter, the remaining issues to be able to integrate the whole antenna system into the set-top-box environment will be addressed. Firstly, the direct flexible interconnection from the antennas to the PCB mainboard, one of the key problems, is resolved. We have focused on the research for interconnection solutions between sub-systems made partly on flexible supports. The final objective consists in replacing conventionally used solutions (coaxial cables + connectors) by low-cost flex to PCB direct connections. Then, the antenna systems, which are printed on the flexible substrate (e.g. paper) and which can be stuck on the plastic sidewall of the set-top-box, are also modelled as a final demonstrator. Polarization diversity induces the use of multiple antennas, as well as multiple interconnections to a main Printed Circuit Board (PCB). The performances of each antenna in the system, as well as the coupling between them, are investigated.

4.2 RF interconnection to PCB mainboard

How to interconnect all RF components and circuits such as antennas, filters, couplers, transmission lines ... printed on flexible substrates with the main PCB structure supporting chipsets and others actives components of a set-top-box? This is a key issue that has been addressed in *chapter 1*. The interconnection solution which consists in using coaxial cable is expensive in terms of implementation cost, so we have investigated for a new ultra-low-cost interconnection solution on paper. The antennas and their interconnection lines are printed on the same paper sheet. Therefore, the last technological breakthrough is the direct interconnection between the flexible feed lines and the main PCB.

This flexible interconnection solution between the antennas and the PCB mainboard must have:

- technological compatibility with the proposed antennas in *chapter 3*
- simplicity and rapidity in implementation
- low cost for mass production

4.2.1 Miniature coaxial cables – Available solutions and limitations

In commercial electronic devices, different interfaces need to be interconnected. Therefore, RF antennas, as well as batteries, or LCD displays, for instance, are usually fixed to the housing box of the equipment and interfaced with the central processing electronic unit through cables and miniaturized multiple input-output connectors.

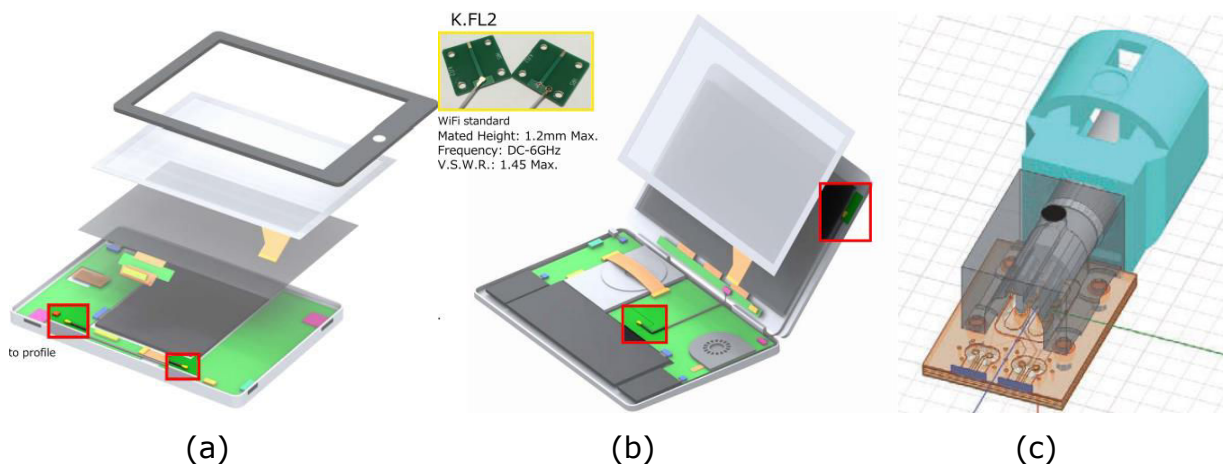


Figure 4-1: Micro-coaxial cables and interconnection – Solutions from industrial markets: (a) Miniature Surface Mounted Connector for Mobile RF devices interconnect; (b) Coaxial connector for wireless laptop connectivity; (c) PCB connector for automotive applications

Even if such techniques are not really low cost, they offer undoubtedly flexibility in terms of test, repairment, RF efficiency. They are still considered in advanced electronic devices as required functionalities tend to promote the integration of various wireless modules in a common environment to cover various design features and functionalities (cohabitation of different standards, necessitating various antennas). In addition, antennas are usually processed on substrates external to the main PCB, so as to address specific constraints such as radiation efficiency (thus using low-loss cost-effective thin substrates), spatial diversity for MIMO schemes (then requiring up to 4x4 colocated antennas per standards and multiple interconnections towards the main PCB).

Commercial wireless systems have consequently strongly encouraged the development of a new family of miniaturized RF connectors and cables, with particular expectations in terms of fast and accurate mounting techniques as well as mass-production for cost-reduction. The Figure 4-2 below describes commercial products of RF surface mounted micro-connectors for such purpose.



Figure 4-2: RF micro connectors from Hirose: Ultra miniature Surface mounted Connectors (50 ohms, high electrical performance up to 6GHz)

In addition, original techniques have been studied to facilitate plug-in and plug-out operations, as well as elastic/flexible board to board clipping or contact solutions to

counteract eventual damages related to temperature variations or mechanical shocks.



Figure 4-3: Different solutions of plug-in coaxial connectors (Rosenberger™): (a) Miniature Plug in connectors; (b) Elastic board to board connectors

For RF antennas, micro-cables are usually directly soldered and connected to the input port, in order to minimize cost and to optimize impedance matching and ground plane continuity. Central pin and shielding structure are usually soldered to the main PCB, considering microstrip configurations (top main line + inner ground plane). This requires usually via holes to promote surface soldered cables, as described in Figure 4-4 below.

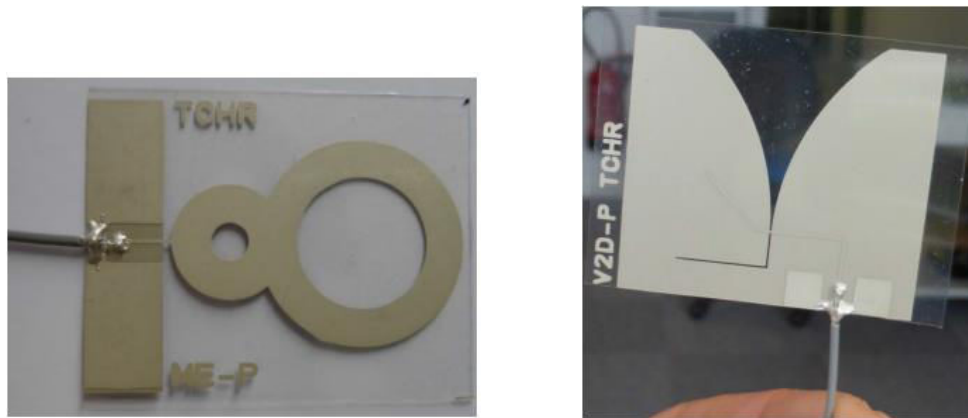


Figure 4-4: View of a coaxial interconnection directly soldered to the PCB (courtesy of Technicolor Connected Home Company)

Such solution brings several drawbacks for mass production:

- A recurrent cost (especially when higher frequencies (above 2 GHz) are considered)
- Non-repairable systems: Cables are soldered, with consequently difficulties to repair and disconnect the attached PCBs
- Difficulties to control undesired coupling and radiating phenomena (EMC constraints)
- Space occupation, especially when multiple antennas systems are considered, thus necessitating to keep sufficient place for soldering operations.
- Some potential mismatching depending on the quality of the soldering operation.

4.2.2 Identification of interconnection solutions compatible with paper & flex technologies - State of the art

Considering previous drawbacks, we target to identify original interconnection techniques/systems to propose multi-access miniature interfaces between a flex support and the main PCB board. This leads to emerging concepts of Flexible Printed Circuit (FPC) and Flexible Flat Cable (FFC) interfaces.

Such consideration becomes a standard expectation for developing highly compact electronic devices, as illustrated in *Figure 4-5* below. Multiples interconnections are required between different subsystems, with different constraints and expectations (robustness, supported currents and powers, operational frequencies and data bit rate, tolerances and achievable dimensions, costs ...).

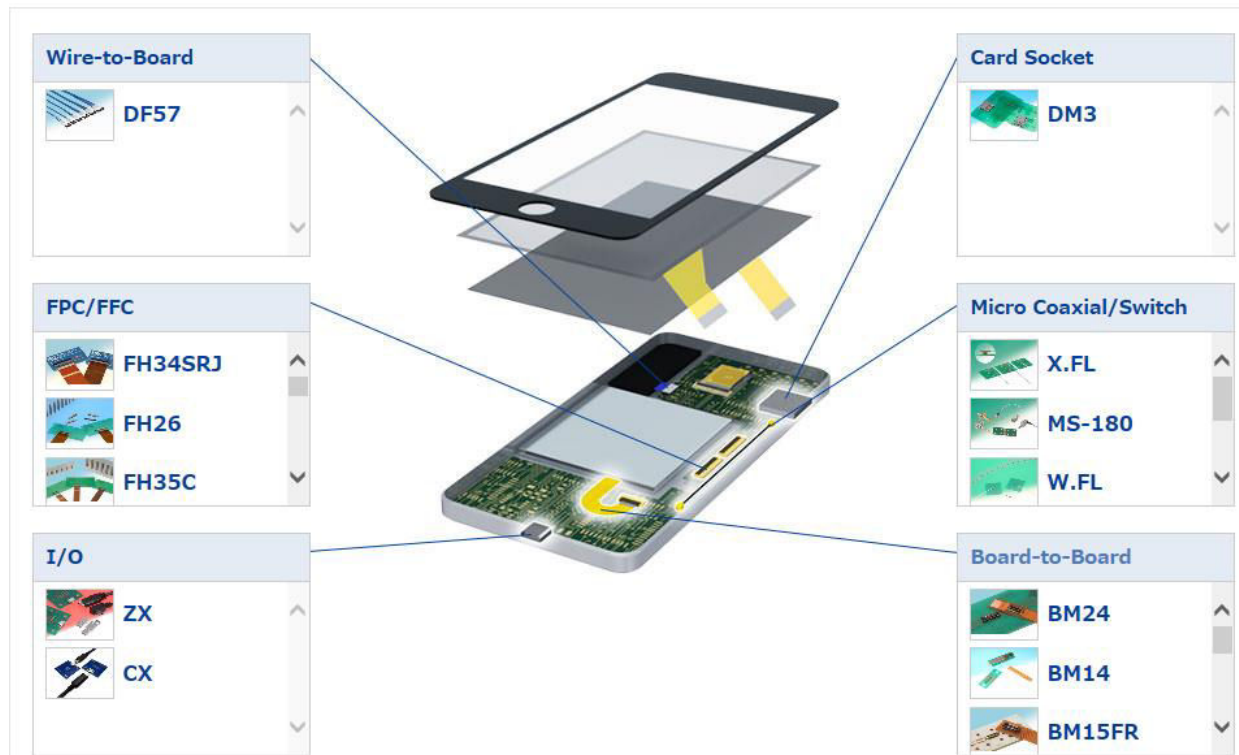


Figure 4-5: Interconnects for commercial electronic devices: a myriad of technical solutions (<https://www.hirose.com/product/en/products/industry/mobile/smartphones/>)

Simple to complex solutions can be identified. Only the most suitable and feasible solutions are presented hereafter. In addition, a specific attention is put on the constraints related to high-frequency requirements, such as conductivity, miniaturization, shielding effects and parasitic EMC ... which are not really considered for the different board-to-board or flex-to-board links presented above.

4.2.2.1 Classical interconnection using conductive glue and assembling techniques

In this conventional method, the use of the vias associated with a weld or conductive glue is simply applied. This corresponds to the natural extension of the coaxial-to-board techniques mentioned before, with an integrated transmission line to replace the expensive coaxial structure.

Clifton Quan et al. from Hughes Electronics have proposed in 1997 a patent, as shown in *Figure 4-6*, about an RF flexible interconnection line for connecting transmission lines in microwave assemblies without the use of coaxial connectors and coaxial cables [Quan 1997]. It operates at microwave frequencies with low RF

distortion, and independently of the flex relative position or twist efforts. RF leakages are also well controlled due to the ideal electrical continuity between ground planes.

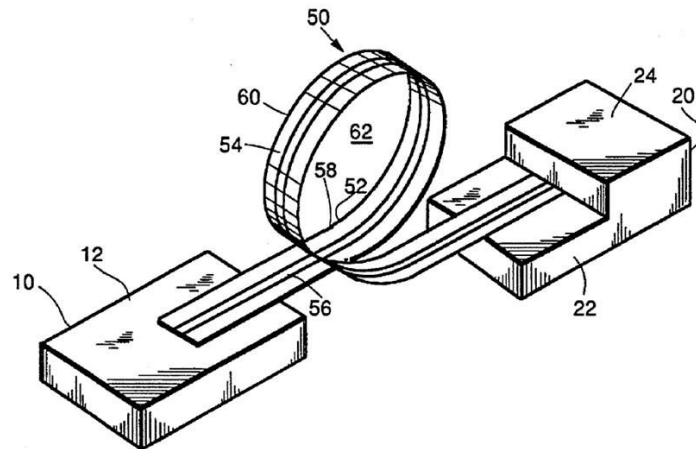


Figure 4-6: Isometric view of a microstrip flexible interconnect circuit

The flexible dielectric material was a 5880 RT/Duroid (TM) or Kapton (TM) having a thickness of 127 μm . The metallic layers were formed on surfaces of the dielectric layer by conventional photolithographic techniques.

The plated through hole is formed through the dielectric layer (52) between the pad (54B') and the center conductor trace (56) to provide connecting pad on the same surface side as the ground plane (54) for surface mount attachment to the circuit board (10').

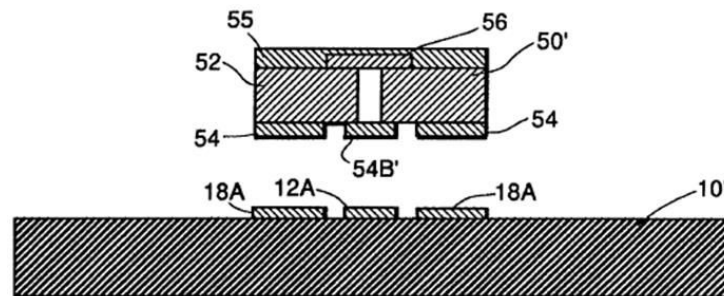


Figure 4-7: Illustration of the interconnection technique between the flexible microstrip line and the strip transmission line on the circuit board.

The flexible interconnection line (50') is attached to the circuit board (10') by conductive epoxy or solder, wherein the pad (54B') is attached to the microstrip center conductor strip (12A), and the pads (18A) are attached to the bottom conductive layer (54) of the interconnection line (50').

This interconnection solution is very simple and ultra-low-cost in term of material and component cost. However, the reliability, repeatability and transparency of the interconnection still have not been verified. In particular, the solder cannot be applied with paper substrates (considering required temperature) and thus the conductive glue remains an alternative approach. Unfortunately, the absorption and the porosity of the paper board tend to disseminate the glue and reduce the accurate control of the connection areas.

4.2.2.2 Interconnect through direct or pseudo-direct compression techniques

A direct contact between a flexible transmission line and a PCB can be obtained considering either a direct metal to metal contact or an interposer interface. Sensitive and cost-effective techniques can, therefore, be avoided and replaced by compression solutions.

4.2.2.2.1 Elastomers as local interposers

The use of elastomeric with vertical conductivity control has been investigated. With such technique, the electrical interconnections are made by means of a layer or sheet medium comprising chains of magnetically aligned, electrically conducting particles or nanowires in a non-conducting matrix material.

William R. Lambert et al. from Lucent Technologies, Inc. have presented in their patent in 1998 a detailed description of this solution [Lambert 1998]. An elastomeric compression interconnect (40) was employed to couple signal from the main circuit board (50) to RF flex circuit lines (36).

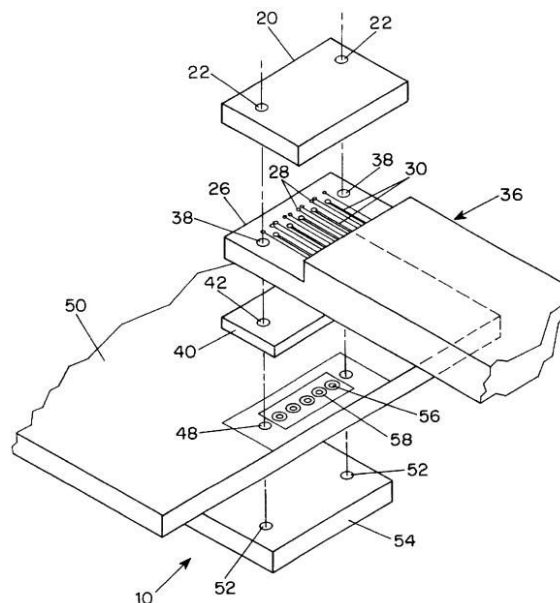


Figure 4-8: Exploded view of a portion of an interconnection system comprising an RF flex circuit, an elastomeric interconnect and a printed circuit board.

The electrical interconnections (46), as illustrated in Figure 4-9, were made by means of a layer or sheet medium comprising chains of magnetically aligned, electrically conducting particles in a non-conducting matrix material (44). In flex circuit (36), the contact pad (92), disposed over the dielectric (26), was coupled to signal line (88) via a through-hole (90). The signal line (70), embedded within circuit board (50), was coupled to a contact pad (74) via a through hole (72).

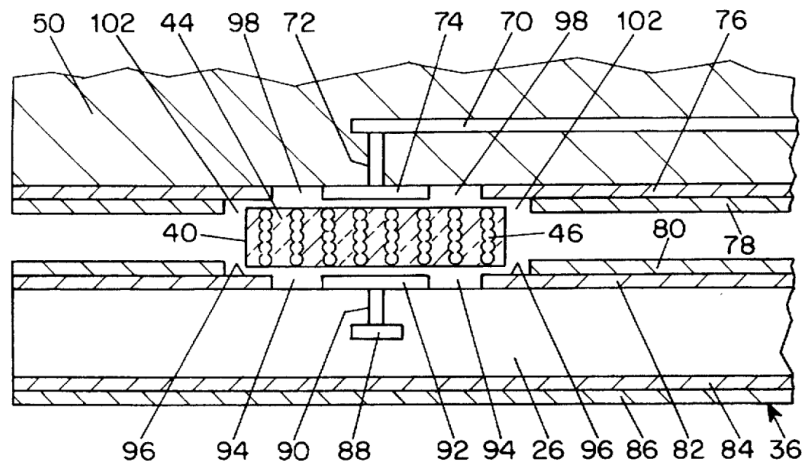


Figure 4-9: Side view of this interconnection system

Finally, a screw ran through holes (22, 38, 42, 48 and 52) to attach the circuit board signal lines and the flex circuit signal lines via compression interconnect (40). Other suitable means of attachment is clamping or bonding. One major difficulty of this method lies in the electrical properties of the elastomeric layer (conductivity and spatial decoupling), especially at RF frequencies, depending on the control of the aligned conductive particles.

4.2.2.2.2 Local miniature contact elements as local interposers

Then, another industrial solution, inspired from elastomeric compression, called SuperButton[®], was also applied by HCD, Inc. (High Connection Density company - <http://hcdcorp.com/index.php>). HCD SuperButton[®] is constructed from Cu-alloy wires surrounded by a polymeric jacket. SuperButton[®] contact elements are assembled into an FR-4 interposer and can be designed to virtually any custom array size or pattern and therefore provide high-performance connectivity for package-to-board, board-to-board, and flex-to-board connections.

It has proved its primacy with features:

- Proven solderless z-axis connector technology that offers exceptional mechanical and electrical performance. A low profile interconnection is achieved (0.8mm thick).
- Excellent choice for high-current, high-frequency, and high-density applications for board-to-board, board-to-flex, and package-to-board interconnect requirements (Experiments announced up to 30 GHz with 1dB insertion loss).
- Electrically efficient connection and consistent resistance value from pin to pin (<10mΩ).
- Cost reduction with enhanced performance for any standard, non-standard footprint with varied, asymmetric and irregular pitches.



Description of the nanowire-based interposer



Figure 4-10: SuperButton® industrial solution for elastomeric compression interconnect
Combining the robust SuperButton® contactor design with the versatility of a flex circuit creates new alternatives to resolve growing interconnect challenges:

- High Density Interconnect (0.5mm pitch available)
- Low profile connector and vertical signal path
- Solderless compression system
- High frequency (up to 26GHz)

Therefore, it offers a very good electrical and mechanical performance which makes it an interesting choice for board-to-flex applications.

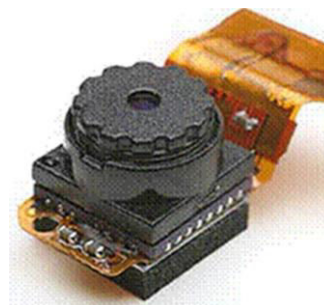
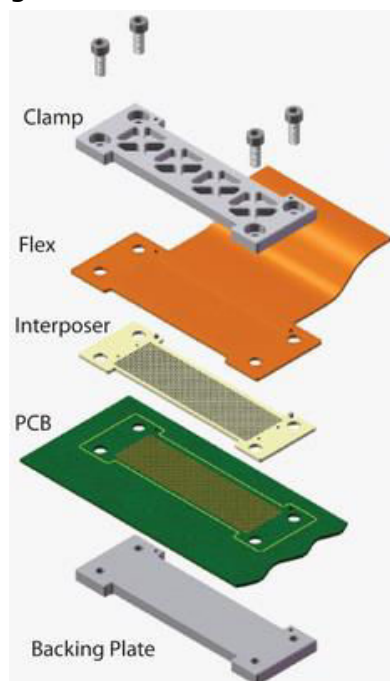


Figure 4-11: Application of SuperButton® in interconnection for Flexible Circuit Board (FPC)
This solution is quite attractive. However, it remains expensive and induces also drawbacks concerning the control of the interposer design (density, number of vertical pins and reproducibility, misalignment, RF behavior ...).

Remarkable progress has nevertheless been accomplished with proposed ultra-low-profile FPC interconnections using, for instance, micro-spring design into an over-molded thermoplastic carrier.

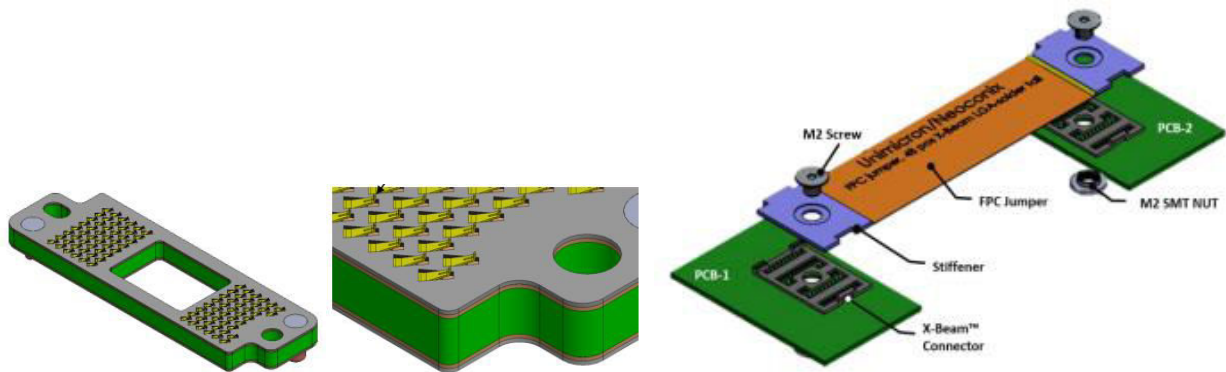


Figure 4-12: TI DLP® Technology Interposer Family from Neocomix™ (www.neoconix.com)

4.2.2.3 ZIF (zero insertion force) connector for RF applications

4.2.2.3.1 Clipping mechanism for low-cost mounting interconnects

Various manufacturers propose different solutions for high-density miniaturized interconnection to flex circuit, such as Molex™ for instance ([http://www.molex.com/molex/products/group?key=wire to board connectors&channel=products](http://www.molex.com/molex/products/group?key=wire%20to%20board%20connectors&channel=products)).

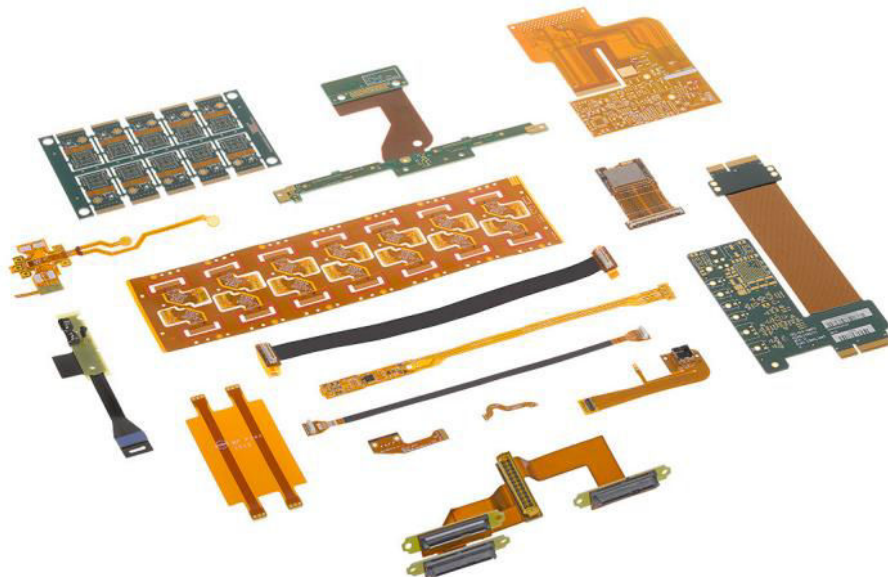


Figure 4-13: Different solutions for Flexible Circuit Board (FPC) to Board interconnections

The first identified category corresponds to "stack" connectors for board-to-board or flex-to-board interfaces, benefiting from remarkable progress in the miniaturization of connectors, plastic packaging/supporting structures and sub-metallic parts (micro pins). The size reduction trend nowadays is illustrated in Figure 4-14 below, inspired from Molex™ solutions.

SlimStack™ Connectors

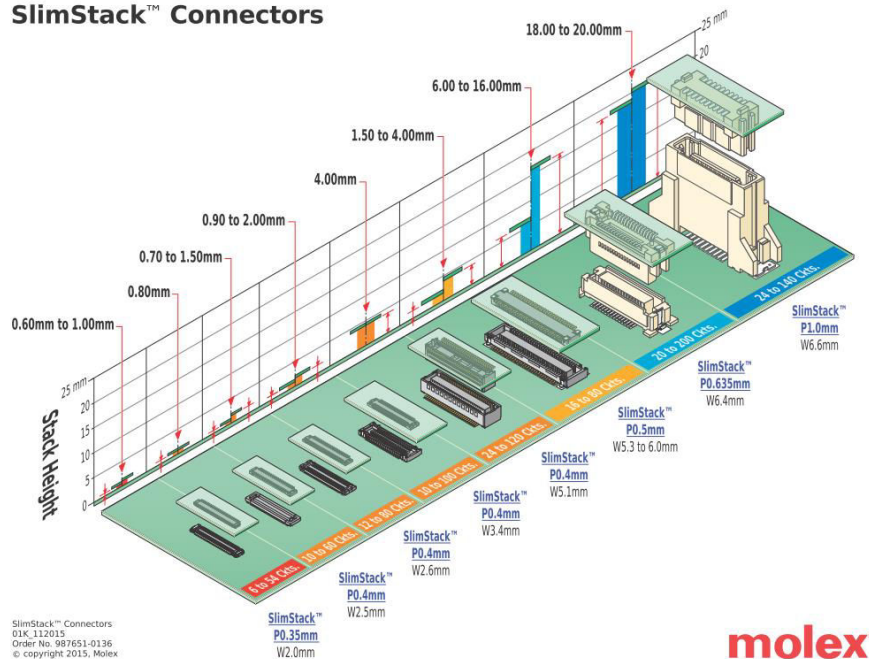


Figure 4-14: SlimStack™ Board-to-Board Connectors

The second category Micro FFC/FPC Connectors are available in a variety of fine-pitch styles including BackFlip and Easy-On actuators to fix the flex to a PCB.

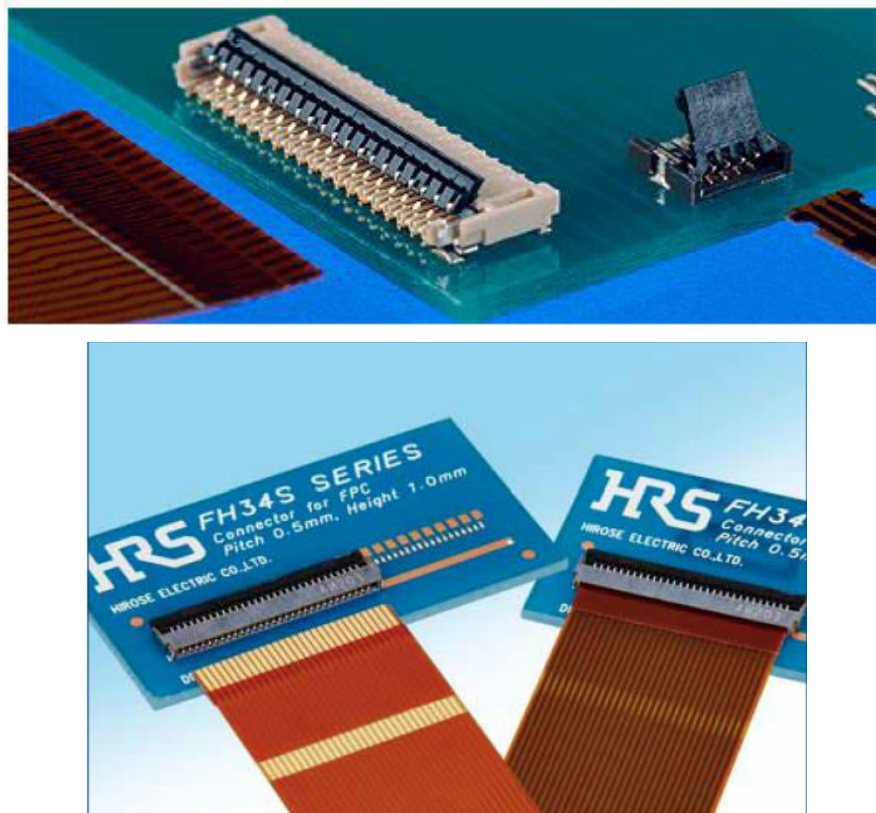


Figure 4-15: FFC/FPC connections with clipping - illustration

The rotating actuator opens from the back of the connector, assuring reliable electrical and mechanical connection.

4.2.2.3.2 ZIF connector solution

The ZIF connectors, which are surface mounted components (SMC), show interesting characteristics for the interconnection between FPC (Flexible Printed Circuit)/ FFC (Flexible Flat Cable) and PCB mainboard:

- Low-profile (for example, height of 1mm and width of 4 mm) for space saving applications.
- Top and bottom contact with design flexibility.
- Easy FPC insertion and reliable electrical connection: In more detail, the rotating actuator, which opens from the back of the connector, allows easy insertion of FPC and provides a tactile sensation when fully closed, assuring reliable electrical and mechanical connection.
- Compatible with two kinds of standard FPC thickness: 0.2 or 0.3 mm thick

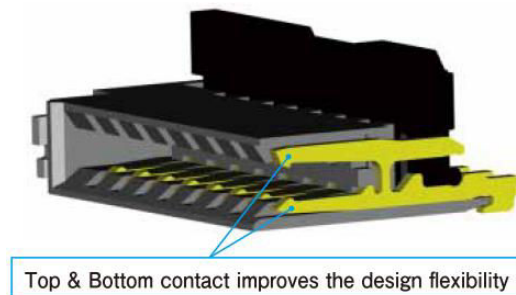
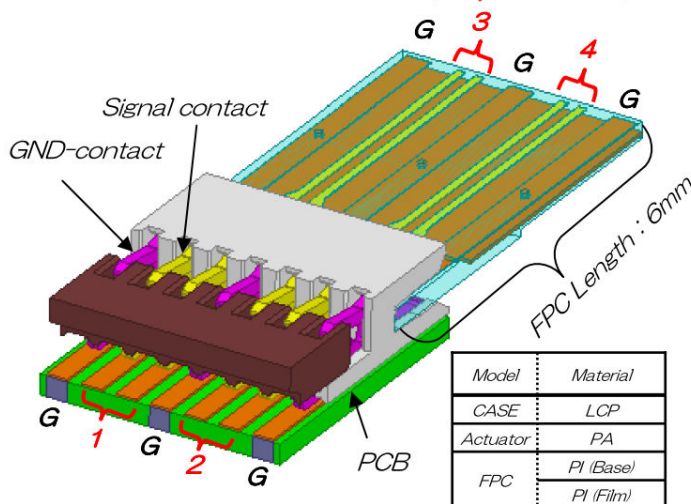


Figure 4-16: Perspective view of a SMC type ZIF connector

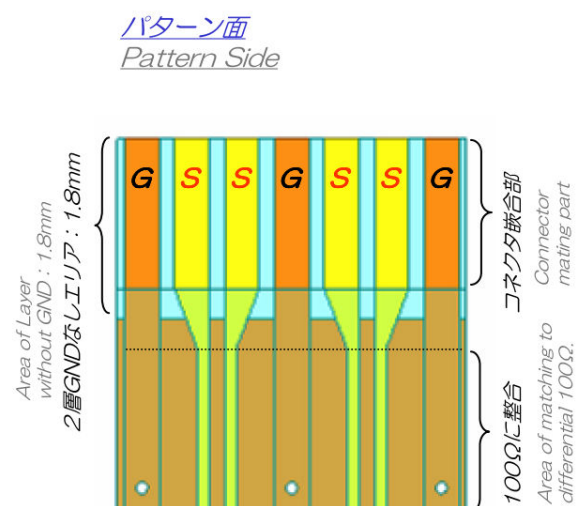
They are often used to transfer digital signals like eDP (a DisplayPort standard for digital communication) or USB in differential mode.

As described in Figure 4-17 below, alternative ground and main signal contacts can be exploited to interconnect efficiently flex coplanar lines with a connector mounted on the main PCB with differential lines access.

FH34SRJ Model (Top contact)



FPC Model



※基板実装部パッドおよびFPCのインピーダンスは差動100Ωに整合
※ Impedance of PCB pad and FPC is matching to differential 100Ω.

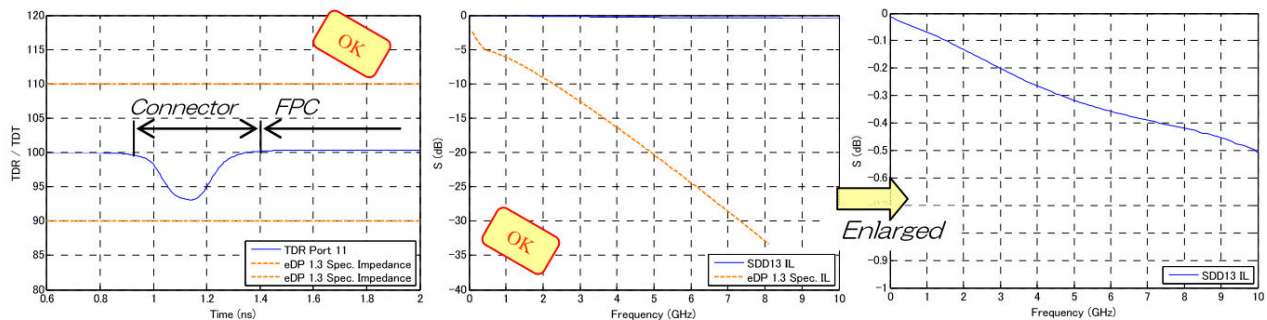
Figure 4-17: Modeling of the interconnection between FPC and PCB card through the ZIF connector [FH34-SRJ]

The documents, provided by Hirose™ manufacturer, show that it can transfer data with transmission speed up to 10 Gb/s. The insertion losses are also very low, about 0.5 dB up to 12 GHz for a 6mm long FPC line (insertion losses of 50Ω transmission line on LCP: about 0.28 dB/cm at 10 GHz).

FH34SRJ For eDP 1.3 — Spec Line

Differential Impedance
@130ps(20-80%)

Differential Insertion Loss



No.	Test Description	Requirement	Result
2-1	Differential Impedance	rise time @ 130 ps(20-80%) 100 ohm ± 10 %	Pass
2-2	Differential Insertion Loss (Cable-Connector Assembly Specification)	$-8.7 \times \sqrt{f/f_0} - 0.072$ ($0.1 < f \leq f_0/3$) $5.68 \times \sqrt{f} - 5.3 \times f - 6.52$ ($f_0/3 < f \leq 8.1$) $f_0 = 1.35 \text{ GHz}$	Pass

Figure 4-18: Simulation results of FH34SRJ connector for eDP 1.3 standard

Therefore, its use for RF applications is totally feasible. However, the frequency limit must be investigated later, especially in terms of impedance control and insertion loss.

The interconnection through the ZIF connector shows a very high reliability and repeatability. Its cost is a little below 1€/connector (for 1000 pieces), so it is not expensive. Most importantly, there is no additional cost paid to the skilled technicians for manually soldering and no need to spend time for soldering. More specifically, the way of realizing connection is very fast and can be applied to mass production in industry. This interconnection solution is certainly compatible with polymer and plastic substrates because these flexible substrates have an excellent mechanical strength enough to resist under the locking force of the ZIF connector. The applicability for paper substrates, and more generally, flex materials at RF frequencies need to be carefully tested.

4.2.3 Investigations: characterization of flexible interconnections using advanced ZIF connectors

Obviously, looking at the state of the art, the most reliable and low-cost solution for interconnection between flexible feed lines and the main PCB is the use of ZIF connectors. There are two issues that need to be verified:

- Whether it can work at radio frequencies up to 6GHz satisfying the required applications
- Whether it is suitable to connect with the paper substrate of the antenna system studied in our research work.

There are too many kinds of connector available in the commercial market. Their features vary from contact with FPC on one side (top or bottom) or on the dual side (top and bottom), thickness compatibility (200 μm or 300 μm), to the number of contacts, and with or without a lock. The manufacturers are also very diverse like Hirose™, Molex™, Amphenol FCI™, TE Connectivity™, Goldenconn™, etc. The properties of these connectors are summarized in *Table 4-1* below. It can be seen that their performance is not too different.

ZIF Connector							
Brand	Height (mm)	Number of contacts	Dual-sides contact	Actuator	Thickness compatibility	Temperature resistance	Current - Voltage (Max)
Hirose™	1	4 - 120	X	Back Flip	200 μm / 300 μm	-55°C to +85°C	0.5 A 50V AC(RMS)/DC
Molex™	1	4 - 32	X	Back Flip	200 μm / 300 μm	-40°C to +85°C	0.5 A 50V AC(RMS)/DC
Amphenol FCI™	0.9	4 - 50		Back Flip	200 μm / 300 μm	-55°C to +85°C	0.4 A 50V AC(RMS)/DC
TE Connectivity™	2.54	4 - 40		Back Flip	300 μm	-55°C to +105°C	
Goldenconn™	2	4 - 60		Front Flip	300 μm	-25°C to +85°C	0.2 A 30V AC(RMS)/DC

Table 4-1: Comparison of some ZIF connectors available in the commercial market

In this thesis, we have identified connectors fabricated by Hirose™, considering advantages in terms of compactness, dual-sides contact possibility, diverse choices, its quality and the certified performance of the interconnections.

4.2.3.1 Interconnection between 2 transmission lines

In order to verify the benefit of these connectors for radio frequency operations, two 50 Ω microstrip transmission lines have been tested, with interconnection through one ZIF connector. The idea herein is that: one line is on a rigid substrate (representing the PCB mainboard); the other line is on the flexible substrate (representing flexible feed lines of the antenna system).

A preliminary test has been done considering two 50 Ω microstrip transmission lines were realized on the same substrate (Teflon™ substrate (thickness 250 μm , $\epsilon_r = 2.2$, $\tan\delta = 0.0003$)): one was soldered with a ZIF connector; the other can be inserted into the opening of this connector to form an interconnection.

This Teflon™ substrate was chosen thanks to its flexibility and its very low loss tangent. The 250 μm thickness was also selected to be compatible with the connector dimensions (acceptable thickness: 300 μm). The copper etching process

yielded the conductive layers of about $17\mu\text{m}$ thick for metallization (so, $250 + 17 * 2 = 284\mu\text{m} < 300\mu\text{m}$).

The FH34 family's connector fabricated by Hirose™ was used thanks to its compact size, the thickness compatibility ($300\mu\text{m}$) and the good performance of the interconnection. In addition, it offers many choices about top/bottom contacts or dual-sides contacts and about the number of contacts (from 4 to 50).

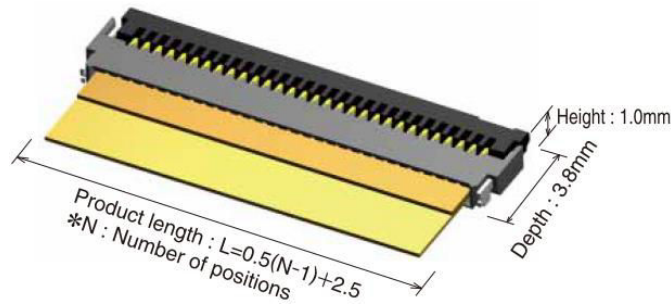
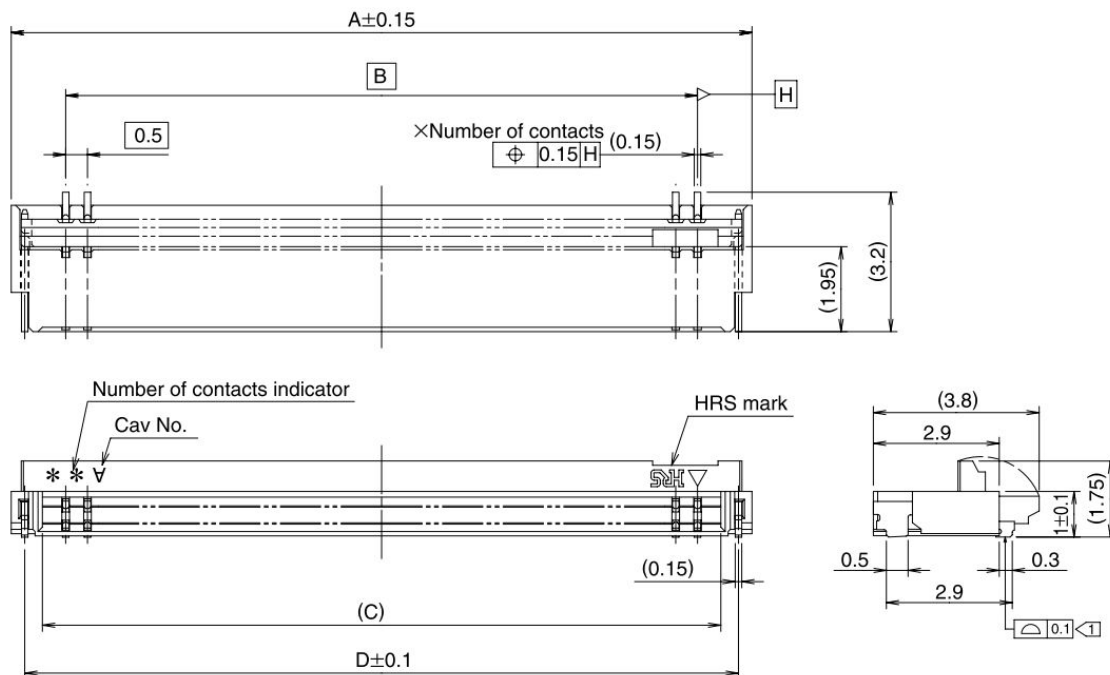


Figure 4-19: Illustrated model of FH34 family's connector

The designs were realized based on the dimensions inside FH34 family's connector provided by the datasheet, as shown in Figure 4-20 below. In particular, the most important details are: the width of each contact pin is 0.15 mm and the distance between the two adjacent contact pins is 0.5 mm . [FH34]



Unit: mm

Part Number	Number of Contacts	A	B	C	D
FH34SJ-4S	4	4	1.5	2.53	3.38

FH34SRJ-8S	8	6	3.5	4.53	5.38
------------	---	---	-----	------	------

Figure 4-20: Connector dimensions of FH34 family (FH34SJ: contacts only on the top of the flex line. FH34SRJ: contacts on the both sides of the flex line)

Two possible configurations have been developed: (a) contacts on only one side of the flex line combining with vias realization and (b) contacts on both sides of the flex line. The vias were realized manually in this trial run.

4.2.3.1.1 Configuration 1: Contacts on top side of the flex line only

The FH34SJ-4S connector was used for this configuration. It has 4 contacts only on the top of the flex line. So, 2 contact tracks in the middle are used for the signal line and 2 contact tracks at the edges are used for the ground plane. The design for the interconnection is presented in Figure 4-21 below.

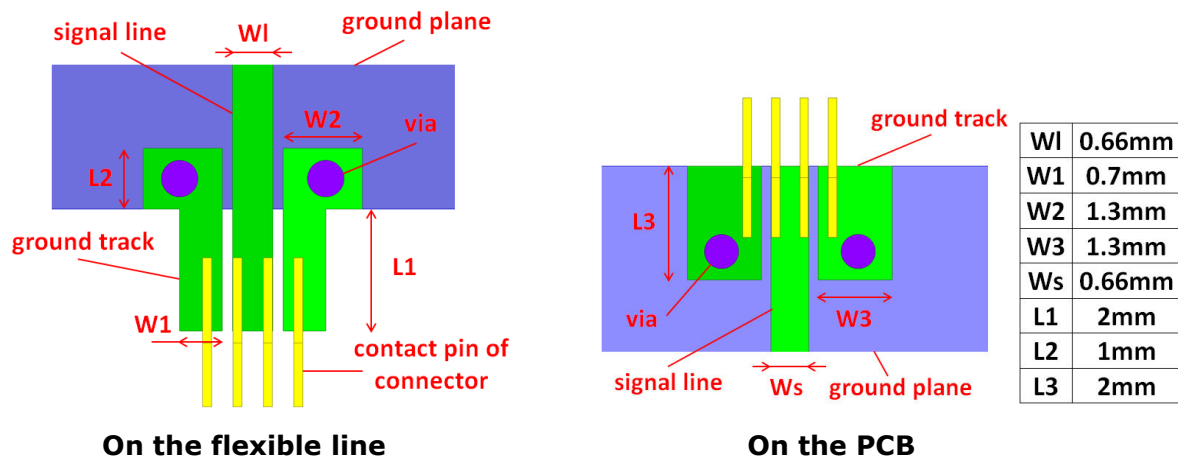
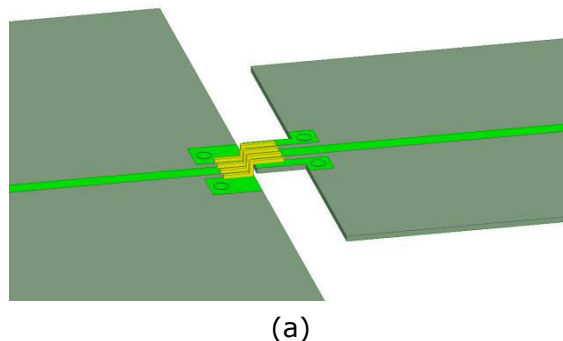
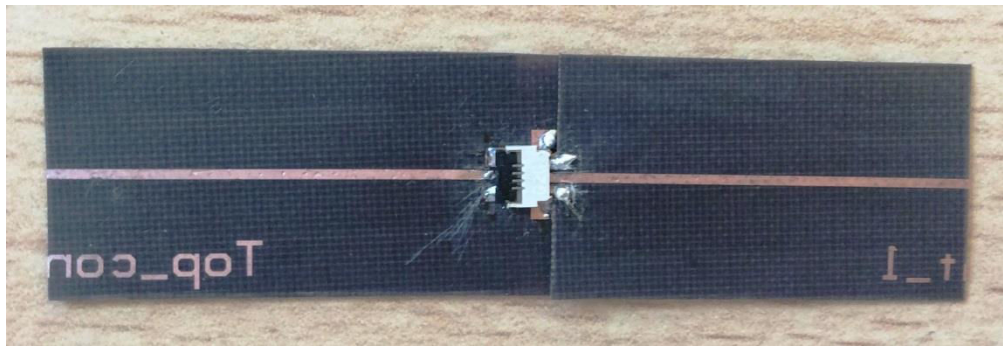


Figure 4-21: Design for the interconnection in the case of using connector with contacts on top side of the flex line

The simulation model on HFSS™ is illustrated in Figure 4-22a. In reality, the detailed model of this connector, provided by Hirose on its website, is far more complex. However, in order to simplify the modelling and the simulation, a simpler model was established, considering only metallic parts, neglecting therefore complex plastic forms. The plastic support of the connector and its back-flip rotating actuator were removed and the metallic contact pins were modelled as the straight copper pins. Obviously, these simplifications have almost no effect on the performance of the connector.

Each transmission line has a length of 30 mm and a width of 0.66 mm corresponding to 50Ω impedance. Two vias must be realized on the flex line in order to have contact with the ground plane.





(b)

Figure 4-22: Simulation model (a) and prototype (b) of the interconnection using connector with contacts on top side of the flex line

The performance of these two transmission lines through the tested connector are presented in Figure 4-23 below. The measurement is not totally smooth due to resonances between the two edges of the metallic support with the two ground planes of the two microstrip transmission lines. However, the agreement with the simulation results remains fairly good. The measured S_{21} exhibited additional losses than simulation, due to extra losses of the two SMA connectors as well as the ZIF connector (dielectric losses of the connector housing material neglected) not included in the ideal simulation. In addition, the via holes have been realized manually with certainly some imperfections of the connection to ground plane, leading ohmic losses.

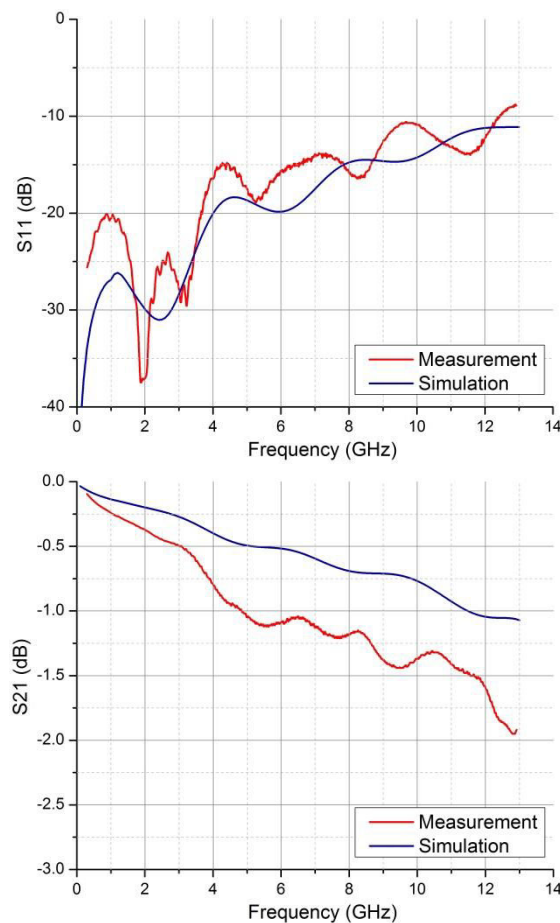


Figure 4-23: S_{ij} parameters of the transmission line through ZIF connector having contacts on top side of the flex line

We can notice that the impedance matching is very good for frequencies below 3 GHz, and it is gradually degraded by rising in higher frequencies (-10 dB in X band). The measured insertion losses over the 6cm length of two transmission lines through the connector were about -0.5 dB at 2.4 GHz and -1.1 dB at 5.5 GHz. We have also verified the insertion losses of a 50 Ω transmission line of 6cm length on Teflon: -0.27 dB at 2.4 GHz and -0.47 dB at 5.5 GHz. Therefore, the insertion losses through the connector are estimated to about -0.23 dB at 2.4 GHz and -0.63 dB at 5.5 GHz. Its performance is validated at least up to X band.

4.2.3.1.2 Configuration 2: Contacts on both sides of the flex line

In this configuration, the FH34SRJ-8S connector fabricated by Hirose was applied. We have chosen the connector type having the least number of contacts as possible of FH34 family available on the market. It has 8 contacts on both sides (top and bottom) of the flex line.

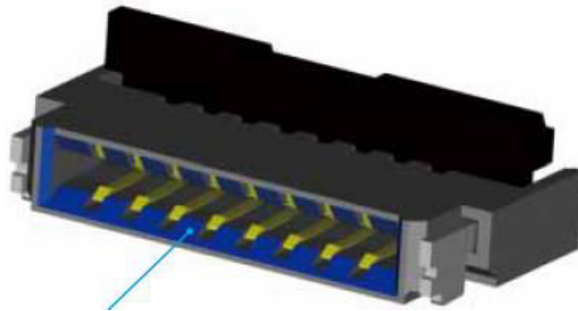


Figure 4-24: Description of the top-bottom contacts

So, 2 central contact tracks are used for the main signal line and 3+3 contact tracks at the edges are used for the ground plane connections. The design for the interconnection is presented in Figure 4-25 below.

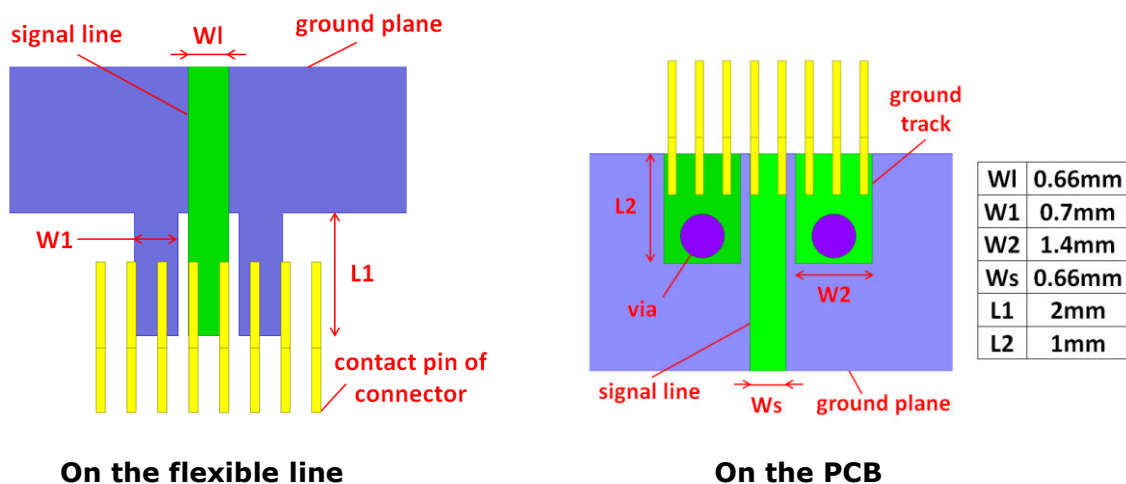
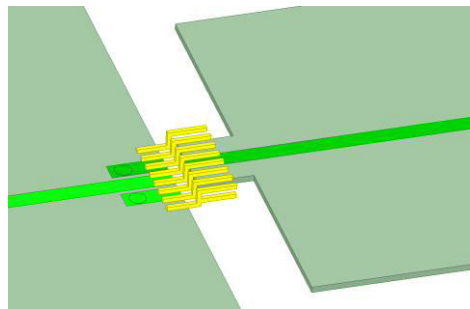
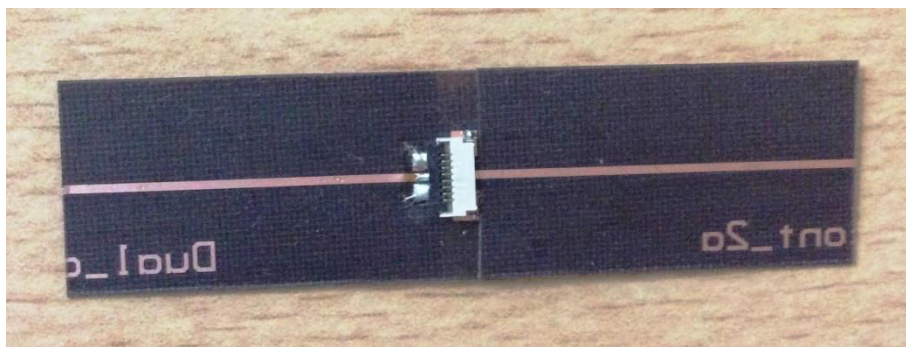


Figure 4-25: Design for the interconnection in the case of using connector with contacts on both sides of the flex line

The benefit of this configuration is that the ground plane continuity is easily achieved using bottom connections. The simulation model on HFSS™ is illustrated in *Figure 4-26a*. Of course, a simplified model was also established to perform the modeling and accelerate the simulation task. The plastic support of the connector and its back-flip rotating actuator were also removed and the metallic contact pins were modelled as the straight copper pins.



(a)



(b)

Figure 4-26: Simulation model (a) and prototype (b) of the interconnection using connector with contacts on both sides (top and bottom) of the flex line

A good agreement between the measurement and the simulation of S_{ij} parameters were also observed, as depicted in *Figure 4-27* below. By comparing with the performance of the interconnection using a connector with contacts only on top side of the flex line, this configuration had slightly more insertion losses. But it allows eliminating the two vias on the flex line. Therefore, the via realization process on the paper substrate is not required anymore.

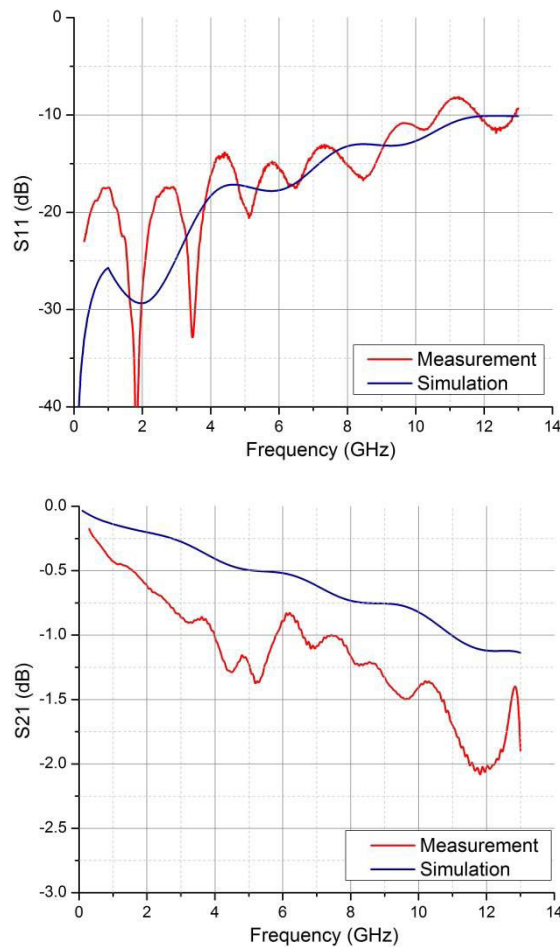


Figure 4-27: S_{ij} parameters of the transmission line through ZIF connector having contacts on both sides (top and bottom) of the flex line

The insertion losses over the 6cm length of two transmission lines through this connector were about -0.7 dB at 2.4 GHz and -1.2 dB at 5.5 GHz. So, the insertion losses through the connector are about -0.43 dB at 2.4 GHz and -0.73 dB at 5.5 GHz.

4.2.3.2 Interconnection from antenna to PCB mainboard

In order to prepare the final demonstrator, we have tested the transition from one antenna on flexible substrate to the feed line on PCB mainboard. The antenna screen-printed on E4D-200 paper was inserted into a ZIF connector, previously soldered on the Teflon™ substrate for interconnection with the 50Ω microstrip transmission line, as illustrated in Figure 4-28 and Figure 4-30.

The FH34SRJ-8S connector, with top and bottom contacts towards the flex line as described above, has been used to avoid the use of the two via holes on the flex line.

The feed line etched on Teflon™ (thickness 250μm, $\epsilon_r = 2.2$, $\tan\delta = 0.0003$) is 3 cm long, with a width of 0.66 mm (Cu metallization thickness: 17μm). The soldering and via realization on Teflon™ were manually made. For industrial

production, they would be done through conventional and perfectly controlled metallization process. Once again, the top-bottom contact connector permits to avoid the realization of via holes in the paper board.

The design for the interconnection has a little change, mainly the width of the signal line on the paper substrate (0.56 mm width) to be compatible with 50 ohm.

Two kinds of antenna (a monopole and a dipole) screen-printed on E4D-200 paper have been tested.

a/ Interconnection with monopole antenna:

The interconnection was tested in two cases: antenna only and antenna stuck on a small piece of ABS plastic (2.7mm x 4.7mm x 2.55mm), as shown in *Figure 4-28a* and *Figure 4-28b*, respectively. A simulation model was also realized on HFSS™ to compare with the measurement, cf. *Figure 4-28c*.

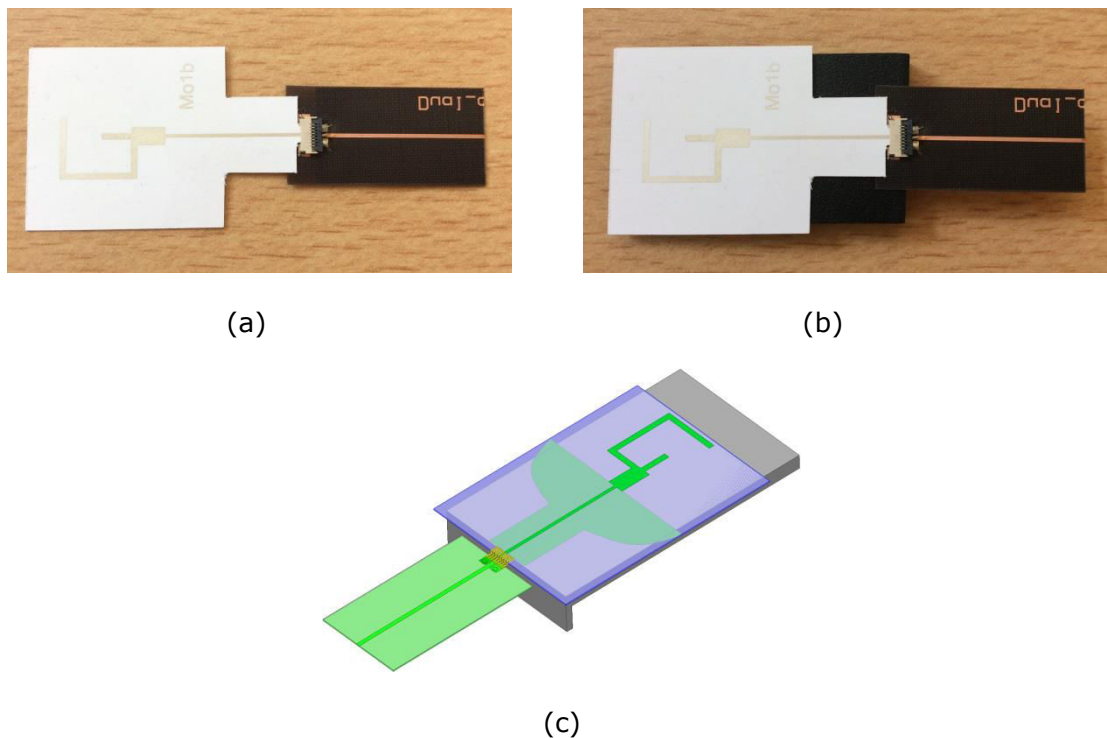


Figure 4-28: Prototype (without ABS (a) and with ABS (b)) and HFSS simulation model (c) of the interconnection from feed line on PCB to monopole antenna screen-printed on paper

During the measurement, we have faced difficulties to establish correct contacts between the interconnection line on paper and the ZIF connector, mainly due to the thickness compatibility. The total thickness of E4D-200 paper (210μm) + 2 layers of conductive ink on both sides (7.6μm x 2) is not enough to have an ideal contact when inserting into the ZIF connector (compatible thickness: 300μm). In addition, the horizontal space between the center line on top side and the ground tracks on bottom side (of the interconnection part on paper) is very narrow. Therefore, the contact between the interconnection line on paper and the ZIF connector is not

tight and remains very sensitive. Thence, we have encountered a great deal of difficulty in measuring the prototypes.

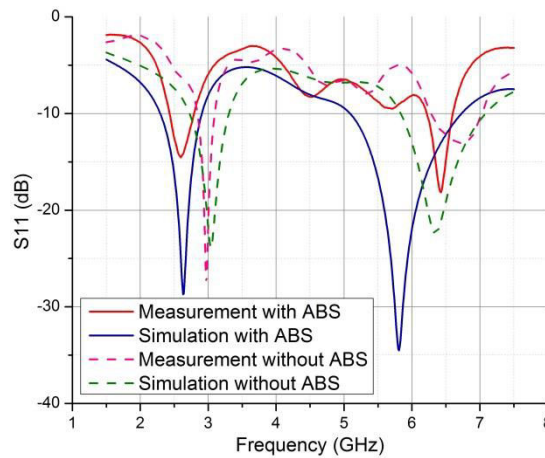


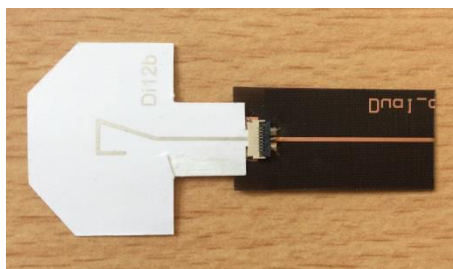
Figure 4-29: Return loss of the monopole antenna screen-printed on paper with taking into account the interconnection with the feed line on PCB

However, the received results are still very encouraging. It can be seen a good agreement between the measurement and HFSS™ simulation for S_{11} parameter in both cases, especially at low frequency. The influence of contacts is more serious and visible at the higher resonance frequency of the tested dual-band antennas.

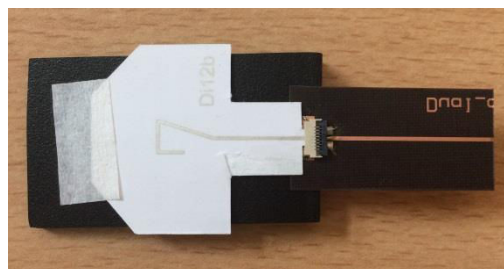
Moreover, the description of the connector is simplified and manual via realization brings undoubtedly some discrepancies. In case of sticking on a small piece of ABS plastic, the resonance frequencies of the antenna shift toward lower desired values as predicted by simulation.

b/ Interconnection with dipole antenna:

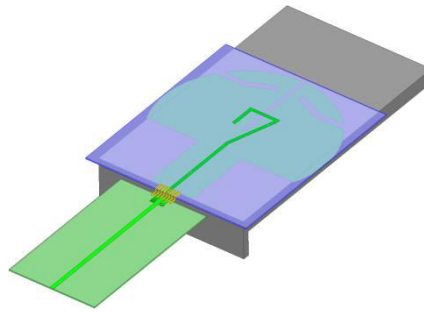
The interconnection with a dipole antenna was also tested in two cases with and without ABS plastic backside support. The results were then compared with the HFSS™ simulation. The problem of contacts control remains, which make the measurements rather difficult.



(a)



(b)



(c)

Figure 4-30: Prototype (without ABS (a) and with ABS (b)) and HFSS simulation model (c) of the interconnection from feed line on PCB to dipole antenna screen-printed on paper

A reasonably good accordance is obtained between the measurement and the simulation of S_{11} parameters in both cases. In case of sticking on a small piece of ABS plastic, the dual-band behavior of the dipole antenna emerges clearly, as exhibited in Figure 4-31, yielding a 1st frequency of 2.53 GHz (0.21 GHz bandwidth @ VSWR=2) and a 2nd frequency of 5.5 GHz (2.22 GHz bandwidth @ VSWR=2). It covers the two desired frequency bands.

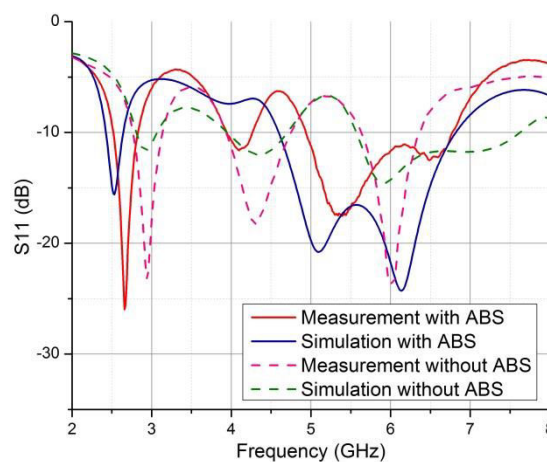


Figure 4-31: Return loss of the dipole antenna screen-printed on paper taking into account the interconnection with the feed line on PCB

4.2.4 Conclusion

In general, we have demonstrated that ZIF connectors can be considered as an innovative solution for connecting RF antennas to PCB, resolving the use of expensive coaxial cables not appropriate with electronic consumers markets.

Experimentations have been performed on several transmission lines and basic antennas to validate the expected performances. Insertion losses through ZIF connector remain quite small and acceptable, at least up to 6 GHz (about -0.4 dB at 2.4 GHz and -0.7 dB at 5.5 GHz). In addition, it also allows the elimination of soldering operations in comparison with micro coaxial cable solution.

The encouraging results mentioned above show the feasibility of this alternative in solving the interconnection requirement. Of course, there are still some problems that need to be optimized or improved.

The contact between the interconnection part on paper and the ZIF connector is not tight and very sensitive. This can be improved by substituting thicker paper substrates, more compatible with ZIF connectors.

For repeated use in long-term, the paper substrate can be damaged. However, if another flexible substrate like polymer is used, it would be very appropriate, especially in terms of mechanical strength.

For the perspective, the optimization of the transition by improving the impedance matching will be realized. The mismatching is caused by the transition from microstrip line to CPW line. Therefore, in order to minimize its influence, we could reduce the length of the CPW part or modify the dimensions of the CPW part (it should be remembered herein that the distance between the contact pins of the connector is fixed at 0.15 mm) or add a complementary matching stub. We could also either minimize or compensate for the parasitic effect of manual soldering and via realization.

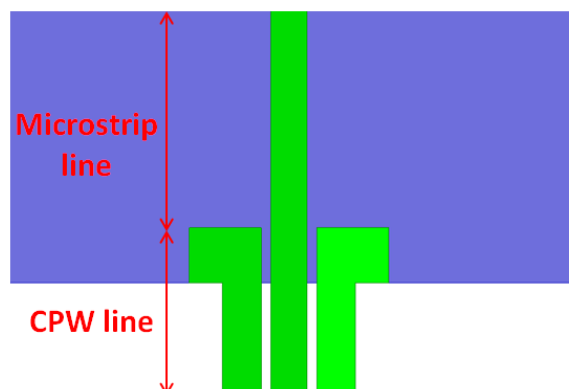


Figure 4-32: Transition from microstrip line to CPW line in the interconnection

4.3 Antenna system on flexible substrate

As we have mentioned in *chapter 1*, the objective of this thesis is creating an antenna system, printed on a flexible substrate (e.g. paper), which can be stuck on the plastic sidewall of the set-top-box and has the direct interconnection to the PCB mainboard without using coaxial cable. The characterization of flexible substrate and the antenna design are presented in the previous *chapters 1* and *2*, the direct interconnection to PCB mainboard is also presented above. So, we have all elements for the construction of the antenna system.

We have developed different models of antennas stuck on 2 sides of set-top-box for polarization diversity. The design features have to be done taking into account the coupling phenomena between closed-proximity structures. The height of the set-top-box is fixed to 3mm according to specifications, so the size of the antennas is

very limited. The *Figure 4-33* below gives an overview of the expected configuration, using spatially distributed antennas (for radiation patterns and consequently special diversity): system of 3 monopole antennas and system of 3 dipole antennas.

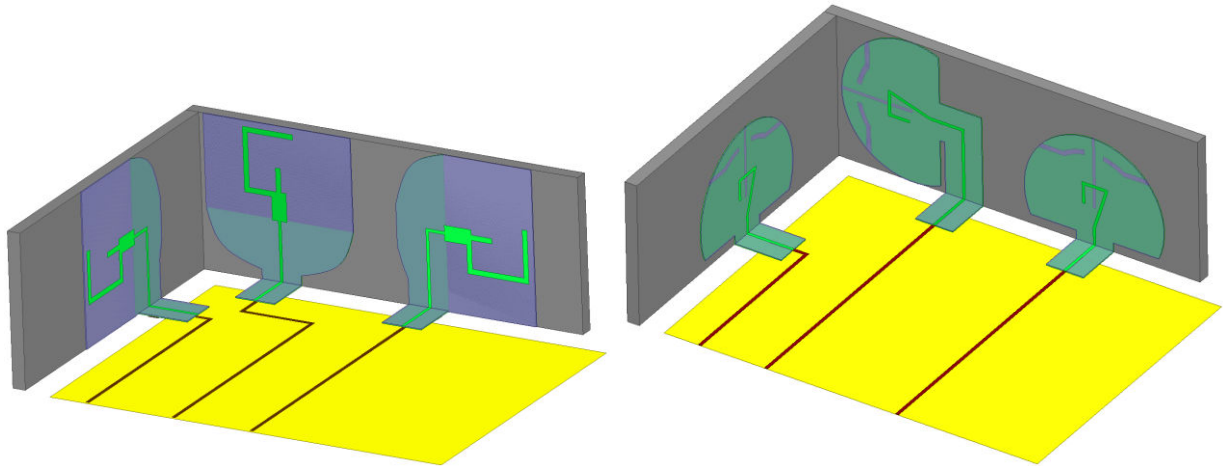


Figure 4-33: Model of the antenna system stuck on the plastic sidewall of set-top-box: (a) 3 monopole antennas and (b) 3 dipole antennas

The most important requirements are:

- the two impedance bandwidths of each antenna must satisfy the two bands of IEEE.802.11a/b/g/n/ac WLAN standards
- the omnidirectional radiation pattern
- the isolation between the antennas above 20 dB.

4.3.1 Three dual-band Wi-Fi monopole antenna

The 3 monopole antennas are arranged at positions as shown in *Figure 4-34* below. The 3 H-planes are orthogonal (or 3 E-planes orthogonal) in order to minimize the coupling between them. The distances between the antennas are small enough for the good isolation (> 20 dB) between them. The dimensions of all 3 antennas have been adjusted by parametric optimization in order to achieve the good resonance frequencies and desired bandwidths taking into account the presence of the ABS plastic sidewalls on which the antennas are stuck. The ground plane of each monopole was truncated to 10 mm if compared with the dual-band Wi-Fi monopole designed in *Figure 3-10* in order to reduce the insertion losses in the feed line. The form factor of this new ground plane was also changed to reduce the size and the printing area of the antenna. The feed lines were reduced to the maximum.

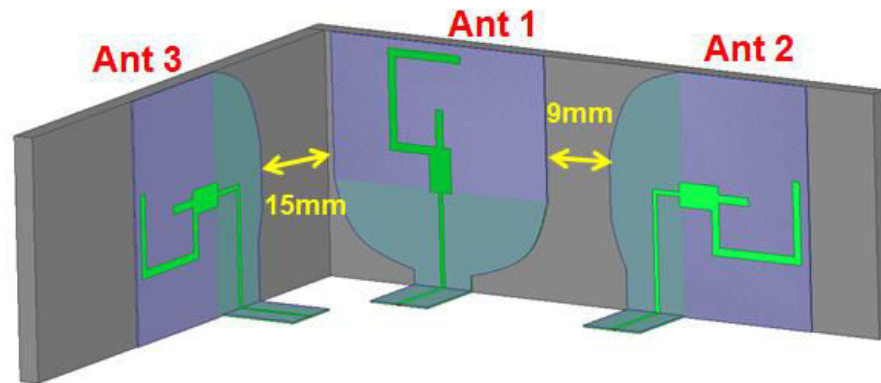


Figure 4-34: Simulation model of the 3 monopole antennas stuck on the plastic sidewall of set-top-box in the case without PCB ground plane

The isolation between two dual-band Wi-Fi monopole antennas in function of angle α has been verified, as shown in Figure 4-35. Obviously, the coupling effect is minimum ($S_{21} < -20$ dB in both frequency bands) when $\alpha = 90^\circ$. In this case, two H-planes of the two antennas are perpendicular (or otherwise two E-planes perpendicular).

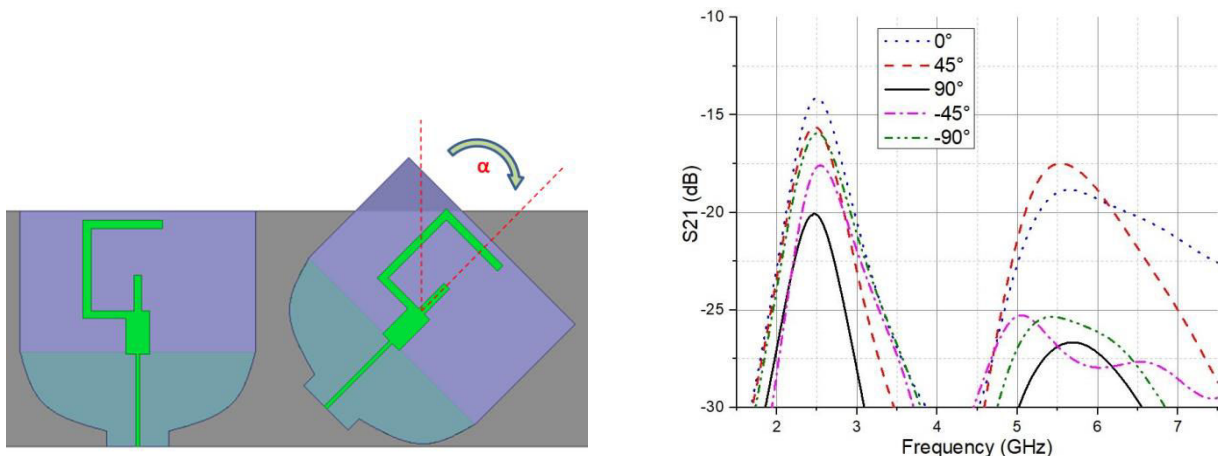


Figure 4-35: Coupling between the two dual-band Wi-Fi monopole antennas in function of angle α

The isolation between two monopole antennas *Ant1* and *Ant2* in function of the distance d_{12} between them has been also investigated by parametric simulation, as shown in Figure 4-35. It can be noted that the closer two antennas are, the more significant coupling effect they exhibit. So, the 9mm distance is enough to have a good isolation between these two monopoles.

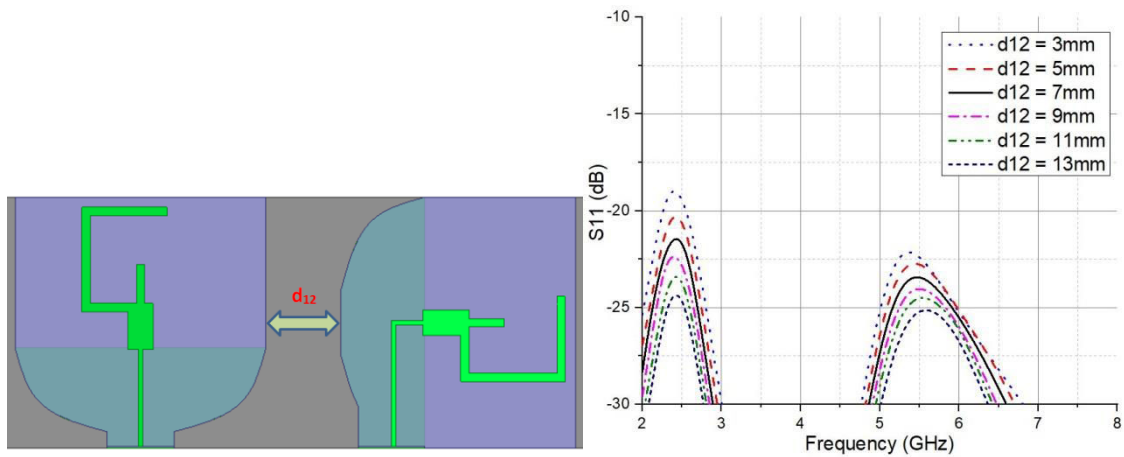


Figure 4-36: Coupling between the two dual-band Wi-Fi monopole antennas Ant 1 and Ant 2 in function of the distance d_{12} between them

The simulated return loss of each monopole in the system, as depicted in Figure 4-34, and the coupling between them are shown in Figure 4-37 below.

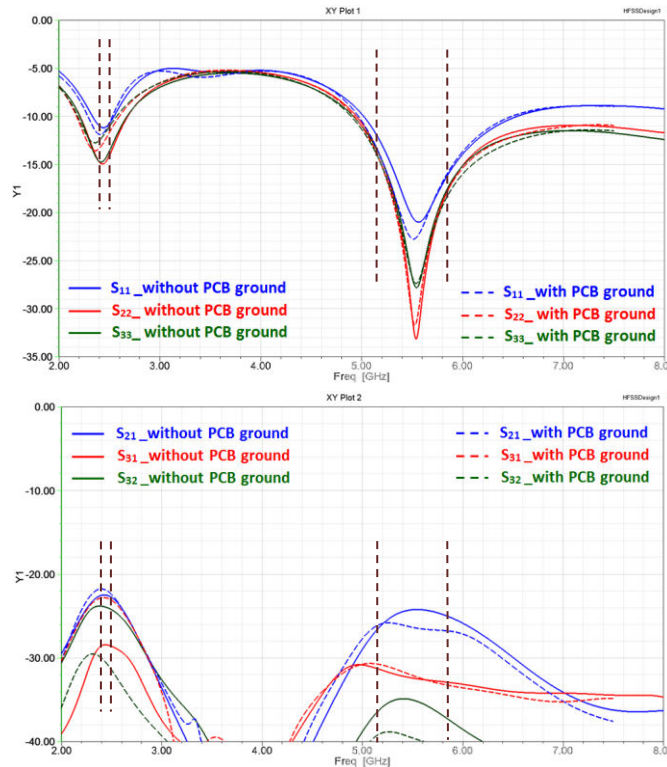


Figure 4-37: Simulated return loss and S_{ij} coupling coefficients of each antenna in the system in both cases: with and without PCB ground plane

We can notice that the dual bands for WLAN applications are satisfied and all isolations between the antennas are above 20dB. We have simulated in two cases: without PCB ground plane and with PCB ground plane ($60 \times 80 \text{ mm}^2$) at the bottom of the set-top-box. Clearly, the S_{ii} return losses and the S_{ij} coupling coefficients in both cases were almost unchanged, cf. Figure 4-37 above. Only, the radiation pattern of each antenna was deformed due to the presence of the PCB ground plane at the bottom of the set-top-box. In the case without PCB ground plane, the radiation pattern of each antenna was omnidirectional as illustrated in Figure 4-38a. However, when adding the copper ground plane to the simulation, we have seen

that the radiation patterns (towards the PCB ground plane) were deformed and directed toward the outside of the set-top-box (*Figure 4-38b*). This is completely normal when the antennas are introduced into the set-top-box environment because all the parasitic metal parts (e.g. hard disk drive, shielding covers, heat-sinks, Ethernet/USB/HDMI/SATA connectors, cables etc.) can impair the antenna performance. Therefore, to solve this problem, the antennas need to be located far from the ground plane. However, with the size and integration constraints in the set-top-box, this is extremely difficult to implement.

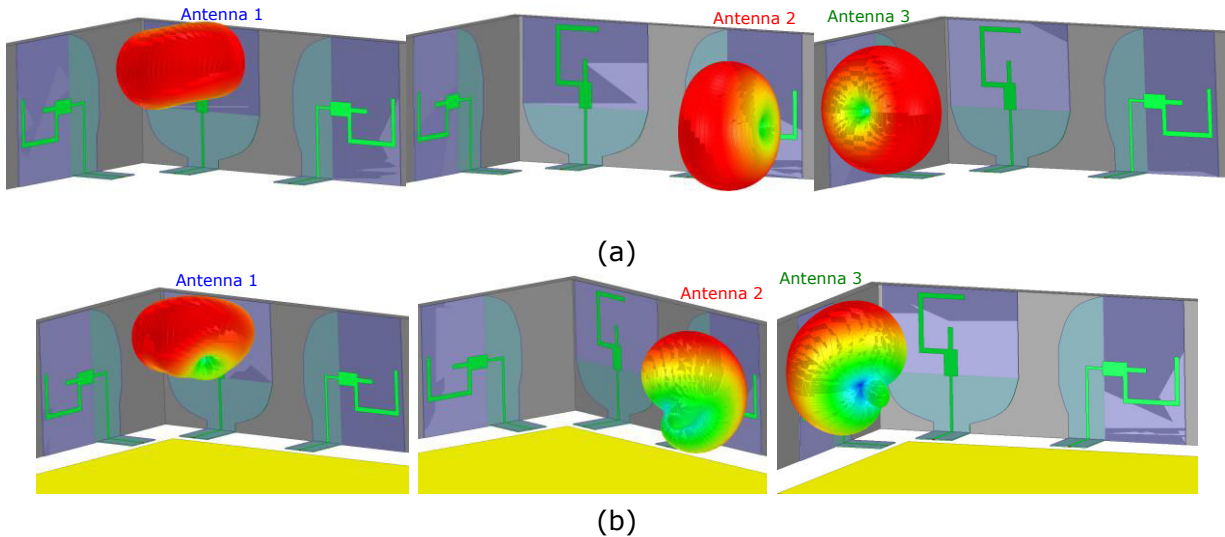


Figure 4-38: Simulated 3D Radiation pattern of each monopole at 2.45 GHz in the case: (a) without PCB ground plane and (b) with PCB ground plane

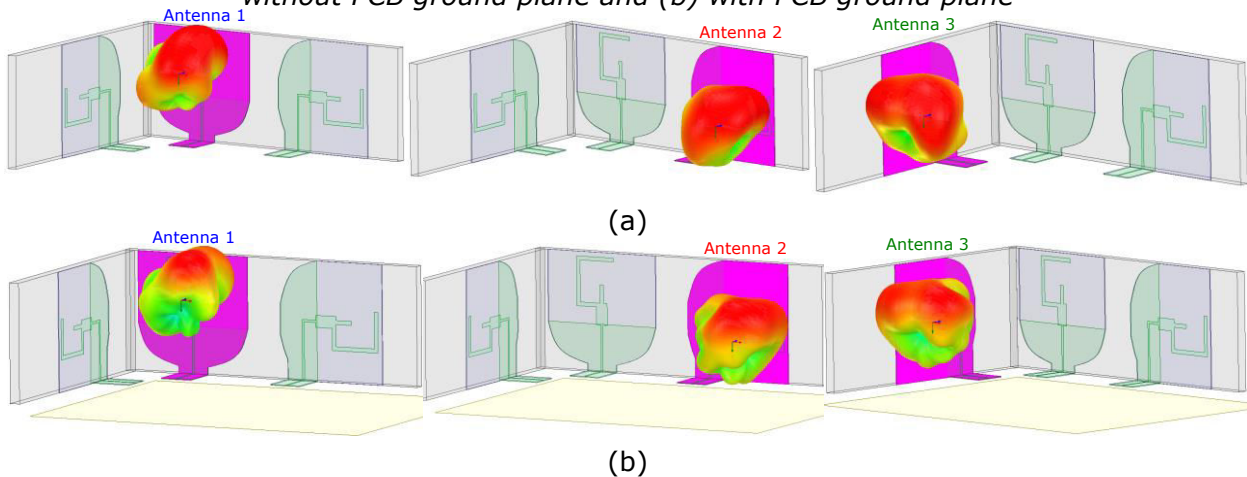


Figure 4-39: Simulated 3D Radiation pattern of each monopole at 5.5 GHz in the case: (a) without PCB ground plane and (b) with PCB ground plane

In the case with PCB ground plane, excluding losses in the feed line, the simulated max realized gains and total efficiency of the Antenna 1 were 2.11dBi and 55.2% at 2.45 GHz and 4.89dBi and 77.7% at 5.5 GHz respectively. For the Antenna 2, these values were 2.87dBi and 60.8% at 2.45 GHz and 5.6dBi and 81.5% at 5.5 GHz respectively. And for the Antenna 3, these values were 2.24dBi and 57.1% at 2.45 GHz and 5.32dBi and 79.8% at 5.5 GHz respectively. These performances are entirely reasonable. At 5.5 GHz, the impedance matching is better, so the efficiency is higher. The Antenna 1 is located in the middle of the system and is affected by the other two antennas, so its performance is a little lower.

Comparison	Frequency (GHz)	Max realized gain (dBi)	Total efficiency (%)
Antenna 1	2.45 GHz	2.11 dB	55.2%
	5.5GHz	4.89 dB	77.7%
Antenna 2	2.45 GHz	2.87 dB	60.8%
	5.5GHz	5.6 dB	81.5%
Antenna 3	2.45 GHz	2.24 dB	57.1%
	5.5GHz	5.32 dB	79.8%

Table 4-2: Simulation results of the 3 monopole antennas stuck on the plastic sidewall of set-top-box in the case with PCB ground plane

The three monopole samples were screen-printed on E4D-200 paper. The feed line circuit was also realized on Teflon substrate by a copper etching process to imitate the PCB mainboard, cf. Figure 4-40.

Since the contact between the interconnection part on E4D-200 paper and the ZIF connector is not tight, mostly because of the thickness compatibility as mentioned in section 4.2.2.2 above, we have not yet folded the paper interconnection line to create the final 3D configuration like the model in Figure 4-33a. In addition, another concern related to the risk of micro-cracking of the silver ink deposit due to folding must be checked further. Therefore, temporarily, we have to survey the antenna system in a planar state, as illustrated in Figure 4-40.

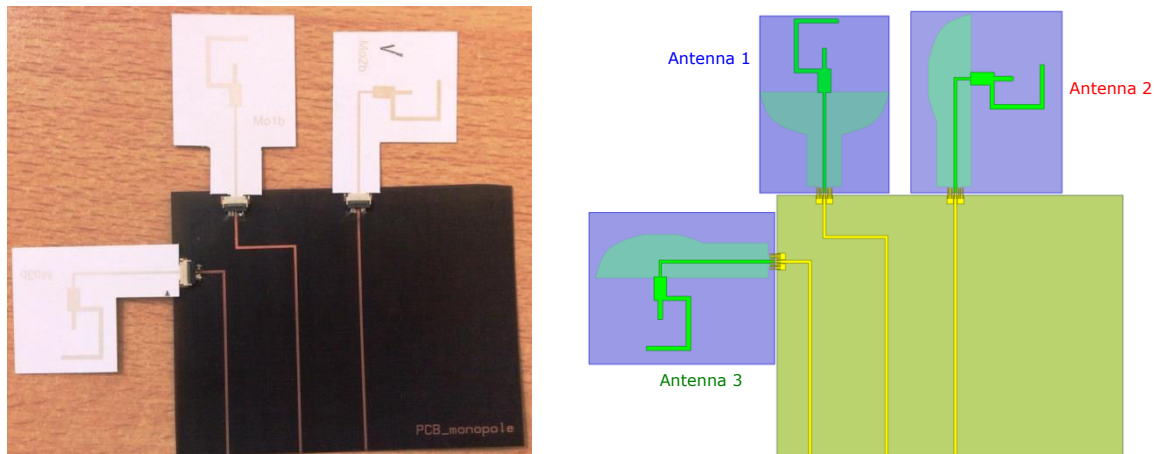


Figure 4-40: Prototype [L] and simulation model [R] of the system with 3 monopole antennas in the planar state

The very good agreements were obtained between the measurement and the HFSS simulation of S_{ii} and S_{ij} , cf. Figure 4-41. These antennas have not yet been stuck on the plastic sidewall of the set-top-box so it is easy to understand that the frequency bands do not correspond to the requirements (absence of dielectric support).

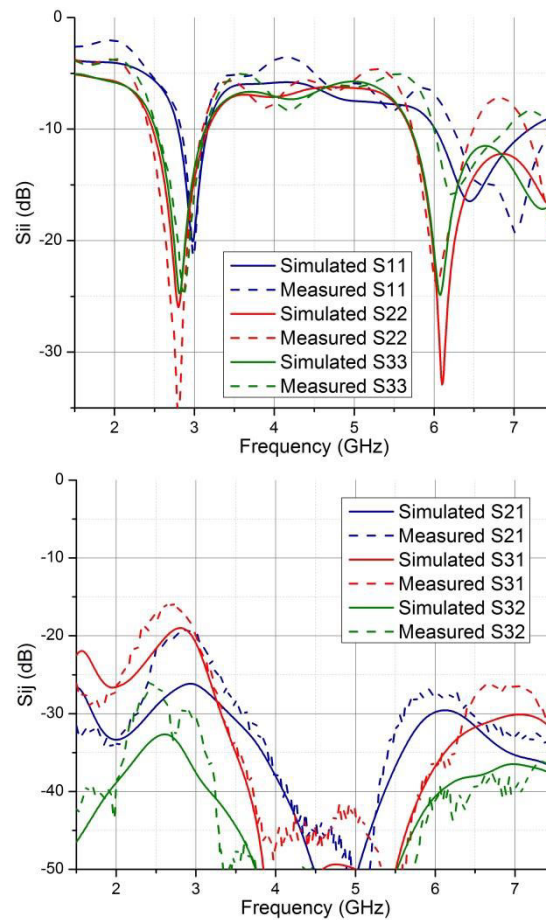


Figure 4-41: Return loss and S_{ij} coupling coefficients of each antenna in the system in the planar state

The couplings between the antennas are below -20 dB except for the case of S_{31} because two H plans of antennas 1 and 3 in the planar state are parallel. Therefore, this system design of 3 monopole antenna can be validated.

4.3.2 Three dual-band Wi-Fi dipole antenna

To create another radiation pattern configuration and expand the bandwidth, especially on 2nd frequency, we have also developed another system with 3 dipoles. The 3 dipole antennas are oriented, as shown in Figure 4-42 below, so that the 3 H-planes (or 3 E-planes) are orthogonal to each other. The distances between the antennas were also calculated enough for the good isolation between them. The dimensions of all 3 antennas have been designed by parametric optimization in order to achieve the good resonance frequencies and desired bandwidths when being stuck on the ABS plastic sidewall.

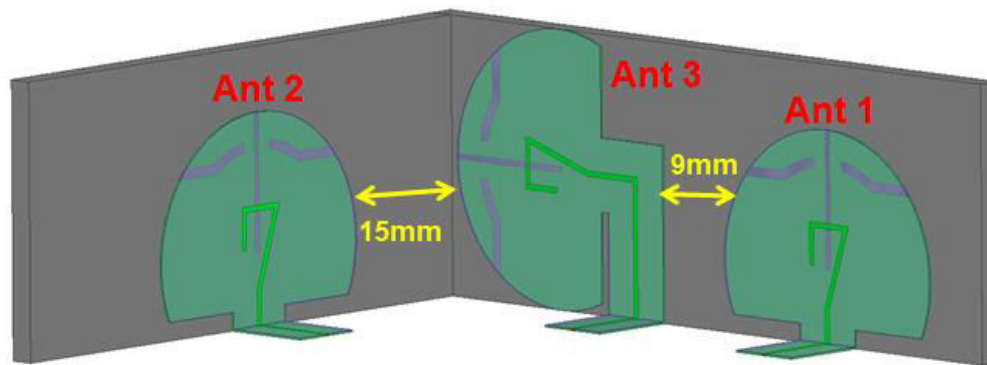


Figure 4-42: Simulation model of the 3 dipole antennas stuck on the plastic sidewall of set-top-box in the case without PCB ground plane

The simulated return loss of each dipole and the coupling between them are shown in Figure 4-43 below.

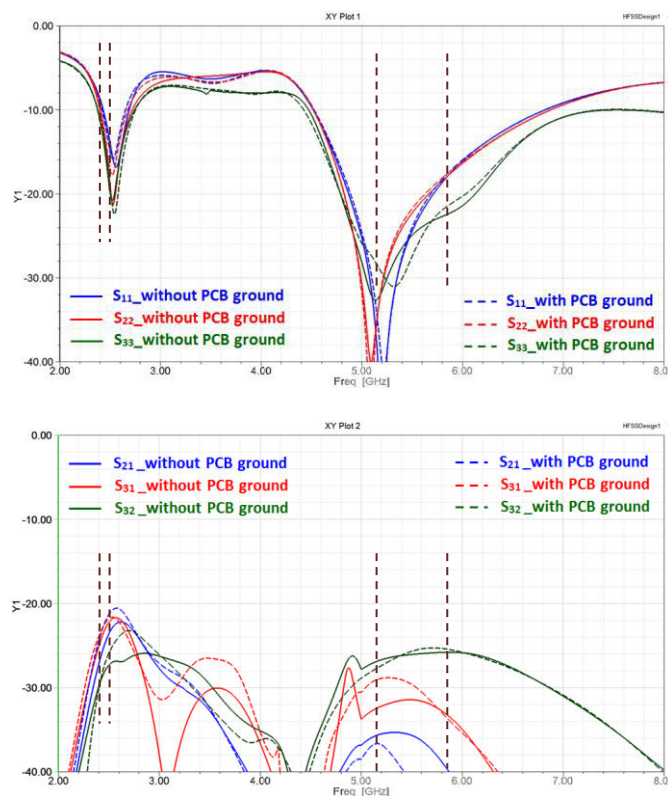


Figure 4-43: Simulated return loss and S_{ij} coupling coefficients of each antenna in the system in both cases: with and without PCB ground plane

It can be seen that the dual bands required for WLAN applications are satisfied and all isolations between the antennas are above 20dB. We have also simulated in two cases: without PCB ground plane and with PCB ground plane (60 x 80 mm²) at the bottom of the set-top-box. Like in the previous configuration with 3 monopole antennas, the S_{ii} return losses and the S_{ij} coupling coefficients were almost unchanged, as shown in Figure 4-43 above. Only, the radiation pattern of each antenna was deformed due to the presence of the PCB ground plane at the bottom

of the set-top-box. When adding the copper ground plane to the simulation, the radiation pattern of each antenna was no longer omnidirectional as illustrated in *Figure 4-44a*; it was strongly deformed and directed toward the outside of the set-top-box (*Figure 4-44b*). At 5.5 GHz, the antennas were already directional toward the outside of the electronic box, so the presence of the PCB ground plane did not significantly affect the radiation patterns of the antennas, as shown in *Figure 4-45*.

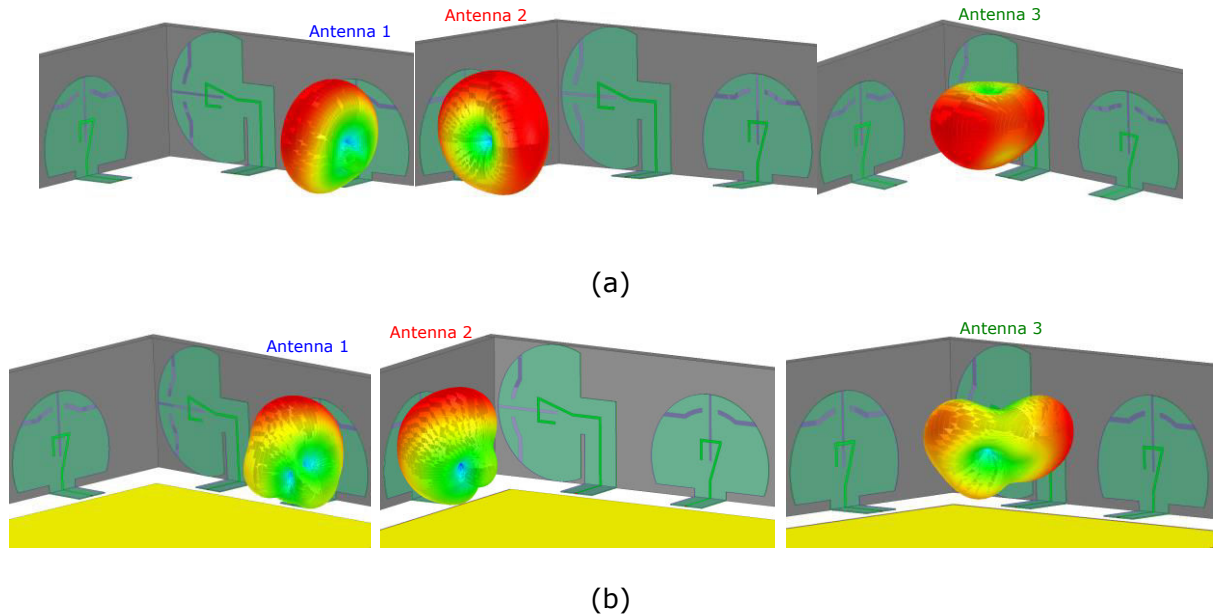


Figure 4-44: Simulated 3D Radiation pattern of each dipole at 2.5 GHz in the case: (a) without PCB ground plane and (b) with PCB ground plane

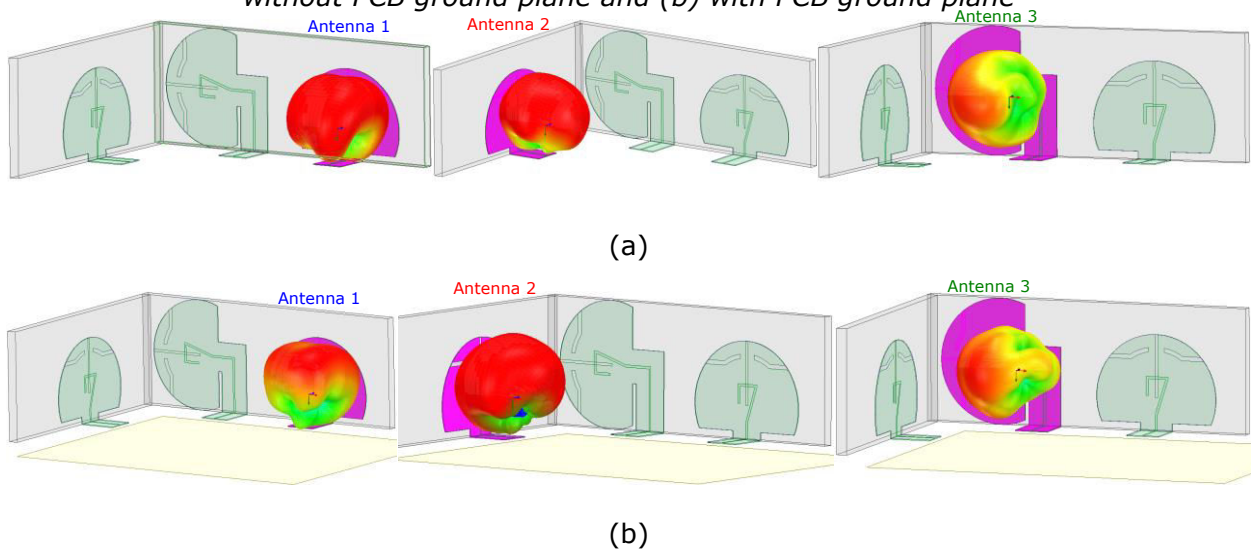


Figure 4-45: Simulated 3D Radiation pattern of each dipole at 5.5 GHz in the case: (a) without PCB ground plane and (b) with PCB ground plane

In the case with PCB ground plane, excluding losses in the feed line, the simulated max realized gains and total efficiency of the Antenna 1 were 2.52dBi and 48.2% at 2.45 GHz and 5.58dBi and 92.4% at 5.5 GHz respectively. For the Antenna 2, these values were 1.11dBi and 55.7% at 2.45 GHz and 5.28dBi and 92.2% at 5.5 GHz

respectively. And for the Antenna 3, these values were 1.68dBi and 65.1% at 2.45 GHz and 5.01dBi and 97.5% at 5.5 GHz respectively. At 5.5 GHz, the impedance matching is better, so the efficiency is higher.

Comparison	Frequency (GHz)	Max realized gain (dBi)	Total efficiency (%)
Antenna 1	2.45 GHz	2.52 dB	48.2%
	5.5GHz	5.58 dB	92.4%
Antenna 2	2.45 GHz	1.11 dB	55.7%
	5.5GHz	5.28 dB	92.2%
Antenna 3	2.45 GHz	1.68 dB	65.1%
	5.5GHz	5.01 dB	97.5%

Table 4-3: Simulation results of the 3 dipole antennas stuck on the plastic sidewall of set-top-box in the case with PCB ground plane

Due to the problem of contact at ZIF connector as well as difficulty in folding paper without damaging the antenna feed line, we have also investigated the antenna system just in the planar state, as illustrated in Figure 4-46.

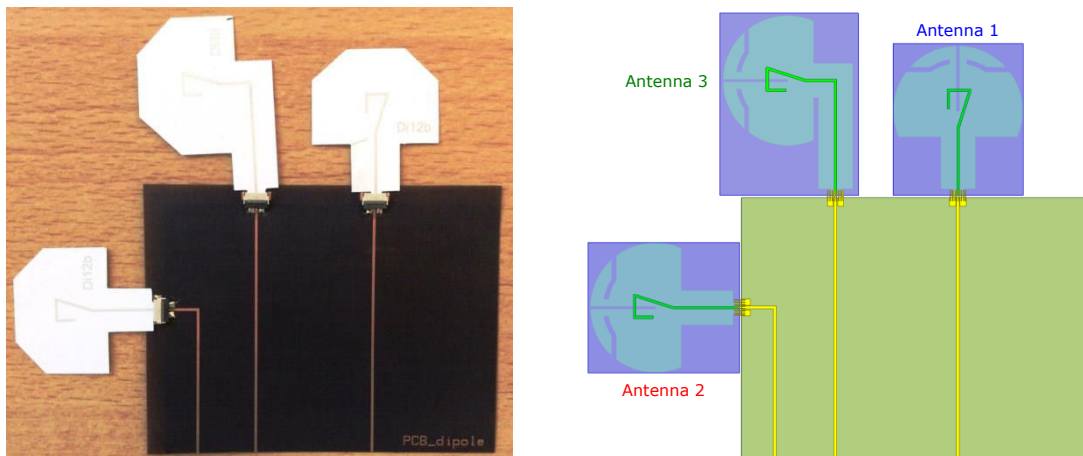


Figure 4-46: Prototype [L] and simulation model [R] of the system with 3 dipole antennas in the planar state

The measurements of S_{ii} and S_{ij} correspond fairly well with the HFSS simulations, as shown in Figure 4-47. These antennas have not yet been stuck on the plastic sidewall of the set-top-box so it is easy to understand that they do not have the characteristics of the dual-band antenna as required.

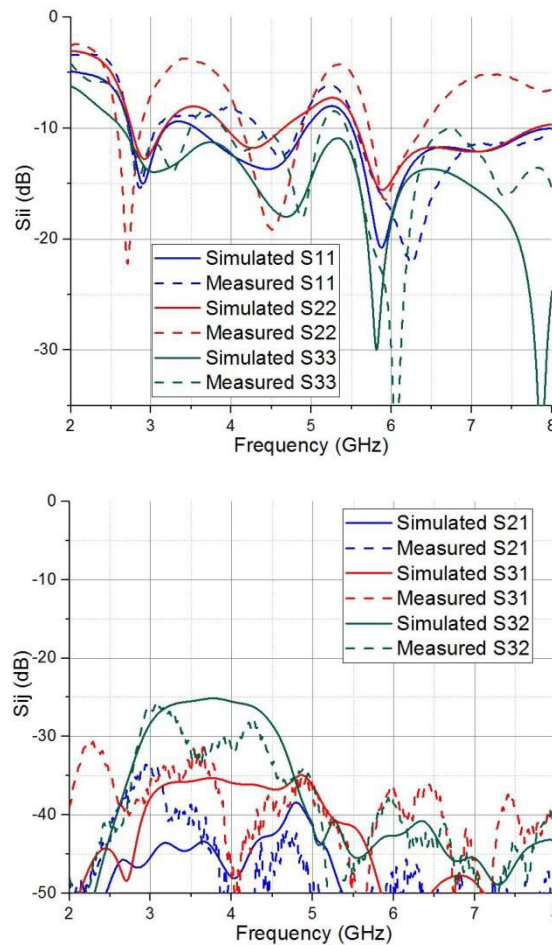


Figure 4-47: Return loss and S_{ij} coupling coefficients of each antenna in the system in the planar state

The measurements showed that the couplings between the antennas were very good, below -20dB. Therefore, this system design of 3 dipole antenna can be validated.

Thus, we have presented the antenna systems which are printed on a paper substrate and have a direct interconnection to the PCB mainboard. The measurements show very similar results with the simulations even if the contact between the interconnection part on paper and the ZIF connector remains not very tight and the measurement conditions in the laboratory are not ideal. The isolations of the 3 antennas in the planar state are superior to 20dB, enough to meet the requirement. These results prove also the operation of the ZIF connectors and the transition between the feed lines on a classical substrate and the antennas screen-printed on a paper substrate.

4.4 Conclusion of chapter 4

In general, we have demonstrated two antenna systems that can be stuck on the inner sidewall of the set-top-box for multimedia applications. These two systems of 3 antennas (monopole and dipole) were designed for polarization diversity. This polarization diversity solution leads to a minimization of inter-antenna coupling

effects (good isolation between antennas (> 20 dB)). Its dimensions have been calculated well to stick on ABS plastic sidewall. They have two resonance frequencies and two associated bandwidths as required (2.4 – 2.5 GHz and 5.15 – 5.85 GHz). Their radiation patterns are also almost omnidirectional. The radiation efficiency is fairly good, superior to 50% (excluding the insertion losses in the feed line), in spite of the dielectric losses of the paper substrate and metallic losses of the silver ink deposit that we have mentioned many times in this thesis.

The measurements correspond very well with the simulations. That shows a reliability and repeatability of the design procedure.

All results prove also the operation of ZIF connectors as an innovative interconnection solution without the use of coaxial cables.

Although the final 3D demonstrator is not yet implemented, the ideas herein are very clear, and they can be further developed in the future.

For the perspective, we must find the way to fold the printed lines on paper and construct the system of 3 antennas in 3D configuration. Then, the 3 antennas will be really stuck on the 3D support of ABS plastic. So, the manner in which the paper antenna is stuck on plastic must be investigated. The measurements of the return loss, radiation pattern, realized gain of each antenna and the S_{ij} coupling between them will validate the design.

The antennas should also be printed on the new paper (or polymer) substrates, which are more compatible with ZIF connectors (e.g. thickness 250 μ m) in order to fix the interconnection. Of course, it is best to use polymer combined with a quality metallization (e.g. aluminum etching on PET) to minimize the losses and optimize the radiation efficiency.

Connectors having a great number of contact tracks can be advantageously used, once multi-access interconnections are properly controlled on different subs RF bands. More specifically, one large connector can handle the interconnection of all 3 antennas with the corresponding feed lines on PCB mainboard instead of utilizing 3 small connectors in order to reduce the cost. We can also use connectors cheaper than Hirose connector (for example Goldenconn) even though their performance is slightly inferior. Thence, the cost of realizing the interconnection will be extremely cheap.

For miniaturization purpose, we could reduce the dimensions of the antennas by using the plastic support which has the relative dielectric constant ϵ_r as high as possible for shielding of the set-top-box or by developing the 3D configuration associated with meandered lines for antenna structure.

General conclusions and perspectives

Contributions of this thesis

Paper is an ancient, universally recognized material that has been instrumental in bringing about major changes in society over the centuries. Nowadays, used in papers and boards industries with a production of about 100 million tons in Europe [Web], this cellulosic material is a green, renewable and recyclable commodity product. And, in the scope of this thesis, we have introduced it to a new function in order to face today's challenges.

Paper material has very interesting properties, in particular, the thermal and mechanical dimensional stability for the printing of electronics compared to, for example, plastics. As main printing substrate, traditional papers and cardboards have led to the development of specific knowledge in printing technology and long-term experience in large area roll-to-roll (R2R) printing processes. In addition, paper materials show many advantages such as very low production cost, very high flexibility, light weight, and biodegradability in the environment. Of course, the strategic orientation for a large use of the cellulosic material for printed electronics in the high-frequency domain exhibits some main limitations such as: very important electromagnetic losses ($\tan\delta$ closed to 0.05 instead of 0.004 for the Kapton for example), limited electrical conductivity level for the metallic nanoparticle inks used (around 2×10^6 S/m), difficulties and challenges for manufacturing vias holes, multi-layers structures and vertical interconnections for system hybridization, lack of robustness and no competitive with respect to traditional connector technologies over the time. Despite these barriers and these weaknesses, leading to new scientific works, these alternative substrates and processes appear as a suitable and interesting solution for cost reduction and a huge lower environmental impact for electronic systems if cellulosic based materials are used. Therefore, we have decided to explore the use of these cellulosic substrates for home networking applications at high frequencies.

In this dissertation, we have studied thoroughly the electromagnetic properties of the paper substrate as well as the associated metallization method for using it at radiofrequency. The characterization process was performed precisely over an ultra wide frequency band. We have also developed the antenna design on this flexible substrate to prepare for the final antenna system demonstrator. Many prototypes of elementary antennas were realized in order to validate the screen-printed paper technology.

We have recognized that the performance of the paper antennas along with others paper-based RF components and circuits is fairly low mainly because of dielectric losses in the paper substrate and metallic losses in the silver ink deposit.

Specifically, we can notice that the insertion losses on the 50Ω transmission lines are too much: about 0.76 dB/cm at 5.5 GHz. This significantly decreases the transmitted power in the feed line, especially for example in our case when we need to connect the antennas with a PCB mainboard by a long interconnection line. These loss issues are also the most important problem in my research work even though our printing technology is not mature and still far behind the inkjet printing technology of Tentzeris group, the leading research group in the domain of RF components and circuits on paper substrate. Obviously, with such performances, this technology can not satisfy technical specification requirements given. But in other applications more simple, such as wireless sensor nodes or RFID tags, it can completely prove as the potential and interesting solution for a new generation of ultra-low-cost "green" wireless electronics. In these applications, low radiation efficiency is not very criticized; but the low-cost aspect is the most important element in order to be realized in mass production amounts.

Then, we have also developed an innovative low-cost solution for the direct and flexible interconnection from the antennas to the PCB mainboard by using the ZIF connector. The measurements show clearly that this type of connection can work well at least up to 6 GHz. This can also be applied to the direct connection of the RF components and circuits to the PCB in other types of electronic box.

Finally, we have demonstrated two antenna systems that can be stuck on the inner sidewall of the set-top-box for multimedia applications. These two systems of 3 antennas (monopole and dipole) were designed for polarization diversity. Its dimensions have been calculated well to stick on ABS plastic sidewall. They have two resonance frequencies and two associated bandwidths as required (2.4 – 2.5 GHz and 5.15 – 5.85 GHz). Although the final 3D demonstrator is not yet implemented, the ideas herein are very clear, and they can be further developed in the future.

In general, RF components on paper in recent years have paved a road towards sustainable development in order to create a new generation of flexible electronics: ultra-low-cost and environmentally friendly. However, they just enough acceptable for the applications which are simples and do not require a high radiation performance, for example, wireless sensor nodes, RFID tags ...

Future perspectives

This research will also contribute to introducing deeper and deeper smart electronic devices in our living environment, generating greater interactivity and functionalities between the digital, industrial and living worlds. Traceability, interaction beyond the conventional identification networks will take advantage of the new technological breakthrough resulting from this thesis work, by exploiting a new interactive environment between RF-Sticker based communicating objects and Connected-Home devices. Consequently, this will result in an enhanced connectivity within the home-networks, interconnecting various objects and devices and offering by this way new services to the consumer.

However, there are still a lot of issues need to be further researched to complete the desired final demonstrator.

About the "printed paper" technology, we have to optimize the mounting/sticking on dielectric supports (transparency of the adhesive film, reliability, reproducibility, ...), optimize the bending/folding of conductive patterns (without degradation of the quality of the printed patterns (e.g. absence of microcracks), ...), extend the possibilities of this "printed paper" technology (metallized vias, multilayer substrates (paper/paper sealing), ...) and complete the evaluation between two technologies: printed paper (Ag) vs etched flexible polymer.

For printed RF devices on paper, we must decrease the insertion losses, especially in the feed lines (prioritize solutions so that paper become "transparent" (coplanar waveguide, coplanar stripline)) and optimize the interconnection between the printed paper and the CMS ZIF connector (technological and electrical improvement).

At the antenna system level, we need to finalize the design of the multi-antenna demonstrator (constitution and configuration of the system) as well as the characterization of the associated performances (return loss, radiation pattern, realized gain and total efficiency of each antenna, S_{ij} coupling between them, ...) and simplify the interconnection between antenna system and PCB mainboard by using multi-port connector (assembly simplification, cost reduction, etc.).

If we would like to reduce the losses and improve the performance of the flexible antennas, we can replace the "paper + screen-printing" techno by "PET + aluminum etching", for example. In this case, the system performance will be much improved while keeping the flexibility of the design. The way how to design an antenna on a flexible substrate does not change, the solution of RF interconnection from the flexible lines to the PCB mainboard remains the same. Therefore, other following researchers can inherit my researches and quickly transfer to the flexible polymer substrate. And that is a good solution for meeting the specification requirements.

ANNEX A: Measurement of conductivity of ink deposit

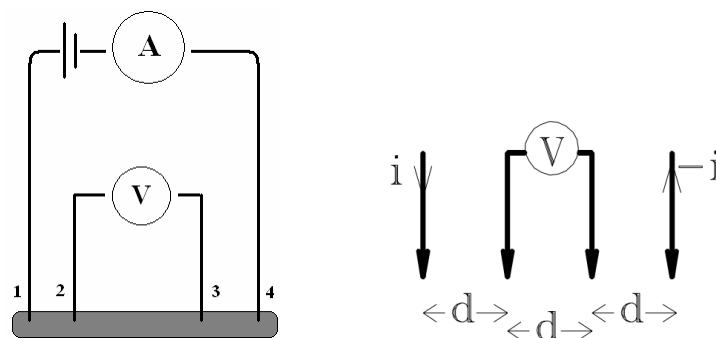
We have used a 4-point method for DC conductivity measurement. This method is an electrical impedance measuring technique that uses separate pairs of current-carrying and voltage-sensing electrodes to make more accurate measurements than the simpler and more usual 2-point method. It is normally used to measure sheet resistance of thin films.

The separation of current and voltage electrodes eliminates the lead and contact resistance from the measurement. This is an advantage for precise measurement of low resistance values.

a/ Principle:

The instrument based on the 4-point measurement work on the following principle:

- Two current leads, 1 and 4, comprise a two-wire current source that circulates current through the resistance under test.
- Two potential leads, 2 and 3, provide a two-wire voltage measurement circuit that measures the voltage drop across the resistance under test.
- We can compute the value of resistance from the measured values of current and voltage.



The 4 points are aligned and placed far from the edges of the conductive layer to be characterized in order to ensure the assumption of the infinite plane.

Since the ink thickness e is negligible with respect to the other dimensions ($e < 0.25 \times d$), a two-dimensional conduction model can be constructed which gives:

$$\frac{V}{I} = K \times \frac{\rho}{e} \quad (\text{A-1})$$

where K is a characteristic dimensionless coefficient of 2D geometry (depending on the shape of the contours, the position of the contacts, ...). [Smits 1958]

The K coefficient can be analytically calculated in a few very simple particular cases, for example for 4 equidistantly aligned points on an infinite layer: $K = \frac{\ln 2}{\pi}$ (or practical value: $1/K = 4.5324$).

In reality, we must measure the resistivity at many positions on the silver ink layer in order to calculate the average value of resistivity, and then the average value of conductivity. From (A-1), we have a formula for calculating the average conductivity:

$$\sigma = \frac{1}{\rho} = \frac{I}{4.5324 \times e \times \bar{U}} \quad (\text{A-2})$$

$$\bar{U} = \frac{U_1 + U_2 + \dots + U_n}{n} = \frac{\sum_{i=1}^n U_i}{n} \quad (\text{A-3})$$

where U_i is the voltage between 2 voltage-sensing electrodes measured at each position on the conductive layer, I is the intensity of the current supplied by 2 points at the extremities, e is the thickness of the conductive layer, \bar{U} is the average voltage measured at n different positions on the conductive layer, n is the number of measurements.

In order to estimate the error of the conductivity measurement, we have set up the following formulas:

$$\Delta U_1 = |\bar{U} - U_1|$$

$$\Delta U_2 = |\bar{U} - U_2|$$

.....

$$\Delta U_n = |\bar{U} - U_n|$$

$$\text{Average error of voltage: } \Delta U = \frac{\sum_{i=1}^n |\Delta U_i|}{n} \quad (\text{A-4})$$

$$\text{From (A-2), we have: } \ln(\sigma) = \ln\left(\frac{I}{4.5324 \times e \times \bar{U}}\right)$$

$$\Leftrightarrow d[\ln(\sigma)] = d[\ln(I) - \ln(U) - \ln(e)]$$

$$\Leftrightarrow \frac{d\sigma}{\sigma} = \frac{dI}{I} - \frac{dU}{U} - \frac{de}{e}$$

$$\text{So, we have the formula of the relative error: } \frac{\Delta\sigma}{\sigma} = \frac{\Delta I}{I} + \frac{\Delta U}{U} + \frac{\Delta e}{e} \quad (\text{A-5})$$

Clearly, the conductivity accuracy depends simultaneously on the precision of the current intensity supplied by the equipment, the precision of the voltage measurement and the precision of the thickness of the conductive layer, in which the thickness measurement has the most important influence to the relative error.

b/ Results:

The current intensity supplied by the generator is set at 0.5A assuming that the current error is negligible. We have measured at 15 different positions on the silver ink layer in order to calculate the average value of conductivity. The average voltage measured at different positions on the conductive layer is 9.63 ± 0.22 (mV) for recto layer and 9.72 ± 0.01 (mV) for verso layer. The thickness of the screen-printed deposit is 7.6 ± 2.07 μm , as presented in *chapter 2*.

Therefore, by applying (A-2) and (A-5), the average DC conductivity calculated is $(1.51 \pm 0.45) \times 10^6$ [S/m] (error 29.8%) for recto layer and $(1.49 \pm 0.41) \times 10^6$ [S/m] (error 27.5%) for verso layer.

ANNEX B: Dielectric properties of ABS plastic

Before characterizing the dielectric properties of the ABS plastic material, we have examined its parameters on the internet. Its characteristics may vary slightly depending on the composition of the material or the different manufacturers. In the datasheet published on <http://www.matweb.com/>, we could find: $\epsilon_r = 2.6 - 3.5$; $\tan\delta = 0.004 - 0.09$.

We have then carried out the same characterization procedure as the flexible substrate in *chapter 2* based on the microstrip transmission line method.

In fact, a small piece of ABC plastic (5 cm x 3 cm) was cut from the set-top-box shell. It has a thickness of 2.48 mm, measured with thickness meter. Then, a microstrip transmission line prototype with 50 mm of length and 2 mm of width was realized with adhesive copper on this ABS piece. The adhesive copper comprises a 25 μ m thick adhesive layer and 40 μ m thick copper layer with an average DC conductivity of about 3.94×10^7 S/m.

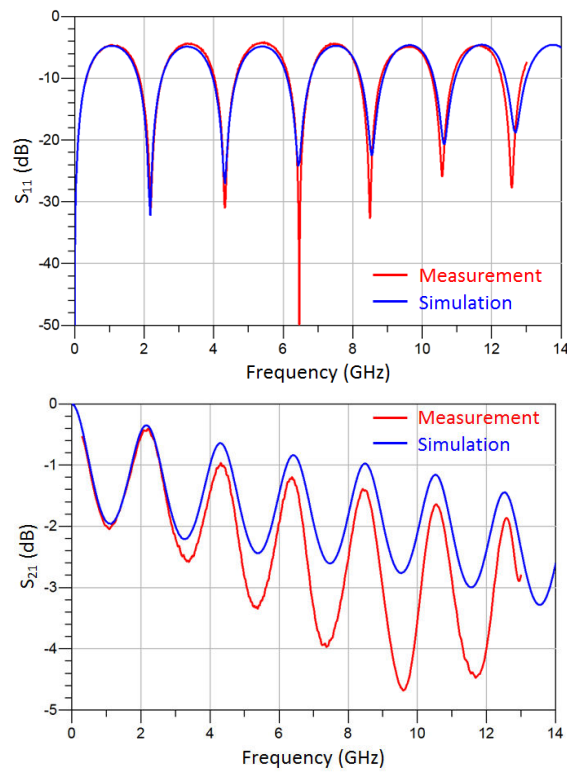
The thickness of the adhesive layer (25 μ m) in copper tape is very small in comparison with the plastic thickness (2.48 mm). The impact of this adhesive layer on the dielectric characterization process of ABS plastic is consequently negligible. Therefore, we can apply analytical calculations, as presented in *section 2.2.2.1*, to rapidly calculate the relative permittivity at each resonance frequency.

For loss tangent, the values of $\tan\delta$ are also chosen so that the retro-simulation has the best agreement with the measurement at each resonance frequency (taking into account the insertion losses related to connectors).

The characterized dielectric properties (relative permittivity and loss tangent) of ABS plastic are reported in the Table below:

ABS_plastic (2.5 mm thickness)						
Resonance mode	1	2	3	4	5	6
f (GHz)	2.18	4.33	6.46	8.50	10.57	12.57
ϵ_r	2.69	2.74	2.77	2.86	2.90	2.96
$\tan\delta$	0.023	0.031	0.028	0.027	0.026	0.024

An average value of dielectric properties ($\epsilon_r = 2.75$ and $\tan\delta = 0.027$) was also applied in the Momentum simulation in order to compare with the measurement results of S_{ij} . A good agreement between simulation and measurement was observed over a wide frequency band up to 13 GHz, as showed in Figure below.



Furthermore, these characterized values show a good concordance when compared to the values given by the datasheet.

In summary, the dielectric properties of ABS plastic are: $\epsilon_r = 2.69 - 2.76$ and $\tan\delta = 0.027$ (in the range of 2 to 6 GHz).

REFERENCES

- [Abouzahra 1979]:** M. D. Abouzahra and L. Lewin, "Radiation from microstrip discontinuities," *IEEE Trans. Microw. Theory Tech.*, vol. MTT-27, no. 8, pp. 722-723, Aug. 1979.
- [Abutarboush 2012]:** H. F. Abutarboush and A. Shamim, "Paper-Based Inkjet-Printed Tri-Band U-Slot Monopole Antenna for Wireless Applications," in *IEEE Antennas and Wireless Propagation Letters*, vol. 11, pp. 1234-1237, 2012.
- [Abutarboush 2014]:** H. F. Abutarboush and A. Shamim, "Wide frequency independently controlled dual-band inkjet-printed antenna," in *IET Microwaves, Antennas & Propagation*, vol. 8, no. 1, pp. 52-56, January 8 2014.
- [Abutarboush 2015]:** H. F. Abutarboush, M. F. Farooqui and A. Shamim, "Inkjet-Printed Wideband Antenna on Resin-Coated Paper Substrate for Curved Wireless Devices," in *IEEE Antennas and Wireless Propagation Letters*, vol. 15, pp. 20-23, 2016.
- [Alimenti 2010]:** F. Alimenti, F. Alimenti, V. Palazzari, G. Orecchini, G. Pinca, P. Mezzanotte, M. M. Tentzeris and L. Roselli, "Crossed dipole frequency doubling RFID TAG based on paper substrate and ink-jet printing technology," 2010 IEEE MTT-S International Microwave Symposium, Anaheim, CA, 2010, pp. 840-842.
- [Alimenti 2011-2]:** F. Alimenti, G. Orecchini, M. Virili, V. Palazzari, P. Mezzanotte and L. Roselli, "Design of paper-substrate dipole antennas magnetically coupled to UHF RFID silicon chips," 2011 IEEE International Conference on RFID-Technologies and Applications, Sitges, 2011, pp. 219-222.
- [Alimenti 2012]:** F. Alimenti, P. Mezzanotte, M. Dionigi, M. Virili and L. Roselli, "Microwave Circuits in Paper Substrates Exploiting Conductive Adhesive Tapes," in *IEEE Microwave and Wireless Components Letters*, vol. 22, no. 12, pp. 660-662, Dec. 2012.
- [Alimenti 2015-1]:** F. Alimenti, V. Palazzari, C. Mariotti, M. Virili, G. Orecchini, L. Roselli and P. Mezzanotte, "24-GHz CW radar front-ends on cellulose-based substrates: A new technology for low-cost applications," 2015 IEEE MTT-S International Microwave Symposium, Phoenix, AZ, 2015, pp. 1-4.
- [Amin 2012-1]:** Y. Amin, Q. Chen, L.-R. Zheng, and H. Tenhunen, "Development and analysis of flexible UHF RFID antennas for "green" electronics," *Progress In Electromagnetics Research*, Vol. 130, pp. 1-15, 2012.
- [Amin 2012-2]:** Y. Amin, Q. Chen, H. Tenhunen, L.-R. Zheng, "Performance-optimized quadrate bowtie RFID antennas for cost-effective and eco-friendly industrial applications," *Progress In Electromagnetics Research*, Vol. 126, pp. 49-64, 2012.
- [Anagnostou 2010]:** D. E. Anagnostou, A. A. Gheethan, A. K. Amert and K. W. Whites, "A Direct-Write Printed Antenna on Paper-Based Organic Substrate for Flexible Displays and WLAN Applications," in *Journal of Display Technology*, vol. 6, no. 11, pp. 558-564, Nov. 2010.
- [Ayman 2016]:** Ayman S. Al-Zayed and V. A. Shameena, "Planar Dual-Band Monopole Antenna with an Extended Ground Plane for WLAN Applications," *International Journal of Antennas and Propagation*, vol. 2016, Article ID 6798960, 10 pages, 2016.
- [Bhattacharya 2007]:** S. K. Bhattacharya, M. M. Tentzeris, L. Yang, S. Basat and A. Rida, "Flexible LCP and Paper-based Substrates with Embedded Actives, Passives, and RFIDs," *Polytronic 2007 - 6th International Conference on Polymers and Adhesives in Microelectronics and Photonics*, Odaiba, Tokyo, 2007, pp. 159-166.

- [Bisognin 2013]:** A. Bisognin, C. Luxey, G. Jacquemod, F. Ferrero, D. Titz, J. Thiellex, W. Wei, H. Happy and P. Brachat, "Antenna on PEN substrate for millimeter-wave applications," 2013 IEEE Antennas and Propagation Society International Symposium (APSURSI), Orlando, FL, 2013, pp. 684-685.
- [Carroll 1995]:** J. Carroll, M. Li and K. Chang, "New technique to measure transmission line attenuation," IEEE Trans. Microw. Theory Tech., vol. 43, no. 1, pp. 219-222, Jan. 1995.
- [Chuang 2007]:** L.-C. Kuo, H.-R. Chuang, Y.-C. Kan, T.-C. Huang & C.-H. Ko, "A Study of Planar Printed Dipole Antennas for Wireless Communication Applications," Journal of Electromagnetic Waves and Applications, Volume 21, 2007 - Issue 5.
- [Cook 2012-1]:** B. S. Cook and A. Shamim, "Inkjet Printing of Novel Wideband and High Gain Antennas on Low-Cost Paper Substrate," in IEEE Transactions on Antennas and Propagation, vol. 60, no. 9, pp. 4148-4156, Sept. 2012.
- [Cook 2013-1]:** B. S. Cook, Y. Fang, S. Kim, T. Le, W. B. Goodwin, K. H. Sandhage and M. M. Tentzeris, "Inkjet catalyst printing and electroless copper deposition for low-cost patterned microwave passive devices on paper" – Electronic Materials Letters 2013, Vol. 9, No. 5, pp. 669-676.
- [Cooper 2012-2]:** J. R. Cooper and M. M. Tentzeris, "Novel "smart cube" wireless sensors with embedded processing/communication/power core for "smart skins" applications," 2012 IEEE Sensors, Taipei, 2012, pp. 1-4.
- [Coupez 2012]:** Coupez Jean-Philippe, Charaabi Zied, Hemery Jeremie, Person Christian, "Dual Fin antenna," US2012/0112967 patent application 2012.
- [Nothorn 2007]:** D. Nothorn, "Emerging Plastic Films for Flexible Electronics Substrates," MSE 542, Flexible Electronics.
- [Denneulin 2011]:** A. Denneulin, J. Bras, A. Blayo, C. Neuman, "Substrate pre-treatment of flexible material for printed electronics with carbon nanotube based ink," in Applied Surface Science, Vol. 257, Issue 8, 2011, pp. 3645-3651.
- [Lo Hine Tong 2016]:** D. L. H. Tong, A. A. Manga, P. Minard, A. Delattre, L. Crowther-Alwyn and P. Borel, "Comparative study of WLAN dual-band monopole antennas printed and etched on paper and PET substrates," 2016 46th European Microwave Conference (EuMC), London, 2016, pp. 1243-1246.
- [Elsherbeni 2010]:** T. Elsherbeni, K. ElMahgoub, L. Sydänheimo, L. Ukkonen, A. Elsherbeni and F. Yang, "Laboratory scale fabrication techniques for passive UHF RFID tags," 2010 IEEE Antennas and Propagation Society International Symposium, Toronto, ON, 2010, pp. 1-4.
- [Farooqui 2014-2]:** M. F. Farooqui, C. Claudel and A. Shamim, "An Inkjet-Printed Buoyant 3-D Lagrangian Sensor for Real-Time Flood Monitoring," in IEEE Transactions on Antennas and Propagation, vol. 62, no. 6, pp. 3354-3359, June 2014.
- [FH34]:** Datasheet of FH34 family's connector provided by Hirose.
- [FH34-SRJ]:** High Speed Connector EM Simulation of FH34SRJ Series
- [Gonçalves 2014-1]:** R. Gonçalves, A. Duarte, R. Magueta, N. B. Carvalho and P. Pinho, "RFID tags on paper substrate for bottle labelling," Science Direct Procedia Technology, Vol. 17, 2014, pp 65-72.
- [Gonçalves 2014-2]:** R. Gonçalves, N. B. Carvalho, R. Magueta, A. Duarte and P. Pinho, "UHF RFID tag antenna for bottle labeling," 2014 IEEE Antennas and Propagation Society International Symposium (APSURSI), Memphis, TN, 2014, pp. 1520-1521.
- [Göttel 2013]:** B. Göttel, S. Beer, H. Gulan and T. Zwick, "Ultra broadband millimeter-wave antenna fabricated on flexible substrate," 2013 IEEE Antennas and Propagation Society International Symposium (APSURSI), Orlando, FL, 2013, pp. 5-6.
- [Hammerstad 1975]:** E. O. Hammerstad and F. Bekkadal, "Microstrip Handbook," Univ. Trondheim, Trondheim, Norway, ELAB Rep., STF 44 A74169, Feb. 1975.

- [Hong-Duc 2016]:** Hong-Duc Nguyen, J.-P. Coupez, V. Castel, C. Person, A. Delattre, L. Crowther-Alwyn and P. Borel, "RF Characterization of Flexible Substrates for New Conformable Antenna Systems", 10th European Conference on Antennas and Propagation (EuCAP), Davos, 2016, pp. 1-5.
- [Hsuan-ling 2011]:** Hsuan-ling Kao; Cheng-Lin Cho; Chih-Sheng Yeh; Bo-Wen Wang; Jing-Yi Ke; Li-Chun Chang, "RF bandpass filter on flexible substrate fabricated with inkjet printing technology".
- [Hsuan-Yu 2012]:** H. Y. Chien, C. Y. D. Sim and C. H. Lee, "Compact size dual-band antenna printed on flexible substrate for WLAN operation," 2012 International Symposium on Antennas and Propagation (ISAP), Nagoys, 2012, pp. 1047-1050.
- [Janezic 1999]:** M. D. Janezic, J. B. Jarvis, "Full-Wave Analysis of a Split-Cylinder Resonator for Nondestructive Permittivity Measurements," IEEE T-MTT, 1999, vol. 47, N10, pp. 2014-2020.
- [Jyoti 2011]:** J. R. Panda, A. S. R. Saladi, R. S. Kshetrimayum, "A compact printed monopole antenna for dual-band RFID and WLAN applications", Radioengineering n°20, pp.464-467, June 2011.
- [Kent 1998]:** G. Kent, "An evanescent-mode tester for ceramic dielectric substrates," IEEE Trans. Microwave Theory & Tech., vol. 36, no. 10, pp. 1451-1454, October 1998.
- [Kim 2013-2]:** S. Kim, A. Traille, H. Lee, H. Aubert, K. Yoshihiro, A. Georgiadis, A. Collado and M. M. Tentzeris, "Inkjet-printed sensors on paper substrate for agricultural applications," 2013 European Microwave Conference, Nuremberg, 2013, pp. 866-869.
- [Kharrat 2013]:** I. Kharrat, G. Eymin Petot Tourtollet, J. M. Duchamp, P. Benech, P. Xavier and T. P. Vuong, "Design and realization of printed on paper antennas," 2013 7th European Conference on Antennas and Propagation (EuCAP), Gothenburg, 2013, pp. 3199-3202.
- [Kharrat 2014]:** I. Kharrat, P. Xavier, T.-P. Vuong, J.-M. Duchamp, Ph. Benech and G. Eymin Petot Tourtollet, "3D compact rectenna for anti-counterfeiting application," 2014 44th European Microwave Conference, Rome, 2014, pp. 664-667.
- [Kharrat 2015]:** I. Kharrat, P. Xavier, T. P. Vuong, J. M. Duchamp, P. Benech and G. Eymin Petot Tourtollet, "Low-Loss Paper Substrate for Printed High Efficiency Antennas at 2.45 GHz," in IEEE Antennas and Wireless Propagation Letters, vol. 14, pp. 1400-1403, 2015.
- [Konstas 2009]:** Z. Konstas, A. Rida, R. Vyas, K. Katsibas, N. Uzunoglu and M. M. Tentzeris, "A novel "Green" inkjet-printed Z-shaped monopole antenna for RFID applications," 2009 3rd European Conference on Antennas and Propagation, Berlin, 2009, pp. 2340-2343.
- [Kutner 2005]:** M. H. Kutner, C. J. Nachtsheim, J. Neter, and W. Li, Applied Linear Statistical Models, 5th ed. New York: McGraw-Hill, 2005.
- [Lambert 1998]:** "RF flex circuit transmission line & interconnection method", US Patent.
- [Latti 2005]:** K. Latti, J. -M. Heinola, M. Kettunen, J. -P. Strom and P. Silventoinen, "A Review of Microstrip T-resonator Method in Determination of Dielectric Properties of Printed Circuit Board Materials," 2005 IEEE Instrumentation and Measurement Technology Conference Proceedings, Ottawa, Ont., 2005, pp. 62-66.
- [Latti 2007]:** K. P. Latti, M. Kettunen, J. P. Strom and P. Silventoinen, "A Review of Microstrip T-Resonator Method in Determining the Dielectric Properties of Printed Circuit Board Materials," in IEEE Transactions on Instrumentation and Measurement, vol. 56, no. 5, pp. 1845-1850, Oct. 2007.
- [Li 1981]:** S. Li, C. Akyel and R. G. Bosisio, "Precise Calculations and Measurements on the Complex Dielectric Constant of Lossy Materials Using TM010 Cavity Perturbation Techniques", IEEE Trans. on Microwave Theory and Techniques, Vol. 29, pp. 1041-1048, No. 10, 1981.

- [Liu 2014-2]:** Xueli Liu, Shun Yao, S. V. Georgakopoulos, B. S. Cook and M. M. Tentzeris, "Reconfigurable helical antenna based on an origami structure for wireless communication system," 2014 IEEE MTT-S International Microwave Symposium (IMS2014), Tampa, FL, 2014, pp. 1-4.
- [Lolli 2012]:** F. Lolli, M. Virili, G. Orecchini, M. Dionigi, F. Alimenti, P. Mezzanotte and L. Roselli, "Electromagnetic Characterization of Paper-Glue Compound for System-in-Package on Paper (SiPoP) Future Developments," in IEEE Microwave and Wireless Components Letters, vol. 22, no. 10, pp. 545-547, Oct. 2012.
- [Markovic 2007]:** D. Markovic, B. Jokanovic, M. Marjanovic, and M. Djordjevic, "Improved method for measurement of the dielectric properties of microwave substrates using microstrip t-resonator," in Proc. Instrumentation and Measurement Technology Conf., May 1-3, 2007, pp. 1-3.
- [Mariotti 2013]:** C. Mariotti, F. Alimenti, P. Mezzanotte, M. Dionigi, Marco Virili, S. Giacomucci and L. Roselli, "Modeling and characterization of copper tape microstrips on paper substrate and application to 24 GHz branch-line couplers," 2013 European Microwave Conference, Nuremberg, 2013, pp. 794-797.
- [Merilampi 2007]:** S. Merilampi, L. Ukkonen, L. Sydänheimo, P. Ruuskanen, and M. Kivikoski, "Analysis of Silver Ink Bow-Tie RFID Tag Antennas Printed on Paper Substrates," International Journal of Antennas and Propagation, vol. 2007, pp. 1-9, 2007.
- [Merilampi 2009]:** S. Merilampi, T. Laine-Ma, P. Ruuskanen, "The characterization of electrically conductive silver ink patterns on flexible substrates", Microelectronics Reliability, Volume 49, Issue 7, July 2009, pp. 782-790.
- [Monti 2012]:** G. Monti, L. Catarinucci, C. Vasanelli and L. Tarricone, "3D patch antenna using a cardboard substrate for RFID reader applications," 2012 42nd European Microwave Conference, Amsterdam, 2012, pp. 884-887.
- [Morgan 1949]:** S. P. Morgan, "Effect of surface roughness on Eddy current losses at microwave frequencies," J. Appl. Phys., vol. 20, no. 4, pp. 352-362, Apr. 1949.
- [Moro 2012]:** R. Moro, M. Bozzi, S. Kim and M. M. Tentzeris, "Novel inkjet-printed substrate integrated waveguide (SIW) structures on low-cost materials for wearable applications," 2012 42nd European Microwave Conference, Amsterdam, 2012, pp. 72-75.
- [Moro 2013]:** R. Moro, S. Kim, M. Bozzi, M. M. Tentzeris, "Inkjet-printed paper-based substrate-integrated waveguide (SIW) components and antennas," International Journal of Microwave and Wireless Technologies, 2013, pp. 197-204.
- [Orecchini 2010]:** G. Orecchini, L. Yang, M. M. Tentzeris and L. Roselli, "High directivity passive UHF RFID tag with dual-radiating-body antenna," 2010 IEEE Antennas and Propagation Society International Symposium, Toronto, ON, 2010, pp. 1-4.
- [Orecchini 2011-1]:** G. Orecchini, F. Alimenti, V. Palazzari, A. Rida, M. M. Tentzeris and L. Roselli, "Design and fabrication of ultra-low cost radio frequency identification antennas and tags exploiting paper substrates and inkjet printing technology," in IET Microwaves, Antennas & Propagation, vol. 5, no. 8, pp. 993-1001, June 6 2011.
- [Orecchini 2011-2]:** G. Orecchini, M. M. Tentzeris, L. Yang and L. Roselli, "'Smart Shoe': An autonomous inkjet-printed RFID system scavenging walking energy," 2011 IEEE International Symposium on Antennas and Propagation (APSURSI), Spokane, WA, 2011, pp. 1417-1420.
- [Pauw 1977]:** L. J. Van der Pauw, "The radiation of electromagnetic power by microstrip configurations," IEEE Trans. Microw. Theory Tech., vol. MTT-25, no. 9, pp. 719-725, Sep. 1977.
- [Phan 2016]:** H. P. Phan, T. P. Vuong, P. Benech, P. Xavier, P. Borel and A. Delattre, "Printed flexible wideband microstrip antenna for wireless applications," 2016 International Conference on Advanced Technologies for Communications (ATC), Hanoi, 2016, pp. 384-387.

- [Polyakov 2004]:** A. Polyakov, T. Grob, R. A. Hovenkamp, H. J. Kettelarij, I. Eidner, M. A. de Samber, M. Bartek and J. N. Burghartz, "Comparison of via-fabrication techniques for through-wafer electrical interconnect applications," 2004 Proceedings. 54th Electronic Components and Technology Conference (IEEE Cat. No.04CH37546), 2004, pp. 1466-1470 Vol.2.
- [Quan 1997]:** "Microstrip Flexible Printed Wiring Board Interconnect Line", US Patent.
- [Ramade 2012]:** C. Ramade, S. Silvestre, F. Pascal-Delannoy, B. Sorli, "Thin film HF RFID tag deposited on paper by thermal evaporation," International Journal of Radio Frequency Identification Technology and Applications, 2012, Vol.4, No.1, pp.49 - 66.
- [Rathore 2010]:** A. Rathore, R. Nilavalan, H. F. AbuTarboush and T. Peter, "Compact dual-band (2.4/5.2GHz) monopole antenna for WLAN applications," 2010 International Workshop on Antenna Technology (iWAT), Lisbon, 2010, pp. 1-4.
- [Riedell 1989]:** C. H. Riedell, M. Kay, R. Pomerleau, M. Steer, J. Kasten and M. Basel, "Dielectric Characterization of Printed Circuit Substrates," IEEE Proceedings - 1989, pp. 102-106.
- [Rida 2008]:** A. Rida, R. Vyas, Li Yang, C. Kruesi and M. M. Tentzeris, "Low Cost Inkjet-printing Paper-Based Modules for RFID Sensing and Wireless Applications," 2008 38th European Microwave Conference, Amsterdam, 2008, pp. 1715-1718.
- [Saghlatoon 2014]:** H. Saghlatoon, L. Sydänheimo, L. Ukkonen and M. Tentzeris, "Optimization of Inkjet Printing of Patch Antennas on Low-Cost Fibrous Substrates," in IEEE Antennas and Wireless Propagation Letters, vol. 13, pp. 915-918, 2014.
- [Saintsing 2014]:** C. Saintsing, B. S. Cook, and M. M. Tentzeris, "An origami inspired reconfigurable spiral antenna," in ASME Int. Design Eng. Techno. Conf. Comput. Inform. Eng. Conf., Buffalo, NY, USA, Aug. 2014.
- [Shaker 2010]:** G. Shaker, M. Tentzeris and S. Safavi-Naeini, "Low-cost antennas for mm-Wave sensing applications using inkjet printing of silver nano-particles on liquid crystal polymers," 2010 IEEE Antennas and Propagation Society International Symposium, Toronto, ON, 2010, pp. 1-4.
- [Shaker 2011-1]:** G. Shaker, S. Safavi-Naeini, N. Sangary and M. M. Tentzeris, "Inkjet Printing of Ultrawideband (UWB) Antennas on Paper-Based Substrates," in IEEE Antennas and Wireless Propagation Letters, vol. 10, pp. 111-114, 2011.
- [Schneider 1969]:** M. V. Schneider, "Microstrip lines for microwave integrated circuits," Bell Syst. Tech. J., vol. 48, no. 5, pp. 1421-1444, May/Jun. 1969.
- [Smits 1958]:** F. M. Smits, "Measurement of sheet resistivities with the four-point probe", in The Bell System Technical Journal, vol. 37, no. 3, pp. 711-718, May 1958.
- [Tentzeris 2010]:** M. M. Tentzeris, A. Traille, H. Lee, A. Rida, V. Lakafosis and R. Vyas, "Inkjet-printed paper/polymer-based "green" RFID and Wireless Sensor Nodes: The final step to bridge cognitive intelligence nanotechnology and RF?," 2010 IEEE Sensors, Kona, HI, 2010, pp. 1273-1276.
- [Tentzeris 2012-1]:** M. M. Tentzeris, R. Vyas, V. Lakafosis, A. Traille, H. Lee, E. Gebara and M. Marroncelli, "Inkjet-printed RFIDs for wireless sensing and anti-counterfeiting," 2012 6th European Conference on Antennas and Propagation (EUCAP), Prague, 2012, pp. 3481-3482.
- [Tentzeris 2012-2]:** M. M. Tentzeris, R. Vyas, V. Lakafosis, T. Le, A. Rida and S. Kim, "Conformal 2D/3D wireless modules utilizing inkjet printing and nanotechnology," Microwave Journal, 2012, Vol. 55, Issue. 2.
- [Tobjörk 2011]:** D. Tobjörk and R. Österbacka, "Paper electronics," Advanced Materials 2011, Vol. 23, Issue. 17, May 3, 2011, pp. 1935-1961.
- [Traille 2009]:** A. Traille, L. Yang, A. Rida, V. Lakafossis and M. M. Tentzeris, "Novel miniaturized antennas for RFID-enabled sensors," 2009 IEEE Sensors, Christchurch, 2009, pp. 912-915.

- [Traille 2014]:** A. Traille, A. Coustou, H. Aubert, S. Kim and M. M. Tentzeris, "Technology for fully printable and rollable ground penetrating radar (GPR) systems," 2014 IEEE Antennas and Propagation Society International Symposium (APSURSI), Memphis, TN, 2014, pp. 334-335.
- [Vena 2013]:** A. Vena, E. Perret, S. Tedjini, G. Eymin Petot Tourtollet, A. Delattre, F. Garet and Y. Boutant, "Design of Chipless RFID Tags Printed on Paper by Flexography," in IEEE Transactions on Antennas and Propagation, vol. 61, no. 12, pp. 5868-5877, Dec. 2013.
- [Virili 2015]:** M. Virili, L. Roselli, F. Alimenti, P. Mezzanotte, S. Moscato, L. Silvestri, M. Bozzi and L. Perregrini, "GRETA approach towards new green material technologies," 2015 International EURASIP Workshop on RFID Technology (EURFID), Rosenheim, 2015, pp. 9-15.
- [Vyas 2007]:** R. Vyas, A. Rida, Li Yang and M. M. Tentzeris, "Design and Development of a Novel Paper-based Inkjet-Printed RFID-Enabled UHF (433.9 MHz) Sensor Node," 2007 Asia-Pacific Microwave Conference, Bangkok, 2007, pp. 1-4.
- [Vyas 2008]:** R. Vyas, A. Rida, Li Yang and M. M. Tentzeris, "Design, integration and characterization of a novel paper-based wireless sensor module," 2008 IEEE MTT-S International Microwave Symposium Digest, Atlanta, GA, USA, 2008, pp. 1305-1308.
- [Vyas 2009]:** R. Vyas, V. Lakafosis, A. Rida, N. Chaisilwattana, S. Travis, J. Pan and M. M. Tentzeris, "Paper-Based RFID-Enabled Wireless Platforms for Sensing Applications," in IEEE Transactions on Microwave Theory and Techniques, vol. 57, no. 5, pp. 1370-1382, May 2009.
- [Walki 2012]:** "Walki-4E technology: a new, sustainable way of producing RFID antennas", www.walki.com.
- [Yen-Liang 2003]:** Yen-Liang Kuo and Kin-Lu Wong, "Printed double-T monopole antenna for 2.4/5.2 GHz dual-band WLAN operations," in IEEE Transactions on Antennas and Propagation, vol. 51, no. 9, pp. 2187-2192, Sep 2003.
- [Yao 2014-1]:** S. Yao, X. Liu, S. V. Georgakopoulos and M. M. Tentzeris, "A novel tunable origami accordion antenna," 2014 IEEE Antennas and Propagation Society International Symposium (APSURSI), Memphis, TN, 2014, pp. 370-371.
- [Yao 2014-2]:** S. Yao, X. Liu, S. V. Georgakopoulos and M. M. Tentzeris, "A novel reconfigurable origami spring antenna," 2014 IEEE Antennas and Propagation Society International Symposium (APSURSI), Memphis, TN, 2014, pp. 374-375.
- [Yang 2007-1]:** L. Yang, A. Rida, R. Vyas and M. M. Tentzeris, "RFID Tag and RF Structures on a Paper Substrate Using Inkjet-Printing Technology," in IEEE Transactions on Microwave Theory and Techniques, vol. 55, no. 12, pp. 2894-2901, Dec. 2007.
- [Yang 2007-2]:** L. Yang and M. M. Tentzeris, "Design and characterization of novel paper-based inkjet-printed RFID and microwave structures for telecommunication and sensing applications," in IEEE MTT-S Int. Microw. Symp. Dig., Jun. 2007, pp. 1633-1636.
- [Yuan Zhu 2016]:** Yuan Zhu, Min Quan Li and Hong Qing He, "A compact dual-band monopole antenna for 4G LTE and WIFI utilizations," 2016 IEEE MTT-S International Microwave Workshop Series on Advanced Materials and Processes for RF and THz Applications (IMWS-AMP), Chengdu, 2016, pp. 1-4.
- [Zou 2002]:** G. Zou, H. Gronqvist, P. Starski, and J. Liu, "Characterization of liquid crystal polymer for high frequency system-in-a-package applications," IEEE Trans. Adv. Packag., vol. 25, no. 4, pp. 503-508, Nov. 2002.
- [Web]** Confederation of European Paper Industries - CEPI countries.

PUBLICATIONS

1. Hong-Duc Nguyen, J.-P. Coupez, V. Castel, C. Person, A. Delattre, L. Crowther-Alwyn and P. Borel, "RF Characterization of Flexible Substrates for New Conformable Antenna Systems", 2016 10th European Conference on Antennas and Propagation (EuCAP), Davos, 2016, pp. 1-5.
2. H.-D. Nguyen, J.-P. Coupez, V. Castel, C. Person, A. Delattre, L. Crowther-Alwyn, P. Borel, "Monopôle Wifi bi-bande sur substrat papier pour l'intégration de systèmes antenaires conformables, faible coût", 20èmes Journées Nationales Micro-Ondes (JNM), 16-19 mai 2017 à Saint-Malo.
3. Ch. Person, Duc NGuyen, J. Ph. Coupez, Ph. Minard, D. Lo Hine Tong, P. Borel , D. Izoard, "Implementing Wideband Monopole/Dipole Antennas on Paper Substrates," 2018 48th European Microwave Conference (EuMC), Madrid, Sept 23-28.
4. Ch. Person, Duc NGuyen, J. Ph. Coupez, Ph. Minard, D. Lo Hine Tong, P. Borel , D. Izoard, "Characterization of Flex to Printed Circuit Board Interconnections using Insertion Connectors," 2018 48th European Microwave Conference (EuMC), Madrid, Sept 23-28.

Titre : Système passif antenne imprimable sur support conformable

Mots clés : Substrat papier flexible, Antenne sur papier, Antennes Wi-Fi bi-bandes, Solution d'interconnexion RF, Intégration au sein du boîtier électronique

Résumé : Au cours des dernières années, en raison de la demande croissante de produits de plus en plus légers, plus petits et moins chers à l'intérieur des appareils portables, l'électronique flexible émerge sur le marché commercial comme une nouvelle génération d'électroniques. Les substrats rigides conventionnels sont remplacés par des matériaux plus minces, flexibles et à faible coût tels que papier, polymère, plastique pour la fabrication des composants et circuits. En même temps, les futurs boîtiers électroniques demandent de plus en plus de nombreux systèmes sans fil afin d'offrir de multiples services et applications (ZigBee/Z-Wave, WLAN, DECT, Bluetooth, RF4CE, 3G/4G, etc.).

À cause de l'intégration d'un très grand nombre d'antennes pour satisfaire l'opération de toutes ces applications, les connectivités deviennent donc un grand défi pour les exigences de coût. C'est pourquoi on voudrait remplacer l'ensemble du système d'alimentation/d'interconnexion à la carte mère PCB par une technologie homogène, collective.

Ce travail de thèse vise à développer une nouvelle technologie "verte" et faible coût dédiée à la conception et réalisation de systèmes antennes et d'interconnexions sur les matériaux flexibles (tels que papier) à base d'encre conductrices et de procédés de fabrication additifs comme impression. Le défi scientifique est de concevoir des systèmes antennes répartis spatialement sur les faces internes en plastique du boîtier électronique sous forme des stickers RF 3D et connectés directement à la carte PCB par une solution innovante, à faible coût pour des applications multimédia sans fil dans la gamme de fréquences de 1.8-6 GHz.

Title : Passive Antenna Systems Printable on Conformable Supports

Keywords : Flexible paper substrate, Antenna on paper, Dual-band Wi-Fi antennas, RF interconnection solution, Integration into electronic box

Abstract :

In recent years, due to the growing demand for lighter, smaller and cheaper electronic products inside portable devices, clothing and packaging materials, flexible electronics is emerging on the commercial market as a new generation of electronics. Conventional rigid substrates will be replaced by thin, flexible, low-cost materials such as paper, polymer, and plastic for the manufacturing of components and circuits. Concurrently with the powerful development of flexible electronics, the future electronic devices have drastically demanded more wireless systems in order to offer multiple services and applications (ZigBee/Z-Wave, WLAN, DECT, Bluetooth, RF4CE, 3G/4G, etc.).

Because of the integration of a great number of antennas to satisfy the operation of all these applications, the connectivities thus become a big challenge for cost constraints. This is the reason why we would like to replace the entire interconnection system with the PCB mainboard by a homogeneous, collective technology.

This thesis work aims at developing "green", low-cost and innovative technology devoted to the design and realization of antenna systems and interconnections on flexible materials (such as paper) based on conductive inks and additive manufacturing processes like printing. The scientific challenge lies on the design of spatially distributed antenna systems on the internal plastic sidewall of the electronics box in the form of 3D RF stickers and directly connected to the PCB mainboard by an innovative, low-cost solution for wireless multimedia applications in the frequency range of 1.8-6 GHz.